VERIFICATION AND VALIDATION OF A TRANSIENT HEAT EXCHANGER MODEL

A thesis submitted in partial fulfillment
of the requirements for the degree of
Master of Science in Engineering

By

JAYME LEE CARPER
B.S., Wright State University, 2010

2015

Wright State University

WRIGHT STATE UNIVERSITY

GRADUATE SCHOOL

August 31, 2015

I HEREBY RECOMMEND THAT THE THESIS PREPARED UNDER MY SUPERVISION BY Jayme Lee Carper ENTITLED Verification and Validation of a Transient Heat Exchanger Model BE ACCEPTED IN PARTIAL FULFILLMENT OF THE REQUIREMENTS FOR THE DEGREE OF Master of Science in Engineering.

Rory A. Roberts, Ph.D.
Thesis Director

George Huang, Ph.D.
Chair
Department of Mechanical and Materials Engineering
College of Engineering and Computer Science

Committee on
Final Examination

Scott K. Thomas, Ph.D.

J. Mitch Wolff, Ph.D.

Robert E.W. Fyffe, Ph.D.
Vice President for Research and
Dean of the Graduate School

ABSTRACT

Carper, Jayme Lee. M.S., Egr., Wright State University, 2015.
Verification and Validation of a Transient Heat Exchanger Model

---

A statistical based verification and validation process is applied to the transient modeling of a shell and tube heat exchanger. A generic model of a heat exchanger was developed based on first principles as a sub-system of a larger thermal system model. This model was originally created without any experimental data, as it was not readily available. To provide the data necessary to apply the validation process, a thermal emulator was designed and built that allowed control of all system inputs to the heat exchanger, while also providing the instrumentation to record all required data. A wide test matrix was chosen to fully encompass the expected operational envelope of the heat exchanger. Focus on the collection of experimental data was the minimization of uncertainty, as these uncertainties were amplified once they were propagated through the validation process.

The validation process encompasses the completion of sensitivity and uncertainty analyses, uncertainty propagation, verification, and validation. Once these steps were completed using a set of non-ideal experimental data, uncertainty in the transient heat exchanger model is quantified. This manuscript proposes a way to complete the validation process without replicate data sets by utilizing known information about the physical process. At the completion of the process, both uncertainties and model form error are quantified for the system outputs and a statistical validation metric is applied. These outputs help to define whether or not the model captures the physical process to a

satisfactory degree while also highlighting avenues for improvement if the uncertainty is deemed too large for the intended application.

TABLE OF CONTENTS

LIST OF FIGURES

Page

LIST OF TABLES

Page

NOMENCLATURE

Symbols

$A\ or\ SA$	surface area
D	hydraulic diameter
$\dot{E}$	energy flow, rate
$\dot{Q}$	heat flow, rate
R^2	coefficient of determination
T	temperature
$\dot{T}$	temperature, rate
c_{p}	specific heat
cv	control volume
h	heat transfer coefficient
k	thermal conductivity
m	mass
$\dot{m}$	mass flow, rate
t	time
v	fluid velocity
$\dot{v}$	volumetric fluid flow, rate
Δ	uncertainty, measurement
θ	phase, electrical power
μ	dynamic viscosity
ρ	density
σ	standard deviation / uncertainty, analytical
σ^2	variance
τ	time constant
Nu	Nusselt number
OD	outer diameter
Pr	Prandtl number
Re	Reynolds number

Sen	sensitivity

Subscripts

hx	heat exchanger
i	inlet, fluid
i	input
i	integer, variable index
k	integer, variable index
n	number of inputs
o	outlet, fluid
o	output
s	shell
store	storage, transient term
t	time, selected data point
t	tube
x	variable

Abbreviations

A-D	Anderson-Darling
AAD	absolute area deviation
AFRL	Air Force Research Laboratory
ANOVA	analysis of variance
AOA	angle of attack
ASME	American Society of Mechanical Engineers
CDF	cumulative distribution function
CLA	coefficient of rolling moment
CNA	coefficient of yawing moment
CYA	coefficient of side force
DAQ	data acquisition
EMI	electromagnetic interference
IPCC	Intergovernmental Panel for Climate Change
ISO	International Organization for Standardization
K-S	Kolmogorov-Smirnov
NIST	National Institute of Standards and Technology
ODE	ordinary differential equation
PDF	probability density function
PRESS	predicted residual error sum of the squares
PRTD	platinum resistance temperature detector
RQPE	Energy & Power Branch, Aerospace Systems Directorate
RTD	resistance temperature detector
RZPE	Energy & Power Branch, Propulsion Directorate
SRQ	system response quantity
T2T	Tip-to-Tail
USB	Universal Serial Bus
V&V	verification and validation
VI	Virtual Instrument (LabView program)
WSU	Wright State University

ACKNOWLEDGEMENTS

I would like to first thank my advisor, Dr. Rory Roberts, for his financial support and guidance throughout this project; he sought to add me to an ongoing project that he had despite my limited knowledge about the subject material and the modeling tools. As he is an expert in Matlab and Simulink, I learned how to use current modeling tools and tips quickly & efficiently, as well as the additional background information on the modeling of heat exchangers, thermal systems, and environmental control systems. I truly believe that without these opportunities that he provided for me, I would not have been able to secure the job that I currently have.

Dr. Roberts was able to help me overcome a major downfall that I possess: the lack of ability to focus on a topic without direction. He managed to provide the guidance necessary such that progress was able to be made, but in such a way that it was solely up to me to force myself to make this progress. I'm sure progress was not always made at the rate that either of us would have preferred, but it helped me to develop ways to shape my management of efforts on large, open-ended projects like this. This helped to build my self-confidence of project management, to accept the responsibility of my engineering decisions, as well as learning how to make progress without necessarily having to be constantly under extreme time constraints. These skills will be invaluable in my engineering career.

Additionally, I'd like to extend a sincere thank you to Dr. Wolff & Dr. Yerkes of AFRL/RQPE for their financial support of this project (Prime Contract: FA8650-11-C-2200) and to Dr. Doty of UD for the development of the verification and validation process that these efforts are based upon. I'd also like to extend a thank you to Dr.

Thomas of WSU for his useful input and guidance, despite not having taken his course in thermal fluid measurements that would have provided the necessary background information to complete my measurements and calibration quickly. He managed to teach me the material that I required in his spare time, as well as provide ideas for how to process some of the data that was collected.

I'd like to thank Scott Eastbourn for his prior modeling efforts that my work evolved from, companionship as both a colleague in school and at work, and most importantly, for his friendship. I am glad to have a friend with similar two (and one) wheeled interests, grateful that I was able to work with him, and excited for the amazing opportunity that his job offers he and his wife. I was sad to see them move across the country while he chases his dream, but now I have more of a reason than ever to travel.

And finally, I'd like to say thank you to my daughter Olivia: you haven't been here through the entire project, but you have provided me the direction, reason, and drive to finish school and move on to the next phase of my life. I had no idea what the next phase of my life was going to be, but since finding out that it is to be a parent, I am looking forward to the coming years more than ever. I can't wait to see what kind of awesome adventures we will have as you grow up.

INTRODUCTION

It is all too common for researchers to accept the outputs of a model as the deterministic truth, as opposed to recognizing that there is uncertainty associated with the system response quantities (SRQs). Some of these are inherent variations that exist in the measurement of real life quantities like random noise, or aleatory uncertainty, assumptions about the way the process actually functions, and the way these assumptions are modeled, or epistemic uncertainty.

When a way to improve the accuracy of the model is desired, it becomes necessary to validate the model in order to quantify the degree to which the model outputs agree with the experimental data. Validation is truly useful when properly completed in a quantitative fashion. Quantitative means more than merely having a value associated with an answer: it means that an answer must be provided along with a measure of the uncertainty in that answer. In fact, according to ASME standards, an answer is considered incomplete unless it has an uncertainty associated with it. This reinforces the importance of a validation technique that is capable of quantifying uncertainties.

Validation is a process used to quantify accuracy of a model. Model validation is a complex and often times ambiguous category, and as such, is often overlooked or simplified. Unfortunately, it is often completed in a qualitative fashion by visually measuring the agreement between SRQs; however, this process is completely unacceptable for engineers to utilize in practice as a speculative judgment by an engineer can have costly results.

This primary goal of this thesis is to document the process by which a thermal fluids component, specifically a shell and tube heat exchanger, is modeled and then subsequently validated. These modeling efforts are driven by a real-world application and as such, the degree to which the model can be trusted is information that is both relevant and required. In order to complete the validation efforts, experimental data will need to be collected and utilized to anchor the model. The validation process encompasses the completion of sensitivity and uncertainty analyses, uncertainty propagation, verification, and validation. These efforts will apply a previously developed statistical based process to a set of non-ideal experimental data. This process emulates a scenario when a researcher does not have access to a preferred quantity and type of data. Once validated, the heat exchanger model may be integrated with other validated sub-system components to help quantify possible system-level improvements.

BACKGROUND

The need for a validation technique arose from modeling efforts on a Tip-to-Tail (T2T) thermal model of a long ranger strike fighter.[1] The T2T model was developed wholly using no proprietary information; this freed the model from stringent controls over its use. As a direct result of the decision to exclude all proprietary information, most models were developed based on "First Principles," but in a generic sense. This meant that the models were based on relations that reflect the physical phenomena occurring, or stated another way, that the models were developed using equations that are widely accepted to govern the physics that occur. Many equations relating to heat transfer and thermal fluids are generic and can be applied to many situations, but apply to complex situations with varying accuracy.

A generic model of a heat exchanger was developed and implemented within the T2T model where it served its purpose to transfer thermal energy from one working fluid to another. It is necessary to note two important points regarding these modeling efforts:

1.) The model had been developed in a generic sense, such that it could be applied to various heat exchangers with minimal modification.
2.) It was completed with no comparison to or validation from experimental results.

Despite these aspects, the model transferred thermal energy and gave outputs that reasonably made sense (visual "validation"). However, it was quickly determined that to truly be useful, the model's accuracy, or lack thereof, would need to be quantified. The quantification of such accuracy would be obtained by following a validation process and applying it to this specific thermal fluids problem.

In order to validate the heat exchanger model, experimental data was required. Conveniently, the Energy and Power Branch of the Air Force Research Laboratory's Propulsion Directorate (AFRL/RQPE, formerly RZPE) possessed a shell and tube heat exchanger being utilized in a laboratory test loop for which additional information was sought. Specifically, the transient performance of the heat exchanger was desired as it was being used to cool an electrical generator, but this information was not readily available. This proved to be an ideal scenario for Wright State University (WSU) researchers to apply a validation process, as briefly described above, that would generate a useful model for both parties. The T2T modeling efforts would be able to continue with a validated heat exchanger model and be able to quantifiably trust the answers, to an estimated degree of certainty. This ultimately would allow the final answers from the entire T2T model to become more robust and accurate; as sub-system models are validated and then combined, true system interactions are feasibly captured.

AFRL/RQPE could stand to benefit from a validated heat exchanger model as well, for several reasons. One reason is equivalent to the reasons that WSU researchers stood to benefit: system level interactions could be studied among the various thermal fluids components with more certainty. By quantifying the uncertainty, the surety that the answer is what it is claimed to be is identified. A further benefit to a partnership with AFRL was alleviation of the highly constrained operational envelope of the electrical generator, as it had extremely limited operating hours before costly overhauls. Examining a wide operating envelope of the heat exchanger while installed in the test loop would require introducing undue wear on the generator; removing the heat exchanger from the loop would allow the full operating range to be examined without

negatively affecting the generator. Another benefit to this partnership was the lack of necessary instrumentation on the AFRL test loop; proper instrumentation would be required to accurately capture the thermal performance of the heat exchanger.

All of these aspects showed that it was necessary to develop a separate test loop, a thermal emulator, for the purposes of collecting experimental data on the thermal performance of the heat exchanger. The experimental data would then be used to validate the heat exchanger model that had been previously developed. Constructing the test loop in WSU laboratory space would allow instrumentation selection to be governed by the overall SRQs that were desired. Furthermore, this arrangement would allow instrumentation calibration to be conducted in the exact environment that it would be used, ensuring that the calibration was valid during the data collection phase of the experiments.

LITERATURE REVIEW

This section provides a review of the most influential documents that guided the efforts of this thesis. The first paper is a document that develops and applies a statistical based verification and validation technique to a dynamic, nonlinear electrical circuit. This effort proved to be a tenet for which this thesis is based, applying the techniques as best as possible to the thermal fluids problem. The second document also helps to lay the groundwork for verification and validation efforts in a statistical way, with a special emphasis placed on statistical sampling. The last document is a guide published by ASME that aims to outline, in a generic sense, the basic steps necessary for verification and validation.

Nonlinear Uncertainty Quantification, Sensitivity Analysis, and Uncertainty Propagation of a Dynamic Electrical Circuit – Doty, A. P. – 2012 [2]

This document is similar to the work being completed in this thesis; emphasis is on uncertainty analysis, sensitivity analysis, and uncertainty propagation. The author applies knowledge learned in previous works to a simple electrical circuit comprised of a resistor, an inductor, and a capacitor. Modeling and experimentation with such a system proved advantageous in the scope of the uncertainty work; an exact analytical solution was derived with which to compare experimental results. Several techniques used by the author on an electrical system are applied to a larger-scale thermal fluids problem.

The author begins with referencing previous works and prior efforts to implement a statistical based validation methodology and why such a methodology is necessary. Providing an answer along with the degree to which that answer is known to be true (or

the degree that it is *not* known to be true) introduces integrity to a solution by attempting to quantify the error present in the answer. Without error listed, an answer is considered incomplete. In order to document the error, or uncertainty, properly, several steps need to be taken, the first of which is always identifying the sources of and characterizing the uncertainty. This process must be completed for both the physical experiment as well as the simulation, as both do not necessarily have all of the same inputs. After all sources of uncertainty have been identified, they must be quantified. It is often times necessary to either take the same measurement several times or to use a sufficient sampling rate to gather a large number of data points, dependent upon the value being characterized. In the event of a cumbersome number of variables, the sequential perturbation technique may be used as a numerical method to propagate the uncertainty in a measurement.

Like the other inputs of the system, the uncertainty of the input voltage step change also required quantification. In the case of a transient change in either the input or output, such as a step change, it is possible to have uncertainties that likewise change with time. One way to handle the uncertainties in this type of situation entails representing the input in terms of the standard deviation as a function of time. In the author's case, many trials were conducted and the standard deviation was computed at the same point in time across all trials. It is shown that the trends of the plot of the standard deviation agree with the step change in data well; the region that exhibits the most change with time has the highest standard deviation, whereas time progresses and the results shift toward steady-state, the standard deviation approaches zero.

Next, data acquisition tool uncertainties are quantified, as well as those associated with numerical approximation. Several validation metrics are discussed in the document,

but two of which are not statistically significant. The Area Validation Metric is used when a proper sampling methodology is implemented with the verification and validation process. The Absolute Area Deviation (AAD) metric calculates the area between the experimental and simulated values as a quantitative way to show agreement, or lack thereof. The Anderson-Darling k-sample test is mentioned as one validation metric that is statistically significant; this test helps a researcher determine if samples indeed originated from the same probability distribution. If the test is evaluated to be true, then the samples are considered interchangeable, and thus, one set of values can be used in place of the others, i.e., the model outputs can be used to predict an experimental output.

The next step in the process is to attempt to minimize model form error. Model form error is the error present due to the way that the model is used to represent the system under question. This can be characterized initially as large disparities between both responses and trends in responses, and it shows whether or not the physical processes actually occurring in the experiment are successfully captured by the model. Attempts to minimize the model form error ultimately lead to a model that more accurately represents the physical phenomena occurring in the experiment and provide a calibrated model over the range of inputs specified.

The last few steps in the process involve conducting the sensitivity analysis and the uncertainty analysis, which are often conducted simultaneously. The sensitivity analysis shows how responsive an output is to variations in the inputs, and the uncertainty analysis scales these variations to show the variation in outputs due to the specific inputs that are used. A recent study incorporates a modified sensitivity coefficient for uncertain input data that allows the use of a technique that normally would not apply to nonlinear

problems. This novel approach makes it simpler to track uncertainties through a problem, regardless of the linearity or nonlinearity of the problem.

As one of the last few steps, the uncertainty values are propagated through the model. It is noted that the propagation of the uncertainty values actually involves the variance, as opposed to the explicit uncertainty. Input variables are then coded to be represented by probability density functions (PDF). The PDFs are then verified to be true cumulative distribution functions (CDF), which can in turn be used to represent the input variables via sampling techniques. It is important to note that this step is necessary if any type of sampling methodology is to be implemented on the input variables.

The results begin with presenting the differences in the dynamic voltage from the experiment and the model. The results were initially compared using the AAD mentioned above as a qualitative way to discern the disparity between the outputs. Next, the uncertainties were compared by plotting the standard deviations as a function of time. In the case of the dynamic input voltage, the author found that the model under predicted the amount of uncertainty in comparison to the experiment. Results from the sensitivity and uncertainty analyses of each of the inputs were plotted and displayed as functions of time. A critical inference is noted: the sensitivities and uncertainties are functions of time due to the fact that the input is dynamic. The dynamic nature of the input results in all of the outputs having dynamically changing uncertainties. This type of analysis allows the quantification of uncertainties in both steady-state and transient regions.

After quantifying uncertainties, the author completes verification and validation. Verification was purely a check to ensure that the model was implemented correctly; this was achieved by comparing the results from the experiment to the analytical solutions

that were solved using various techniques. All outputs were in general agreement, concluding that the model in fact represented the physical processes occurring within the system. The last step of the process was statistical validation. The author chose to implement the Anderson-Darling k-sample test which is a statistical test to determine if two samples of data could have been drawn from the same population. Several different comparisons were made using the test, including averaging values at the same point in time across all replicate tests; the test indicated that the samples were not drawn from the same population. This implies that the model was not able to be statistically validated via the Anderson-Darling k-sample test. Despite this determination, the sensitivity and uncertainty were still generated and are useful for the purposes of quantifying the error in the model outputs.

Statistical Analysis and Assessment of Missile Performance Characteristics – Doty, J. H. – 2012 [3]

This document serves as a cornerstone for which all of the work in this thesis is based. The author explains in great detail the process by which uncertainty analysis, uncertainty quantification, sensitivity analysis, and uncertainty propagation are performed and applied to a problem when utilizing a surrogate model. Special emphasis is also placed on the choice of sampling methodology and the resultant effects on the System Response Quantities (SRQs). The main goal of study was to quantify how sensitive and uncertain the SRQ is to an input with a specified amount and type of uncertainty. In order to do complete the exercise, a deterministic model was used with the assumption of no uncertainty in the experimental data.

In this specific case, the coefficients of rolling moment (CLA), of yawing moment (CNA), and of side force (CYA) were examined as a function of the angle of attack (AOA). Experimental data was provided from wind tunnel tests completed on an FG5 generic missile. It is noted that for the purposes of the study, experimental data was assumed to be exact with no experimental uncertainty, as the focus was on uncertainty propagation.

The response surface design methodology was selected for representation of the data as it can capture possible nonlinearities that may exist within the data. These surrogate models prove useful from the standpoint that their derivatives are easily calculable for the propagation of uncertainty, as well as the fact that they are statistically based and supported by analysis of variance (ANOVA). The first step in the process was to transform the data into non-dimensional coded values that are presented on a scaling of -1 for the low value to +1 for the high value. This step was necessary as the surrogate model fitting is best performed in terms of the coded variables.

A form of the model was first postulated and later adjusted based upon various selection criteria. In this analysis, a 6^{th} order polynomial was first selected, but later it was found that a 3^{rd} order polynomial represented the data better. The coefficient of determination (R^2), the adjusted R^2, the predicted residual error sum of the squares (PRESS), and the predicted R^2 are all utilized as metrics to determine which surrogate best represented the data. Desirable characteristics were low PRESS values (close to zero) and the rest of the selection criteria as close to one as possible. If all values are approaching the desirable point, but one begins to change direction, it may be indicative

that higher orders of the model form do not capture the data as accurately as a lower order form and introduce additional error.

Background information on uncertainty is given, starting with explaining the two types of uncertainty: aleatory and epistemic. Aleatory uncertainty is sometimes referred to as irreducible uncertainty as it is due to the random variation that inherently exists in all physical quantities, and can be represented by a probability distribution. Epistemic uncertainty is due to lack of knowledge and therefore, the uncertainty cannot be precisely known. Despite the differences in the types of uncertainty, they are both still represented in terms of the standard deviation, σ. It is stated that the aleatory and epistemic uncertainties are rarely summed directly due to interactions and nonlinearities; therefore, the need for sensitivity analyses and uncertainty propagation arise.

Sensitivity analyses provide a way to apportion uncertainty of the outputs to uncertainties in the inputs of the model. It is becoming increasingly common to perform both uncertainty and sensitivity analyses in parallel, as the results are nearly identical, merely scaled versions of each other. The suggested (from literature) methodology for a sensitivity analysis, from a global perspective, involves utilizing the Taylor-series based approach for approximation, yielding a partial derivative to represent the sensitivity on a localized basis. A disadvantage to the localized sensitivity technique is that the partial derivatives are generally evaluated in a linear fashion and, therefore, lack the ability to capture nonlinearities that may be present. A suggested technique to include nonlinear effects is to weight the sensitivity by a normalizing factor comprised of uncertainties: this modified sensitivity coefficient is merely the standard deviation of the input divided by the standard deviation of the output. With known standard deviations (uncertainties) of

the inputs and the outputs, as well as the partials of the surrogate models determined, the sensitivities are easily calculable.

The next step in the process was to propagate the uncertainties, which quantified the effects of the uncertainty of the inputs on the outputs for the specific case under question. It is shown that the uncertainty, σ, is actually squared before it is propagated; this indicates that it is in fact the variance, σ^2, that propagates the uncertainty through the model. This is easily seen below in Equation (1).

$$\sigma^2_{x_{input} \rightarrow SRQ_k} = (Sen^{SRQ_k}_{x_{input}})^2 (\sigma^2_{x_{input}}) \quad (1)$$

This equation shows that the process involves multiplying the square of the sensitivity of an output to an input by the variance of the input to yield the propagated uncertainty effects as a variance. This equation is applied to the system for all SRQs and all inputs to the system to yield all propagated uncertainties. It is worth noting that the implementation of the surrogate model to represent the data was beneficial for uncertainty propagation as this made computing the required partial derivatives a simple task.

The author then switched focus to the importance of the effect of different sampling methodologies utilized when quantifying uncertainties. In order to utilize a sampling technique such as Monte Carlo or Latin Hypercube, the first step of the process is to determine the probability density function (PDF) that represents the input(s) to the system. Then, the PDF must be proven to be a true density function by summing the points within the PDF; this value must equal unity. If the summation of points does equal unity, then the PDF may be represented as a cumulative probability density function (CDF). This CDF, when inverted, allows the user to map the CDF back to the input of

the system. It is not possible to calculate the required values for the uncertainty analysis based upon sampling once the CDF has been determined.

The author then uses the CDFs to propagate uncertainties through two different sampling methodologies, pseudo-random and low-discrepancy sequence, for use in Monte Carlo simulations. The final results were compared and differences between the sampling techniques were quantified, and recommendations were made to utilize low-discrepancy sequence sampling over pseudo-random sampling whenever possible for better representation while minimizing the number of samples required. Lastly, it is important to note that a large aspect of the efforts were possible by making the assumption upfront that there was no error in the reference solutions that were generated from experimental data. This assumption eased the modeling efforts for the purposes of placing emphasis on discerning the differences between the sampling techniques.

Standard for Verification and Validation in Computational Fluid Dynamics and Heat Transfer – ASME – 2009 [4]

The American Society of Mechanical Engineers periodically issues standards to cover best-practices for common issues encountered in the field. In recent years, there has been much emphasis placed on verification and validation (V&V), which concerns assessing the accuracy of a computational model. Specifically, the process that one uses to reach and complete validation is what this document aims to provide guidance on. The end goal with V&V is the validation aspect, which serves to determine how accurately a model represents a real life phenomenon, within the perspective of its intended use. Several important points are made about implementing V&V while describing a possible

process to follow that could apply to fluid dynamics or heat transfer computational problems.

One of the first points stressed is that validation cannot occur without experimental data to compare to the model outputs. It also aims to apply internationally agreed upon definitions of uncertainty, such as International Organization for Standardization (ISO) standards, and concepts to errors in both experimental and computational efforts. Another key point is that in an ideal situation, the researchers responsible for the modeling efforts and those responsible for the experiments will be working together towards the end goal of validation. In practice, this can prove to be difficult or sometimes impossible. In the case of creating a model based upon data from a journal article, there is virtually no interaction between researchers and thus, validation could become difficult or infeasible.

In order to follow the validation process, a brief overview is offered that defines important terms and aspects necessary for successful verification and validation. First, validation error is defined as the difference between the simulation and the experimental data values. This error is then shown to be equal to the simulation error minus the experimental error. These errors are then broken down into three categories: modeling assumptions and approximations (model form error), numerical solution, and output error due to simulation input parameter errors. The key objective of validation is to estimate the model form uncertainty and to use this value, along with the validation error, as metrics for validation.

The next steps in the process are code and solution verification. Code verification is intended to identify the error for a known solution to the governing mathematical

equations. This step is noted to differ from solution verification in that solution verification estimates errors for a solution that is typically unknown. Code and solution verification are declared to be purely mathematical operations that do not involve the experimental data, as this data is taken into account in the validation step. The standard states that the best way to implement code verification is with an exact analytical solution to test the mathematical relationships and that this solution be sufficiently complex to encompass all terms of the governing equations. One technique for finding an exact analytical solution is outlined. Solution verification follows and is used as an estimate of error, typically completed via systematic grid refinement studies when applied to grid-based problems such as computational fluid dynamics. One example of a methodology for acquiring an error estimate is via Richardson Extrapolation.

Next, two techniques used to assess the error in simulation outputs due to error in the simulation inputs are explained. The choice of which technique to be used is largely dependent upon whether the researcher is concerned with the local or global view of uncertainty, where local uncertainties are over a small range of parameter values and the global approach is over a larger range of values. The local approach is also known as the sensitivity coefficient method or the perturbation method, while the global approach is known as the sampling method. Next, the validation uncertainty is computed based upon the manner whether the global or local approach was used to estimate the simulation error for various cases. For the case when the experimental validation variable is directly measured, makes an easy task of determining the validation uncertainty as the errors are assumed to be independent. When utilizing the sensitivity coefficient method for this context, it is noted that only nominal values of input parameters along with their standard

deviations are needed, as opposed to requiring knowledge of the form of the distributions. Various approaches for estimating the validation uncertainty are discussed that apply to differing methods used to determine the validation variable.

Finally, the interpretation of both the validation error and validation uncertainty is discussed. The validation error is shown to be an estimate of the model form error and the validation uncertainty is the standard deviation of the estimate of the model form error. From these two pieces of information, information can be gleaned relating to the range (probability distribution) that the model form error likely falls within. If the absolute value of the validation error is much larger than the validation uncertainty, then the validation error is roughly equivalent to the model form error. This is useful in that it provides an indication that the model could be improved to possibly reduce the model form error. If the opposite case is true, where the absolute value of the validation error is smaller than the validation uncertainty, then the model form error is likely on the same order of magnitude or smaller than the combination of the numerical, input and experimental uncertainties. This means it falls within the noise of these uncertainties and that changes to the model would not likely result in a better or more accurate result.

MATLAB / SIMULINK MODEL CREATION

A heat exchanger model was developed for use within the T2T thermal model efforts being completed by WSU researchers. This model was based upon a heat exchanger that was to be provided by AFRL/RQPE for the purposes of model validation. The heat exchanger was the Stanley Proctor (now Young Touchstone) SSF-502-2P-EY. This specific model is designed to handle heat loads from 15 – 55 Btu/min-F and flow rates from about 30 – 90 gpm. According to the documentation provided by Young, this heat exchanger utilized a full stainless steel construction, two tube passes, one shell pass with baffles, is 5.12" in diameter, and 18" long. A representative cutaway section is shown below in Figure 1 from a Young Touchstone catalog describing the features of their shell and tube heat exchangers.[5]

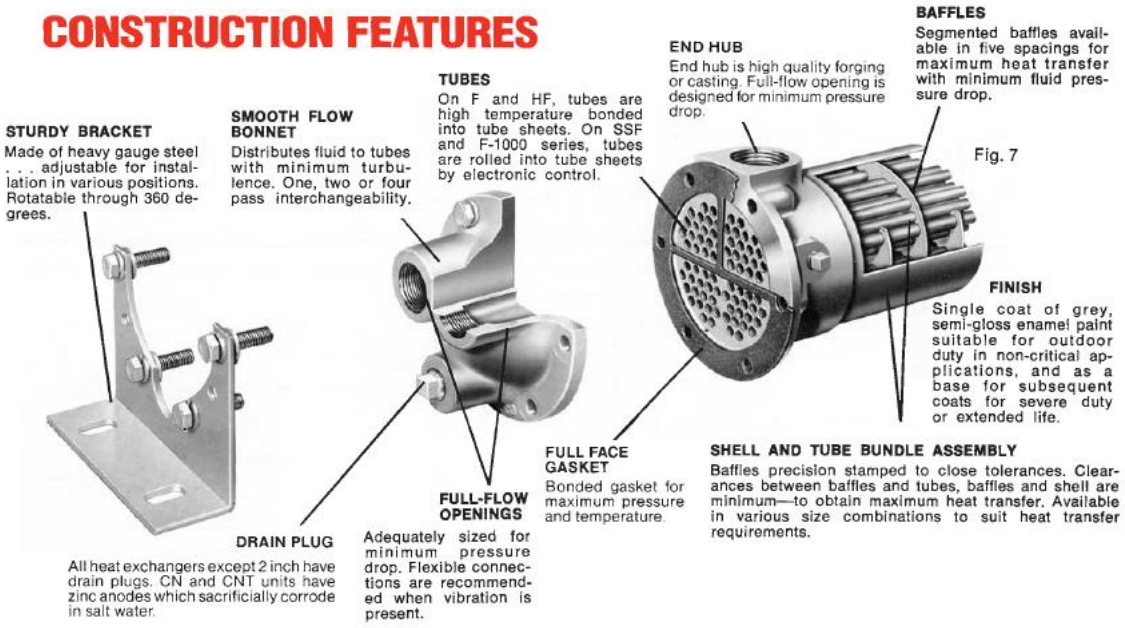

Figure 1: Representative cutaway view of shell and tube heat exchanger

The diagram shows a view of the internal flow paths inside the shell and tube heat exchanger. Specifically, it is easy to tell the function and layout of the baffles with this view; the baffles serve to force the shell fluid to take a serpentine path around the outside of the cooling tubes to maximize heat transfer. A simplified side view of this type of heat exchanger is shown below in Figure 2.

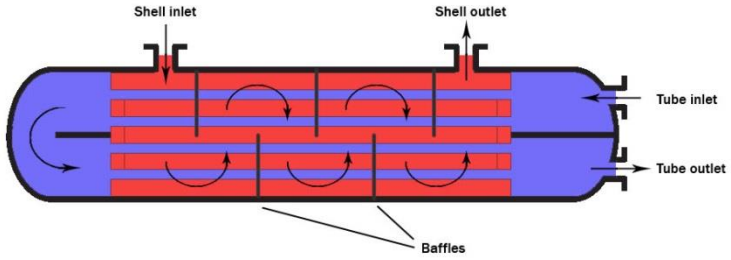

Figure 2: 2-D generic diagram of a 2 pass tube, 1 pass shell with baffles heat exchanger

The shell and tube heat exchanger as shown above in Figure 2 utilizes numerous tubes to carry fluid down the axial length of the heat exchanger and back again. In addition to the external dimensions of the heat exchanger, various additional pieces of information are provided describing the heat exchanger such as the volume of the fluid on the shell and tube side, outer diameter of the tubes and the configuration of the baffles.

The model initially was created based on flat plate relations with flow above and below the plate. An energy balance was maintained between the incoming flow streams and the thermal energy (heat) being transferred through the heat exchanger.[6] This basic layout can be seen below in Figure 3.

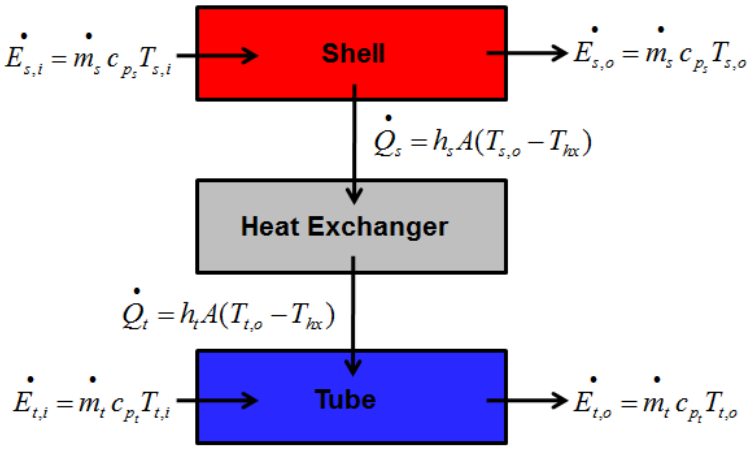

Figure 3: Simplified energy balance of initial heat exchanger model

This energy balance was then applied to a very simple heat exchanger design that utilizes an inner tube carrying one fluid, and an outer tube carrying the other fluid. The implementation of this design is seen below in Figure 4.

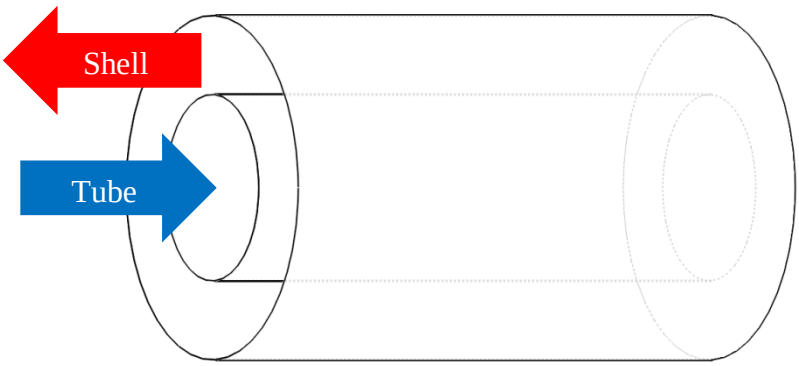

Figure 4: Tube within a tube flow

The cooling fluid is represented as flowing through the inner tube of this simple heat exchanger design. The hot fluid flows around the inner tube in the annular space between the two tubes. When it was determined that experimental data could be

collected from a shell and tube heat exchanger, this simple design was used to represent the actual shell and tube heat exchange geometry in a simplified fashion.

The simplified tube within a tube design in Figure 4 above is applied to the geometry of the SSF-502 heat exchanger. The simplified model is calculated on a per tube basis, meaning that certain defining quantities of the heat exchanger are adjusted based on the number of tubes present in the system. Due to this, the total mass flow rate is divided by the number of tubes present in the system, and calculations are completed for that tube and associated amount of shell fluid. Fluid parameters are calculated based upon the amount of mass flow through a single tube, such as hydraulic diameter and Reynolds number. If a piece of information was not provided by Young Touchstone to use as a basis, relationships between known parameters were used to estimate the unknown quantities. Actual values were recorded once the researchers had possession of the heat exchanger if those values were easy to measure. For example, the number of tubes was simply counted after removing an end cap, and the mass of the heat exchanger was determined by weighing with a scale of known accuracy. These values were used as a starting point to begin to calibrate the model to match experimental data.

Several modifications are made to simplify the complications associated with attempting to model the exact geometry of the heat exchanger. For example, as opposed to making 2 passes with the tubes, in the simplified model, the tubes are represented as a single pass bundle. The baffles that direct and mix the shell fluid are not included in the design. The shell fluid is also represented as co-flow within the model, meaning the shell fluid flows axially in the same direction as the tube fluid, despite the fact that in this heat

exchanger, various degrees of co-flow, counter-flow, and cross-flow are all found locally in different regions.

Initially, the energy balance only contained the terms shown above in Figure 3: energy of flow streams coming in, energy of flow streams leaving, and heat being transferred through the heat exchanger. These terms all represent a steady-state, steady-flow condition, and as such, generally apply only when the system is operating with minimal changes in input and outputs. In order to capture the transient changes in the system, an additional term needs to be introduced in both fluid streams, as well as the mass of the heat exchanger needs to be taken into consideration.

These transient effects come into play as a "storage" term that represents the changing temperature of the fluid streams with time, as well as the changing temperature of the heat exchanger with time. These changes will be shown below in the derivation of the equations utilized within the model.

The equations utilized for both the shell and tube fluid streams are almost identical; as such, they will be presented in tandem. In this fashion, the subscript '*s*' will be used to specify the shell side, and a '*t*' will represent the tube side. Additionally, '*i*' represents fluid at the inlet and '*o*' represents fluid at the outlet. The energy of the fluid stream entering the system is dependent upon the mass flow rate of the fluid streams, the specific heat of the fluids, and the temperature of the incoming fluid.[6]

$$\dot{E}_{s,i} = \dot{m}_s c_{p,s} T_{s,i} \tag{2}$$

$$\dot{E}_{t,i} = \dot{m}_t c_{p,t} T_{t,i} \tag{3}$$

The energy content of the fluid the exiting the system is represented similarly.

$$\dot{E}_{s,o} = \dot{m}_s c_{p,s} T_{s,o} \tag{4}$$

$$\dot{E}_{t,o} = \dot{m}_t c_{p,t} T_{t,o} \tag{5}$$

Next, the heat flow exiting the shell stream and heat flow entering the tube stream are calculated. It is important to note that due to the addition of the mass of the heat exchanger as a transient term, the heat exiting the shell stream does not necessarily equal the amount of heat entering the tube stream for all instances of time.[7] As such, the heat flow is calculated for each stream.

$$\dot{\mathrm{Q}}_s = h_s A_s \left(T_{s,o} - T_{hx}\right) \tag{6}$$

$$\dot{\mathrm{Q}}_t = h_t A_t \left(T_{t,o} - T_{hx}\right) \tag{7}$$

The same tube surface area is used to calculate the heat flow for both fluid streams. The assumption is made that the thickness of the tube is small enough to not make an appreciable difference in surface area from the outside to the inside of the tube. Next, it is necessary to calculate the heat transfer coefficient, h.

$$h = \frac{k\, Nu}{D} \tag{8}$$

Here, D represents the hydraulic diameter of the fluid for each stream. The hydraulic diameter is calculated based upon the calculated inner diameter of the tube, and based upon annular flow for the shell fluid. The Nusselt number is defined as a piecewise function, with different values based upon the calculated Reynolds number.

$$Nu = \begin{cases} 3.66, & Re \leq 10{,}000 \\ 0.23\, Re^{4/5} Pr^{n}, & Re > 10{,}000 \end{cases} \tag{9}$$

$$where, \qquad n = \begin{cases} 0.3, & T_{hx} \leq \dfrac{T_i + T_o}{2} \\ 0.4, & T_{hx} > \dfrac{T_i + T_o}{2} \end{cases} \tag{10}$$

The Nusselt number is a constant for when the Reynolds number is less than 10,000; this indicates laminar flow conditions. When the flow is considered turbulent, the relation given above is used to calculate the Reynolds number, and it is dependent upon whether the surface is experiencing cooling or heating, as specified in Equation (10), as well as the Reynolds and Prandtl numbers.[8] The Reynolds number is defined below in Equation (11) for fluid flow in a pipe or tube.

$$Re = \frac{v\ \rho\ D}{\mu} \tag{11}$$

The Reynolds number is a dimensionless number defined as the ratio of inertial forces to the viscous forces acting on the fluid. It is used to determine state of the fluid, whether laminar or turbulent. It is dependent upon the density of the fluid, the hydraulic diameter of the tube that the flow is contained within, the dynamic viscosity, and the velocity of the fluid.[9] The velocity of the fluid is defined below for fluid in a pipe or tube.

$$v = \frac{4\ \dot{m}}{\pi D^2 \rho} \tag{12}$$

The Prandtl number is the ratio of viscous diffusion to thermal diffusions rates, and is defined below in Equation (13).

$$Pr = \frac{\mu\ c_p}{k} \tag{13}$$

The storage, or transient, terms used in the energy balance are calculated as rates of change of the temperatures for the fluid present in the control volumes of each fluid stream. The mass of fluid in the control volume is required, and this is dependent upon the specific heat of the fluid streams, as well as their respective densities. The control volumes for each fluid stream are defined as the amount of fluid that exists within each side of the heat exchanger.

$$\dot{E}_{s,store} = cv_s \rho_s c_{p,s} \dot{T}_{s,o} \tag{14}$$

$$\dot{E}_{t,store} = cv_t \rho_t c_{p,t} \dot{T}_{t,o} \tag{15}$$

Each of the terms listed above in Equations (2), (4), (6), and (14), as well as (3), (5), (7) and (15) are combined to represent the flow of energy into and out of each fluid stream below in Equations (16) and (17).

$$\dot{E}_{s,i} - \dot{E}_{s,o} - \dot{Q}_s = \dot{E}_{s,store} \tag{16}$$

$$\dot{E}_{t,i} - \dot{E}_{t,o} - \dot{Q}_t = \dot{E}_{t,store} \tag{17}$$

Next, substitutions are made for what each term is comprised of, as defined above.

$$\dot{m}_s c_{p,s} T_{s,i} - \dot{m}_s c_{p,s} T_{s,o} - h_s A_s \left(T_{s,o} - T_{hx}\right) = cv_s \rho_s c_{p,s} \dot{T}_{s,o} \tag{18}$$

$$\dot{m}_t c_{p,t} T_{t,i} - \dot{m}_t c_{p,t} T_{t,o} - h_t A_t \left(T_{t,o} - T_{hx}\right) = cv_t \rho_t c_{p,t} \dot{T}_{t,o} \tag{19}$$

Now, terms are distributed and grouped such that the desired output quantities are together.

$$cv_s \rho_s c_{p,s} \dot{T}_{s,o} + (\dot{m}_s c_{p,s} + h_s A_s) T_{s,o} = \dot{m}_s c_{p,s} T_{s,i} + h_s A_s T_{hx} \tag{20}$$

$$cv_t \rho_t c_{p,t} \dot{T}_{t,o} + (\dot{m}_t c_{p,t} + h_t A_t) T_{t,o} = \dot{m}_t c_{p,t} T_{t,i} + h_t A_t T_{hx} \tag{21}$$

It is obvious that Equations (20) and (21) above are first-order linear ordinary differential equations (ODE). Once the ODEs are solved, it is found that the output temperatures for the fluid streams are functions of the input temperatures, as well as the temperature of the heat exchanger. The input temperatures are known, however the temperature of the heat exchanger needs to be determined to fully define the output temperatures of the fluid streams. The temperature of the heat exchanger changes with time, and therefore is represented as a rate.

$$\dot{Q}_{net} = m_{hx} c_{p,hx} \dot{T}_{hx} \tag{22}$$

The heat used in this calculation is the net heat on the mass of the heat exchanger. This net heat is the summation of the heat from and to each fluid stream.

$$\dot{Q}_{net} = \dot{Q}_s + \dot{Q}_t \tag{23}$$

Now that an equation has been defined that relates the changing temperature of the heat exchanger to the heat loads from the fluid streams, substitutions are made per the definitions of these terms above.

$$m_{hx} c_{p,hx} \dot{T}_{hx} = h_s A_s \left(T_{s,o} - T_{hx}\right) + h_t A_t \left(T_{t,o} - T_{hx}\right) \tag{24}$$

Now, terms are distributed and grouped such that the desired output quantities are together.

$$m_{hx} c_{p,hx} \dot{T}_{hx} + (h_s A_s + h_t A_t) T_{hx} = h_s A_s T_{s,o} + h_t A_t T_{t,o} \tag{25}$$

Again, easily recognizable is a first-order linear ordinary differential equation. Now it is easy to see that Equations (20), (21), and (25) form a system of coupled ODE's. Due to the fact that these equations are highly coupled and that the fluid properties are a function of temperature, a numerical solver that steps incrementally in time is required to determine the results. This is implemented via the use of Matlab's ode45 solver. The output temperatures of the fluid streams are dependent upon the temperature of the heat exchanger, and the temperature of the heat exchanger is dependent upon the output temperature of both fluid streams.

THERMAL EMULATOR DESIGN & CONSTRUCTION

A layout for the thermal emulator was developed. This layout was created by taking into account several important budgetary, operation, repeatability, and resource concerns. These important design factors are presented in this section.

First, the system needed to be capable of reproducing the flow conditions that were seen at the AFRL facility. The general ranges of fluid flow rates and expected temperatures, as well as fluid type was indicated to WSU researchers by AFRL staff. These conditions are listed below in Table 1.

Table 1: Estimated fluid conditions in AFRL laboratory experiment

	Fluid Type	Estimated Temperatures	Estimated Flow Rates	Estimated Pressures
Units	[-]	[°C]	[gpm]	[psi]
Shell Fluid (Hot)	MIL-PRF-7808 (Oil)	< 105	< 10	< 100
Tube Fluid (Cold)	Water	~ 12.5	< 10	< 100

These expected flow conditions proved constraining during the initial development of the thermal emulator design. Specifically, the MIL-PRF-7808 oil coupled with the high temperatures made instrumentation selection difficult. Instrumentation would have to be capable of withstanding long term exposure to the fluid in question and at the specified temperatures, all while providing accurate measurements. Due to the fact that the viscosity of the oil is a function of temperature, accurate flow rate measurements would be costly, if feasible. These constraints caused two important changes to be made to the operating conditions: it was decided that the thermal emulator would run with water as the working fluid on both sides of the heat exchanger, and that

the maximum temperature seen on the shell side would be reduced such that operating conditions for water would not introduce phase change effects into the study. These changes can be seen below in Table 2.

Table 2: Estimated fluid conditions in WSU thermal emulator

	Fluid Type	Estimated Temperatures	Estimated Flow Rates	Estimated Pressures
Units	[-]	[°C]	[gpm]	[psi]
Shell Fluid (Hot)	Water	20 - 80	2 - 6	< 65
Tube Fluid (Cold)	Water	~ 12	2 - 6	< 65

The change in shell side fluid facilitated selection of flowmeters that were within the scope of the available budget, as the viscosity of water experiences minimal change with respect to temperature when it is in the fluid state. The lower temperatures contributed to this as well, and it also made the selection of a fluid reservoir, heating method, and pumping system much simpler.

WSU's laboratory environment contained several thermal fluids experiments that had been unused for many years. These fluids apparatuses all were comprised of various lengths and diameters of copper pipe, V-port valves, gate valves, ball valves, elbows, tees, unions, and an electric centrifugal pump. These fluids apparatuses had to be disassembled to make space for the thermal emulator experiment. During this disassembly, it was determined that many of the pipe and pipe fittings could be re-purposed for the new thermal emulator. A box tube rolling stand from one of the old fluids experiments was also able to be repurposed as it simplified access to the thermal emulator from both sides in the event that adjustments or repairs were necessary. An added benefit of this acquisition of pipe, fittings, and rolling stand helped to extend the

budget of the study; more funds could be allocated to a proper data acquisition (DAQ) system and instrumentation purchases.

To further extend this ease of access and modification, each major component was designed to have unions on either side of it in the event that any individual component required replacement, adjustment, or cleaning. This decision proved invaluable during leak tests after the initial soldering was complete. Additionally, a bypass pipe was added to the design after it was mostly complete, and it required minimal time for modification due to the nature of the rolling stand design.

One of the primary outputs desired from the thermal emulator, in addition to the steady-state output temperatures, was the quantification of the transient response of the system to a step change in temperature input on the shell side of the heat exchanger. In order to do this, the thermal emulator would need to be capable of delivering consistent fluid flow (temperature and flow rate) on both the shell (hot) and the tube (cold) sides of the heat exchanger long enough for the output temperatures to reach steady-state. This goal governed the first major design considerations for the system. The selection of a commercial hot water heater as a means to heat the fluid and store it would require modification to facilitate faster heating of the fluid on the shell side of the heat exchanger and provide a consistent output temperature from the fluid reservoir to the input of the heat exchanger during the experimental tests cases, as it was determined that the water supply from the lab did not provide water to cover the temperature range desired, and that fluctuations in the flow rate were common.

It was determined that two electric hot water tanks, plumbed in series, would be required; this arrangement of hot water tanks serve two purposes:

1.) The tanks provide ample thermal mass to ensure a relatively constant temperature of supply water for the hot side of the heat exchanger.
2.) They serve as the storage tanks for the water as it is being heated, providing a large thermal mass.

A centrifugal pump is incorporated within the loop to circulate the water within the tanks as it is being heated, as well as to pump the water through the hot side of the heat exchanger at a relatively constant pressure and flow rate. Although pressure is something that is not explicitly being modeled currently in the heat exchanger blocks, by having a constant pressure supply, it will be easier to make fine adjustments to the valve that controls the mass flow rate through each side of the heat exchanger.

Each hot water tank has two heating elements; an upper element and a lower element. The standard wiring of each hot water tank only operates one heating element at a time, as a measure to conserve energy. The upper element is used to first heat the water in the upper portion of the tank, where hot water is drawn for use. After the water in the top portion of the tank is heated, the upper element is turned off, and the lower element is powered to heat the rest of the tank. This method for heating allows the almost instantaneous draw of hot water, even when the majority of hot water has been depleted, by utilizing the fact that a temperature gradient naturally will exist within the tank, from the bottom where cold water is drawn in, to the top. The tanks were modified in the following ways to better adapt them to the requirements of the experiment:

1.) The dip tube was removed, which brought in the cold water from the top of the tank, and introduced it to the body of water at the bottom of the tank.

Now, water enters the top of the tank, and is dumped directly onto the top of the volume of water within each tank.

2.) The drain at the bottom of the tank was removed, and now, water is drawn from the bottom of each tank, as opposed to the top.

3.) The top of each tank has two hookups: one is now used to introduce fresh water into the system; the other is used for recirculation as well as to purge any air from the system. This air purge hookup is also the location where air will be drawn into the tank when the water is drained from the bottom and a vacuum is created that could lead to hydro lock.

4.) The original thermostats have been removed for two reasons:

   a. They did not allow the water to be heated up to the desired temperature.

   b. They did not allow explicit control over the temperature. Each heating element is directly wired to one of two electro-mechanical relays that are controlled by a LabView Virtual Instrument program (VI) which handles all data acquisition from the system.

These modifications may seem counter-intuitive with respect to the original design of the hot water tanks, but they are necessary and serve the intended purposes in the experiment well. The water will constantly be circulated to help minimize thermal gradients and the water will be drawn from the bottom of the tanks which will allow the possibility to completely utilize all water in each tank, thus providing ample run time for each test case.

In order to control the temperature, a program within LabView has been written that monitors all temperatures within the system, flow rates, and pressures. The LabView

program was intended to be coded such that it would automatically control the heating elements by activating or deactivating a relay module, based on the monitored temperatures of the system; through initial shakedown tests it was determined that this functionality would not be required, and that manual control of the heating elements would be sufficient. This system allows a fine control over the temperature of the system, as opposed to the original thermostats, as it has the capability of monitoring all temperatures in the loop, as well as allowing the researcher the ability to modify temperatures as necessary.

The heat exchanger requires two separate water supplies for testing, one for each side of the heat exchanger, the shell side (hot), and the tube side (cold). Each side of the heat exchanger will require both a hot and cold water line hooked up to the system for precise temperature control. The path that the water takes for the tube side of the heat exchanger is as follows: the water is drawn into the system from the hot and cold taps on the wall and enters a small mixing chamber that is used to maintain a specified constant temperature of supplied water. After the mixing chamber, the water enters a filtration system that is used to prohibit large particles from causing potential damage to the flow meters. The documentation with the flow meters specifies that particles larger than 150 microns must be filtered; the filters in use filter down to 5 microns, nominally. The filters are a cartridge style and various choices are available for style of filter, as well as the nominal size of particles that each filter is capable of removing from the water. The chamber that houses the filter is a clear polycarbonate which allows easy visual inspection for a qualitative estimation of how clogged they have become. A more quantitative way of determining if the filters require changing is merely to monitor the

flow rates through the LabView program. Normal water pressure from the wall (about 55 psi) is capable of pumping more than the maximum 7.5 gallons per minute that the flow meter can handle through the system. If the filter is beginning to restrict flow, the water supply flow rate will begin to drop.

After the filter, the water flows through a long straight section of pipe used as a flow straightener. This long section of pipe allows the fluid to fully develop the flow profile prior to entering the flow meter, a requirement for accurate flow rate measurements. After the flow meter, a gate valve is used to control the total flow rate through the tube side of the system. The water then enters the tube side of the heat exchanger on the top port located on the side of the heat exchanger. The water flows laterally down the length of the heat exchanger, makes a 180 degree turn, then returns along the length, and exits the heat exchanger on the same side that it entered at the bottom port. The water is then dumped to the drain. Important physical parameters like pressure, temperature, and flow rate are all measured along the flow path of the thermal emulator system. Pressure and temperature readings are taken as close as possible to the inlets of the heat exchanger, as well as at the outlets.

The shell side of the system is generally laid out in the same way, with a few additional components. Hot and cold water is drawn from the taps on the wall and mixed in an identical mixing chamber as used on the tube side. The water exits the mixing chamber and can either be directed into the reservoir for recirculation, or it can bypass the reservoir. If the bypass is used, the water is directed through an identical filter as used on the tube side, and then through a flow straightening section of pipe. Then the water flows through the flow meter, gate valve, and enters the shell side on the top of one end of the

heat exchanger. The water flows around the tubes as directed by several baffles, then exits the heat exchanger at the top of the opposite end that the water entered. This water is then dumped to the drain. Temperature and pressure readings are taken at the same respective locations as on the tube side.

If the water is not bypassed directly to the shell side of the heat exchanger, it enters the reservoir for recirculation, and if necessary, heating. The reservoir system is comprised of two forty gallon electric hot water heaters that are piped in series, as previously mentioned. The water enters the first tank through one of two hookups on the top of the tank. During filling, the second hookup on the top of the tank is used as a vent to expel air from the tank as it is filled with water. After the tank is full of water, a valve on the vent side is closed, and now water is forced out the bottom drain of the first tank and piped to the inlet on the top of the second tank. The second tank also utilizes the second hookup as a vent to expel air from the system. Once the second tank is filled, the vent valve is closed and water flows out through the bottom drain to the centrifugal pump. After the pump, a valve is used to either direct the flow to the filter, and subsequently into the shell side of the heat exchanger, or to direct the water back to the first tank for recirculation. In this case, the vent valve is also attached to the second inlet on the first tank and when closed, creates a closed system for recirculation.

If the heating elements in the water tanks are powered, approximately 13 kW of heat is transferred to the water in the system. Power calculations were completed to determine if the existing wiring in the WSU laboratory was capable of providing the required current draw in the event that all four heating elements were powered. As long as the elements were wired such that three of the elements were configured in a wye

configuration on a 208 V three-phase supply, the current draw would stay under the maximum allowable by the wiring in the building and circuit breakers. The fourth element would be powered from a separate 208 V supply line.

When the tanks were filled and the heating elements were initially powered to verify functionality, it was found that the water at the surface of the elements boiled almost instantaneously, which can rapidly destroy the heating elements. This was determined by audibly hearing the water boil within the tanks, and subsequent examination of the design specifications of the hot water tank confirmed this was the case. The design specifications explicitly state that the tank must be pressurized in order to prevent the heating elements from burning out. This is normally not an issue when the hot water tank is being used as intended in a consumer's home; however, this was not the case for the purposes of the experiment. Keeping the system under pressure would raise the boiling point of the water, but the circulation of the water by the centrifugal pump is prohibited by this higher bulk pressure, as revealed through testing. It was determined through experimentation that as long as the water was being circulated through the tanks by the pump, the heating elements could be operated without the risk of the elements burning out as the circulating water carried away the super-heated water, and thus kept the element temperature cool enough to prevent them from burning out rapidly. The circulation of the water also served to maintain a relatively constant temperature of water throughout the entire reservoir system.

The vents from both tanks are connected to a single, clear, acrylic tank. This tank serves four distinct purposes:

1.) It serves as a simple qualitative way to determine when both water heaters are completely full by containing a small amount of over-flow water once water heaters are full.
2.) It vents air to atmosphere as the water heaters are being filled.
3.) It draws atmospheric air into the water heaters as they are being drained to prevent hydro lock.
4.) It acts as an expansion tank as the water is heated.

The tank has a float-operated valve mechanism that cuts off the air vent to atmosphere in the event that excessive water floods the tank. This same valve allows air to be drawn into the system when the water level drops while the pump is draining the water heaters. This vent to atmosphere is through a hose that is run to the drain next to the experiment. From this drain location, the atmospheric air is drawn or purged from the system, and in the event that the tank overflowed with water, it would merely be pushed directly into the drain. The tank is also used to determine when pressure needs to be relieved from the system when the heating elements are activated and the water is being heated. If the pressure inside the system rises too much as the water is being heated, the centrifugal pump will no longer be able to circulate water; the tank serves as an indicator as to whether the hot water heaters are at atmospheric pressure or if there is positive pressure present within the system.

All of these functions are described in more detail below in the experimental procedure section with Figure 6 being a diagram of the emulator and Table 9 serving as the legend identifying the label for each component in the system along with a description of functionality. Photos of the construction of the thermal emulator as well as

the completed emulator are found in APPENDIX A: THERMAL EMULATOR DESIGN & CONSTRUCTION.

INSTRUMENTATION SELECTION & CALIBRATION

Instrumentation was a key aspect of this project, in that all measurements taken on the thermal emulator needed to be taken with minimal error introduced into the readings. One way to accomplish this is to allocate more money from a budget on the instrumentation. Generally speaking, instrumentation can provide higher accuracy for the trade-off of higher expense.[10] With uncertainty quantification as an emphasis for this work, it was necessary to obtain the highest accuracy readings possible as the measurements would have an effect on both the answers from the experimental results, as well as the computational results from the model.

The first steps in the process were to identify what measurements were required from the thermal emulator and then to rank them according to their relative importance. With a transient thermal step being introduced on the shell side of the heat exchanger, temperature at both the inlet and outlet would be required, as well as the corresponding temperatures for the tube side. In an ideal scenario, the flow rates would be kept constant through the entire process, but this was not practically possible; thus flowmeters for each side of the heat exchanger were also necessary. The last pieces of data that could be gathered from the heat exchanger were the pressures at the inlet and outlet for both the shell and tube sides of the heat exchanger.

With the three measurements identified, they are then ranked. Pressure readings are not taken into account within the current Simulink model of the heat exchanger, and as such, they are the lowest priority. Pressure readings are not necessary to complete the calibration of the model, but are taken in the event that future studies introduce a model form that utilizes pressure. Temperature readings are arguably some of the most

important measurements for the system as they help to provide a view of how much thermal energy has been transferred from one fluid stream to the other. However, in order to fully utilize the temperatures differences for energy calculations, it is also necessary to know the flow rate with time. As the highly accurate flow measurements are required along with the fluid temperatures in order to calculate the total thermal energy transferred, they are regarded as important as temperature readings. This results in a ranking of required measurements with flow rates and temperatures as most important and pressure readings as ancillary.

Now that the measurements are ranked according to importance, the next step is to identify the amount of funds available to dedicate to the instrumentation and data acquisition (DAQ) hardware. By the point that the instrumentation was to be selected and purchased, a portion of the budget had already been allocated to purchasing all materials necessary to finish construction of the thermal emulator, while minimizing purchases by utilizing any salvageable supplies from the lab at WSU. This process was detailed in the previous section.

Flowmeters

Flowmeters can range in price from several hundred to several thousand dollars, all depending on the fluid conditions for which the flowmeter is intended to be used. The conditions in the thermal emulator did not present a situation that warranted a purchase of the most expensive flowmeters on the market; however, high accuracy was still a requirement within the constraints of the budget. After reviewing possible options from Omega, a well-known supplier of scientific instrumentation, a flowmeter was selected for

use on both the shell and tube sides of the heat exchanger. The FTB-102 is a turbine-style flowmeter that utilizes user replaceable steel ball bearings to enable high accuracy measurements and features a flow range that encompasses those that are expected to be seen in the thermal emulator as defined above in Table 2. The FTB-102 features a low mass rotor for fast dynamic responses, provides a wide range of linear flow readings from 0 – 7.5 GPM, and boasts an accuracy of ± 0.5 % of the reading.[11] The flowmeter also comes from Omega pre-calibrated for water, which was one of the selling points to selecting this particular device over others, along with the price.

Turbine flowmeters produce a low-level frequency signal that must be converted and amplified for ease of use with a DAQ system by a signal conditioner. All flowmeters purchased from Omega have the option of being ordered with signal conditioner already attached and adjusted to provide the desired output signal. In this case, the FLSC-28 signal conditioner was selected as it requires an 8 – 40 V power source, provides a 0 – 5 V analog signal for measurement, and provides a ± 0.5 % full scale accuracy.[12]

Calibration of Flowmeters

As mentioned previously, the flowmeters came from Omega already calibrated for water. Several flow rates were checked for each flowmeter and were found to differ from the stated calibration from the manufacturer via a rough estimation; this led to the need to fully calibrate each of the flowmeters while installed in the thermal emulator exactly as it was intended to be used. This arrangement would help to ensure that the readings measured during the data collection process would not be biased or changed due to differences between the calibration setup and the experimental setup.

In order to calibrate the flow meters, a large bin was used to gather a specified mass of water and the amount of time to reach the desired mass was recorded; this calibration methodology is known as the 'flying start and stop.'[13] A large 45 gallon drum was used to store the water during the calibration tests and was marked at 20, 30, and 40 gallon levels. This was completed by repeatedly measuring the mass of water in a graduated flask using a digital scale (Ohaus EB6) with an uncertainty of ± 0.2 g and adding it to the drum.[14] The mass of the water was converted to a volume based upon the temperature of the water available from the cold water tap in the laboratory. The total mass of water for each flask was documented by measuring the flask mass once full with water as well as after the flask was drained into the drum. Uncertainties for each measurement were recorded and added together to obtain a total uncertainty for the final specified volumes of water marked in the bin.

Several set point flow rates were selected to encompass the flow ranges that were to be tested in the thermal emulator. Three data points were collected for each specified flow rate set point and the tests were conducted in a random order. The table showing the calibration data points for the shell side flowmeter is shown below in Table 3.

Table 3: Flowmeter calibration set points, tube side flowmeter (FM2)

Flow Rate, Target	Flow Rate, Claimed	Volume, Actual	Time, Target	Test Number	Time, Actual	Voltage, Average
[Volts]	[GPM]	[gal]	[sec]	[#]	[sec]	[Volts]
1	1.5	20.00522	800	T1	802.29	1.001033
1	1.5	20.00522	800	T14	811.79	0.992874
1	1.5	20.00522	800	T15	814.103	0.989264
1.3333	2	20.00522	600	T2	602.293	1.337425
1.3333	2	20.00522	600	T13	589.798	1.370995
1.3333	2	20.00522	600	T16	599.501	1.343963
2	3	30.00036	600	T3	594.003	2.021528
2	3	30.00036	600	T12	599.401	2.008122
2	3	30.00036	600	T17	604.595	1.989912
2.6666	4	40.000093	600	T4	595.299	2.67581
2.6666	4	40.000093	600	T11	598.793	2.663476
2.6666	4	40.000093	600	T18	598.893	2.662933
3.3333	5	40.000093	480	T5	477.101	3.326318
3.3333	5	40.000093	480	T10	474.598	3.346757
3.3333	5	40.000093	480	T19	475.595	3.340734
4	6	40.000093	400	T6	390.499	4.042693
4	6	40.000093	400	T9	393.197	4.021301
4	6	40.000093	400	T20	395.997	3.99043
4.3333	6.5	40.000093	369.23	T7	368.79	4.275033
4.3333	6.5	40.000093	369.23	T8	362.3	4.353597
4.3333	6.5	40.000093	369.23	T21	362.7	4.351603

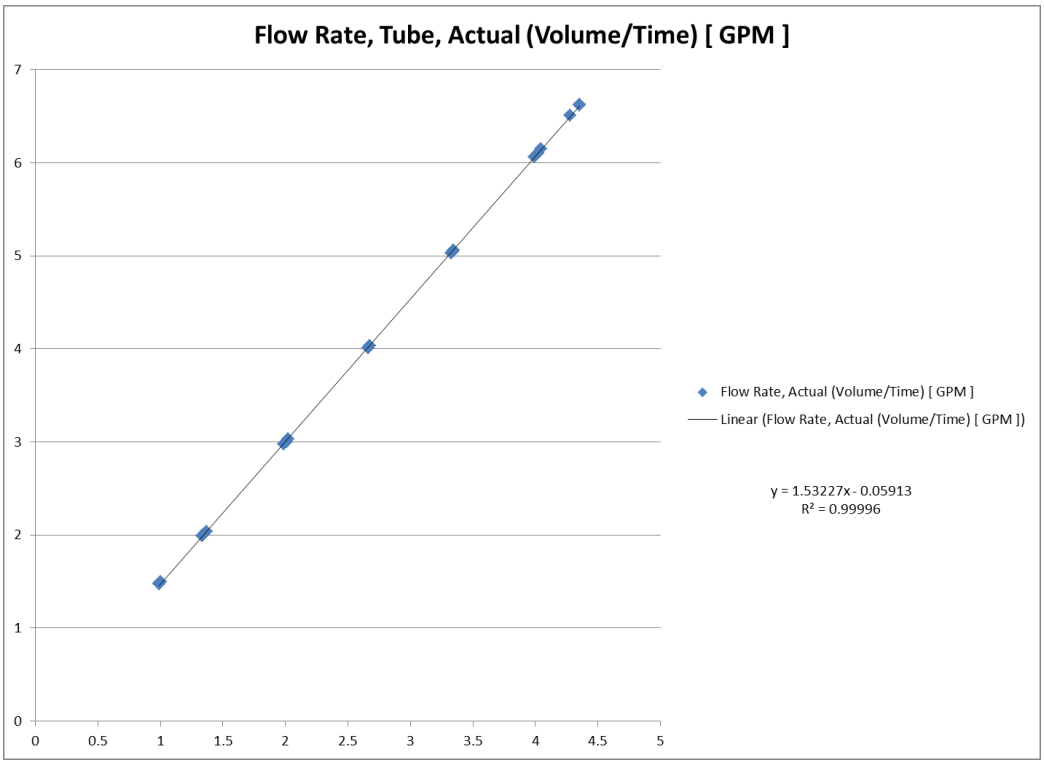

Figure 5: Calibration data points and curve fit, tube side flowmeter

As seen above in Figure 5, a calibration line was created by plotting actual average voltage values versus target flow rate voltages that correspond to the desired flow rates. After fitting a line to the data points, an equation is generated that feeds in the current voltage measured from the flowmeter and provides a voltage between 0 and 5 Volts that is scaled linearly from 0.75 to 7.5 GPM. The calibration line fit of the data points is displayed on the plot and is shown to have an R^2 value of 0.99996 implying excellent data prediction with line fit. The calibration equation is entered into the LabView VI to transform the measured voltage into one that accurately relates to the true scale of the flowmeter.

The process shown above for the tube flowmeter is identical to the one used for the shell flowmeter; this data is found in APPENDIX B: INSTRUMENTATION CALIBRATION.

Flowmeter Uncertainties

There are several places where uncertainty shows up in the calculations of the flow rates. The flowmeter itself has an uncertainty of ±0.5% of the reading (gpm), while the signal conditioner has an uncertainty of ±0.0025 Volts for the output analog signal. This first step is to identify the sources of uncertainty that will play into the calibration and final measurements of the flow rate. The calibration uncertainty for the flowmeters is represented as

$$\Delta\dot{v}_{cal} = \Delta\dot{v}_{signal\ conditioner} + \Delta\dot{v}_{flowmeter} + \Delta\dot{v}_{99\%} + \Delta\dot{v}_{best\ fit} \qquad (26)$$

where $\Delta\dot{v}_{signal\ conditioner}$ is the uncertainty due to the voltage output of the signal conditioner, $\Delta\dot{v}_{flowmeter}$ is the uncertainty due to the output signal from the flowmeter,

$\Delta\dot{v}_{99\%}$ is the maximum value of the 99% confidence interval calculated for each of the calibration flow measurements, and $\Delta\dot{v}_{best\ fit}$ is the maximum deviation from the calibration best fit line. A 99% confidence interval is chosen as it provides a more conservative estimate for the errors than does the typically used 95% confidence interval. The values used to calculate $\Delta\dot{v}_{cal}$ are shown below in Table 4, below.

Table 4: Flowmeter calibration uncertainties

	$\Delta\dot{v}_{signal\ cond}$ [± gpm]	$\Delta\dot{v}_{flowmeter}$ [± gpm]	$\Delta\dot{v}_{99\%}$ [± gpm]	$\Delta\dot{v}_{best\ fit}$ [± gpm]	$\Delta\dot{v}_{cal}$ [± gpm]
FM1 (shell)	0.00375	0.0375	0.004406359	0.019848822	0.065505181
FM2 (tube)	0.00375	0.0375	0.004292144	0.020936406	0.066478551

The flowmeter uncertainties are specified by the manufacturer as ± 0.5 % of the reading, however, the uncertainty used in Table 4 is calculated based upon the maximum flow rate that the flowmeter is designed to measure. This is a more conservative approach to estimating the uncertainty of the measurements than using ± 0.5 % of each reading. With the calibration uncertainty calculated for the flowmeters, it is now possible to define the uncertainty in each measurement. Traditionally, for steady-state cases, this would be calculated as

$$\Delta\dot{v}_{measurement} = \Delta\dot{v}_{cal} + \Delta\dot{v}_{measurement,99\%}\ , \tag{27}$$

where $\Delta\dot{v}_{measurement,99\%}$ is the 99% confidence interval of the flow measurement that was made with the flowmeter. While this is useful for a steady-state analysis, it automatically introduces additional error into uncertainty calculations when measuring dynamic signals as the nature of dynamic signals will bias the confidence interval. In order to estimate the uncertainty associated with the measurement of dynamic flow rates, the uncertainties associated with the DAQ system are added to the calibration uncertainty to yield the total estimated uncertainty in the measurements as

$$\Delta\dot{v}_{measurement} = \Delta\dot{v}_{cal} + \Delta\dot{v}_{DAQ} \ . \quad (28)$$

The uncertainty associated with the DAQ system for flow rate is represented by $\Delta\dot{v}_{DAQ}$ and is calculated in the data acquisition section below, but presented with the flowmeter uncertainties in Table 5, below.

Table 5: Total flowmeter uncertainties

	$\Delta\dot{v}_{cal}$ [± gpm]	$\Delta\dot{v}_{DAQ}$ [± gpm]	$\Delta\dot{v}_{measurement}$ [± gpm]
FM1 (shell)	0.065505	0.004845	0.070350181
FM2 (tube)	0.066479	0.004845	0.071323551

It is important to note that the uncertainties provided by the manufacturer for the flowmeters and the signal conditioners have different units. The signal conditioner uncertainty is given in volts, as the output signal is an analog voltage measurement. The output signal from the flowmeter is actually a measure of pulses per second (counting the number of rotations of the turbine wheel), but the uncertainty is given as a percentage of the reading in terms of the final output value of gpm. In order to calculate the uncertainties for the flow measurements and have them be useful, all uncertainties need to be converted to the same type of unit. All voltage uncertainties were converted to flow uncertainties in terms of gpm based upon the given flow range that the flowmeters are designed to measure and the full scale voltage outputs from the from the signal conditioner.

Another important note is that the DAQ uncertainty needs to be included in the final total flow measurement uncertainty because even though the flowmeter was being calibrated in-situ, it was not be calibrated against another flowmeter of known accuracy. If it were, the DAQ uncertainty would already be included and quantified within the calculation of the calibration uncertainty.

Thermocouples

Thermocouples were selected to gather the necessary temperature measurements from the system. There are innumerable choices for thermocouple styles and types, varying in length, diameter, materials, and intended applications. In order to select the appropriate thermocouples for use in the thermal emulator, an automated tool was utilized on Omega Engineering's website; by answering questions related to the intended application, the tool helps the user to select the best thermocouples for the task. The end result was the selection of KQXL-116G-12 thermocouples for use in the system. These specific thermocouples feature excellent stability at very high temperatures, are a standard type 'K' thermocouple with a 1/16" diameter sheath, and have low thermal drift. Furthermore, the thermocouples are grounded, which means that the sensing element touches the sheath, thus improving the dynamic response of the thermocouple as thermal energy can more easily flow from the fluid, through the sheath to the sensing wire junction.[15]

Calibration of Thermocouples

Thermocouples can feature high accuracy measurements, dependent upon the specific type of thermocouple being used, manufacturing tolerances, and the accuracy of the calibration. In order to achieve a high accuracy calibration for the thermocouples, the outputs must be compared to a temperature detector of known uncertainty. WSU has a platinum resistance temperature detector (PRTD or RTD) available for the purposes of calibration that has a National Institute of Standards and Technology (NIST) traceable

uncertainty. Both RTD and thermocouples are placed into a chiller bath (Lauda RC20) filled with water.[16] The chiller bath is set to various temperature set points that encompass the temperature range that the thermocouples are intended to see. In this case, the chiller was adjusted from 5 to 95 °C in 10 °C increments. After equilibrium has been reached at each temperature, a several hundred data points are recorded from all thermocouples and from the RTD. It is important to note that the DAQ system used for calibration was the exact same setup to be used during experimentation. Thermocouple wiring was not changed or adjusted in any way between the calibration and the experiment to prevent introducing bias and changing the calibration.

Uncertainty of Thermocouples

With the water bath temperatures from both devices, a calibration line can be created. This calibration line will take a raw input from a thermocouple as an input and output the corresponding RTD temperature. The uncertainty of this calibration for each thermocouple is calculated as

$$\Delta T_{cal} = \Delta T_{RTD} + \Delta T_{bath,99\%} + \Delta T_{best\ fit}\ , \tag{29}$$

where ΔT_{cal} is the calibration uncertainty for each thermocouple, ΔT_{RTD} is the NIST traceable uncertainty of the RTD, $\Delta T_{bath,99\%}$ is the 99% confidence interval of the chiller bath temperature as read by the RTD, and $\Delta T_{best\ fit}$ is the maximum deviation from the best fit calibration line. The NIST traceable uncertainty for the RTD is stated to be ± 0.0033 °C.[17] The percentage for the confidence interval is a value that can be selected by the researcher; it is common to use 95%, as opposed to the 99% confidence interval used in the calibrations. The higher the confidence interval percentage chosen, the higher the

uncertainty for $\Delta T_{bath,99\%}$ will be; 99% was chosen to be a more conservative estimation over the more common 95%. Regardless, it was found that the confidence interval was the smallest contributor to total thermocouple calibration uncertainty, with the deviation from the calibration curve being the largest. The values used to calculate ΔT_{cal} are shown below in Table 6.

Table 6: Thermocouple calibration uncertainties

	ΔT_{RTD} [± °C]	$\Delta T_{bath,99\%}$ [± °C]	$\Delta T_{best\ fit}$ [± °C]	ΔT_{cal} [± °C]
TC07 / Shell, Inlet	0.0033	0.004038907	0.176049405	0.183388311
TC08 / Shell, Outlet	0.0033	0.004038907	0.170331009	0.177669916
TC09 / Tube, Inlet	0.0033	0.004038907	0.173996165	0.181335072
TC10 / Tube, Outlet	0.0033	0.004038907	0.198882705	0.206221611

With the calibration uncertainty calculated for each thermocouple, it is now possible to define the uncertainty in each measurement. Traditionally, for steady-state cases, this would be calculated as

$$\Delta T_{measurement} = \Delta T_{cal} + \Delta T_{measurement,99\%} \ , \tag{30}$$

where $\Delta T_{measurement,99\%}$ is the 99% confidence interval of the temperature measurement that was made with the thermocouple. While this is useful for a steady-state analysis, it automatically introduces additional error into uncertainty calculations when measuring dynamic signals as the nature of dynamic signals will bias the confidence interval. As with the flowmeter measurements, the uncertainties associated with the DAQ system would normally be added to the calibration uncertainty to yield the total estimated uncertainty in the measurement. Due to the fact that the thermocouples were calibrated in-situ against another temperature sensing device (RTD) of known certainty, the actual DAQ uncertainty of the thermocouple module was included and quantified within the

calculation of the calibration uncertainty for each thermocouple. This means that the total uncertainty of the thermocouples can be estimated to be

$$\Delta T_{measurement} = \Delta T_{cal} \ . \tag{31}$$

This results in the total thermocouple uncertainties shown below in Table 7.

Table 7: Total thermocouple uncertainties

	$\Delta T_{measurement}$ [± °C]
TC07 / Shell, Inlet	0.183388311
TC08 / Shell, Outlet	0.177669916
TC09 / Tube, Inlet	0.181335072
TC10 / Tube, Outlet	0.206221611

It is worth noting that for all thermocouples, the maximum deviation occurred at either the 5 or the 95 °C data point. This is attributed the fact that these temperatures were the furthest from the ambient temperature in the laboratory and therefore, the chiller had the most difficulty maintaining the set point due to the larger temperature difference to the environment. If these data points were not necessary, the uncertainty of the thermocouples could have been reduced further.

Pressure Transducers

Pressure transducers are capable of reading both positive and negative pressures, as well as gauge and absolute values. The transducers that were selected for the system were the PX319-100A5V which are designed to measure absolute pressure and cover a range of 0 – 100 psia. As typical water pressures from the laboratory do not exceed 55 psia, the selected range was more than enough to accommodate typical variations in pressure. These specific transducers offer a full error band of ±2% to include the effects from linearity, hysteresis, repeatability, thermal hysteresis, and thermal errors, all

applicable over the pressure range that the transducers were intended to be used. The transducers require the same voltage supply as the flowmeters and also feature an analog 0 – 5 Volt output signal.[18]

Calibration of Pressure Transducers

WSU does not have the capability to calibrate pressure transducers, and as such, the 5 point calibration that was completed by Omega was utilized. This calibration shows the highly accurate pressures that were fed into the transducer along with the actual output voltage. From these points, a line can be created to provide the conversion from measure voltage to actual pressure. Due to the 0 – 5 Volt output and the fact that the pressure range was 0 - 100 psia, merely multiplying the output voltage by a factor of 20 provided the measured pressure in psia.

Uncertainty of Pressure Transducers

Uncertainties of the measured pressures can be calculated similarly to the methods used above for the thermocouples and the flowmeters. The uncertainties were not actually calculated due to the pressure data not being utilized in the model. The spec sheets that detail the calibration procedure are attached in the appendix such that the uncertainty can be calculated if it is necessary at a later date.

Data Acquisition (DAQ) System

DAQ is the hardware interface that is responsible for translating the signals generated by instrumentation into a digital, computer readable signal. DAQ systems are

often chosen based upon the intended application, budget constraints, and required accuracy. In this experiment, the National Instruments CompactDAQ chassis was selected as the backbone of the total DAQ system. The CompactDAQ chassis features 4 bays for hot-swappable input/output modules that allow a system to be tailored to any specific need, as well as a standard universal serial bus (USB) interface to the DAQ computer and software.[19] With the chassis chosen, it is now possible to select the individual modules that will handle the specific inputs and outputs to the system.

Voltage Module

Voltage measurements were made using the NI-9205, one of various voltage measurement modules. The NI-9205 features 32 channels (16 differential channels), ±10 DC Volt analog input signals, 16-bit analog to digital conversion, and up to 250 kS/s. The flowmeters with signal conditioners output an analog voltage from 0 -5 Volts, as well as the pressure transducers; this module is capable of handling all necessary voltage measurements from the system, as well as any foreseeable additional instrumentation. Each module lists necessary specifications and uncertainty information. For the NI-9205, Voltage readings based on a ±5 Volt range will have an absolute accuracy of 3,230 μV.[20] This absolute accuracy takes into account gain, noise, and offset errors. This value is denoted as ΔV_{DAQ} and is necessary when calculating the uncertainties associated with any instrumentation that outputs an analog voltage signal that is read by this module. This voltage uncertainty has units of volts, but must be transformed to the proper units when voltages are measured to represent another physical value. For example, 3,230 μV over the ±5 Volt range will correspond to ±0.004845 gpm over the 0.75 – 7.5 gpm range that

the flowmeter is designed to measure. This uncertainty is used above to calculate the total uncertainty for the flow measurements.

Thermocouple Module

Thermocouple measurements were made using an NI-9213 module. This module is capable of reading 16 differential thermocouple channels and features built-in cold junction compensations. This module offers the choice of two different data collection modes: high speed or high resolution. In high speed mode, the module is capable of making up to 75 samples per second at the cost of less accuracy and resolution. In high speed mode, the sampling rate is dropped to a maximum of 1 sample per second (for all channels being utilized), but sports a measurement sensitivity and accuracy that is an order of magnitude smaller than for high speed mode. The specifications detail the information that defines the errors that can affect the final temperature readings: gain, offset, differential and integral nonlinearity, quantization, noise, lead resistance, and cold junction compensation errors. All of these values are provided individually for calculation or are all combined in a chart that represents the maximum error over the given temperature range. For type 'K' thermocouples, at room temperature, with the module set to high resolution mode, the typical error, ΔT_{DAQ}, is approximately ±0.8 °C over the temperature range that the thermocouples will be subjected to within the thermal emulator (approximately 5 – 80 °C).[21]

Relay Control Module

The heating elements in the fluid reservoirs were controlled via the NI-9481 module. This module is a 4 channel single pole, single throw, electromechanical relay control module. By flipping a switch on or off from within the LabView VI, the control module is capable of opening or closing 4 separate low power relays.[22] These low power relays were used to switch on and off the solid state, high power, electromechanical relays that controlled the power to the heating elements within the fluid reservoirs. The control module relay is possible to be controlled automatically from the VI based upon system measurement, but it was found that manual operation of the relays was sufficient to reach the operating temperatures for each test. It is important to note that AC electrical power was wired directly through the control module which was located directly next to the thermocouple and voltage modules within the DAQ chassis. In order to prevent electromagnetic interference (EMI) from the AC signals from interacting with the low-level DC signals from the thermocouples and other measurements, all AC wiring was shielded and grounded. The shielding was tested via a wireless clamp-style voltage meter to prove that EMI effects on the DC measurements had been eliminated.

Photos of the thermocouple and flowmeter calibration procedures can be found in APPENDIX B: INSTRUMENTATION CALIBRATION.

EXPERIMENTAL PROCEDURES

A well-defined test plan was necessary in order to be able to produce results in a consistent manner. Following a test plan also served to minimize bias introduced to the system due to minor variations between test runs. The first step was to define the inputs to the system and over what ranges they would be controlled. The main inputs to the heat exchanger were flow rates of the fluid on both the shell and tube sides, temperatures at the inlets and outlets, as well as pressures at the inlets and outlets. The ranges over which these parameters would need to be tested were initially defined based on conditions that were seen by the heat exchanger that was being utilized in the AFRL laboratory experiments, and then adapted to the specific design of the thermal emulator to be used at WSU's laboratory. This information was all previously discussed and the ranges of test conditions can be seen in Table 2, above.

With the fluid conditions defined, it is then necessary to determine how many and what configuration of tests to conduct. To cover the flow rate ranges, three set points were used: low, middle, and high. This covered the entire spectrum of the flow rate ranges provided without leaving large gaps between points. The range of inlet temperatures on the shell side was a much larger range, and since this value could be virtually any value with the given range, it was decided to use more set points with the temperature than with flow rates. The total range of temperature to be covered in the experiment was 60 °C. Since the shell inlet temperature was expected to cover such a wide range and with no information about where it would typically be within that range, it was decided to use more set points for the temperature than with the flow rates. The temperature was broken up into seven set points total, each varying by 10 °C.

The next step in the process was to determine what sort of test plan to utilize. With the limited knowledge of the fluid conditions and typical operating conditions, a full factorial design was selected. A full factorial design involved conducting a test at each possible combination of parameter set points. For the selection of three set points for both the shell and tube flow rates and seven set points for the temperature, this yields a total of 63 combinations, and thus, 63 tests. For the specific type of tests that were being conducted and due to the nature of the testing equipment used, this proved to be a time-consuming and arduous process. Due to the results of preliminary tests with the thermal emulator, the amount of time required to conduct each test, and the time constraints upon possession of the test article, a single replicate was selected; this means the true test plan became an unreplicated, full factorial design.[23]

In an ideal situation, more than a single replicate of each test point would be conducted to prevent the possibility of measuring noise. The need to minimize the number of tests can become necessary when the number of individual factors becomes large, or when the cost, with respect to either time or money, becomes too large. It is possible for additional factors to play into this determination as well. For example, in this specific case, it was determined that producing an exact replicate of a transient temperature change for the same test point was extremely difficult. If additional replicates were feasible with respect to time, it is possible that even a small number of replicates could have introduced more variance into the data than it would have eliminated due to the lack of reproducibility for an exact transient change.

This decision to only run one replicate of each test provides an additional useful purpose for this research. With non-ideal data, it is still necessary to utilize the

experimental data for the purposes of the model validation. This scenario is similar to utilizing data provided in a journal paper as only the best data or mean values are provided; rarely are all data points for all replicates provided or accessible. In these cases, it still may be desirable to use the data to form a functional model. It is the hope that the process utilized in this research will be applicable to similar situations.

The set points for each parameter result in 63 total tests, but to minimize bias error in the testing process, it is necessary to randomly conduct the tests. JMP, a graphically based statistical package, was used to generate the randomly ordered test matrix. This test matrix is found below in Table 8.

Table 8: Test matrix, randomized by JMP

Test Number	Pattern	Flow Rate, Shell [GPM]	Flow Rate, Tube [GPM]	Temperature, Shell [C]	Test Number	Pattern	Flow Rate, Shell [GPM]	Flow Rate, Tube [GPM]	Temperature, Shell [C]
1	214	4	2	50	33	122	2	4	30
2	314	6	2	50	34	313	6	2	40
3	224	4	4	50	35	137	2	6	80
4	226	4	4	70	36	123	2	4	40
5	115	2	2	60	37	113	2	2	40
6	332	6	6	30	38	221	4	4	20
7	326	6	4	70	39	112	2	2	30
8	317	6	2	80	40	336	6	6	70
9	124	2	4	50	41	132	2	6	30
10	231	4	6	20	42	223	4	4	40
11	134	2	6	50	43	114	2	2	50
12	211	4	2	20	44	126	2	4	70
13	327	6	4	80	45	321	6	4	20
14	133	2	6	40	46	311	6	2	20
15	237	4	6	80	47	127	2	4	80
16	136	2	6	70	48	216	4	2	70
17	234	4	6	50	49	116	2	2	70
18	335	6	6	60	50	337	6	6	80
19	227	4	4	80	51	111	2	2	20
20	323	6	4	40	52	217	4	2	80
21	236	4	6	70	53	233	4	6	40
22	316	6	2	70	54	235	4	6	60
23	131	2	6	20	55	222	4	4	30
24	213	4	2	40	56	324	6	4	50
25	117	2	2	80	57	325	6	4	60
26	215	4	2	60	58	125	2	4	60
27	212	4	2	30	59	333	6	6	40
28	121	2	4	20	60	232	4	6	30
29	331	6	6	20	61	225	4	4	60
30	322	6	4	30	62	135	2	6	60
31	315	6	2	60	63	312	6	2	30
32	334	6	6	50					

Once the test matrix was completed, the next step was to formulate the plan for how each test was to be conducted. This would require a clearly defined step-by-step process to follow to minimize mistakes and help ensure that all 63 tests would be

conducted in a similar fashion. The thermal emulator was designed to accommodate a large temperature gradient being introduced on the shell side of the heat exchanger, and in order to complete this action, several phases of the testing were defined:

1.) Warm-up,

2.) Filling fluid reservoirs,

3.) Recirculation and heating (if necessary),

4.) Adjustment of shell gate valve, and

5.) Testing.

Each valve in the thermal emulator has a specific purpose, and in some cases, more than one purpose, dependent upon which phase of testing is being run at the time. These valves are seen labeled in the following process and instrumentation diagram of the experimental thermal emulator.

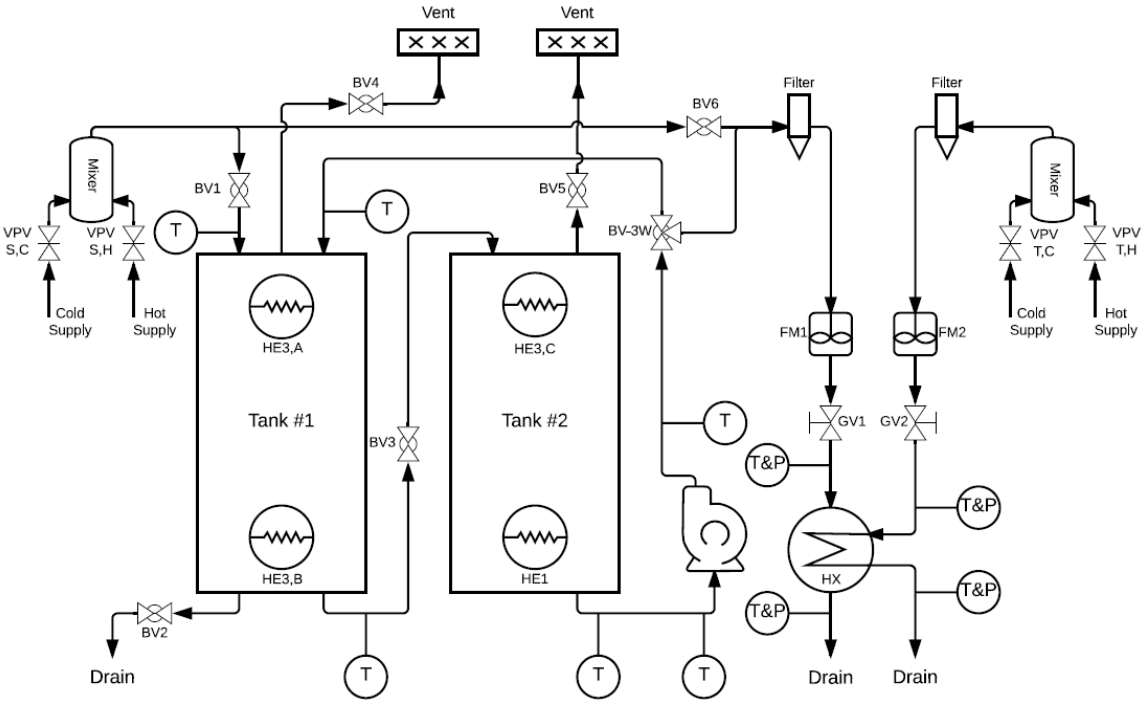

Figure 6: P&ID of experimental thermal emulator

Although it is possible to see all flow control valves and instrumentation in this diagram, it is not intuitive to tell what purpose each valve fulfills. A table was constructed that contains the label, name, and function for each valve and controlled component within the system. This information is found in Table 9, below.

Table 9: Control labels, names, and functions

Label	Name	Function
VPV-S,C	V-port valve, shell side, cold	Fine control of cold water flow rate into the system on the shell side of the emulator
VPV-S,H	V-port valve, shell side, hot	Fine control of hot water flow rate into the system on the shell side of the emulator; also used to control bypass flow rate
VPV-T,C	V-port valve, tube side, cold	Fine control of cold water flow rate into the system on the tube side of the emulator; also used to control bypass flow rate
VPV-T,H	V-port valve, tube side, hot	Fine control of hot water flow rate into the system on the tube side of the emulator
BV1	Ball valve, 1	Binary flow control (on/off); allows fluid into tanks, as well as to bypass recirculation tanks
BV2	Ball valve, 2	Binary flow control (on/off); To drain Tank #1
BV3	Ball valve, 3	Binary flow control (on/off); allows or prohibits flow between Tank #1 and Tank #2
BV4	Ball valve, 4	Binary flow control (on/off); air purge to atmosphere for Tank #1 during filling, and air vent during draining to prevent hydro lock
BV5	Ball valve, 5	Binary flow control (on/off); air purge to atmosphere for Tank #2 during filling, and air vent during draining to prevent hydro lock
BV6	Ball valve, 6	Binary flow control (on/off); allows or prohibits bypass of tanks for shell side
BV-3W	Ball valve, 3-way	Directs flow in 1 of 2 directions: Position #1 recirculates fluid through tanks; Position #2 drains to shell side of hx
GV1	Gate valve, 1	Main control valve for flow rate through shell side of hx
GV2	Gate valve, 2	Main control valve for flow rate through tube side of hx
HE3θ,A	Heating element, 3-phase, element A	1st of 3 heating elements for 3-phase power, cannot be operated independently of other 3-phase elements
HE3θ,B	Heating element, 3-phase, element B	2nd of 3 heating elements that operate in unison, cannot be operated independently of other 3-phase elements

HE3θ,C	Heating element, 3-phase, element C	3rd of 3 heating elements that operate in unison, cannot be operated independently of other 3-phase elements
HE1θ	Heating element, single phase, element 1	Single heating element, can be operated individually and independently from 3-phase heating elements

It is important to note in Table 9 that heating elements 3A, 3B, and 3C are all controlled via a single virtual control from within LabView: due to the nature of 3-phase wiring with resistive heating elements, it is not possible to operate them independently from one another. When the 3-phase heating elements are energized, approximately 10.14 kW of heat is generated within the tanks. The single phase heating element can be controlled independently in LabView from the 3-phase heating elements, and when energized, adds approximately 3.38 kW of heat to the fluid within the tanks.

An image showing the front screen of the LabView VI used to collect data from the thermal emulator is found in Figure 7. All thermocouple outputs are shown across the top of the VI on scales that are adjusted for the expected temperature ranges. At the bottom, the flow rates are seen on dials as well as the raw voltages recorded from the flowmeters. The flow rates seen are after the raw voltages have been adjusted by the calibration equations. Raw voltages were recorded to ease calculation of actual flow rates in the event that the calibration equation changed in the future. Pressures are recorded from the inlets and outlets of the heat exchanger. The left-hand side of the screen has a few values that are entered by the user to control the frequency to record voltage and thermocouple data. The recommended values are noted for future tests.

The right-hand side of the VI has three user operated switches. The top two switches control the power to the heating elements; one switch operates the 3θ power and

the other operates the 1θ power. The switch at the bottom coupled with the tank volume estimator located adjacent; the tank volume is estimated by calculating the total amount of water being expelled from the system by multiplying each flow rate by the amount of time between data points, and summing the total. This total value is subtracted from a user-entered amount of water present in the tanks at the beginning of the test. This information was useful when the next test used the same temperature water as the previous test as input water temperature from the wall could be adjusted to minimize the amount of heating necessary to achieve the proper temperature for the next test.

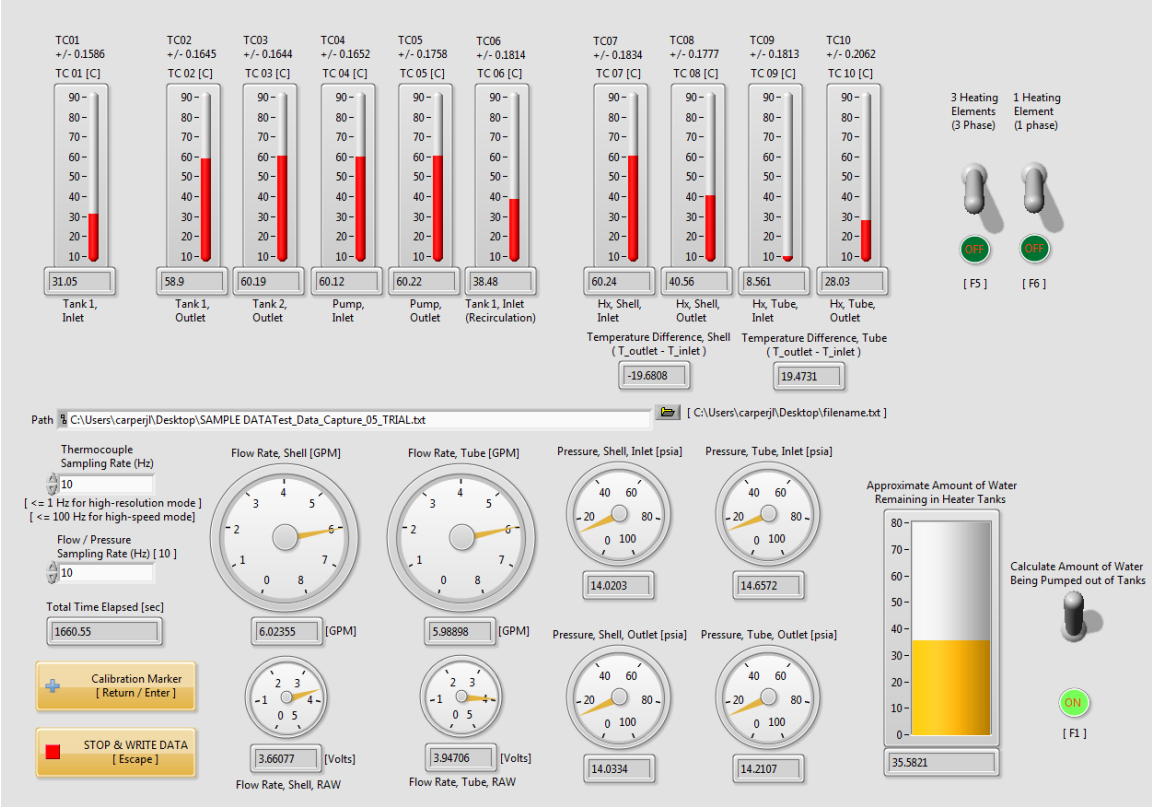

Figure 7: LabView VI used to collect thermal emulator data and control heating elements

Utilizing the information in Figure 6 and Table 9, a detailed procedure was developed that states the position of each valve at the start of each phase of testing as the

steps to follow to complete each phase of testing successfully. These detailed procedures are found in APPENDIX C: EXPERIMENTAL PROCEDURES.

CALIBRATION OF HEAT EXCHANGER MODEL

The Simulink model developed earlier does not identically represent the heat exchanger in question, by design, and therefore will require calibration in order to represent the heat exchanger that was used in the experiment as closely as possible. This calibration process was originally broken down into two major parts: a steady-state and a transient calibration. The steady-state calibration was completed first and deviations from experimental data were calculated, then the transient calibration and deviations were calculated.

Steady-State Calibration

Each experimentally run case has six important factors: four inputs, and two outputs. Each of these inputs and outputs are time varying signals, and near the step change exhibit large transients. The steady-state parameters for the model are to be defined based upon the steady-state values of the inputs and outputs from the experiment. After the step change in temperature was introduced, the experiment was allowed to run for approximately eight minutes to be certain that the model had reached steady-state. The data that was used specifically for the steady-state calibration involves only the last approximately three minutes of the selection. A sample of this data is shown below in Figure 8.

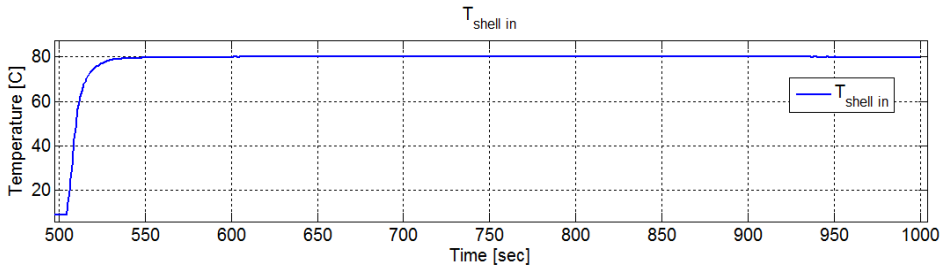

Figure 8: Sample data from experimental Case #19, region shown is center portion of data (~500 – 1000 sec) that captures start of transient as well as steady-state values for the shell input temperatures

For the selection of data used, the number of data points, n, mean, μ, standard deviation, σ, and variance, σ^2, were calculated for the steady-state region. The average values were then used as exact inputs and outputs to the model for each case for the purposes of calibration.

A basic sensitivity analysis was performed on the twelve parameters used to define the heat exchanger model by the sequential perturbation method. This testing methodology involves defining a baseline case with all parameters set to specific values. Each value is then altered up and down by a prescribed amount, in this case 5%, the model run, and outputs compared for each change. By utilizing this method, it was easy to determine which parameters had the largest effect on the steady-state output temperatures from the model. Additionally, this basic sensitivity analysis identified which parameters affect only the transient region of the output variables; they were noted to have no effect on the steady-state outputs.

It is necessary, from a computational standpoint, to attempt to minimize the number of parameters that are being adjusted. Of all of the parameters that were perturbed, eight were identified to have a significant effect on the output. Two of these parameters were not independent variables, and two other parameters had a significantly

larger effect than the rest. These two parameters with the largest effects were the surface area of the tubes and the outer diameter of each tube. While the rest of the parameters were fixed at values that corresponded to physical measurements of the heat exchanger, both the surface area of the tubes and the outer diameter of the tubes were to be adjusted during the tuning process.

Average experimental data values were plugged into the model and all parameters were set to as measured values or given by the manufacturer of the heat exchanger. This initial case was run to provide a rough comparison of the model and experimental outputs. This rough comparison initially showed that the selected model parameters for tuning needed adjustment in order to align the outputs more closely. A first pass at aligning the parameters was completed manually for the purposes of identifying the useful adjustment range of each parameter that would give reasonably accurate results. Once these ranges were selected, a low and high value for each parameter was identified for use in a full two factor factorial analysis. These low and high values are coded to the range [-1, 1] for the regression equation generation. This type of analysis, and the subsequent regression equations that were generated, were then used to fine-tune the parameters for the steady-state calibration.

The full factorial design with two parameters, each with a high and low value, gave four cases total to be run. Each of these four cases were run, for each of the sixty-three cases that experimental data existed for. This resulted in a test matrix of 252 total cases. Each model run takes approximately thirty seconds for initialization and solution calculation on typical personal computer equipment; all of these cases can be run in approximately 2 hours.

For each output of the model for each of these cases, the same values were calculated as were for the experimental data: the number of data points, n, mean, μ, standard deviation, σ, and variance, σ^2 in the steady-state region (the last 100 seconds of the middle portion of each data set). An example of the type of data generated for each of the 4 factorial cases per set of experimental data is found in Figure 9, below, for experimental Case #19.

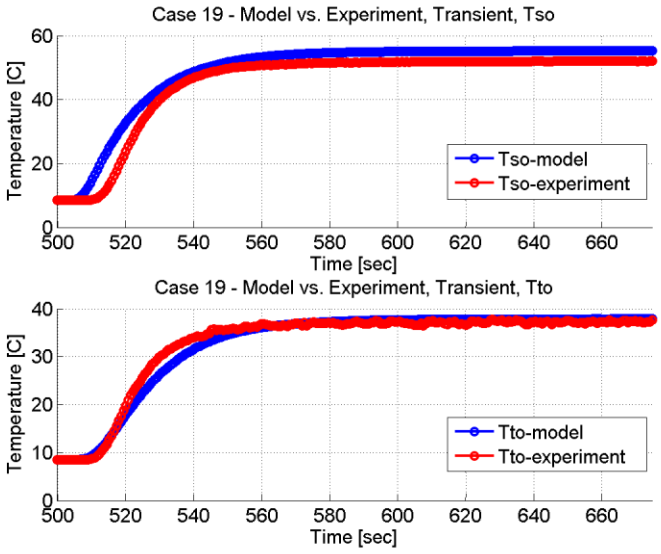

Figure 9: A comparison of model and experimental outputs; steady-state parameter calibration focuses on the last 100 seconds of data

This data was then all entered into a statistical package (JMP) that was used to generate the original test matrix, to calculate a regression equation for each output SRQ. For each of the original 63 cases, these regression equations were set equal to the experimental SRQs, and then the desired parameters were solved for using basic matrix algebra. With the two critical steady-state parameters now specified, the outputs match as closely as is feasibly possible to the experimental outputs for each individual case. If the analyst were only concerned with a single experimental case, these steady-state

parameters would be used as they will generate a minimum difference between the two data sets. This is highlighted in Table 10, below, for all cases for which experimental data exists.

Table 10: Model steady-state parameters and results, individual case

Case #	Parameters		Outputs	
Case(*1*)	SA_t(*1*)	OD_t(*1*)	$\Delta T\_so(1) \rightarrow 0$	$\Delta T\_to(1) \rightarrow 0$
Case(*2*)	SA_t(*2*)	OD_t(*2*)	$\Delta T\_so(2) \rightarrow 0$	$\Delta T\_to(2) \rightarrow 0$
⋮	⋮	⋮	⋮	⋮
⋮	⋮	⋮	⋮	⋮
Case(*63*)	SA_t(*63*)	OD_t(*63*)	$\Delta T\_so(63) \rightarrow 0$	$\Delta T\_to(63) \rightarrow 0$

Optimal steady-state parameters are now known for each individual case. The intent for the model was to be calibrated once to give the best results possible over a broad range of inputs and outputs. In order to accomplish this goal, it was necessary to calculate one value for each of the steady-state parameters identified for each case: SA_t and OD_t. These final parameter values were generated by computing the mean of each parameter across all 63 cases for which they were generated. These mean values were then used as the final optimum values for each of the two steady-state parameters. It is recognized that these final parameter values will not give model outputs that line up identically with experimental outputs for each case, rather, they will generate the best possible model output over the entire range of data used to calibrate the parameters; in this case, that is over the range of all 63 experimental cases. The last step in the process was to calculate and quantify the error associated with using the mean parameter values. Once the parameter values are fixed, the model is run for all sixty-three cases and the output values are compared to experimental outputs to calculate the error for each case.

Transient Calibration

The transient calibration process was intended to be very similar to that used above for the steady-state calibration, in that it would require comparing the experimental and computational outputs in some quantitative fashion. Initially, the results from the model were compared to the experiment for the first manual adjustment of parameters. These initial results revealed that the transient portion of the model outputs did not cause the transients to vary significantly and that the output temperatures were in reasonable agreement with the experimental outputs.

It would still be necessary to calculate the differences between the experiment and the model for the transient regions, so a quantitative way to compare the outputs was implemented. The time varying output signals will be compared by calculating the absolute area deviation (AAD), a metric that is introduced by Roy & Oberkampf[24] as a quantitative way to compare time-varying outputs that were experiencing transient changes. The AAD is essentially a discrete computation of the area between two curves. When the AAD has been minimized, the area, and subsequently the deviation over time, has been minimized.

The AAD was calculated after the steady-state calibration was completed as a way to gauge how much the transients differed prior to completing the transient calibration procedure. It was found that the transient response did not experience large changes when adjusting model parameters, and as such, the transient responses seen after the steady-state calibration procedure were to be accepted and used. The AAD was useful as a quantitative way to determine the differences, but only relatively, in that each case required a set of data to compare to. An example of the computed AAD can be

found below, in Figure 10, of Case #19 data. This image shows the AAD value on each plot after the minimization process outlined above has been completed.

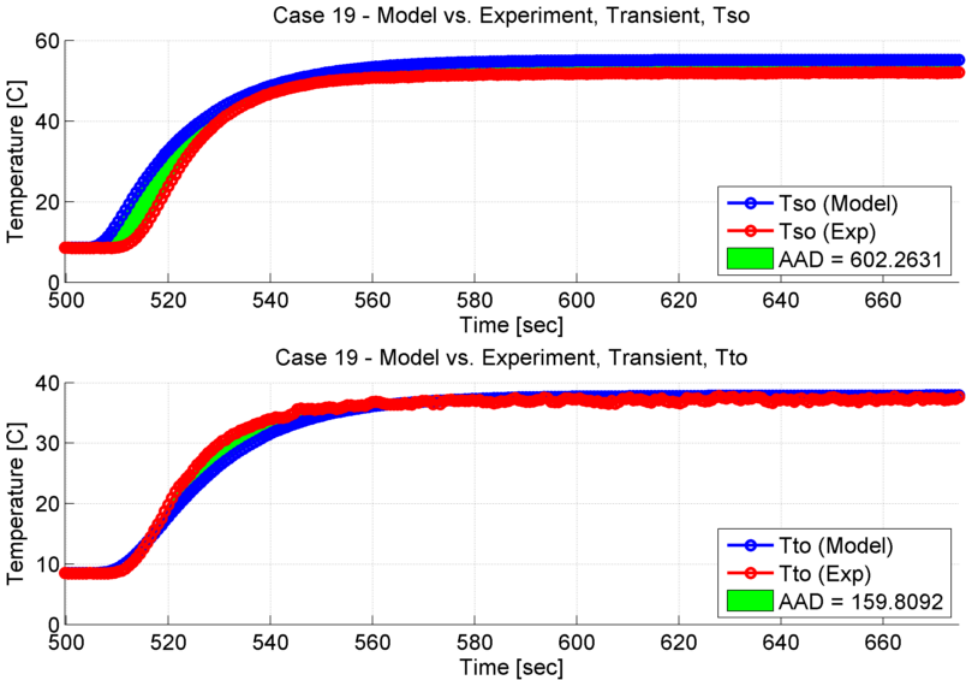

Figure 10: AAD as calculated for Case #19, T_{so} and T_{to}

SENSITIVITY ANALYSIS, UNCERTAINTY ANALYSIS, VERIFICATION, AND VALIDATION

Sensitivity Analysis

Proper quantification of error, or uncertainty, requires a defined process to follow. The following explanation serves to layout the process that will later be used to quantify the error for both experimental and computational data. The error in the outputs from the model will ultimately be compared to the error of the outputs from the experiment. The error in the outputs from the experiment is a value that is relatively easy to calculate as it is only associated with the direct measurement of the output. The output from the model is dependent upon the parameters of the model, as well as the inputs to the model and error associated with these inputs.

The first step to quantify error in the outputs of the model is first to complete a sensitivity analysis. This is a way to assign how much effect the variation of the inputs has on the uncertainty of each of the outputs; in this case, the variation of the inputs is the uncertainty of the inputs. Typically, sensitivity and uncertainty analyses are completed in tandem due to the nature of the values being calculated and how they relate to one another. There are various techniques used to calculate such sensitivities, all ranging in complexity and applicability. Beginning with a function f, expressed by "n" inputs $(x_1, x_2, x_3, \dots, x_n)$ to a system with any number of "k" outputs, the k^{th} output of the system can be referred to as a system response quantity (SRQ) and is a function of the input variables. For any case, this is written as

$$SRQ = f_k(x_i) \text{ for } i = 1, 2, \dots, n \; inputs. \tag{32}$$

For a basic nonlinear combination of variables, Goodman[25] uses a Taylor-series approximation for the functional value of f as

$$f_k(x_i) \approx f_k^0 + \sum_{i=1}^{n} \frac{\partial f_k(x_i)}{\partial x_i} \tag{33}$$

where the second half of Equation (33) is

$$\frac{\partial f_k(x_i)}{\partial x_i} \equiv \text{a derivative of } f_k \text{ with respect to } x_i. \tag{34}$$

The localized sensitivity of function f_k with respect to each input variable is approximated as

$$Sen_k^i \approx \frac{\partial f_k}{\partial x_i}. \tag{35}$$

This formulation is, again, for the localized sensitivity. It is noted by Saltelli[26] that this technique has both advantages and disadvantages. Advantages of this method are how simple the partial derivative is to calculate, supposing that the analytical formulation for function f_k is known. A disadvantage to this methodology is the fact that the sensitivities are generally evaluated in a linear fashion, and as such, is not typically applicable to nonlinear problems. Therefore, a new formulation for the sensitivity must be derived in order to properly quantify the nonlinear sensitivities. According to the Intergovernmental Panel for Climate Change (IPCC)[27], the sensitivity can be modified by incorporating a normalizing coefficient

$$\left\{Sen_{SRQ_k}^{x_i}\right\}_{\sigma_{SRQ_k}} \approx \frac{\sigma_{x_i}}{\sigma_{SRQ_k}} * \frac{\partial SRQ_k}{\partial x_i} \tag{36}$$

where σ_{x_i} is the uncertainty of the input variable x_i and σ_{SRQ_k} is the uncertainty of SRQ_k. The curly braces indicate that the sensitivity has been normalized by the output uncertainty.

Due to the nature of the way the governing equations are derived that represent heat exchanger model and to limitations in the quantity of testing that was able to be completed, all parameters from Equation (36) above must be estimated to some degree. For example, the partial $\frac{\partial SRQ_k}{\partial x_i}$ is the derivative of SRQ_k with respect to input variable x_i, or, the change of SRQ_k with respect to the change of input variable x_i. While this exact term was not recorded, each SRQ_k and each input variable x_i were recorded. Using the definition of the partial derivative

$$\frac{\partial SRQ_k}{\partial x_i} = \frac{dSRQ_k}{dt} * \frac{dt}{dx_i}, \tag{37}$$

it is easy to see that the partial derivative of the output SRQs can easily be calculated due to the fact that all input and output variables were recorded for each experiment. The derivatives with respect to time for each variable is computed numerically, then the resulting data sets are multiplied and divided by each other as Equation (37) above shows, to obtain the desired partial derivative.

Another issue to recognize in Equation (37) is that the standard deviation (uncertainty) is required for the normalizing coefficient as well. This is also problematic, as the standard deviation in this case is a function of time. In a steady-state analysis, the standard deviation would be one value calculated over a range of data points that were not changing with time, to minimize the standard deviation; this is not the case with the current analysis. Due to the inclusion of the large transient in input temperatures, the

outputs change greatly with time, and as such, the typical formulation of the standard deviation does not apply.

One way to mitigate this issue would be to calculate the standard deviation across several replicate data sets, at each point in time, as evidenced by previous research.[2] This technique allows the calculation of a standard deviation that represents that variation of the data at each point in time due to the variation in the data, not necessarily due to the variation as a function of time. In the experiments that were conducted for this study, a single replicate was conducted for each data point due to the length of time required to run each test, as well as the discovery that it was extremely difficult to exactly reproduce a particular transient step-change. As such, it was necessary to formulate a way to estimate the required parameters. Due to the lack of replicate data and the large variation in transients between test points, the technique that was chosen was to calculate the standard deviation of a moving average. The moving average would be calculated as a centered moving average, and always use an odd subset of data points for calculation. For a subset of 5 data points, the moving average is represented as

$$\mu_{moving} = \frac{1}{n}\sum_{t=1}^{n}(x_{t-2}, x_{t-1}, x_t, x_{t+1}, x_{t+2}) \tag{38}$$

where n is the number of data points used in the subset to calculate the moving average. This would be calculated for each point in time, even though it requires the knowledge of past, (x_{t-2}, x_{t-1}), and future data, (x_{t+1}, x_{t+2}). Since this is not possible to know for the beginning and ending data points and the region of time under scrutiny is in the center of a much larger collection of data points, this does not pose an issue. The standard deviation of each data point would then be calculated over each subset of data points similarly to the moving average as

$$\sigma_{\mu_{moving}} = \left(\frac{1}{n} \sum_{t=1}^{n} \left(x_{t-2} - \mu_{moving}, x_{t-1} - \mu_{moving}, x_t - \mu_{moving}, x_{t+1} - \mu_{moving}, x_{t+2} - \mu_{moving}, \right)^2 \right)^{\frac{1}{2}}. \quad (39)$$

The assumptions made in utilizing Equations (38) and (39) are that the data is not experiencing a large change with time during the steady-state regions and that the natural variance in the data between tests would be larger in the transient regions, not explicitly due to the large change with respect to time, but purely due to the large transients providing an opportunity for potential differences.

One important difference to note between these efforts and those of A. Doty is that in his study, 3 inputs to the system were fixed values and only 1 input was a function of time that experienced a large transient. In this study, the experiment has 4 major inputs: two inlet temperatures and two mass flow rates. One inlet temperature is the main driver and experiences the large transient temperature change, while the other inlet temperature is ideally held at a constant temperature. In reality, due to the nature of the experiment in the laboratory environment, the inlet temperature does not stay constant over the duration of the experiment; therefore, all values are recorded as a function of time to reproduce the signal as closely as possible. The mass flow rates are intended to be constant during all tests; however, due to the nature of the experimental setup, they experience relatively small fluctuations with time. As the impact of these fluctuations will not be known until after the data is collected and processed, it was deemed necessary to treat the flow rates as transient variables. This indicates that all outputs from these

efforts, both experimental and computational, are going to have uncertainties that change as functions of time.

As applied to this specific thermal fluids problem, there are two main SRQs of interest: the output temperature from the shell side of the heat exchanger, $T_{s,o}(t)$, and the output temperature from the tube side of the heat exchanger, $T_{t,o}(t)$. The four major inputs to the system are the inlet temperature on the shell side of the heat exchanger, $T_{s,i}(t)$, the inlet temperature on the tube side of the heat exchanger, $T_{t,i}(t)$, and the mass flow rates on the shell and tube side, $\dot{m}_s(t)$ and $\dot{m}_t(t)$, respectively. This is shown as

$$T_{s,o}(t) = f\big(\dot{m}_s(t), \dot{m}_t(t), T_{s,i}(t), T_{t,i}(t)\big) \tag{40}$$

$$T_{t,o}(t) = f\big(\dot{m}_s(t), \dot{m}_t(t), T_{s,i}(t), T_{t,i}(t)\big)\,. \tag{41}$$

According to Equations (37), (40), and (41), above, it will be necessary to calculate the following partial derivatives for the shell outlet temperature

$$\frac{\partial T_{s,o}}{\partial \dot{m}_s} = \frac{dT_{s,o}}{dt} * \frac{dt}{d\dot{m}_s}, \tag{42}$$

$$\frac{\partial T_{s,o}}{\partial \dot{m}_t} = \frac{dT_{s,o}}{dt} * \frac{dt}{d\dot{m}_t}, \tag{43}$$

$$\frac{\partial T_{s,o}}{\partial T_{s,i}} = \frac{dT_{s,o}}{dt} * \frac{dt}{dT_{s,i}}, \tag{44}$$

$$\frac{\partial T_{s,o}}{\partial T_{t,i}} = \frac{dT_{s,o}}{dt} * \frac{dt}{dT_{t,i}}\,. \tag{45}$$

Similarly, the partial derivatives required for the tube outlet temperature will be

$$\frac{\partial T_{t,o}}{\partial \dot{m}_s} = \frac{dT_{t,o}}{dt} * \frac{dt}{d\dot{m}_s}, \tag{46}$$

$$\frac{\partial T_{t,o}}{\partial \dot{m}_t} = \frac{dT_{t,o}}{dt} * \frac{dt}{d\dot{m}_t}, \tag{47}$$

$$\frac{\partial T_{t,o}}{\partial T_{s,i}} = \frac{dT_{t,o}}{dt} * \frac{dt}{dT_{s,i}}, \tag{48}$$

$$\frac{\partial T_{t,o}}{\partial T_{t,i}} = \frac{dT_{t,o}}{dt} * \frac{dt}{dT_{t,i}}. \tag{49}$$

With these partial derivatives calculated, it is now possible to define the sensitivities required for both the shell and tube outlet temperatures. For the shell side, the sensitivities are

$$\left\{Sen_{T_{s,o}}^{\dot{m}_s}\right\} = \frac{\sigma_{\dot{m}_s}}{\sigma_{T_{s,o}}} * \frac{\partial T_{s,o}}{\partial \dot{m}_s}, \tag{50}$$

$$\left\{Sen_{T_{s,o}}^{\dot{m}_t}\right\} = \frac{\sigma_{\dot{m}_t}}{\sigma_{T_{s,o}}} * \frac{\partial T_{s,o}}{\partial \dot{m}_t}, \tag{51}$$

$$\left\{Sen_{T_{s,o}}^{T_{s,i}}\right\} = \frac{\sigma_{T_{s,i}}}{\sigma_{T_{s,o}}} * \frac{\partial T_{s,o}}{\partial T_{s,i}}, \tag{52}$$

$$\left\{Sen_{T_{s,o}}^{T_{t,i}}\right\} = \frac{\sigma_{T_{t,i}}}{\sigma_{T_{s,o}}} * \frac{\partial T_{s,o}}{\partial T_{t,i}}. \tag{53}$$

For the tube side, the sensitivities are

$$\left\{Sen_{T_{t,o}}^{\dot{m}_s}\right\} = \frac{\sigma_{\dot{m}_s}}{\sigma_{T_{t,o}}} * \frac{\partial T_{t,o}}{\partial \dot{m}_s}, \tag{54}$$

$$\left\{Sen_{T_{t,o}}^{\dot{m}_t}\right\} = \frac{\sigma_{\dot{m}_t}}{\sigma_{T_{t,o}}} * \frac{\partial T_{t,o}}{\partial \dot{m}_t}, \tag{55}$$

$$\left\{Sen_{T_{t,o}}^{T_{s,i}}\right\} = \frac{\sigma_{T_{s,i}}}{\sigma_{T_{t,o}}} * \frac{\partial T_{t,o}}{\partial T_{s,i}}, \tag{56}$$

$$\left\{Sen_{T_{t,o}}^{T_{t,i}}\right\} = \frac{\sigma_{T_{t,i}}}{\sigma_{T_{t,o}}} * \frac{\partial T_{t,o}}{\partial T_{t,i}}. \tag{57}$$

Uncertainty Analysis / Uncertainty Propagation

Once the sensitivities and standard deviations of the input variables and output SRQs have been calculated, it is possible to continue with the propagation of uncertainty. Uncertainty propagation is how to determine the effect of the uncertainty of the inputs on the outputs of the system. The uncertainty is actually propagated as the uncertainty squared, or the variance of the inputs. This is represented as

$$\sigma_{x_i \to SRQ_k}^2 = \left[\left(Sen_{x_i}^{SRQ_k}\right)\right]^2 \left(\sigma_{x_i}^2\right). \tag{58}$$

Making the substitution for sensitivity as suggested by the IPCC[27] as it is defined above in Equation (36), the propagated variance becomes

$$\sigma_{x_i \to SRQ_k}^2 = \left[\left(\frac{\sigma_{x_i}}{\sigma_{SRQ_k}}\right)\left(\frac{\partial SRQ_k}{\partial x_i}\right)\right]^2 \left(\sigma_{x_i}^2\right). \tag{59}$$

Substituting the expressions for the shell outlet temperatures into Equation (59) yields

$$\sigma_{\dot{m}_s \to T_{s,o}}^2 = \left[\left(\frac{\sigma_{\dot{m}_s}}{\sigma_{T_{s,o}}}\right)\left(\frac{\partial T_{s,o}}{\partial \dot{m}_s}\right)\right]^2 \left(\sigma_{\dot{m}_s}^2\right), \tag{60}$$

$$\sigma_{\dot{m}_t \to T_{s,o}}^2 = \left[\left(\frac{\sigma_{\dot{m}_t}}{\sigma_{T_{s,o}}}\right)\left(\frac{\partial T_{s,o}}{\partial \dot{m}_t}\right)\right]^2 \left(\sigma_{\dot{m}_t}^2\right), \tag{61}$$

$$\sigma_{T_{s,i} \to T_{s,o}}^2 = \left[\left(\frac{\sigma_{T_{s,i}}}{\sigma_{T_{s,o}}}\right)\left(\frac{\partial T_{s,o}}{\partial T_{s,i}}\right)\right]^2 \left(\sigma_{T_{s,i}}^2\right), \tag{62}$$

$$\sigma_{T_{t,i} \to T_{s,o}}^2 = \left[\left(\frac{\sigma_{T_{t,i}}}{\sigma_{T_{s,o}}}\right)\left(\frac{\partial T_{s,o}}{\partial T_{t,i}}\right)\right]^2 \left(\sigma_{T_{t,i}}^2\right). \tag{63}$$

The equations that represent the tube outlet temperature are similar to Equations (60) through (63); they only differ by substituting the tube outlet temperature, $T_{t,o}$, in as the SRQ variable:

$$\sigma^2_{\dot{m}_s \to T_{t,o}} = \left[\left(\frac{\sigma_{\dot{m}_s}}{\sigma_{T_{t,o}}}\right)\left(\frac{\partial T_{t,o}}{\partial \dot{m}_s}\right)\right]^2 \left(\sigma^2_{\dot{m}_s}\right), \tag{64}$$

$$\sigma^2_{\dot{m}_t \to T_{t,o}} = \left[\left(\frac{\sigma_{\dot{m}_t}}{\sigma_{T_{t,o}}}\right)\left(\frac{\partial T_{t,o}}{\partial \dot{m}_t}\right)\right]^2 \left(\sigma^2_{\dot{m}_t}\right), \tag{65}$$

$$\sigma^2_{T_{s,i} \to T_{t,o}} = \left[\left(\frac{\sigma_{T_{s,i}}}{\sigma_{T_{t,o}}}\right)\left(\frac{\partial T_{t,o}}{\partial T_{s,i}}\right)\right]^2 \left(\sigma^2_{T_{s,i}}\right), \tag{66}$$

$$\sigma^2_{T_{t,i} \to T_{t,o}} = \left[\left(\frac{\sigma_{T_{t,i}}}{\sigma_{T_{t,o}}}\right)\left(\frac{\partial T_{t,o}}{\partial T_{t,i}}\right)\right]^2 \left(\sigma^2_{T_{t,i}}\right). \tag{67}$$

When examining the results of the propagated uncertainties, it is necessary to remove the square of the standard deviation as the uncertainties are not presented in terms of the variance that is propagated. Taking the square root of each side of Equation (58) yields

$$\sigma_{x_i \to SRQ_k} = \sqrt{\left[\left(Sen^{SRQ_k}_{x_i}\right)\right]^2 \left(\sigma^2_{x_i}\right)}. \tag{68}$$

The square root here must be positive definite. To maintain this requirement, an absolute value must be introduced as

$$\sigma_{x_i \to SRQ_k} = + \left|\left(\frac{\sigma_{x_i}}{\sigma_{SRQ_k}}\right)\left(\frac{\partial SRQ_k}{\partial x_i}\right)\right| \sigma_{x_i}. \tag{69}$$

For the final form of Equation (69), the absolute value can be isolated to the partial derivative, as the uncertainties will be positive values. The result is the final form of the propagated uncertainty as

$$\sigma_{x_i \to SRQ_k} = + \left(\frac{\sigma^2_{x_i}}{\sigma_{SRQ_k}}\right)\left|\left(\frac{\partial SRQ_k}{\partial x_i}\right)\right|. \tag{70}$$

Making the necessary substitutions into Equation (70) for the inputs and SRQs yields the following equations for the propagated uncertainties for the shell outlet temperature

$$\sigma_{\dot{m}_s \to T_{s,o}} = + \left(\frac{\sigma_{\dot{m}_s}^2}{\sigma_{T_{s,o}}} \right) \left| \left(\frac{\partial T_{s,o}}{\partial \dot{m}_s} \right) \right|, \tag{71}$$

$$\sigma_{\dot{m}_t \to T_{s,o}} = + \left(\frac{\sigma_{\dot{m}_t}^2}{\sigma_{T_{s,o}}} \right) \left| \left(\frac{\partial T_{s,o}}{\partial \dot{m}_t} \right) \right|, \tag{72}$$

$$\sigma_{T_{s,i} \to T_{s,o}} = + \left(\frac{\sigma_{T_{s,i}}^2}{\sigma_{T_{s,o}}} \right) \left| \left(\frac{\partial T_{s,o}}{\partial T_{s,i}} \right) \right|, \tag{73}$$

$$\sigma_{T_{t,i} \to T_{s,o}} = + \left(\frac{\sigma_{T_{t,i}}^2}{\sigma_{T_{s,o}}} \right) \left| \left(\frac{\partial T_{s,o}}{\partial T_{t,i}} \right) \right|. \tag{74}$$

Similarly, the equations for the propagated uncertainties for the tube outlet temperature

$$\sigma_{\dot{m}_s \to T_{t,o}} = + \left(\frac{\sigma_{\dot{m}_s}^2}{\sigma_{T_{t,o}}} \right) \left| \left(\frac{\partial T_{t,o}}{\partial \dot{m}_s} \right) \right|, \tag{75}$$

$$\sigma_{\dot{m}_t \to T_{t,o}} = + \left(\frac{\sigma_{\dot{m}_t}^2}{\sigma_{T_{t,o}}} \right) \left| \left(\frac{\partial T_{t,o}}{\partial \dot{m}_t} \right) \right|, \tag{76}$$

$$\sigma_{T_{s,i} \to T_{t,o}} = + \left(\frac{\sigma_{T_{s,i}}^2}{\sigma_{T_{t,o}}} \right) \left| \left(\frac{\partial T_{t,o}}{\partial T_{s,i}} \right) \right|, \tag{77}$$

$$\sigma_{T_{t,i} \to T_{t,o}} = + \left(\frac{\sigma_{T_{t,i}}^2}{\sigma_{T_{t,o}}} \right) \left| \left(\frac{\partial T_{t,o}}{\partial T_{t,i}} \right) \right|. \tag{78}$$

Verification

There are two main steps in the verification process: verification of the code and calculation verification. Verification of the code is to ensure that no errors were made

when translating the chosen mathematical formulae to the model format. Calculation verification entails estimating round-off and discretization errors. Discretization errors arise when continuous functions are estimated using small, piece-wise representative sections. All digital calculations are completed using some level of discretization; fortunately, the smallest increment that can be computed is extremely small. For a 64-bit installation of Matlab, the smallest change in double precision floating point numbers that is recognized is on the order of 10^{-16}. Furthermore, each numerical value is stored using 1 of the 64 bits available to designate whether the value is positive or negative and the rest are used to represent the value in scientific notation; of these remaining bits, 52 are reserved for significant digits and 11 are for the exponent.[28] With the high level of precision afforded by using floating point numbers in all calculations, the discretization error can effectively be ignored.

Validation

Validation is the act of determining the degree to which the experimental and computational data agree with each other. This metric could be calculated in various ways. A basic way to evaluate this metric could be merely to include a confidence interval along with an answer. The confidence interval is provided with a percentage and indicates how sure the researcher is that the true value falls within the provided range. For example, if the range is given as a 95% confidence interval, this means that the researcher is 95% sure that the true mean falls within the given range. As this technique is dependent upon having the data, it merely is a way to be sure where the mean of the data truly lies, not that the mean of the generated data is accurate, as in the case of model

generated data. The confidence interval technique requires knowledge of the standard deviation of multiple data points in order to calculate, and as such, is useful for steady state calculations. In the event of highly dynamic data, like transients, this technique could be used across replicate data sets for the same points in time.

Another means of validation is the Absolute Area Deviation (AAD) technique that was briefly discussed earlier, developed by Roy & Oberkampf[29]. The AAD essentially computes the discrete area between two data sets. This is calculated as

$$\text{AAD} = \sum_{i=1}^{n} |T_{experiment,i} - T_{model,i}| \Delta t \tag{79}$$

and is represented by absolute values of the difference from experimental and computational data such that any deviation from the data sets, either above or below, will be added as a cumulative error.

This technique provides a very useful qualitative measurement of agreement between data sets as a discrete value is generated that represents the amount of disagreement. With improvements to the model methodology, it is possible to directly measure improvements to the outputs via a reduction in AAD. This way to measure agreement between data sets for continuous improvements is useful, but it is not a statistical measure of agreement.

An example of a statistically based validation metric is the Anderson-Darling k-sample test. This test was developed based on the Anderson-Darling test, which attempts to answer whether the provided subset of data possibly came from a population with a normal distribution. The test is more sensitive to outliers, and therefore, detects departure

from normality more closely than other typical statistical measurements.[30] In its modified k-sample form, the test utilizes the comparative power of the Anderson-Darling test to determine if it is possible that two subsets of data may have been generated from the same population of data. The Anderson-Darling k-sample test is expressed as

$$n\int_{-\infty}^{\infty}\frac{\{F_{n_i}(x)-H_N(x)\}^2}{H_N(x)\{1-H_N(x)\}}dH_N(x). \tag{80}$$

The Anderson-Darling test statistic is expressed as

$$A_n^2=-n-\sum_{i=1}^{n}\frac{2i-1}{n}\left[\ln\left(F(X_i)\right)+\ln\left(1-F(X_{n+1-i})\right)\right]. \tag{81}$$

With this test metric, it is possible to test sets of data, or to compare individual data points. In this study, the Anderson-Darling k-sample test will be applied to two subsets of data: experimentally gathered data and predicted outputs from the model designed to represent the experiment.[31]

RESULTS & DISCUSSION

The desired SRQ's from the model are the shell and tube outlet temperatures. These temperatures were measured directly during experimentation with the thermal emulator and were calculated using the Simulink model developed above. There were a total of 63 cases that were run, as defined above in Table 8. The inputs to the thermal emulator, the inlet temperature and flow rates, were measured and used as time varying inputs to the model for a direct comparison. As part of the code verification process, the equations used in the model were checked and verified; model outputs were then compared to experimental outputs by running a sample case. This sample case was able to verify that the model results agreed favorably with the experimental results. These results are seen below in Figure 11.

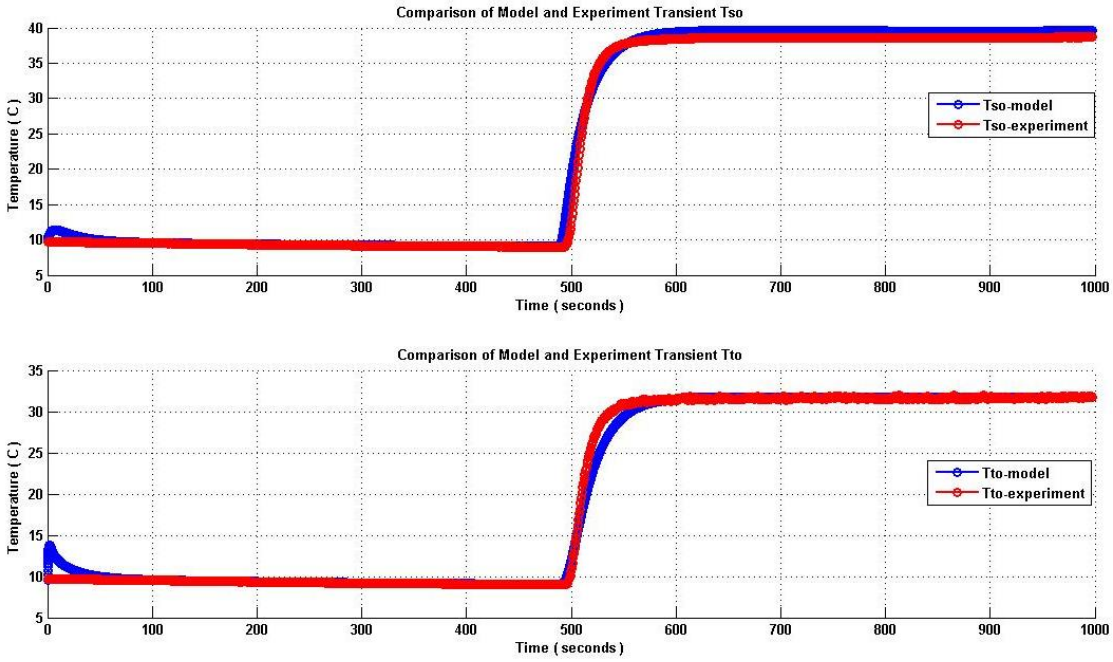

Figure 11: Comparison of shell and tube outlet temperatures, during code verification

Once the code verification was complete and the model was calibrated using the experimental data, steady-state output temperatures for the shell and tube fluid streams were compared to the steady-state values recorded from the thermal emulator experiments. These comparisons are found below.

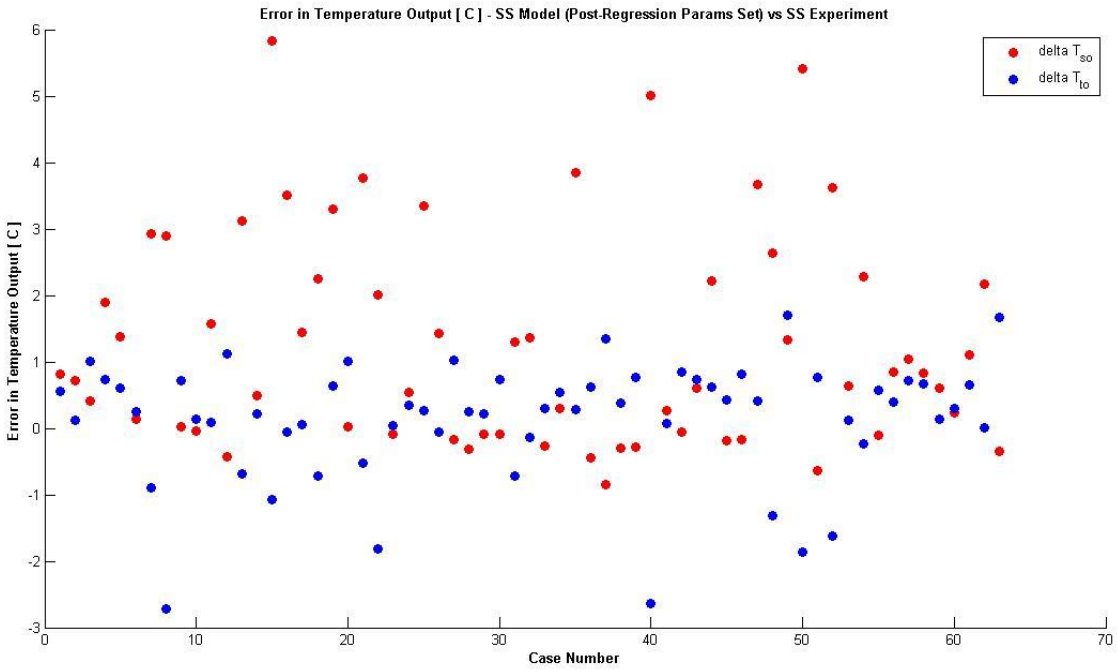

Figure 12: Steady-state outlet temperatures, model vs. experiment

Figure 12 shows that the majority of the differences in outlet temperatures are near 0, indicating small differences for the steady-state outputs. The maximum difference is found on the shell outlet from the model for Case 15, where it over predicts the temperature by about 5.7 °C. In contrast, the tube side has the maximum under predicted temperature for Case 8, with a temperature about 2.9 °C cooler than the experiment.

For the following results, emphasis will be placed on the results from the shell side as it is the side that contained the lubricating oil in the AFRL test loop. The tube

side was considered to be less important as it merely dumped heated water to the drain. More specifically, three different cases of data will be presented. Out of the entire test matrix, these three test cases represent the maximum over prediction of the shell outlet temperature, the maximum under prediction, and the case where the final temperature was the closest. Due to the fact that the transient change in the model started before the change in the experimental data, the only transient cases that can be analyzed are

1.) When the model is initially over predicting the temperature (all cases) and continues to over predict the temperature once the it has reached steady-state, and

2.) When the model is initially over predicting the temperature (all cases) and then under predicts the temperature once it has reached steady-state.

Both of these transient scenarios are encompassed by the three cases chosen for presentation.

Standard Deviations

The standard deviation of the data was required in order to properly calculate the sensitivities of the SRQ's to the inputs. Typically, this is completed by simply calculating the standard deviation across the replicate data sets. For the thermal fluids problem, since the transient region is under scrutiny, these standard deviations would normally be calculated at each point in time across all data sets. Due to the limited data that is provided, another technique was used to estimate what the standard deviation would be with replicate data. This was completed by calculating the standard deviation across a moving average window. The moving average window is denoted by Equation (38). This technique was used to estimate the replicate standard deviations due to the

lack of replicate data as well as the fact that the time constant of the system is rather large when compared to other systems such as those in previous works.[2] With a large time constant, it is possible to collect a large number of data points during the transient portion of the physical process. If fewer data points were collected, it may be unfeasible to truly capture the spread of the data in the transient section. An assumption that is made in utilizing this technique is that for replicate data, the bulk of the deviations would exist in the transient region and that the steady-state would still converge to the same value for separate runs.

The relevant standard deviations for the system inputs and outputs were computed using this moving average technique. This encompassed the standard deviations for the mass flow rate and the inlet temperature for both the shell and tube side, as well as the outlet temperatures for both the shell and tube. Case 15 highlights the scenario when the shell side temperature was over predicted the most out of all cases. The standard deviations for the mass flow rates for both the shell and tube sides of the heat exchanger, the inlet temperatures, and the outlet temperatures are shown below for Case 15.

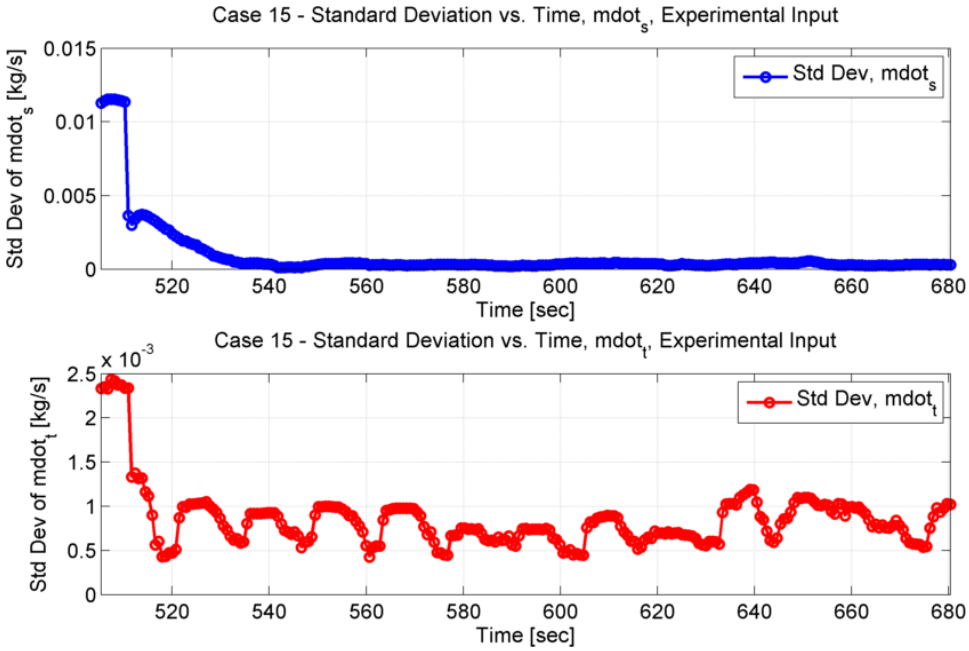

Figure 13: Case 15, Standard Deviation vs. Time for Mass Flow Rates

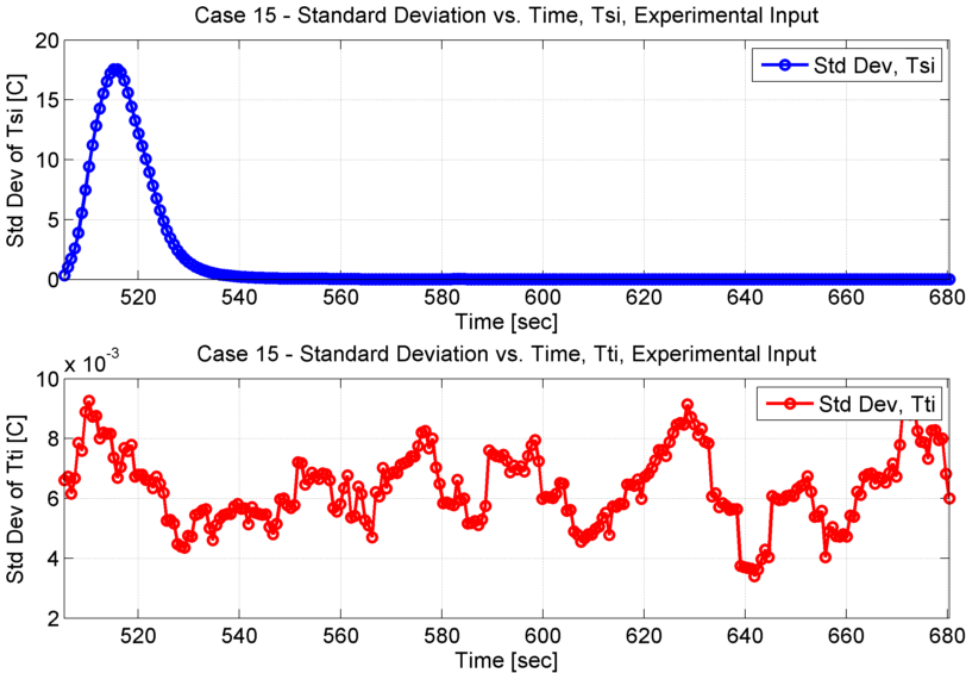

Figure 14: Case 15, Standard Deviation vs. Time for Temperature, Inlets

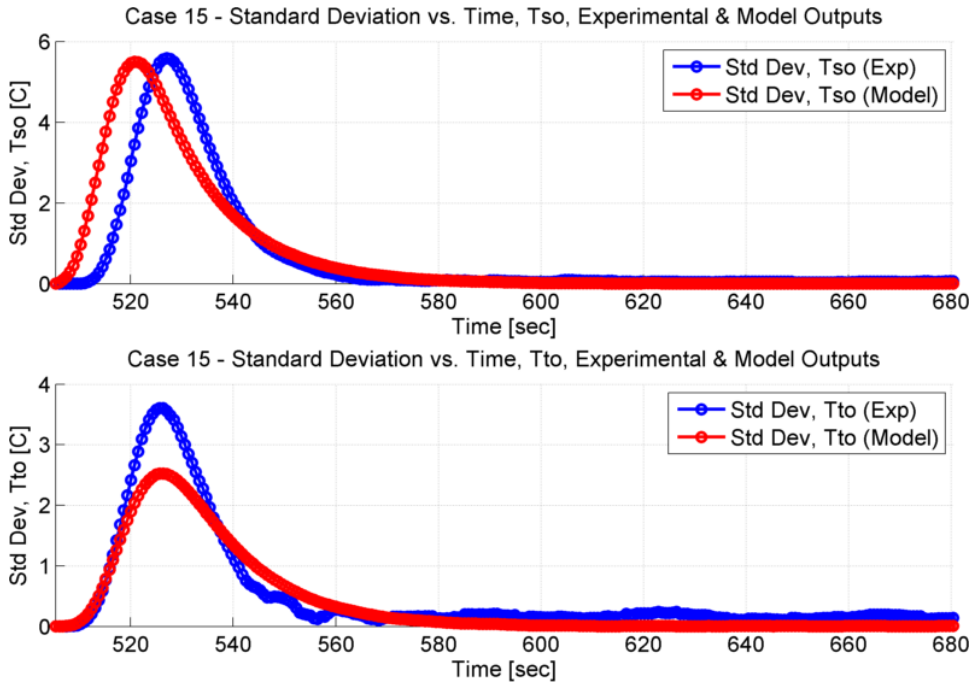

Figure 15: Case 15, Standard Deviation vs. Time for Temperature, Outlets

The standard deviations of the mass flow rates for the shell and the tube fluctuate, but overall, the magnitude of the fluctuations is small, on the order of 1E-3. The initial transient region experiences a larger standard deviation than the steady-state region, as is expected, but it is still the same order of magnitude. The differences in the consistency of the flow rates for both sides of the heat exchanger are especially highlighted in these plots. The shell side water was pumped from a reservoir where the only thing affecting the pressure and flow readings was the gradual change of the water height in the tanks. For the tube side, the water came directly from the laboratory water supply that was provided by the building. Due to this different water source, the experimental data was susceptible to pressure and flow variations that existed due to the water usage within the building.

For the inlet temperatures, the standard deviations begin to differ between the shell and tube. Specifically, there is little deviation for the tube inlet temperature, much like the mass flow rates. This is to be expected as the mass flow rates and the tube inlet temperature were all held as close to constant as was feasible. The shell inlet temperature, however, experiences a large spike in the standard deviation when the step change in temperature is induced. This is also as expected due to the large change in temperature that occurs over a relatively short period of time. This large deviation in the inlet temperature on the shell side is then seen on the outlet temperature for both the shell and tube as well.

Case 37 highlights the scenario when the shell side temperature was under predicted the most out of all cases. The standard deviations for the mass flow rates for both the shell and tube sides of the heat exchanger, the inlet temperatures, and the outlet temperatures are shown below for Case 37.

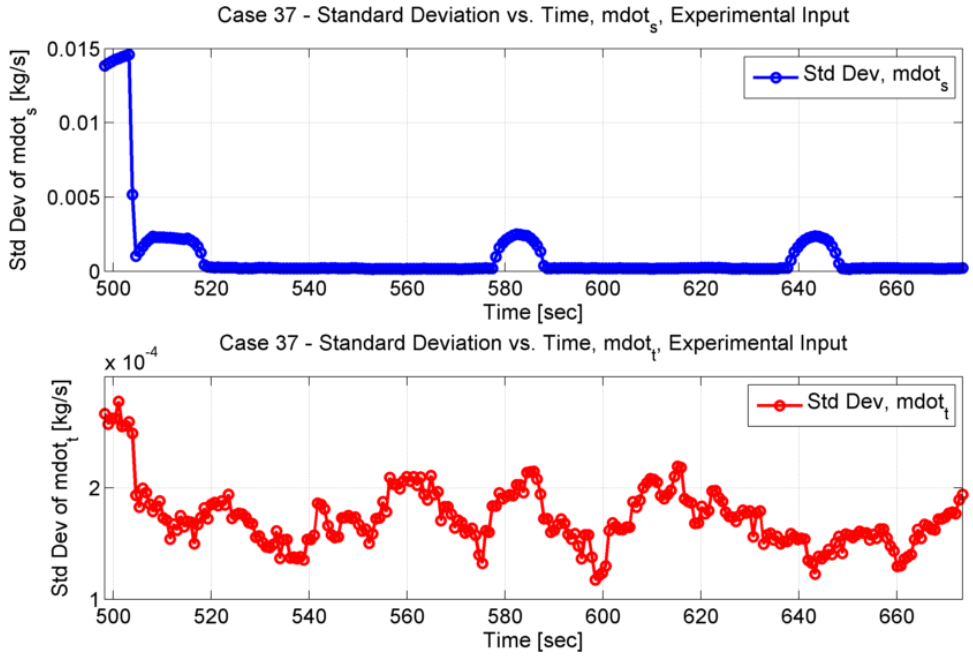

Figure 16: Case 37, Standard Deviation vs. Time for Mass Flow Rates

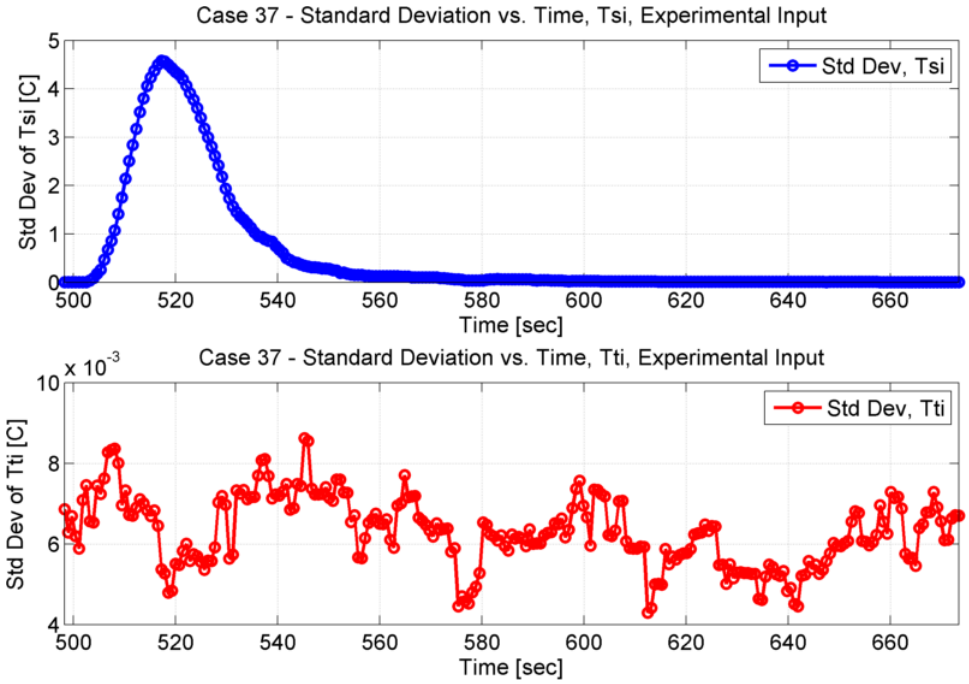

Figure 17: Case 37, Standard Deviation vs. Time for Temperature, Inlets

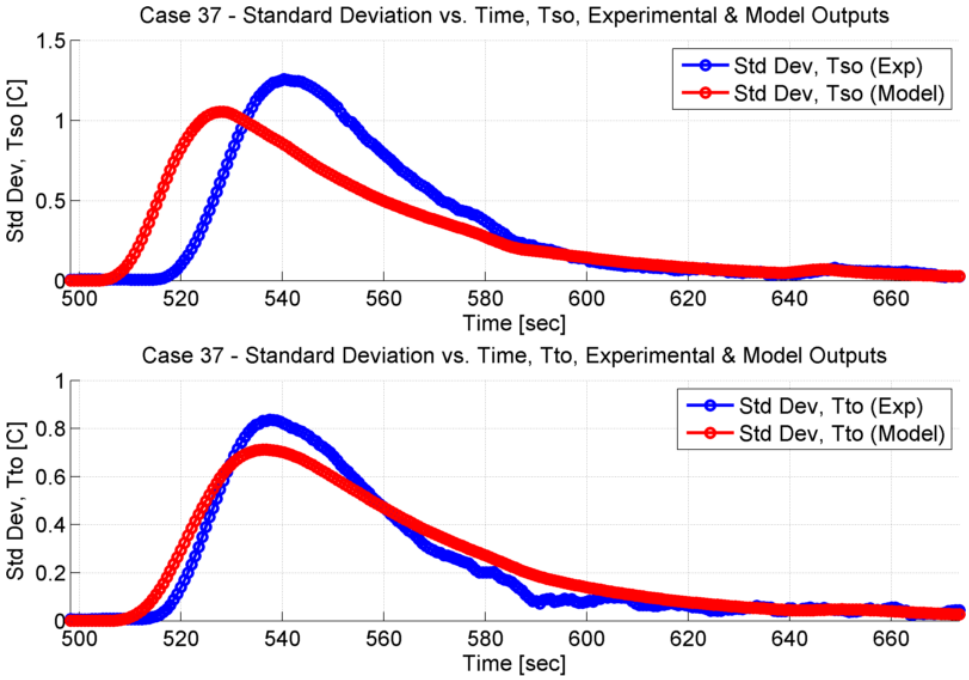

Figure 18: Case 37, Standard Deviation vs. Time for Temperature, Outlets

Much like Case 15, the standard deviations on the mass flow rates for the shell and the tube have small fluctuations for Case 37. An initial spike in deviations is found on the shell side as the flow rate step change is introduced, but this deviation then returns to a negligible value. For the inlet temperatures, again, the shell has a large spike due to the large transient change in temperature, where the tube side has very little deviation due to the nearly constant inlet temperature. The deviations on the shell side are a very smooth and gradual increase and subsequent decrease; this is largely in part due to the relatively large time constant of the heat exchanger system. The tube side inlet temperature fluctuations are all small, on the order of 1E-3. These measurements are expected to be small since the tube inlet temperature is essentially held to a constant. The large deviation that is seen on the inlet temperature for the shell side is again found on the outlet temperature of the shell side, but this time the deviations take longer to gradually respond due to the effect of the mass of the heat exchanger. The outlet temperature on the shell side now sees a similar trend as the tube outlet temperature in that it gradually increases and then decreases, but on the same time scale as the shell outlet temperature.

Finally, Case 42 highlights the scenario when the shell outlet temperatures aligned the closest out of all of the cases. The relevant standard deviation plots are shown below.

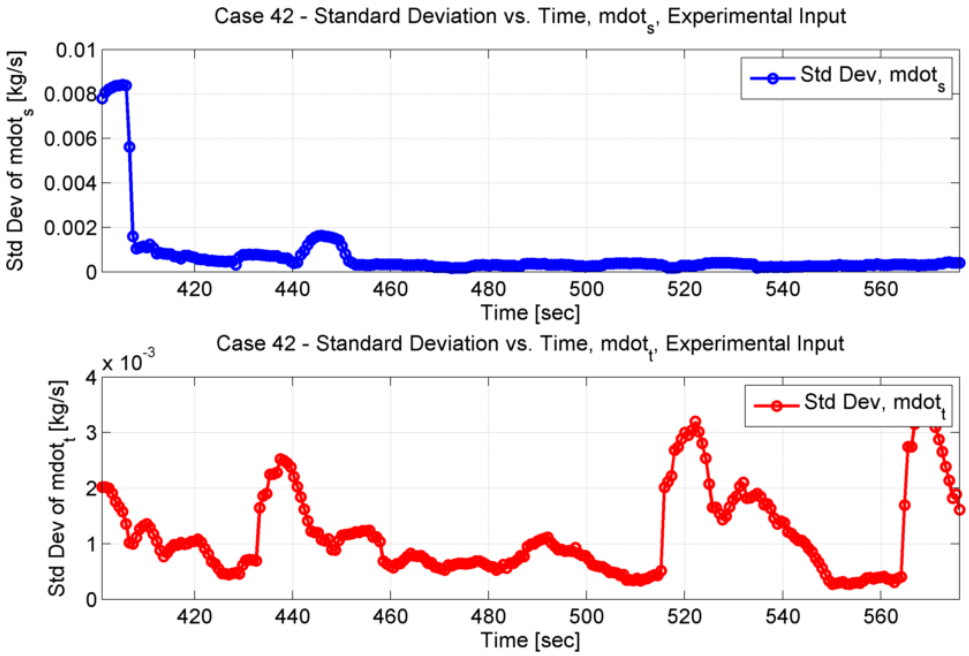

Figure 19: Case 42, Standard Deviation vs. Time for Mass Flow Rates

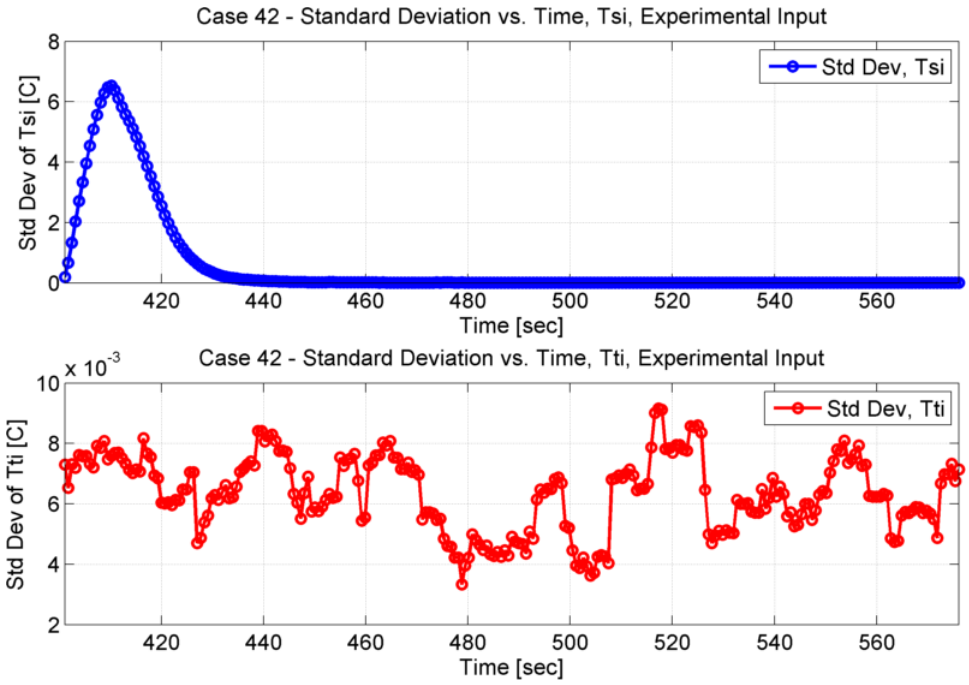

Figure 20: Case 42, Standard Deviation vs. Time for Temperature, Inlets

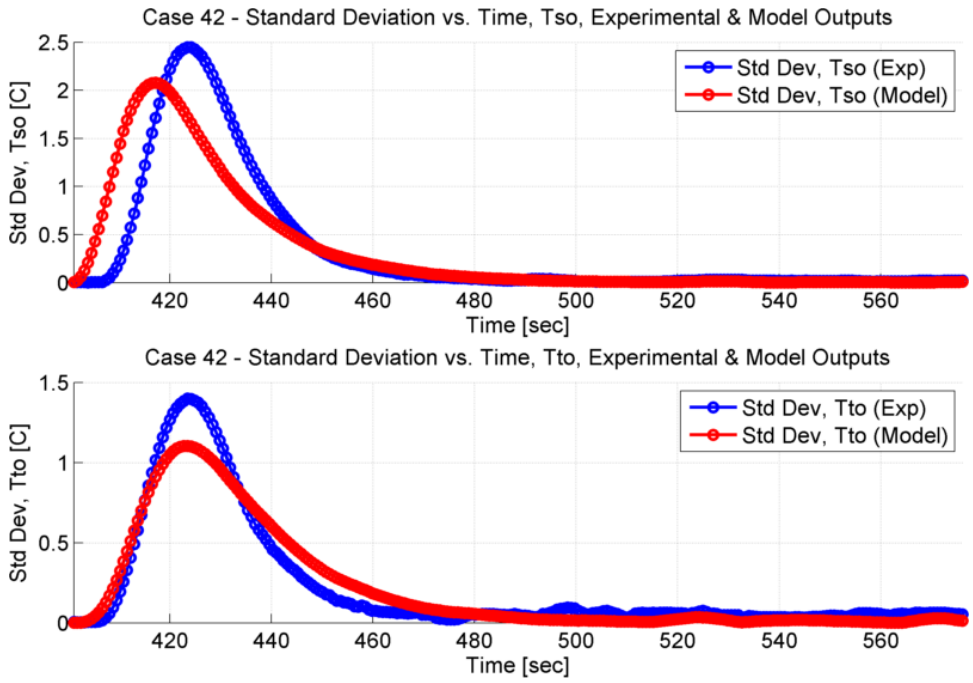

Figure 21: Case 42, Standard Deviation vs. Time for Temperature, Outlets

The standard deviations for Case 42 exhibit the same trends as Cases 15 and 37. Of these trends, one important aspect to note is that for the outlet temperatures, the standard deviations for the experimental data all tend to lag behind those of the model. This trend is a direct result of the same trend that is seen at the inlet for both the experiment and the model; this is discussed in more detail when the output temperatures are compared along with the calculated error.

Sensitivity Analysis

To reiterate, the sensitivity analysis provides a means to determine which input parameter has the largest effect on the desired SRQ's, specifically, with respect to uncertainties. Several other quantities are required in order to complete the sensitivity analysis; these include the standard deviations calculated previously, as well as partial

derivatives of the SRQ's with respect to each inlet parameter. The equations that are used to represent the sensitivity are again called out here for simplicity.

$$\left\{Sen_{SRQ_k}^{x_i}\right\}_{\sigma_{SRQ_k}} \approx \frac{\sigma_{x_i}}{\sigma_{SRQ_k}} * \frac{\partial SRQ_k}{\partial x_i} \tag{82}$$

$$\frac{\partial SRQ_k}{\partial x_i} = \frac{dSRQ_k}{dt} * \frac{dt}{dx_i}, \tag{83}$$

Equation (82) outlines the parameters required to calculate the sensitivity. Specifically, the partial derivative of the SRQ with respect to the inlet variable can be difficult to determine. As such, Equation (83) is utilized; the partials can be determined easily after calculating the derivative with respect to time of each SRQ, as well as each input variable. This means that for the sensitivities of each output temperature, there will be 4 required sensitivities as there are 4 inputs to the system: shell and tube mass flow rates and inlet temperatures for both.

The results will be presented with all inputs affecting the same output variable together for each case; the focus will be the sensitivity of each input from both shell and tube sides on the shell output temperature. The sensitivities of the input variables on the tube outlet temperature experience similar trends as those for the shell outlet temperature, but for completeness, the results are provided in APPENDIX D: RESULTS. First, the equations used to calculate the sensitivity of the inlet variables, shell and tube mass flow rates and shell and tube inlet temperatures, on the shell outlet temperatures are repeated and the results are shown below in Figure 22 and Figure 23.

$$\left\{Sen_{T_{s,o}}^{\dot{m}_s}\right\} = \frac{\sigma_{\dot{m}_s}}{\sigma_{T_{s,o}}} * \frac{\partial T_{s,o}}{\partial \dot{m}_s}, \tag{84}$$

$$\left\{Sen_{T_{s,o}}^{\dot{m}_t}\right\} = \frac{\sigma_{\dot{m}_t}}{\sigma_{T_{s,o}}} * \frac{\partial T_{s,o}}{\partial \dot{m}_t}, \tag{85}$$

$$\left\{Sen_{T_{s,o}}^{T_{s,i}}\right\} = \frac{\sigma_{T_{s,i}}}{\sigma_{T_{s,o}}} * \frac{\partial T_{s,o}}{\partial T_{s,i}}, \tag{86}$$

$$\left\{Sen_{T_{s,o}}^{T_{t,i}}\right\} = \frac{\sigma_{T_{t,i}}}{\sigma_{T_{s,o}}} * \frac{\partial T_{s,o}}{\partial T_{t,i}}. \tag{87}$$

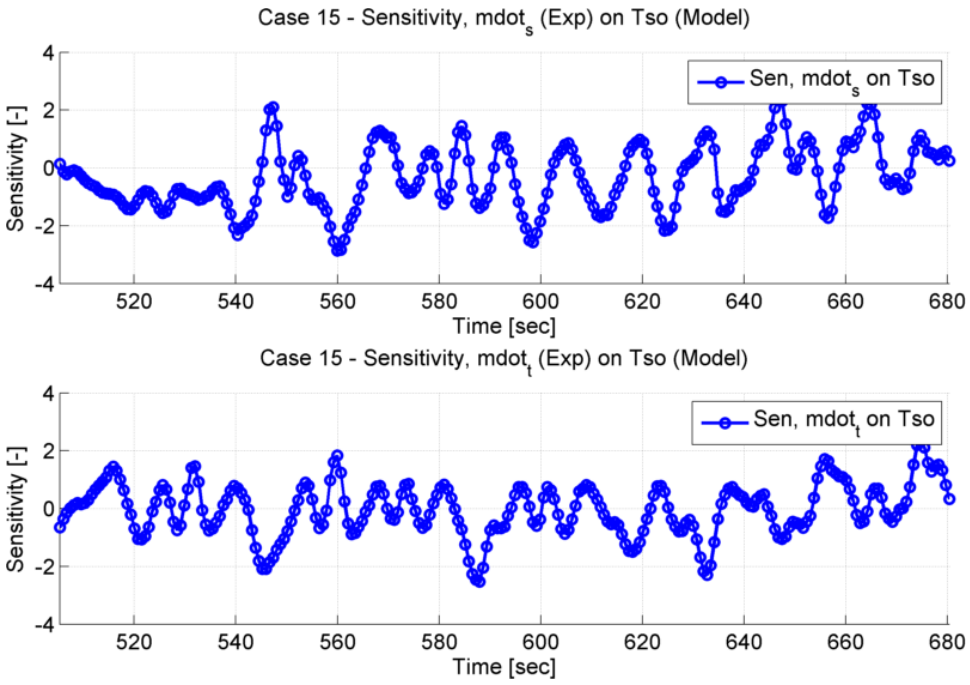

Figure 22: Case 15, Sensitivity of Mass Flow Rates on Shell Outlet Temperature vs. Time

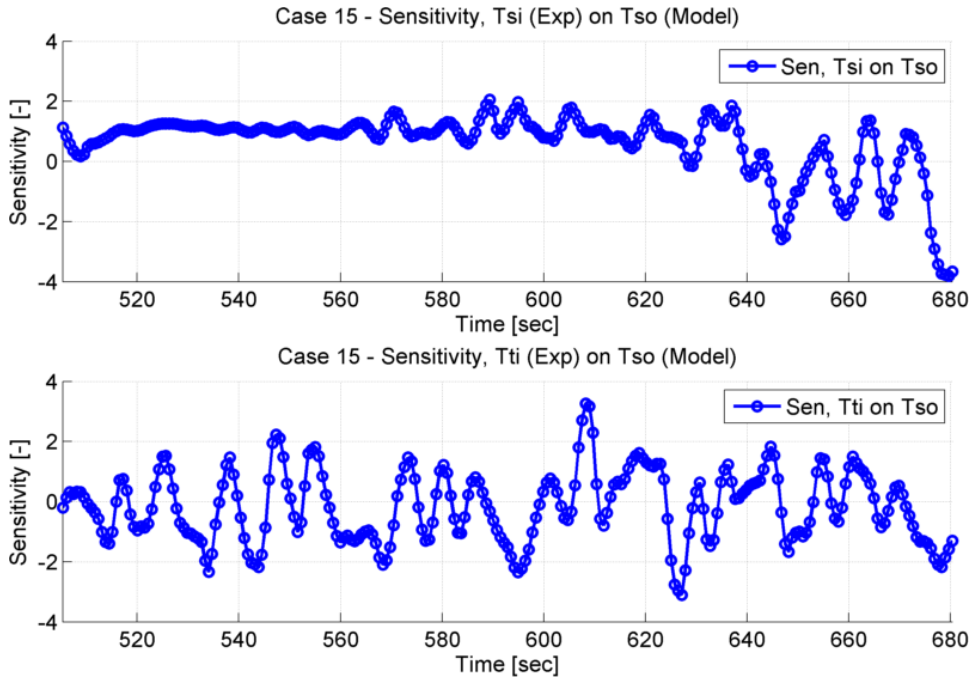

Figure 23: Case 15, Sensitivity of Inlet Temperatures on Shell Outlet Temperature vs. Time

For Case 15, the case where the shell outlet temperature was over predicted the most, it is seen that the sensitivity of the input variables to the system have generally the same effect on the shell outlet temperature. All variations are of the same order of magnitude and seem to randomly fluctuate between the negative and positive values. One interesting difference to note is with the sensitivity of the shell inlet temperature on the shell outlet temperature: the first half of the plot shows a fairly stable positive sensitivity before the data begins to show the same type of random variation that the other inputs show. This would indicate that the variable that the shell outlet temperature is most sensitive to is the shell inlet temperature; thus it is possible to tell that the actual temperature of the shell stream coming into the heat exchanger does affect the shell outlet temperature.

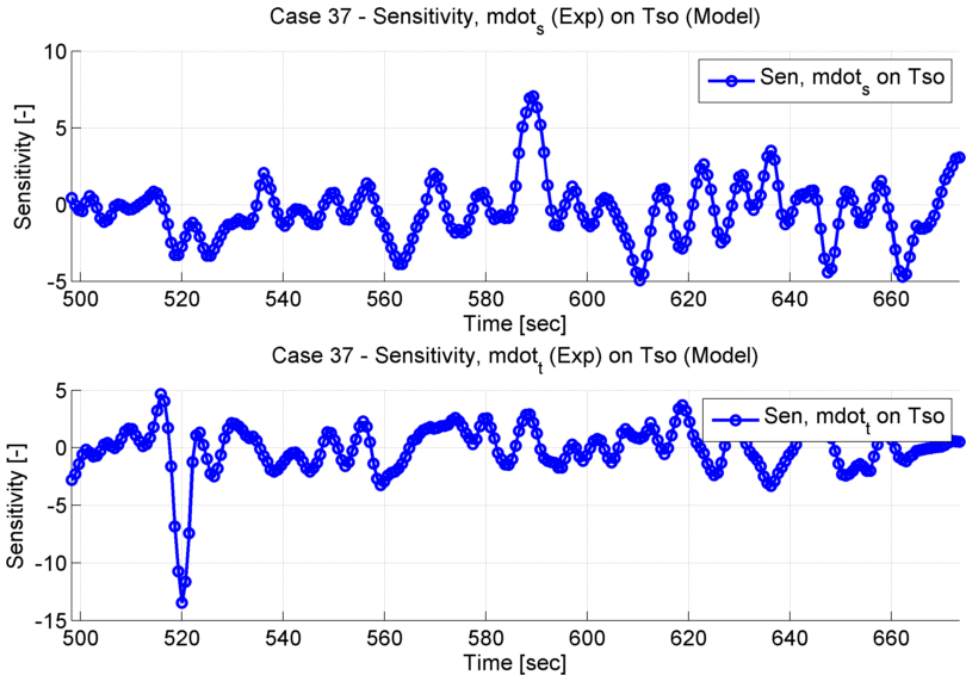

Figure 24: Case 37, Sensitivity of Mass Flow Rates on Shell Outlet Temperature vs. Time

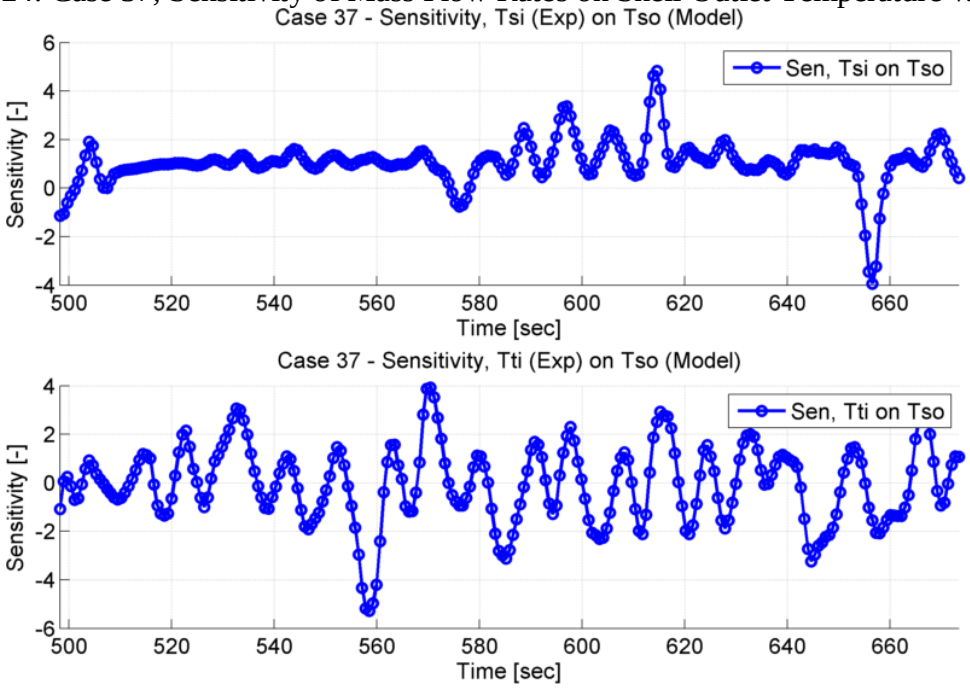

Figure 25: Case 37, Sensitivity of Inlet Temperatures on Shell Outlet Temperature vs. Time

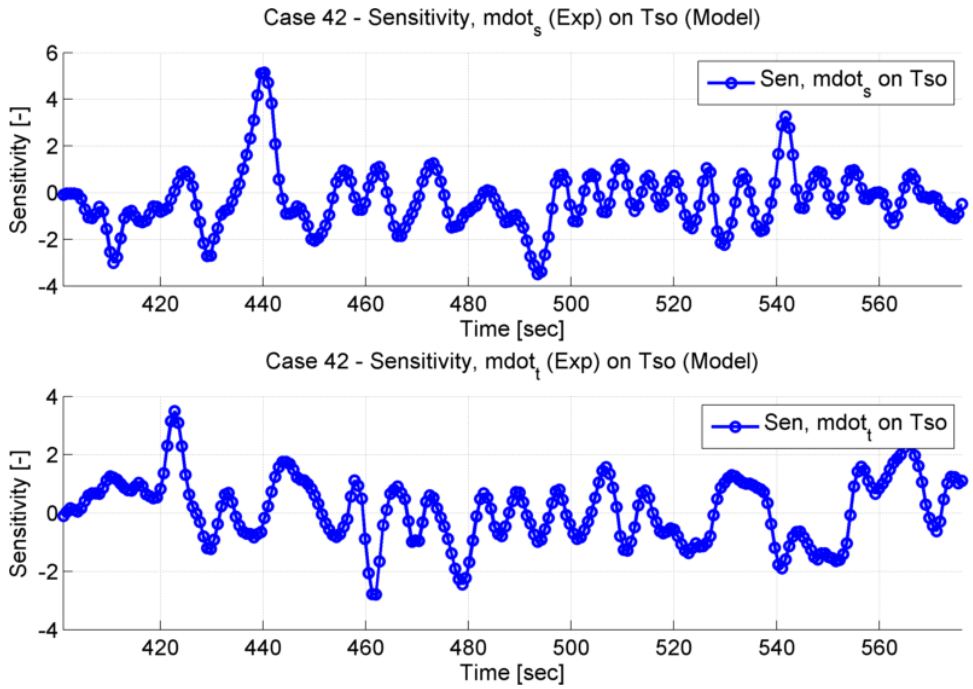

Figure 26: Case 42, Sensitivity of Mass Flow Rates on Shell Outlet Temperature vs. Time

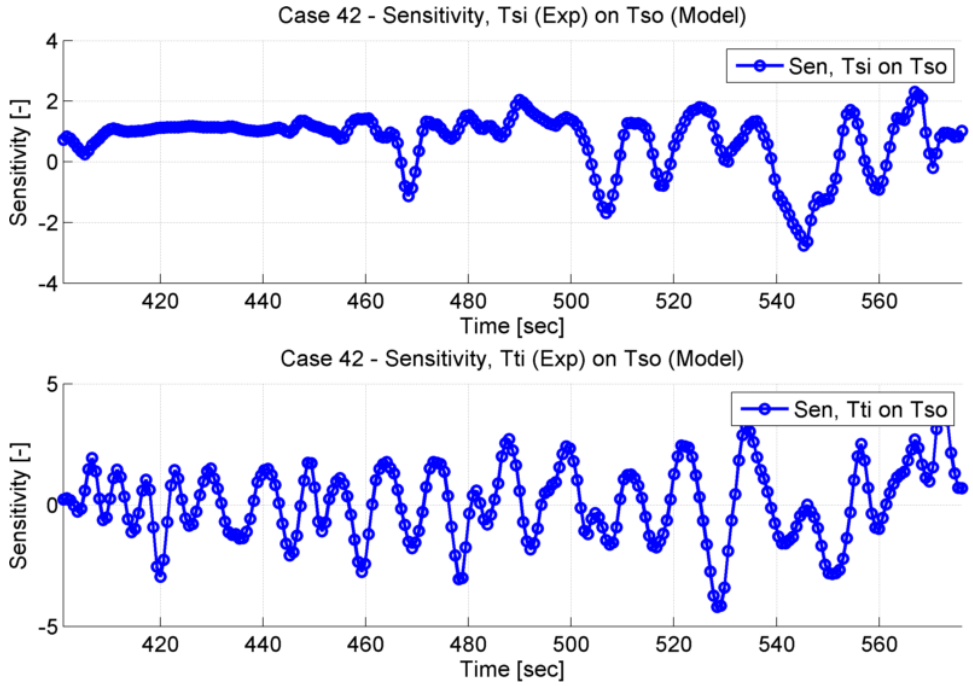

Figure 27: Case 42, Sensitivity of Inlet Temperatures on Shell Outlet Temperature vs. Time

With respect to the sensitivity of the shell outlet temperature to the inlet variables, Cases 37 and 42 show similar trends to Case 15. The orders of magnitude of the sensitivities are all the same and the sensitivities are randomly distributed as both positive and negative values. The exception to this, again as with Case 15, is found with the sensitivity of the shell inlet temperature on the shell outlet temperature. This sensitivity shows that for the first half of the time under examination, after the step change is introduced, the sensitivity of the shell outlet temperature to the shell inlet temperature is generally positive and fairly stable. Beyond the half-way point of the plotted time, this positive sensitivity transitions and begins to fluctuate as both negative and positive with time, in a random fashion, much like the rest of the sensitivities shown.

Uncertainty Propagation

To reiterate, uncertainty propagation provides a means to study the effect of the uncertainty of the inputs on the outputs of the system. In order to complete an uncertainty analysis by the proposed methodology, a sensitivity analysis must be completed first and the standard deviations of the inputs and outputs calculated. The propagation of uncertainties requires that the uncertainties be squared, which means that they are propagated as variances. Several parameters are required in order to complete the uncertainty propagation, specifically the sensitivities are needed, and hence the uncertainties are only propagated after the sensitivity analysis is completed. This is highlighted by repeating Equation (58) and Equation (59) here for simplicity.

$$\sigma^2_{x_i \to SRQ_k} = \left[\left(Sen^{SRQ_k}_{x_i}\right)\right]^2 \left(\sigma^2_{x_i}\right). \tag{88}$$

$$\sigma_{x_i \to SRQ_k}^2 = \left[\left(\frac{\sigma_{x_i}}{\sigma_{SRQ_k}}\right)\left(\frac{\partial SRQ_k}{\partial x_i}\right)\right]^2 \left(\sigma_{x_i}^2\right). \tag{89}$$

Equation (88) shows the dependence of the uncertainty analysis on the sensitivities and Equation (89) shows the values required after making the substitutions as recommended by the IPCC.[27]

The results will be presented with all inputs affecting the same output variable together for each case; the focus will be the uncertainty propagation of each input from both shell and tube sides on the shell output temperature. The uncertainty propagation of the input variables on the tube outlet temperature experience similar trends as those for the shell outlet temperature, but for completeness, all results are provided in APPENDIX D: RESULTS. First, the equations used to calculate the as propagated uncertainty of the inlet variables, shell and tube mass flow rates and shell and tube inlet temperatures, on the shell outlet temperatures are repeated.

$$\sigma_{\dot{m}_s \to T_{s,o}}^2 = \left[\left(\frac{\sigma_{\dot{m}_s}}{\sigma_{T_{s,o}}}\right)\left(\frac{\partial T_{s,o}}{\partial \dot{m}_s}\right)\right]^2 \left(\sigma_{\dot{m}_s}^2\right), \tag{90}$$

$$\sigma_{\dot{m}_t \to T_{s,o}}^2 = \left[\left(\frac{\sigma_{\dot{m}_t}}{\sigma_{T_{s,o}}}\right)\left(\frac{\partial T_{s,o}}{\partial \dot{m}_t}\right)\right]^2 \left(\sigma_{\dot{m}_t}^2\right), \tag{91}$$

$$\sigma_{T_{s,i} \to T_{s,o}}^2 = \left[\left(\frac{\sigma_{T_{s,i}}}{\sigma_{T_{s,o}}}\right)\left(\frac{\partial T_{s,o}}{\partial T_{s,i}}\right)\right]^2 \left(\sigma_{T_{s,i}}^2\right), \tag{92}$$

$$\sigma_{T_{t,i} \to T_{s,o}}^2 = \left[\left(\frac{\sigma_{T_{t,i}}}{\sigma_{T_{s,o}}}\right)\left(\frac{\partial T_{s,o}}{\partial T_{t,i}}\right)\right]^2 \left(\sigma_{T_{t,i}}^2\right). \tag{93}$$

Once the uncertainties have been propagated, the results are the as propagated uncertainties; these values are the result of the process used to propagated the uncertainties and require manipulation. This manipulation is accomplished by taking the

square root to transform the uncertainties from variances to uncertainties in units that are useful. The equations that represent the effect of the uncertainties of each input variable on the uncertainty of the shell outlet temperature are repeated for simplicity and then the results are shown below for the cases under review.

$$\sigma_{\dot{m}_s \to T_{s,o}} = + \left(\frac{\sigma_{\dot{m}_s}^2}{\sigma_{T_{s,o}}} \right) \left| \left(\frac{\partial T_{s,o}}{\partial \dot{m}_s} \right) \right|, \tag{94}$$

$$\sigma_{\dot{m}_t \to T_{s,o}} = + \left(\frac{\sigma_{\dot{m}_t}^2}{\sigma_{T_{s,o}}} \right) \left| \left(\frac{\partial T_{s,o}}{\partial \dot{m}_t} \right) \right|, \tag{95}$$

$$\sigma_{T_{s,i} \to T_{s,o}} = + \left(\frac{\sigma_{T_{s,i}}^2}{\sigma_{T_{s,o}}} \right) \left| \left(\frac{\partial T_{s,o}}{\partial T_{s,i}} \right) \right|, \tag{96}$$

$$\sigma_{T_{t,i} \to T_{s,o}} = + \left(\frac{\sigma_{T_{t,i}}^2}{\sigma_{T_{s,o}}} \right) \left| \left(\frac{\partial T_{s,o}}{\partial T_{t,i}} \right) \right|. \tag{97}$$

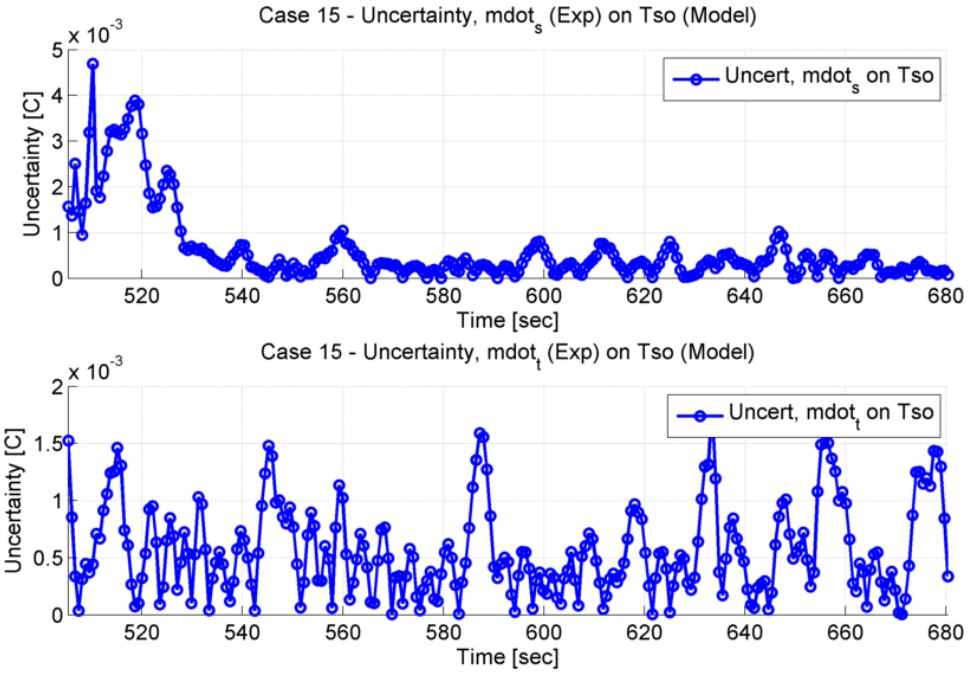

Figure 28: Case 15, Uncertainty of Mass Flow Rates on Shell Outlet Temperature vs. Time

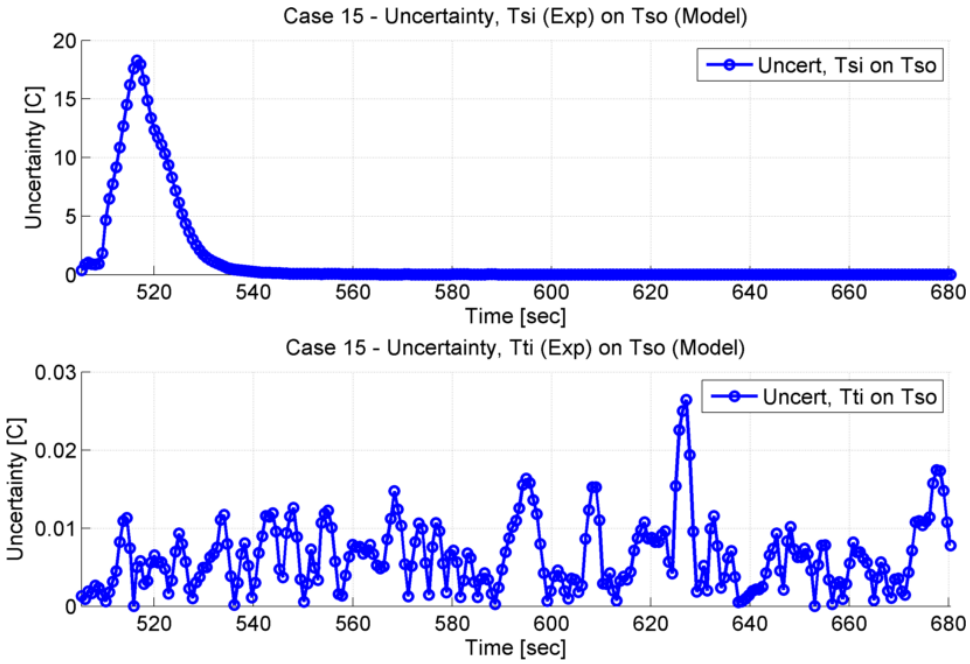

Figure 29: Case 15, Uncertainty of Inlet Temperatures on Shell Outlet Temperature vs. Time

For Case 15, the case where the shell outlet temperature was over predicted the most, the effect of all of the input uncertainties on the shell outlet temperature is examined; Figure 28 and Figure 29, above, show the final uncertainties of the input variables on the shell outlet temperature. Specifically, this shows the effect of the inlet temperature of both the shell and tube fluid streams, as well as the mass flow rates for both the shell and tube fluid streams. The effect of the uncertainties of the mass flow rates for the shell and tube streams on the uncertainty of the shell outlet temperature is negligible; both variables cause uncertainties on the order of 1E-3. The effect of the uncertainties of inlet fluid temperatures shows deviations from the mass flow rates: the effect of the tube inlet temperature on the shell outlet temperature is overall an order of magnitude higher than the mass flow rates, but can still be considered negligible. The uncertainty of the shell inlet temperature on the shell outlet temperature is the one that

shows the most effect, specifically in the transient region when the temperature values are changing the most. The uncertainties spike as high as 18 during the middle of the transient temperature change before they fall off to negligible values once the system reaches steady-state.

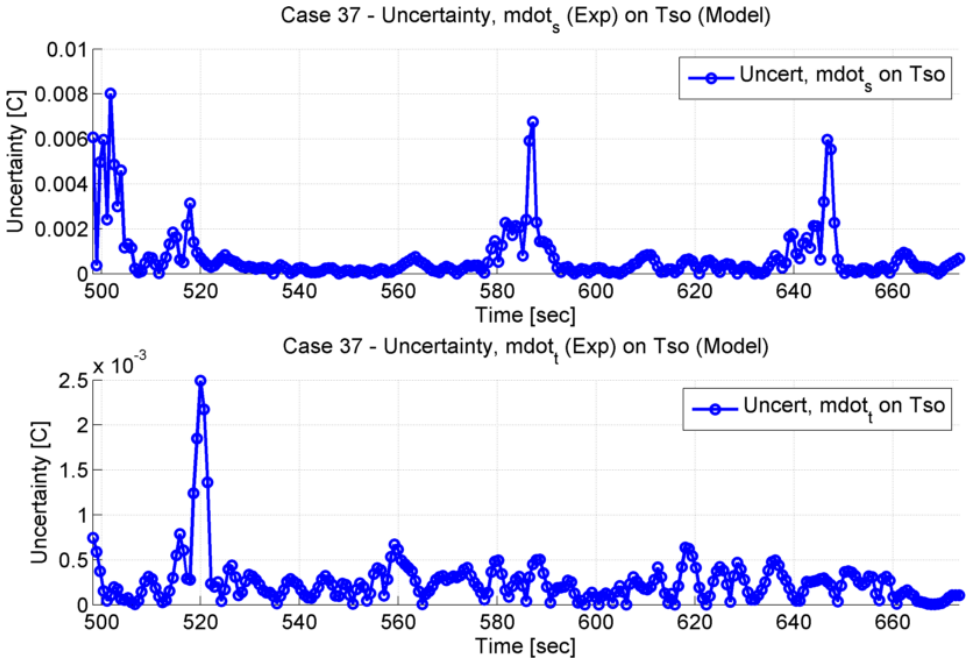

Figure 30: Case 37, Uncertainty of Mass Flow Rates on Shell Outlet Temperature vs. Time

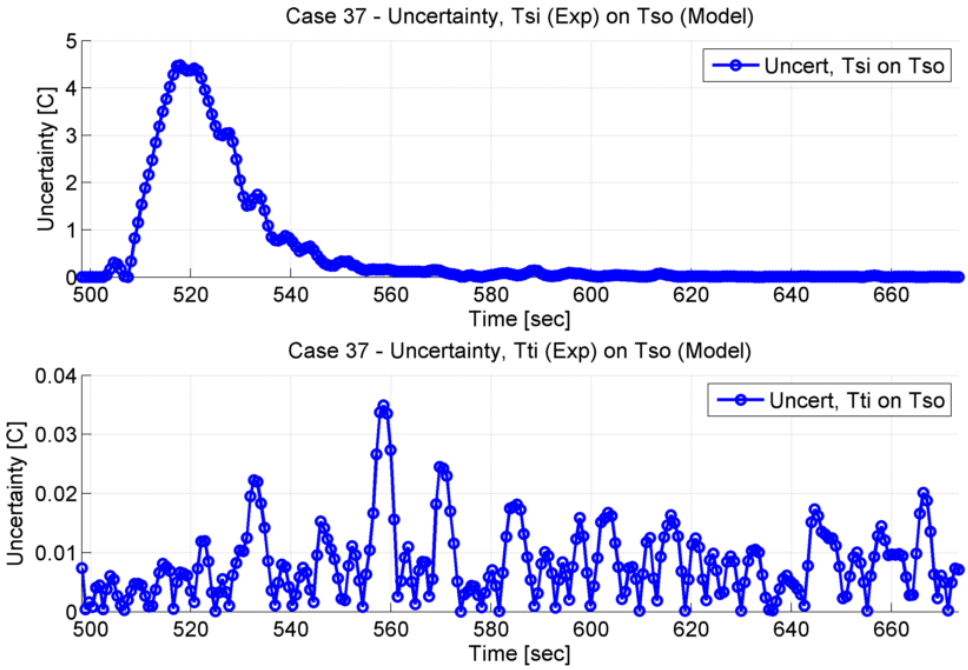

Figure 31: Case 37, Uncertainty of Inlet Temperatures on Shell Outlet Temperature vs. Time

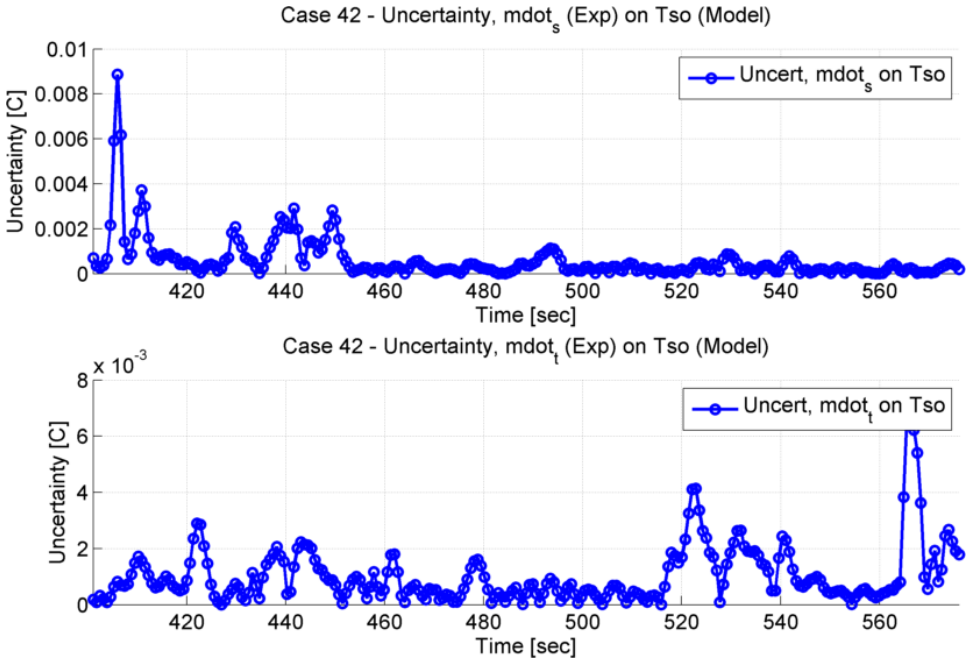

Figure 32: Case 42, Uncertainty of Mass Flow Rates on Shell Outlet Temperature vs. Time

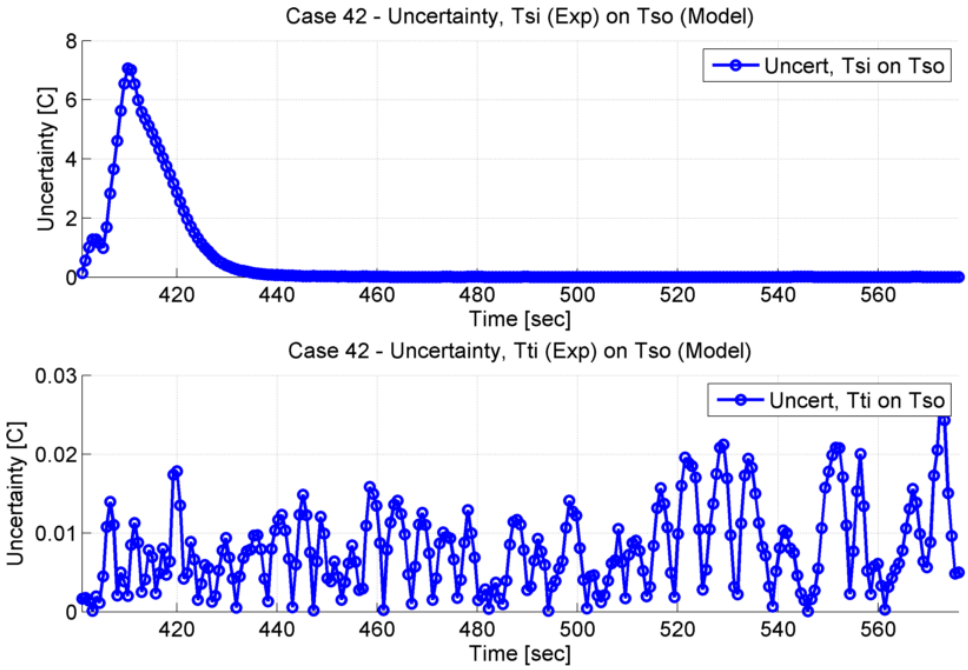

Figure 33: Case 42, Uncertainty of Inlet Temperatures on Shell Outlet Temperature vs. Time

Case 37, where the shell outlet temperature was under predicted the most and Case 42, where the shell outlet temperature aligned the most with experimental values, all exhibit the same trends as the uncertainties of Case 15. The values fluctuate and deviate from Case 15 a bit, but the same order of magnitude of the effect of the uncertainties of the mass flow rates, 1E-3, are found for both of the these cases. The effect of the uncertainty of the tube inlet fluid stream is one order of magnitude higher than the mass flow rates, but still negligible. The shell inlet temperature uncertainty is shown to introduce the most uncertainty on the shell outlet temperature, but only during the transient portion of the test. Once the system reaches steady-state, the uncertainties drop off again to very low values.

When added up, all of these uncertainties give the total uncertainty of the desired output variable with respect to all of the input variables. For the SRQ that has been the

focus of this study, this will show the total uncertainty of the shell outlet temperature with respect to the uncertainty of the mass flow rates of the shell and tube streams, as well as the uncertainty of the shell and tube inlet temperatures. These total uncertainties for the three cases under examination are shown below.

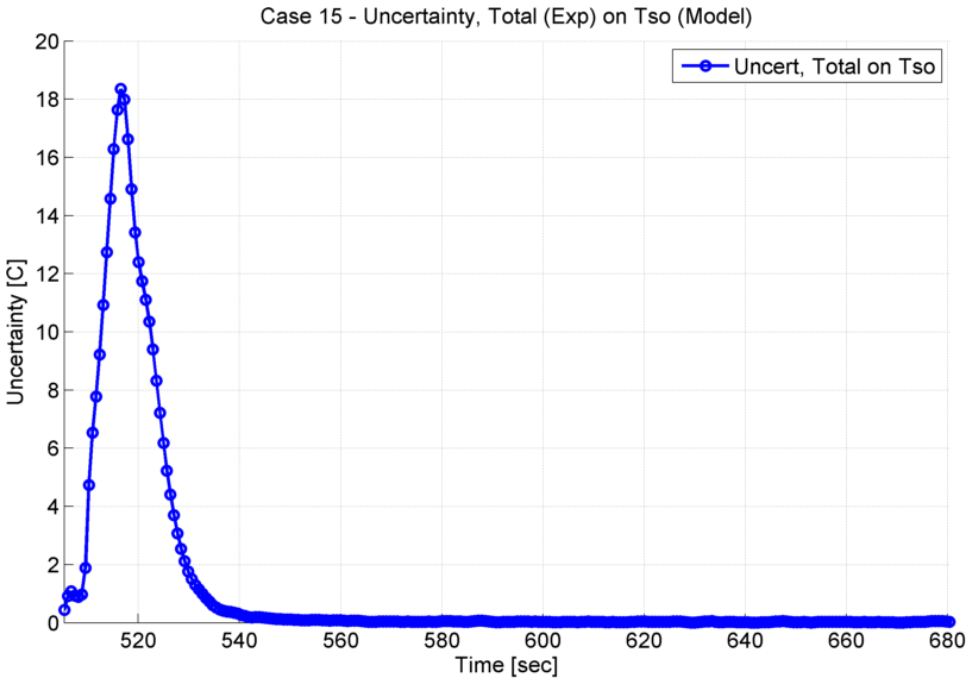

Figure 34: Case 15, Total Uncertainty of Inlet Temperatures & Mass Flow Rates on Shell Outlet Temperature vs. Time

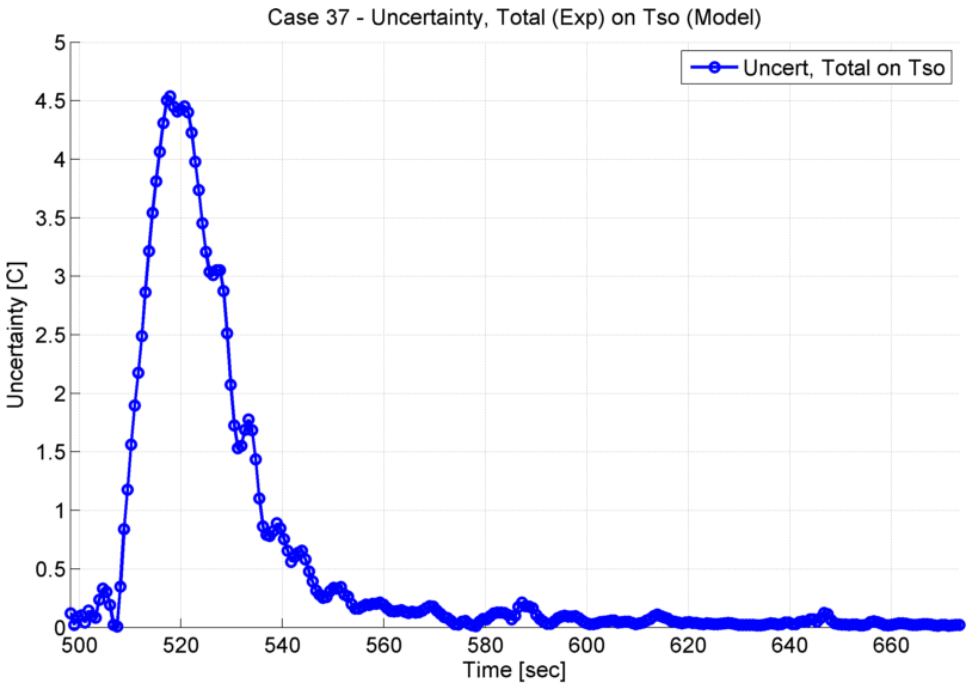

Figure 35: Case 37, Total Uncertainty of Inlet Temperatures & Mass Flow Rates on Shell Outlet Temperature vs. Time

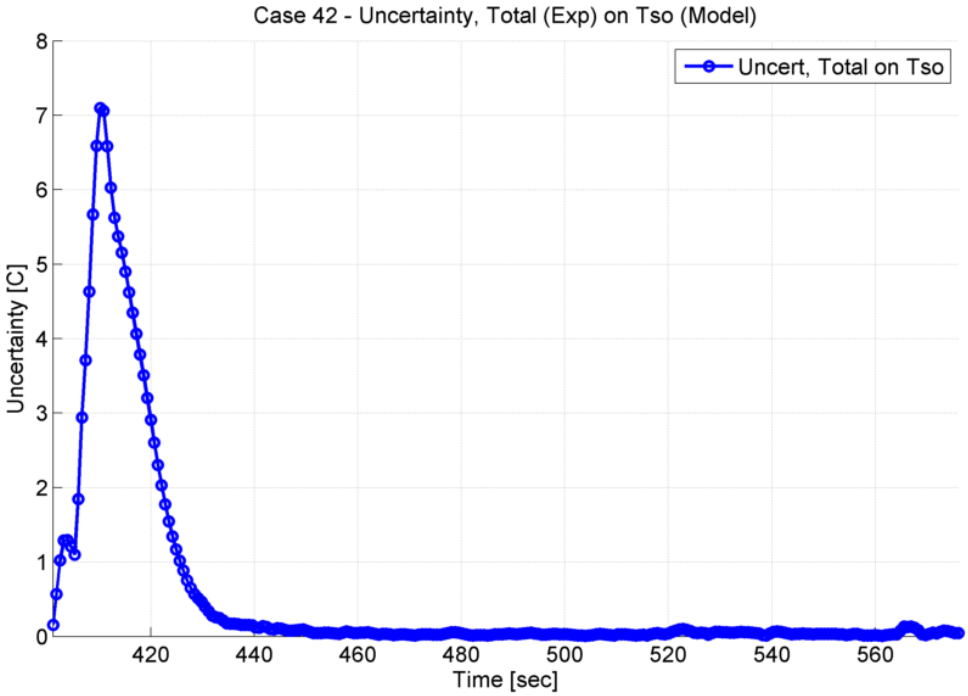

Figure 36: Case 42, Total Uncertainty of Inlet Temperatures & Mass Flow Rates on Shell Outlet Temperature vs. Time

The total uncertainties for all three cases show the same trends, with varying magnitudes. The trends indicate that the bulk of the measurable uncertainty stems from the uncertainty of the shell inlet temperature in the transient region. Once the temperatures reach steady-state, the total uncertainties fall down to values that have little to no impact. Case 15 exhibits the highest uncertainties of the three cases around the 520 second mark with a peak uncertainty value of about 18 degrees C, while Case 37 shows the lowest uncertainty value of about 4.5 degrees C. Case 42 shows a peak uncertainty value between the other two, peaking at about 7 degrees C near 415 seconds.

Shell Outlet Temperatures

One of the final outputs from this study is an examination of how well the Simulink model is capable of predicting the outlet temperatures of the heat exchanger. Specifically, the study is focused on the shell outlet temperature as the tube side was used for cooling purposes by a fluid that was not recirculated. The shell outlet temperatures from the experimentally gathered data, as well as the model outputs, are shown below for Cases 15, 37, and 42.

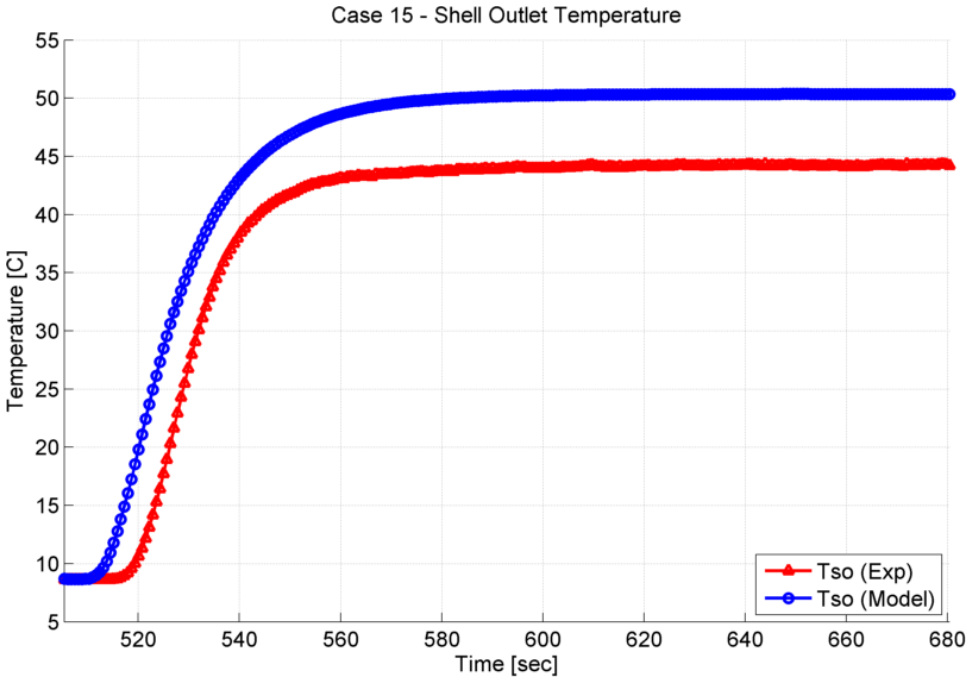

Figure 37: Case 15, Shell Outlet Temperature, Model and Experiment

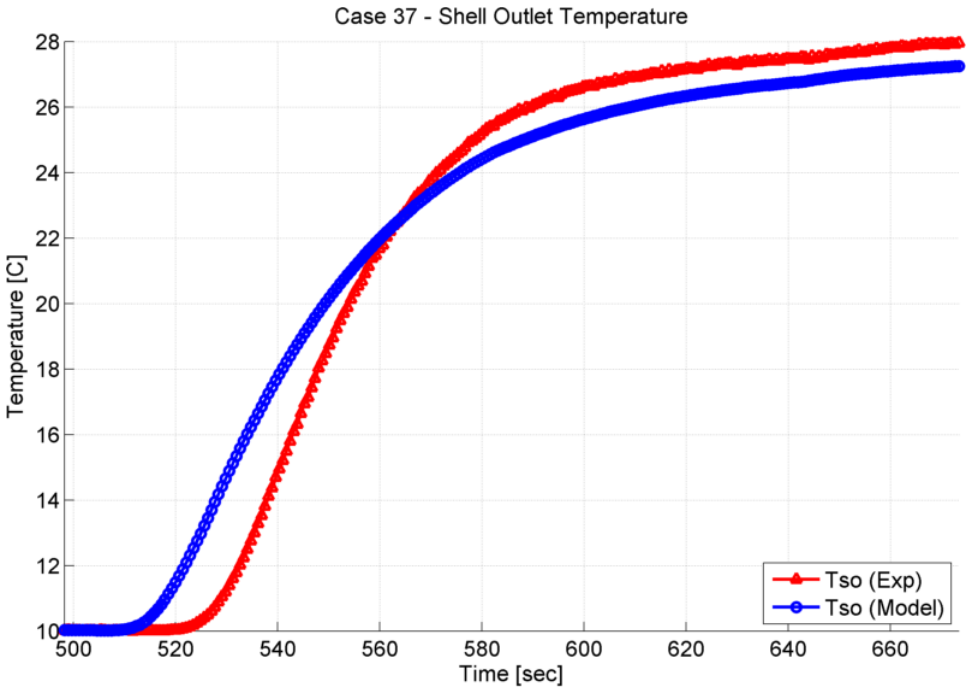

Figure 38: Case 37, Shell Outlet Temperature, Model and Experiment

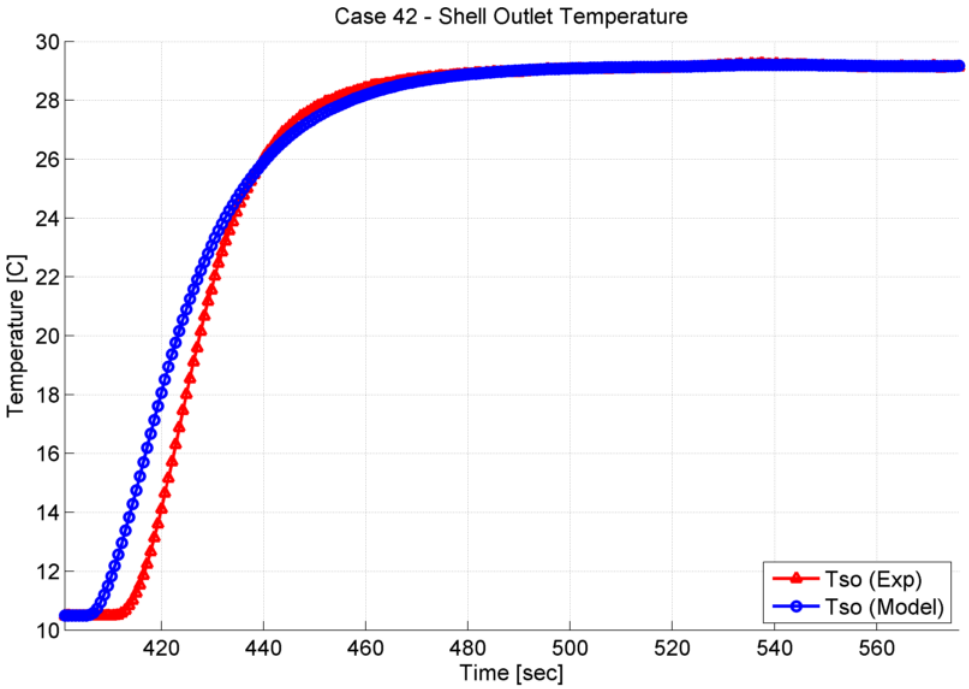

Figure 39: Case 42, Shell Outlet Temperature, Model and Experiment

In Figure 37, above, Case 15 highlights the shell outlet temperatures that were over predicted the most in comparison with the experimental results. It is seen that the model over predicts the outlet temperature all the way through the transient region and through steady-state. Figure 38, above, depicts the shell outlet temperatures for Case 37. Initially, the model over-predicts the shell outlet temperature before it crosses and begins to under-predict the temperature as the outputs reach steady-state. Figure 39, above, shows the outputs from Case 42. In the bulk of the transient region, the model over-predicts the temperature before it settles at a steady-state value very near the experimental steady-state temperature. One consistency through each of these 3 cases, representative of the rest of the total 63 cases, is that the model always over-predicts the shell outlet temperature initially. Qualitatively, the slope of the curve at the onset of the transient temperature change is either very similar or identical to the slope of the transient

change as measured in the experimental data. The key difference is that shell outlet temperature from the model begins to rise before the temperatures in the experiment begin to rise. This indicates that the thermal energy transfer that is occurring between fluid streams in the model has a slight lag on the shell side when compared to what is happening in real life. This indicates that it is possible for the model to represent the physical processes occurring on the shell side of the heat exchanger more accurately. As a way to gauge the accuracy of the model outputs, an analysis of the uncertainties of the outlet temperatures provides additional information.

Shell Outlet Temperatures, With Uncertainties

The uncertainties that have been calculated throughout this effort are ultimately used when analyzing the final SRQ's. In this case, the shell outlet temperature has been reviewed in the previous section to show a general agreement between the model and experiment outputs. Now, the calculated uncertainties are attached to those shell outlet temperatures as the error for each data point. Since the nature of the transient temperature change varies with time, as do the calculated uncertainties, it is found that the error in the output variables also vary with time. The shell outlet temperatures for Cases 15, 37, and 42 are again plotted below, but this time the uncertainties are included as the error bars on each data point.

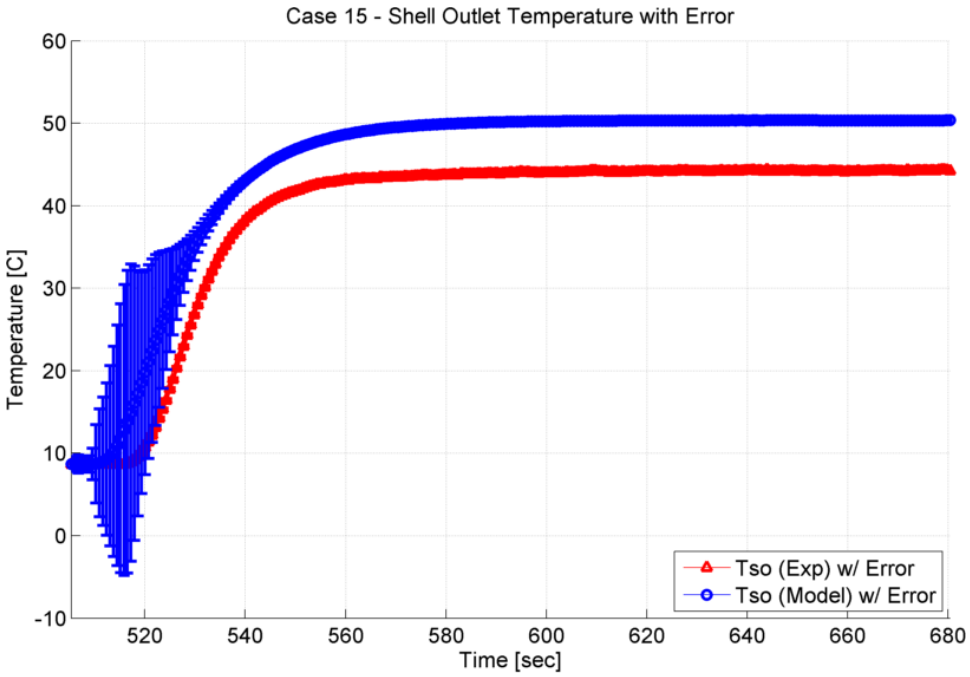

Figure 40: Case 15, Shell Outlet Temperature with Error Bars, Model and Experiment

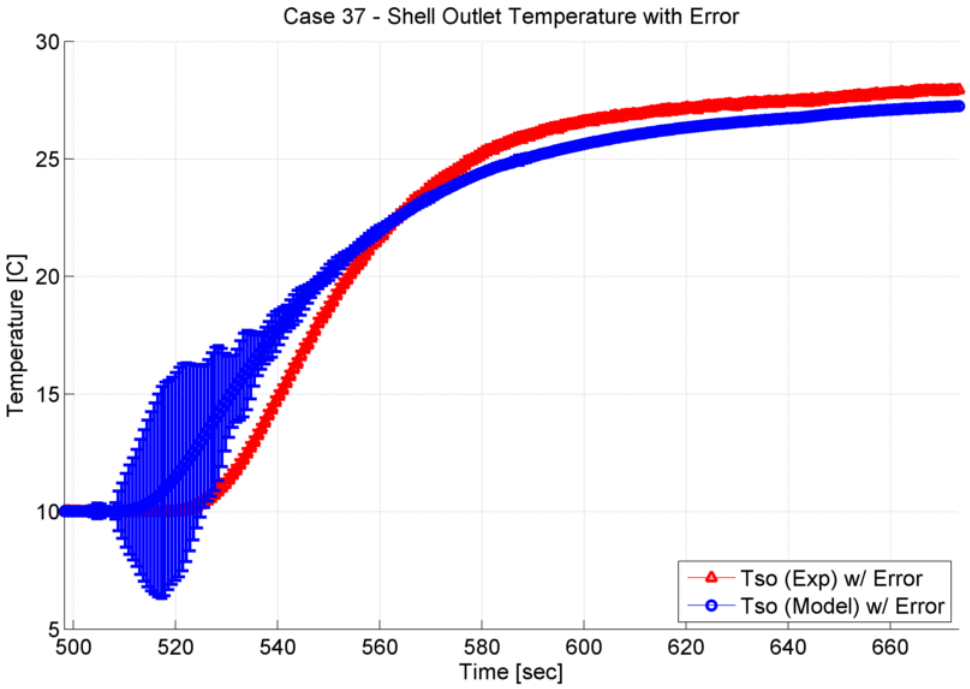

Figure 41: Case 37, Shell Outlet Temperature with Error Bars, Model and Experiment

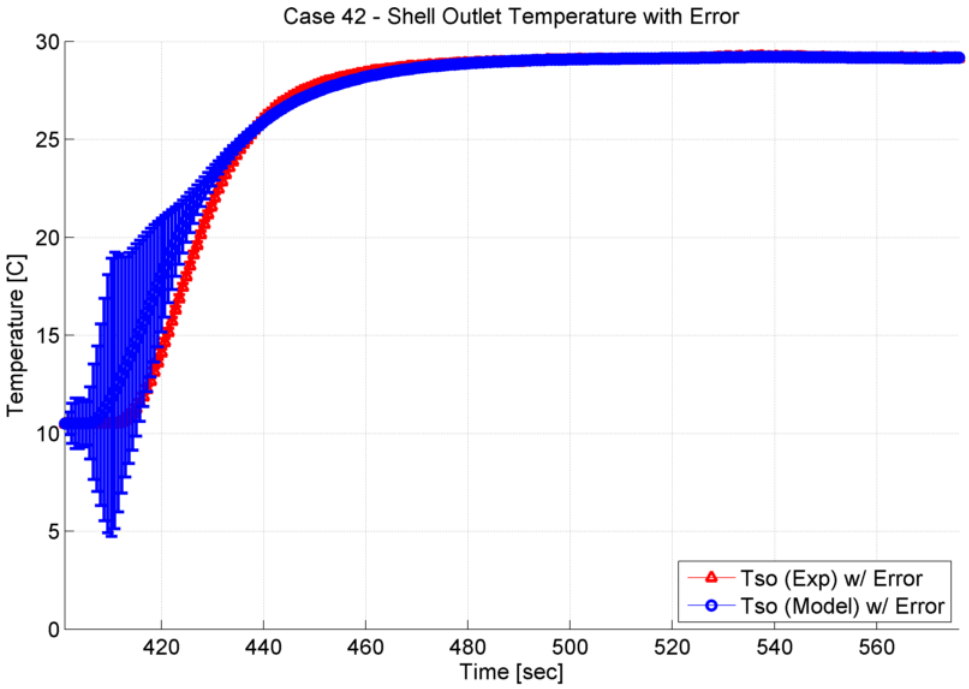

Figure 42: Case 42, Shell Outlet Temperature with Error Bars, Model and Experiment

Similar trends are seen in all three cases with respect to magnitude of the error and the way the error diminishes with time. In all cases, for both model and experimental outputs, the error is much larger in the transient regions than in the steady-state regions. As the step change occurs, the error of the model outputs initially spikes high relative to the actual output temperature before it begins to diminish as the system approaches steady-state. For Case 15, this spike in error reaches as high as ±18 degrees C, whereas Cases 37 and 42 have error spikes of ±4.5 and ±7 degrees Celsius, respectively. These large spikes in error occur at the time when the slope of the derivative is the highest which reflects when the outlet temperature is changing the most. The model output temperatures all exhibit small errors in the steady-state region, on the order of tenths of a degree Celsius.

For Case 42, the error band of the model output for the steady-state region fall within the error band of the experimental outputs. This implies that for this case, the steady-state model output accurately represents the experimental output when taking into account both model and experimental error. For Cases 15 and 37, the error bands of the model outputs lie outsides of the error bands of the experimental outputs. This indicates that for Cases 15 and 37, the model needs to be refined to bring the output in alignment with the experimental results.

The trends that are seen with error in the transient portion of the outputs are representative of the calculated uncertainties. For the experimental outputs, the error is comprised wholly of instrumentation and measurement error. For the model outputs, the error is a function of the measurement error of the experimental inputs, including the instrumentation error, as well as the propagation of the uncertainties through the model. The output uncertainties are highly dependent upon the way that these values are calculated as evidenced by the way the error approaches a steady-state value before the system reaches steady-state. The moving average technique is responsible for this behavior as the technique produces standard deviations that are dependent upon the change of the data with respect to time. All three cases under examination show this trend where the uncertainty spikes to a maximum at the location where the largest change in output temperature is seen, before diminishing as the outputs approach steady-state values.

Time Constant

Another method of analyzing transient data is by examining the time constant of the system. The time constant is traditionally represented as the time that the system requires to reach 63% of its steady-state value. As one of the main goals of this modelling effort was to examine how closely a model can replicate a step-change in temperature, the study would not be complete without comparing the time constants from the experimental data to those generated through the model. This comparison provides useful information as the time constant is an additional way to quantitatively compare the model and experimental outputs. The time constant is also the primary piece of information that would be used to represent the transient physical process in a model with system level interactions.

The time constants were calculated by determining the initial and final outlet temperature during the entire transient portion of the experiment, then finding the time that was required to reach 63% of the final value; this was done for each case for both the model and experimental outputs.

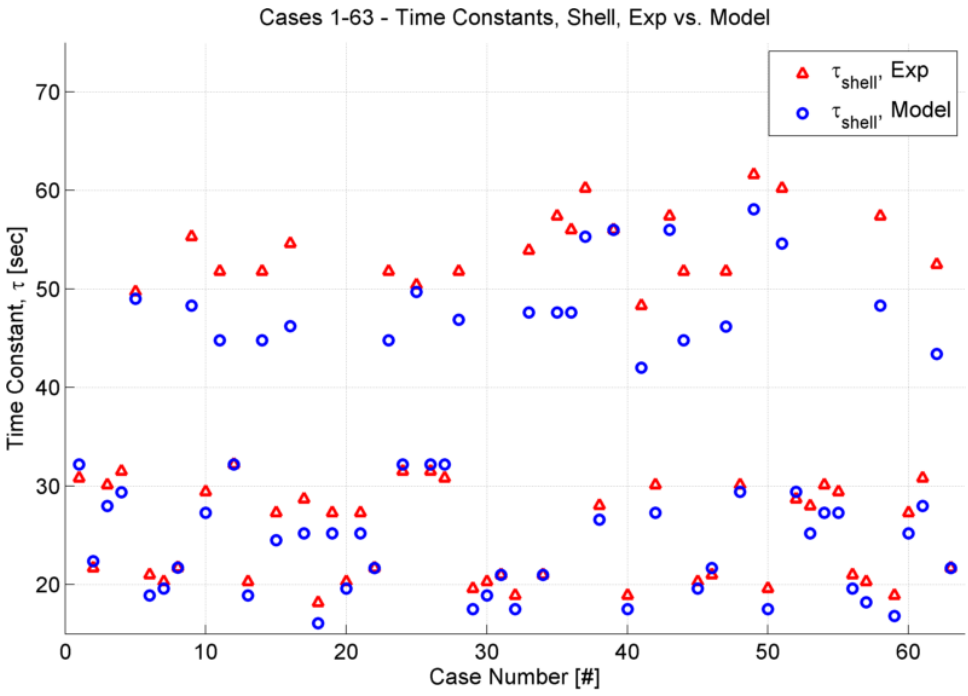

Figure 43: Time Constants, Shell, Experiment vs. Model

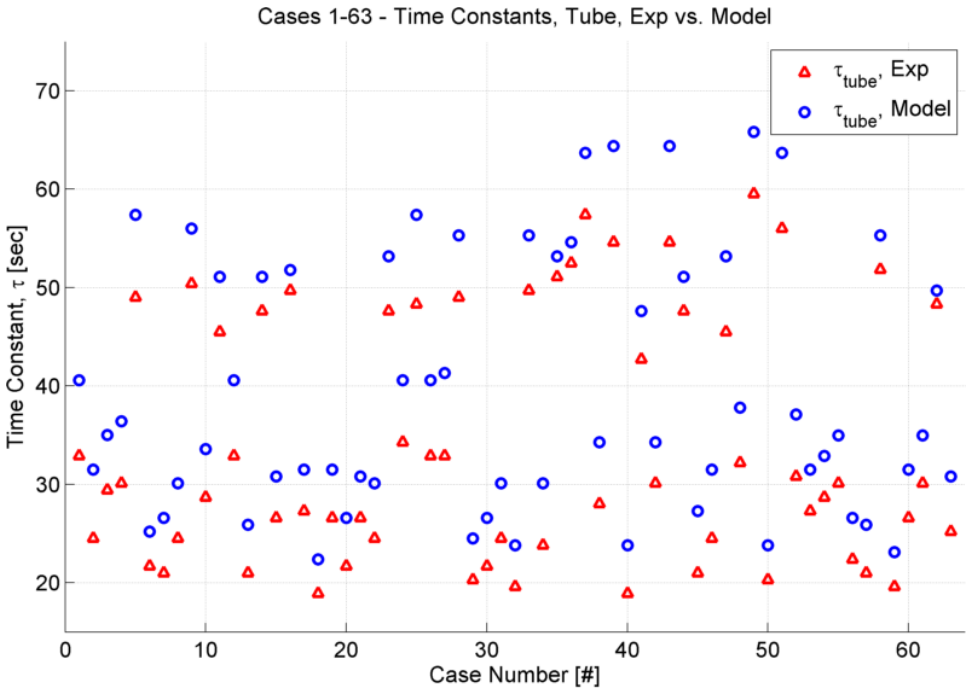

Figure 44: Time Constants, Tube, Experiment vs. Model

At first glance, Figure 43 and Figure 44 show time constants that vary widely when comparing the experimentally gathered values with the model outputs. Two pieces of information can be inferred from these plots. First, it appears as though the predicted time constants from the model show a similar trend as those measured from the experiment, but it is difficult to identify without looking at the data in a different way. Second, it appears that there are at least two different time constants from each set of data, both experimental and model. Each set of time constant comparisons for both the model and experimental data, as generated from both the shell and tube data, are labeled based on corresponding nominal shell flow rate for the each case; these plots are shown below.

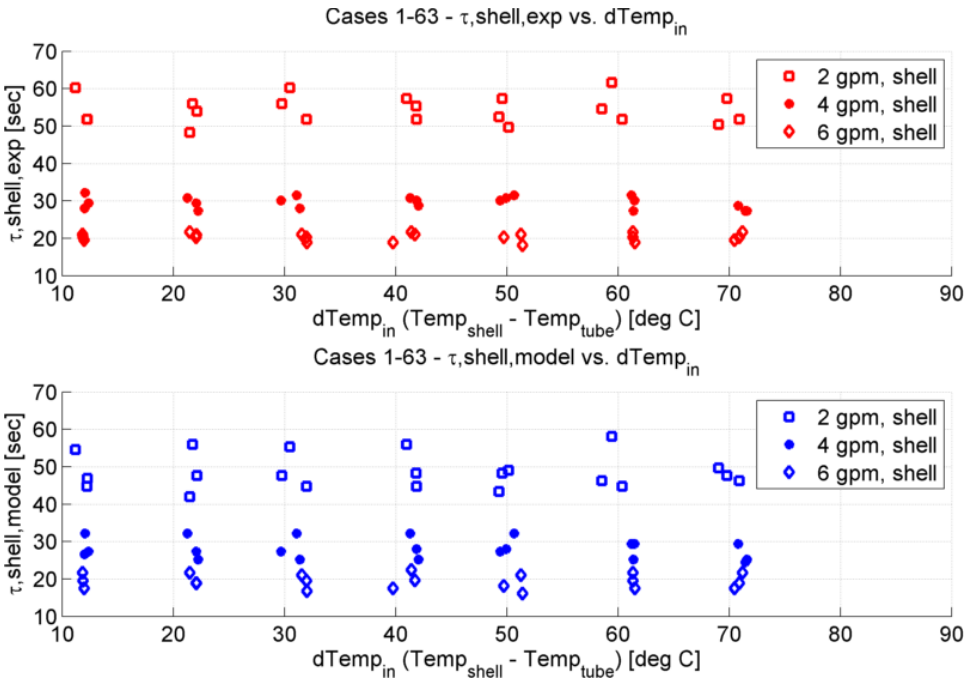

Figure 45: Time Constants, Shell, Experiment vs. Model

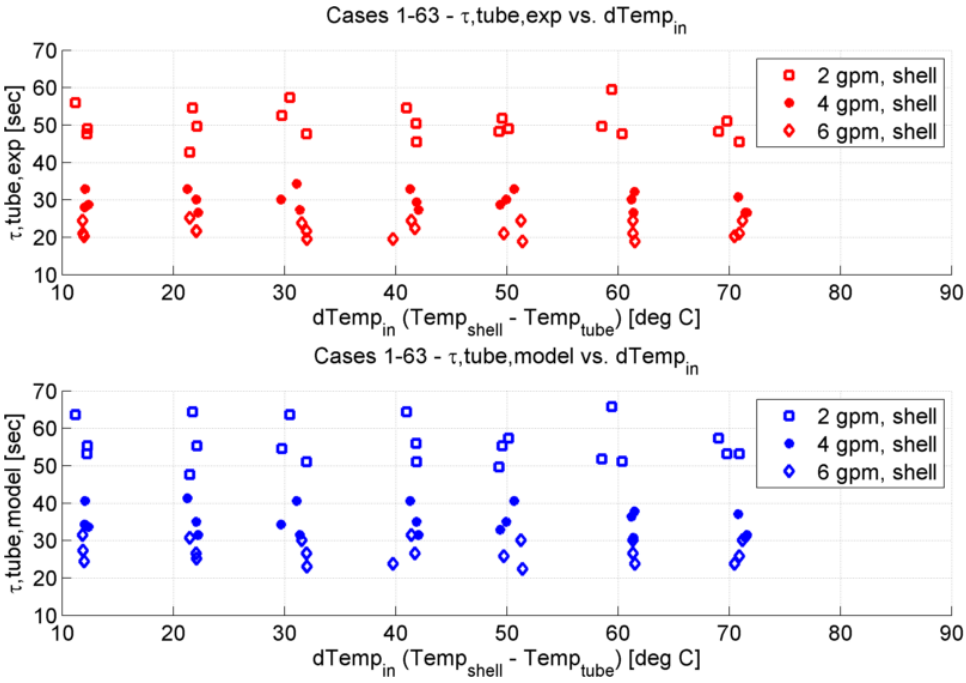

Figure 46: Time Constants, Tube, Experiment vs. Model

After plotting the time constants versus the difference in inlet temperatures, natural groupings of the time constant value form: these groupings coincide with the various set points of flow rate through the shell side of the heat exchanger. It is now easy to see that for a higher flow rate of fluid through the shell side, the time constant value drops. To glean more information about what drives the differences in the time constant value, the Reynolds number as calculated in the model for both the shell and tube sides of the heat exchanger are also plotted against the difference in inlet temperatures; this plot is shown below.

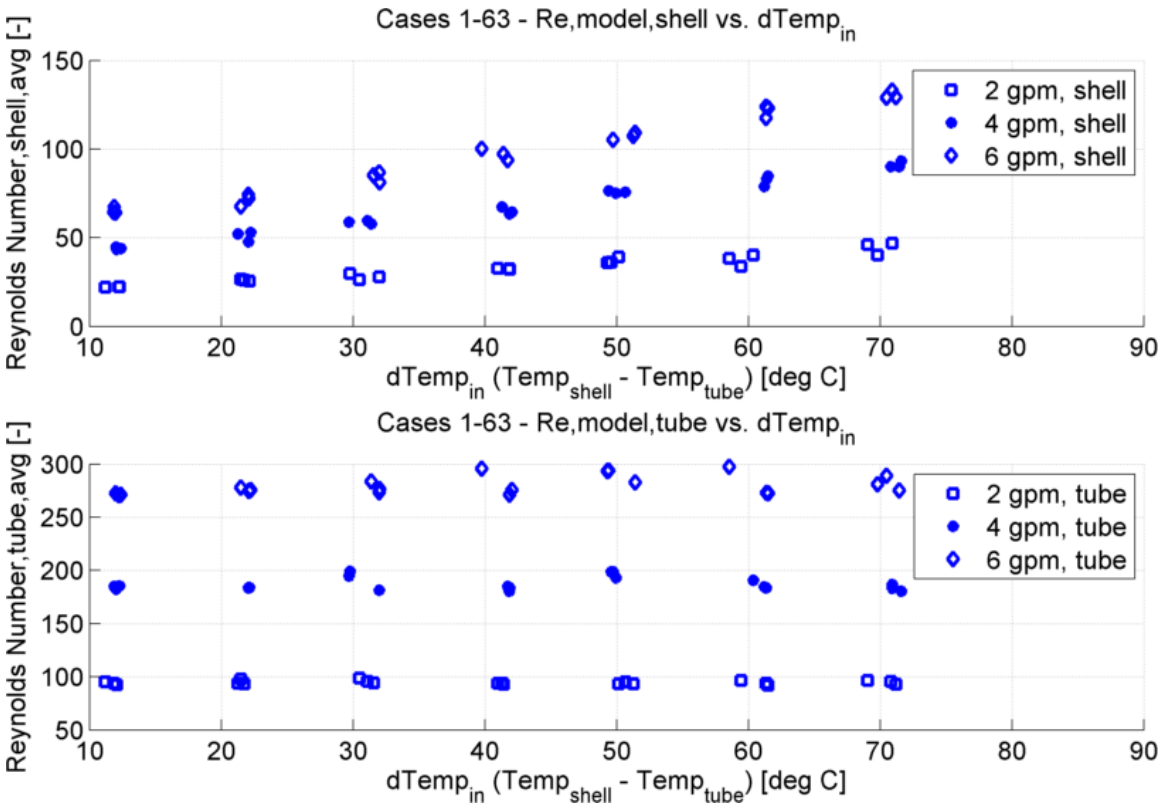

Figure 47: Model Calculated Reynolds Number vs. Difference of Inlet Temperatures, Shell & Tube

The Reynolds number is shown as an average value over the transient region of interest, and thus the shell side of the heat exchanger appears to be driven by both flow rate as well as the change in inlet temperature. When analyzing the Reynolds number on the tube side of the heat exchanger, it is shown that for a constant tube flow rate in the model, the Reynolds number does not change. This indicates that the shell side of the heat exchanger is the primary driver in changes in Reynolds number, and thus, overall time constant.

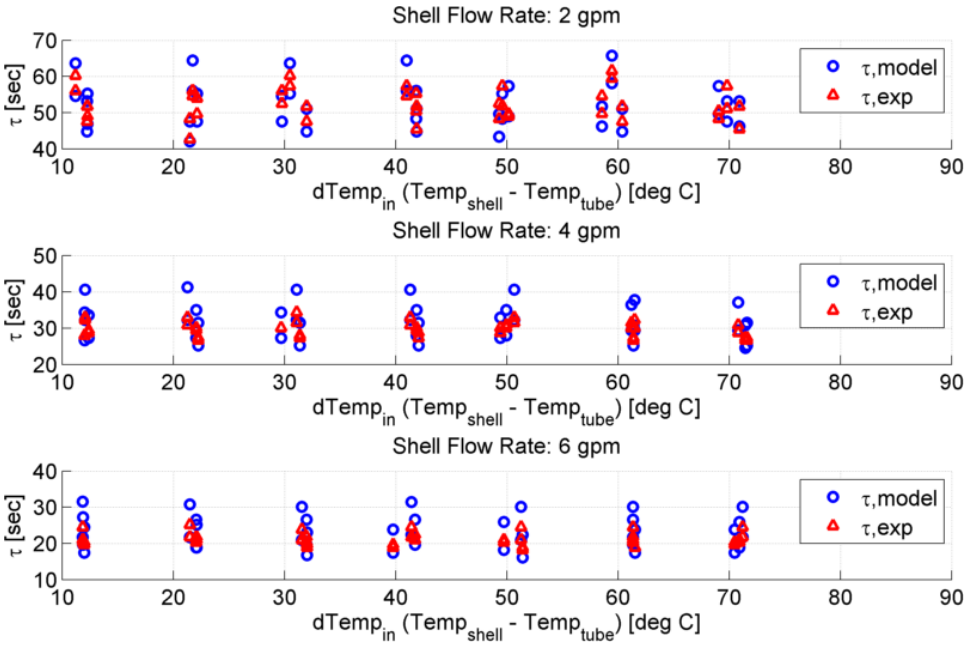

Figure 48: Time Constant vs. Difference of Inlet Temperatures,
Shell & Tube, Model & Experiment

As it was determined above that the shell flow rate is the primary driver in time constant value, the calculated time constants for both the model and experiment were separated into groups based on the shell flow rate value. This results in three different values for the time constant that correspond to the 2, 4, and 6 gpm flow rates on the shell side; the shift in the time constant values can be directly attributed to the changes in shell fluid flow rate and temperature. When the three different time constant values are plotted on the same scaling, it is possible to see that the model predicted time constant values encompass the experimentally calculated time constants. It can also be seen from the plots that as the shell flow rate increases (and thus Reynolds number), the spread in the model predicted time constants decreases. This indicates that the model more closely predicts the time constant of the heat exchanger for the higher shell flow rates used in the experiment versus the lower flow rates.

Although useful, these qualitative analyses do not provide a true answer to whether or not the model is capable of accurately predicting the performance of the tested heat exchanger. In order to attempt to validate the model against the experimental data, the accuracy is measured in a quantitative fashion by applying the Anderson-Darling k-sample test. The k-sample test serves to answer whether or not two sets of data may have been sampled from the same population; in this specific application the test will be used to determine if the time constants as calculated from both the experimental and model data came from the same population. If the test fails to reject the null hypothesis that both sampled data sets came from the same population, then it means that each subset of data may have come from the same population and could either be combined or used interchangeably. For the comparative analysis of experimental data to predicted model data, this means that statistically, the model accurately represents the physical processes occurring within the assumptions used during the analysis of the data. If the test rejects the null hypothesis that both sets of data may have come from the same population, then from a statistical perspective, the data may not be combined or used interchangeably.

Table 11: Anderson-Darling k-sample Test Results

	Adjusted for Ties	Significance Level	A-D Rank Statistic	Standardized A-D Rank Statistic	Probability	Reject Null Hypothesis
τ, Shell	No	5%	2.1226479	1.4966858	0.0770510	NO
τ, Shell	Yes	5%	2.2696288	1.6926370	0.0640761	NO
τ, Tube	No	5%	5.1790447	5.5713970	0.0019844	YES
τ, Tube	Yes	5%	5.3907038	5.8535755	0.0015258	YES

Table 11, above, describes the results of the Anderson-Darling k-sample test. The test was run two different ways in order to both neglect and account for ties, or duplicate data values, within the data sets to be compared; accounting for ties did not change the outcome of the test. The test was run with a typical 5% significance level used to

determine statistical significance and the Anderson-Darling rank statistics were then calculated for the datasets. The rank statistics were compared generating a p-value (probability); if the probability was below 0.05, then the null hypothesis was not rejected. According to the results of the Anderson-Darling k-sample test results, the null hypothesis was not rejected when comparing the time constants on the shell side; statistically this indicates that within the significance level specified, it is possible that both sets of data are from the same population (the data sets are interchangeable). However, for the time constants calculated using the tube side data, the test results did reject the null hypothesis, indicating that the data sets did not come from the same population. As one of the sets failed the test, the conclusion to be made is that the transient data, from the perspective of the time constants, is not capable of being statistically validated.

As a means to support the Anderson-Darling k-sample test results above, plots of the CDF for each set of data (experimental and model) are plotted on top of each other to graphically highlight the differences between the data. Figure 49, below, shows the CDF's for the experimental and model shell time constants, while Figure 50 shows the CDF's for the tube time constants. Visually, it is apparent that the shell time constant CDFs are much closer together than those for the tube time constants, which is commensurate with the results gathered above.

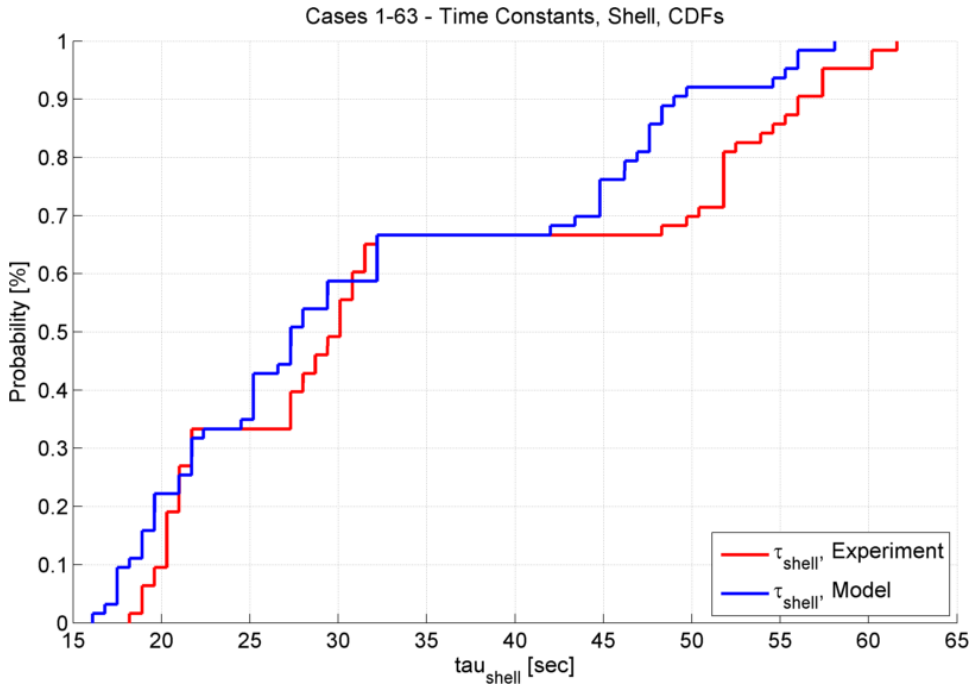

Figure 49: Cumulative Distribution Functions, Time Constant, Shell Experiment vs. Model

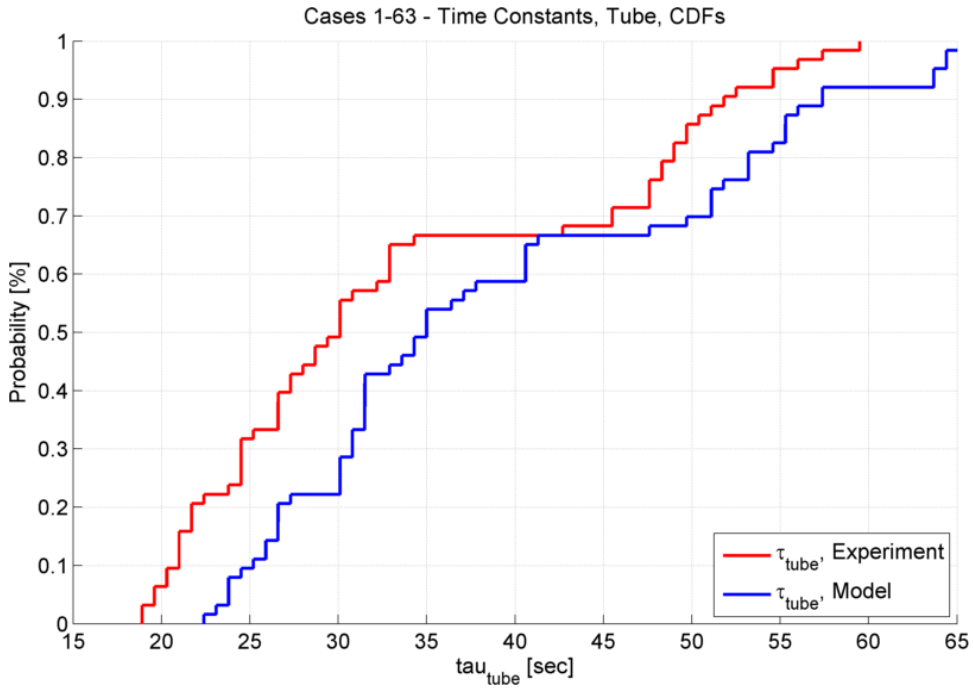

Figure 50: Cumulative Distribution Functions, Time Constant, Tube, Experiment vs. Model

A final check of the results generated above would be to run another statistical validation tool to verify the outcome. The two-sample Kolmogorov-Smirnov (K-S) test is a nonparametric assessment of the differences between empirical distribution functions; a tool similar to the Anderson-Darling k-sample test.[30,32] Key differences are that the K-S test does not require any knowledge of the type of distribution of either sets of data like the Anderson-Darling test does, and the underlying principles of the Anderson-Darling test as applied to the k-sample test result in a test comparison that is much more robust than the K-S test as it is more sensitive to outliers. The null hypothesis for the K-S test is the same as that for the Anderson-Darling k-sample test: that the two sets of data may have come from the same parent population.

Table 12: Two-sample Kolmogorov-Smirnov Test Results

	Significance Level	*p*-value	K-S Test Statistic	Reject Null Hypothesis
τ, Shell	5%	0.0762	0.2222	NO
τ, Tube	5%	0.0090	0.2857	YES

The results of the two-sample Kolmogorov-Smirnov test shown above in Table 12, generate the same conclusions as the more robust Anderson-Darling k-sample test: the two sets of time constant data from the shell side may have come from the same population, however, the time constant data on the tube side did not come from the same parent population.

Final Results

Through a graphical review of the CDF's and the analysis of two sets of statistical test results, it is concluded that it is not possible to statistically validate the model with 95% confidence against the experimental data presented in this manuscript. The

emphasis on a broad operating envelope for which experimental data was collected, coupled with the lack of replicate case data, provides sufficient variability to make statistical validation infeasible. Focus on one single operating condition may provide enough consistent replicate data to statistically validate the model, however, any model predictions beyond that one specific operating condition would not be validated.

CONCLUSIONS

A simplified transient heat exchanger model was developed using First Principles with the intent of quantifying its ability to accurately reflect physical processes. The accuracy of this model was assessed by utilizing previously developed statistically based processes; these processes had not been applied to a thermal fluids problem with relatively large time constants before these efforts. In order to support the statistical validation process, a thermal emulator was designed and built with the specific purpose of providing the necessary experimental data required to support model validation.

The model validation techniques utilized required completing sensitivity and uncertainty analyses, uncertainty propagation, verification, and finally, application of statistically based validation metrics. A method for generating the required partial derivatives and standard deviations across data sets is proposed and used to complete the study in the absence of ideal data. The key findings are noted below:

1. Despite validating the shell side time constant using both the Anderson-Darling k-sample test and the Kolmogorov-Smirnov test, it is not possible to validate the entire heat exchanger model using statistically based validation metrics. This stems from various factors, including: non-ideal data sets, lack of replicate data, data covering a broad operating envelope as opposed to a single focused operating condition, and stringent requirements of validation metrics.
2. The parameters required to complete sensitivity and uncertainty analyses, uncertainty propagation, and validation, are presented for a typical thermal fluids problem. Where parameters may not be easily calculable for this type

of problem, i.e. standard deviations across replicate data sets, an alternative technique for generating the required analysis inputs is presented and applied.

3. Although not validated, the ability of the heat exchanger model to capture both the transient and steady-state physical responses is assessed. Over a broad operating envelope, the heat exchanger model is able to reasonably well capture the trends of both the transient and steady-state behaviors. Model transient outputs tend to rise before the outputs from the experimental data and tend to not rise as quickly as the experiment. Steady-state output predictions may either be within the error bands of the experimentally gathered data, or may be above or below, suggesting that additional model refinement may produce more consistently accurate results.
4. Across a broad operating envelope, the time constant of the system for each set of fluid conditions is not validated statistically; however, the trends are followed quite well. Not only are the minor variations of the time constant captured by the model, but a larger step change in time constant due to flow conditions are captured as well. This proves useful as the time constant across a broad operating envelope is the key parameter that system-level models utilize and rely on from sub-system models.

These efforts highlight both quantitative statistically based techniques, such as the Anderson-Darling k-sample test or the Kolmogorov-Smirnov test, which may be applied to similar thermal fluids system problems in the absence of ideal experimental data for use in validation. Ultimately, the accuracy of the model must be assessed by those

intending to use it via both qualitative and quantitative techniques to determine if the model provides sufficient accuracy for its intended use.

APPENDIX A: THERMAL EMULATOR DESIGN & CONSTRUCTION

Figure 51 shows the initial layout of the thermal emulator in terms of where components were located relative to each other on the rolling stand. Locations were chosen to provide easy access to either the front or back of all major system components. At this phase of construction, no electrical work had been completed and future changes were made to the piping to facilitate the testing goals.

Figure 51: General location of major components on rolling stand

Figure 52 shows the nearly complete thermal emulator. At this phase of construction, minor changes were made to the piping for the purposes of introducing a step change in flow temperature, all instrumentation was connected and tested, and the

entire system was leak tested for various test conditions. The electrical work was also completed by this phase of construction which encompassed running power to the heating elements in the reservoir tanks and verifying that the VI could successfully control the heating elements with user input. Shakedown tests were completed at this phase prior to adding insulation to the heat exchanger, a necessary step for data collection.

Figure 52: Nearly complete thermal emulator

Figure 53 shows the piping at the top of reservoir Tank #1 and the electrical box where power enters the system from the wall. The piping shown is the wall supplied water for the shell side of the heat exchanger. This water is either fed into Tank #1 or bypasses the reservoirs to flow into the shell side of the heat exchanger. The electrical box shown contains the VI-controlled relays that enable or disable power to the heating

elements. Mounted on the top of the electrical box are two indicator lights that show whether the relays are switched on or off. This serves as a safety feature to help prevent the heating elements from being powered inadvertently.

Figure 53: Electrical power for heating elements and piping above Tank #1

Figure 54 shows the bottom of Tank #1 and #2. The piping located at the bottom of the tanks house thermocouples to monitor outlet temperatures. The piping from Tank #1 splits and can either be directed to the drain to empty the tank or up to the inlet of Tank #2. The outlet from Tank #2 leads to the inlet of the pump.

Figure 54: Heating elements and piping at bottom of tanks

Figure 55 shows the top of Tank #2. The thermocouple wires can be seen in yellow; routed together along the box tube rail and out of the way of any pipes. All of the silver wiring that leads to and from the DAQ hardware are AC lines used to power the relays on or off. These wires appear silver because they are shielded to prevent electromagnetic interference to any of the surrounding low voltage DC lines; the relay module is also wrapped in shielding as well. A fan is seen directing cooling air to the bottom of the air vent tank. The air vent tank is made from acrylic and the cooling air was to minimize the temperature at the metal pipe to acrylic interface as much as possible.

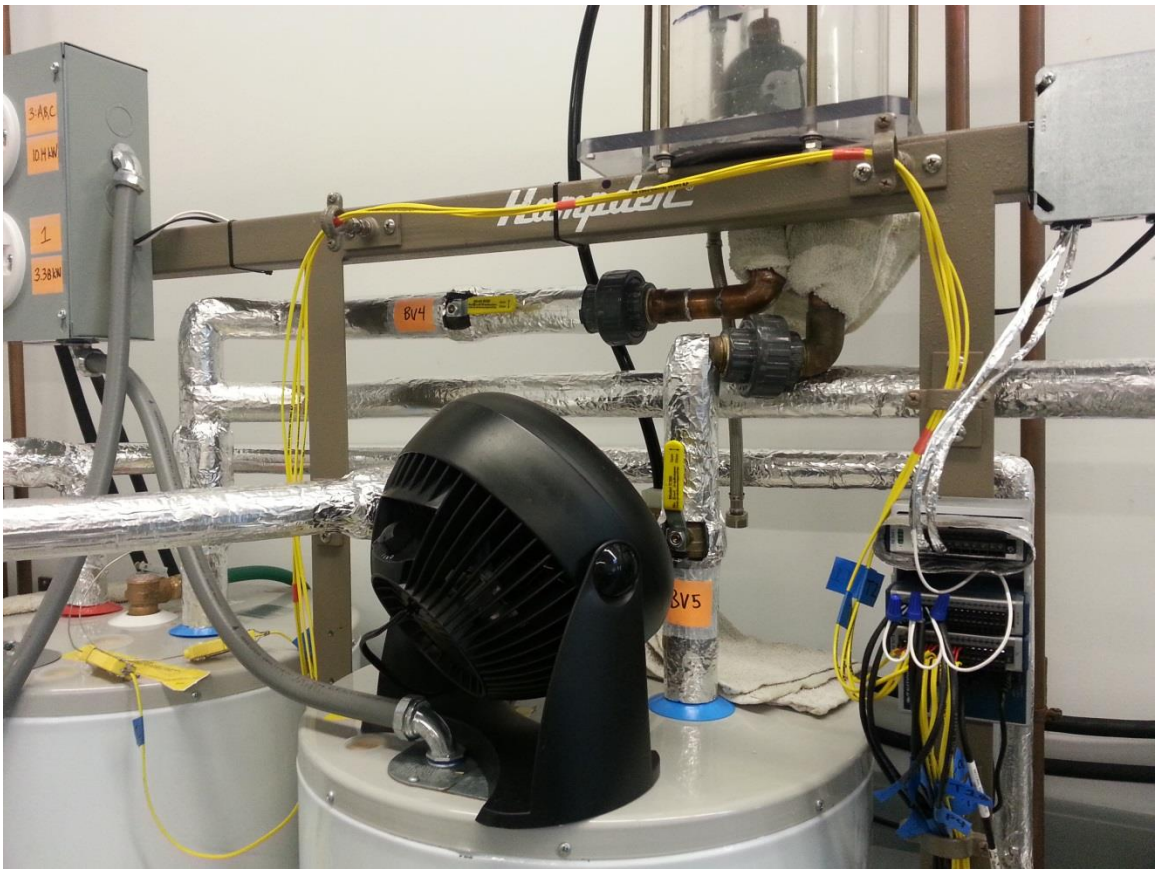

Figure 55: Air vent, piping, DAQ hardware location near top of Tank #2

Figure 56 shows the insulated heat exchanger ready for data collection. This view also shows the locations of the gate valve for flow control, the flowmeters, and all instrumentation located at the inlets and outlets of the heat exchanger. The pump, as well as one of the particle filters, can be seen located on the backside of the rolling frame.

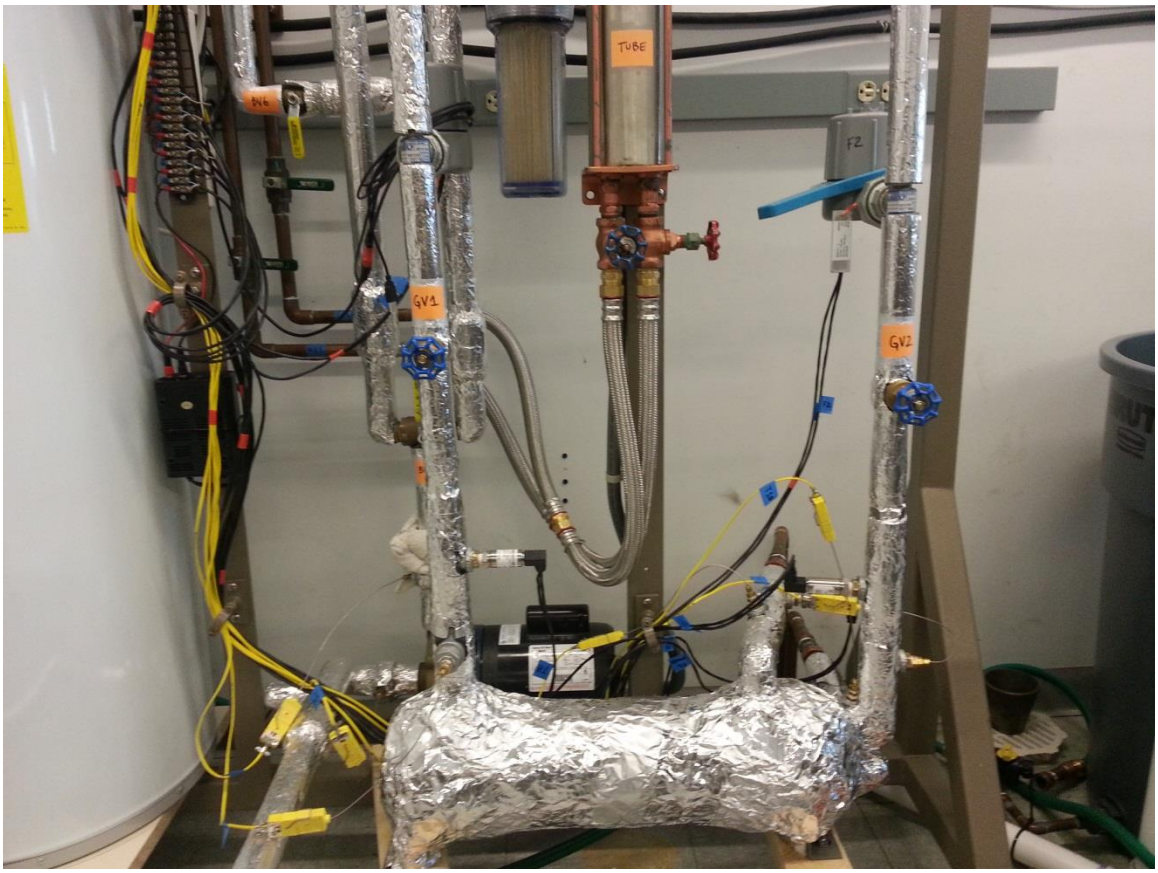

Figure 56: Instrumentation, piping, and insulation near heat exchanger

APPENDIX B: INSTRUMENTATION CALIBRATION

Thermocouple Calibration

Figure 57 shows the thermocouples in the chiller bath and Figure 58 shows a close-up view to see the relative location of the RTD and the thermocouples in the water bath. Just the tip of the RTD houses the sensing element, and as such, the ends of the thermocouples were placed in roughly the same location to minimize any local temperature transients from introducing bias to the calibration.

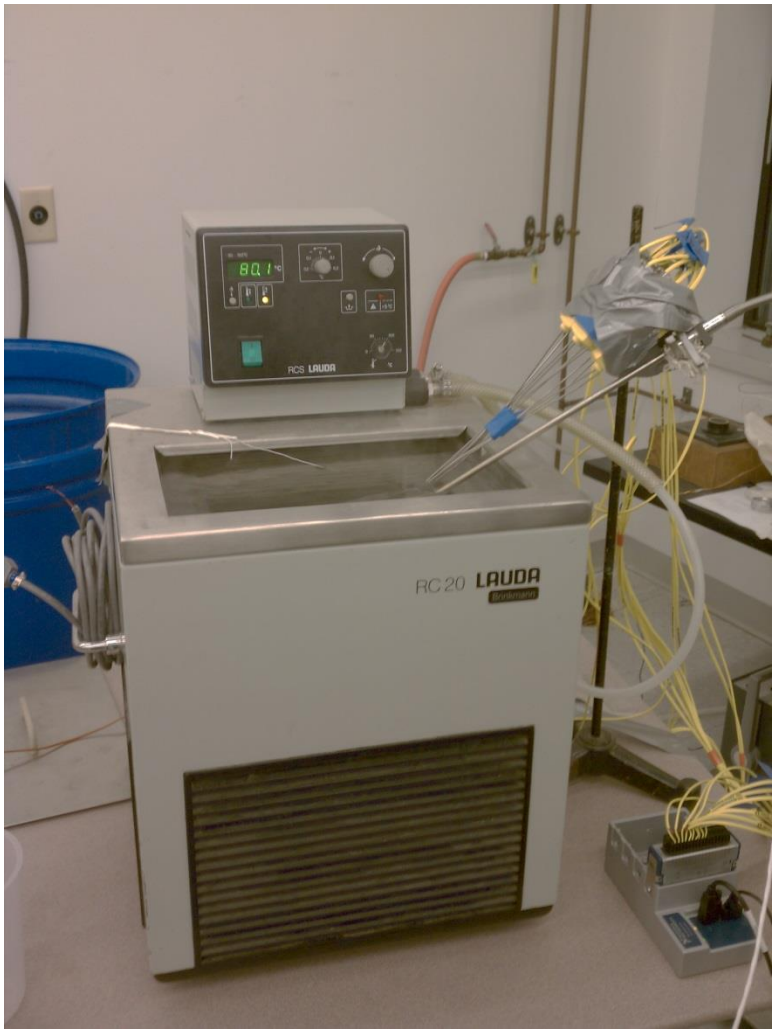

Figure 57: Chiller bath for thermocouple calibration

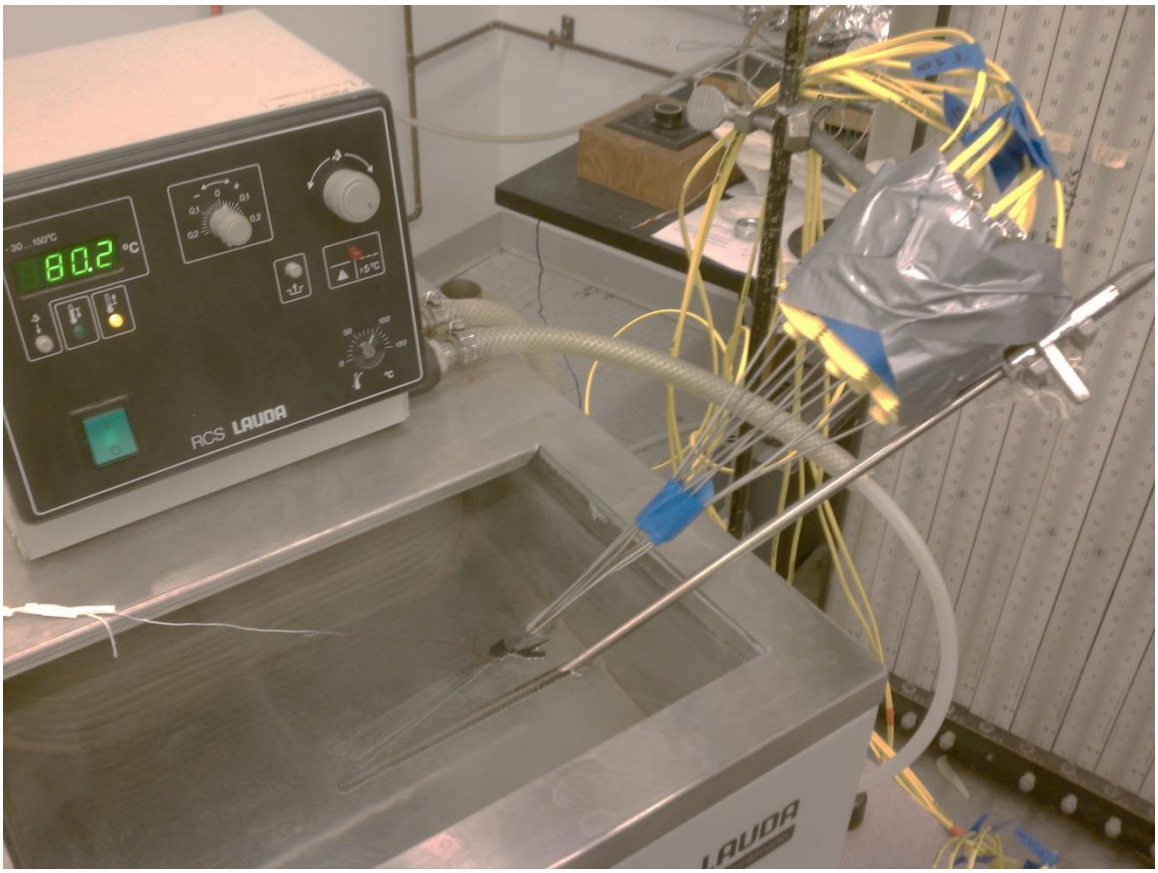

Figure 58: Location of thermocouples and RTD in chiller bath during calibration

The LabView VI used to collect the calibration data is seen in Figure 59. All ten thermocouples were connected to the DAQ hardware with the exact wiring configuration to be used in the thermal emulator and all measurements were made at the same time. The time derivative of each of the measurements was monitored to ensure that the water bath had actually reached steady state prior to collecting temperature measurements. This served to minimize the deviation of the points as close as possible down to the dead band of the temperature controller of the chiller. All thermocouple measurements and RTD readings were read and written to a text file for later analysis.

Figure 59: Labview VI used for thermocouple calibration

Flowmeter Calibration

The flowmeters were calibrated in the thermal emulator in the exact configuration that they were to be used for collecting test data to minimize any shift in the calibration associated with piping configuration changes. A schematic of the flow loop is seen in Figure 66 and a photo of the emulator where the flowmeters are located is found in Figure 60; the flowmeters are denoted with red arrows and are located immediately upstream of the fluid entrance to the heat exchanger for both the shell and tube side.

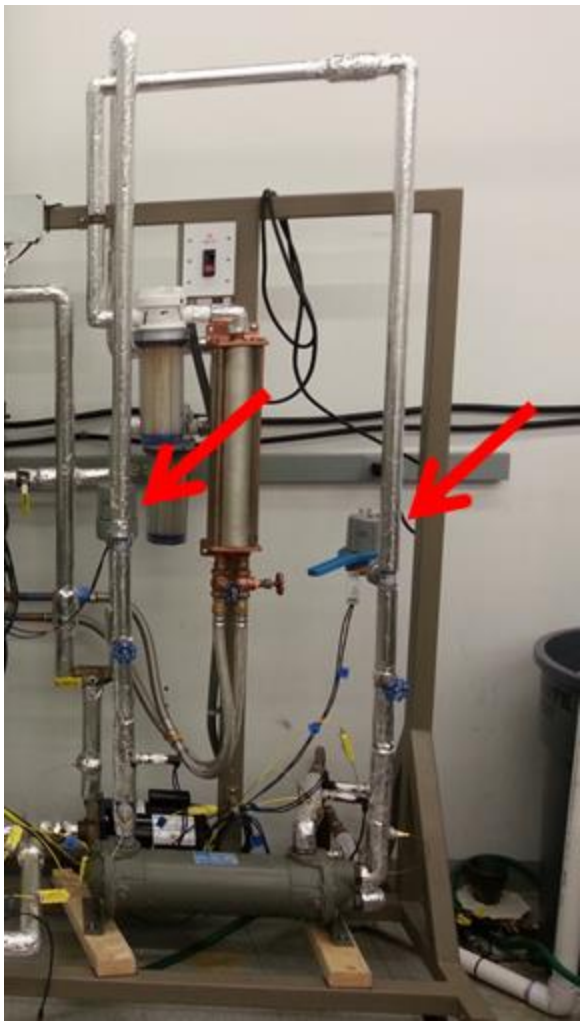

Figure 60: Location of flowmeters in thermal emulator

Figure 61 shows the drain and fill pipes used to direct the water flow for the test. The test was conducted by quickly switching the water flow from the drain tube to the fill tube when the timer was started. It was necessary to maintain the outlet of the hose at the same vertical height to prevent changing the backpressure and thus, the flow rate. The end of the hose was marked with a horizontal line to ensure that it stayed at the same height before and during the test. The potential change in backpressure also led to the design of the top of the drain and fill tubes. A tee fitting was chosen with the front opening left open for the researcher to see. This allowed an easy visual way to ensure

that water had not backed up in the pipes and formed a solid column of water up to the outlet of the hose; this would have changed the backpressure and the flow rates, throwing off the calibration for that calibration data point.

Figure 61: Drain and fill pipes for flowmeter calibration bin

Figure 62 shows the inside of the flowmeter calibration bin. From this view, several volume markings are seen on the inside of the bin. These markings were used to stop the timer for each calibration data point; the total time to fill to a set volume was recorded and used as an average flow rate for that test point.

Figure 62: Flowmeter calibration bin with visible volume markings

The fill tube layout can be seen in Figure 63. The fill tubes incorporated several 45 degree angles, a tall vent tube, and a diffuser piece with several holes at the bottom of the bin. Due to the volumetric flow rate of the water being introduced into the fill tube, without this type of layout, air bubbles were introduced into the bottom of the bin. As the bin filled up, these air bubbles caused the surface of the water to break up and not maintain a smooth surface; this made it difficult to tell the exact point and time at which the bin had been filled to the prescribed volume. The tubing layout allow the air bubbles to be released through the vent tube and the diffuser piece slowed the velocity of the water as it entered the bin through each orifice to a point that it did not froth and swirl.

This allowed the bin to be filled while maintaining a nearly perfectly flat surface, thus it was easy to identify exactly when the bin passed the calibrated volume markers.

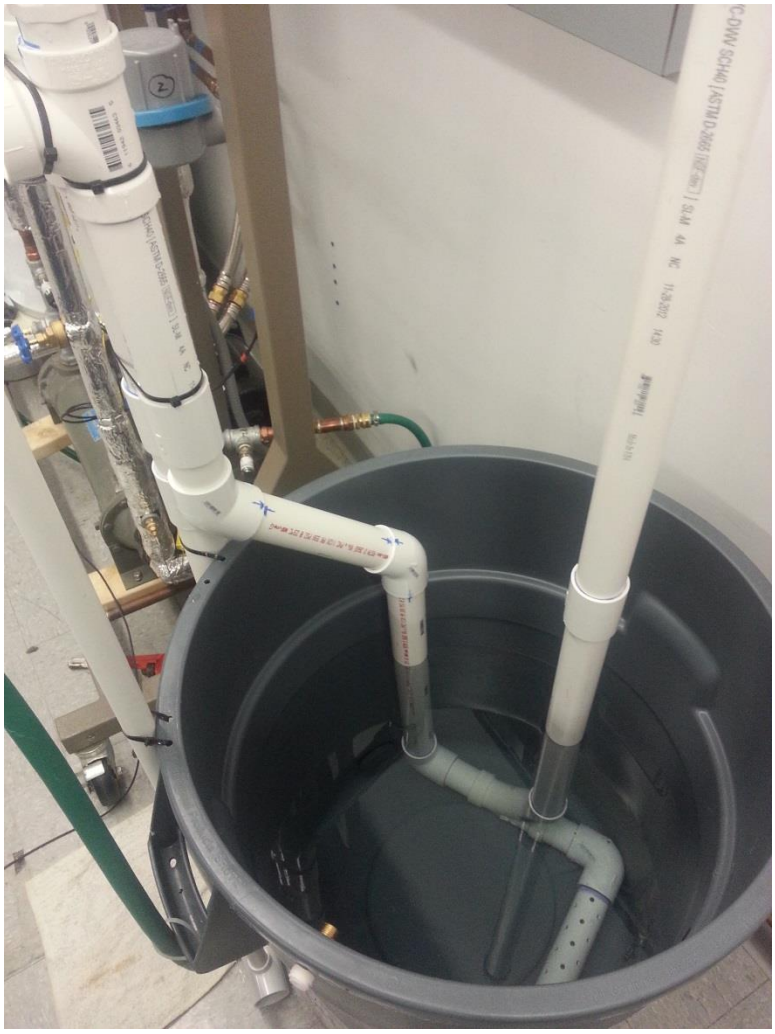

Figure 63: Flowmeter calibration bin fill pipe configuration

The drain pipes can be seen in Figure 64. The white PVC drain tube led directly to the drain and was used to reach a steady flow rate before starting each test. The bottom of the bin had a drain with a built-in cutoff valve. This cutoff valve allowed the bin to be filled during a test, but easily drained without having to manually bucket the water to the drain. After the bin was emptied, all remaining moisture was removed via

the use of an air compressor, a wet-dry vacuum, and a towel to ensure each test started from the same dry bin conditions.

Figure 64: Drain pipe from flowmeter calibration bin

Additional Calibration Data

The data from the shell side flowmeter calibration is included below for completeness. The procedure used to collect the data and determine the calibration is identical to that used for the tube side flowmeter; this information is found in the INSTRUMENTATION SELECTION & CALIBRATION section. The calibration for the shell side flowmeter includes 3 additional calibration data points when compared to

the tube side calibration. These additional data points were added at the 4 gpm set point as the original 4 gpm data was an outlier; these repeated data points showed that the original data point was truly an outlier. It is noted that in Table 13, the original incorrect data point (S4) was not included in the calibration; instead, it is replaced by data points S22, S23, and S24.

Table 13: Flowmeter calibration set points, shell side flowmeter (FM1)

Flow Rate, Target	Flow Rate, Claimed	Volume, Actual	Time, Target	Test Number	Time, Actual	Voltage, Average
[Volts]	[GPM]	[gal]	[sec]	[#]	[sec]	[Volts]
1	1.5	20.00522	800	S1	745.598	1.006336
1	1.5	20.00522	800	S14	749.797	1.001435
1	1.5	20.00522	800	S15	746.2	1.007619
1.3333	2	20.00522	600	S2	559.592	1.336496
1.3333	2	20.00522	600	S13	564.2	1.324752
1.3333	2	20.00522	600	S16	566.7	1.322135
2	3	30.00036	600	S3	554.195	2.009827
2	3	30.00036	600	S12	557.397	1.993729
2	3	30.00036	600	S17	556.292	1.996996
2.6666	4	40.000093	600	S11	551.1	2.663834
2.6666	4	40.000093	600	S18	556.296	2.640468
3.3333	5	40.000093	480	S5	438.7	3.334962
3.3333	5	40.000093	480	S10	440.8	3.3136
3.3333	5	40.000093	480	S19	438.296	3.333636
4	6	40.000093	400	S6	365.5	3.982189
4	6	40.000093	400	S9	363.996	3.996182
4	6	40.000093	400	S20	358.694	4.057604
4.3333	6.5	40.000093	369.23	S7	334.9	4.340329
4.3333	6.5	40.000093	369.23	S8	335.298	4.33719
4.3333	6.5	40.000093	369.23	S21	331.703	4.385608
2.6666	4	40.000093	600	S22	551.998	2.660955
2.6666	4	40.000093	600	S23	550.898	2.667929
2.6666	4	40.000093	600	S24	551.402	2.66347

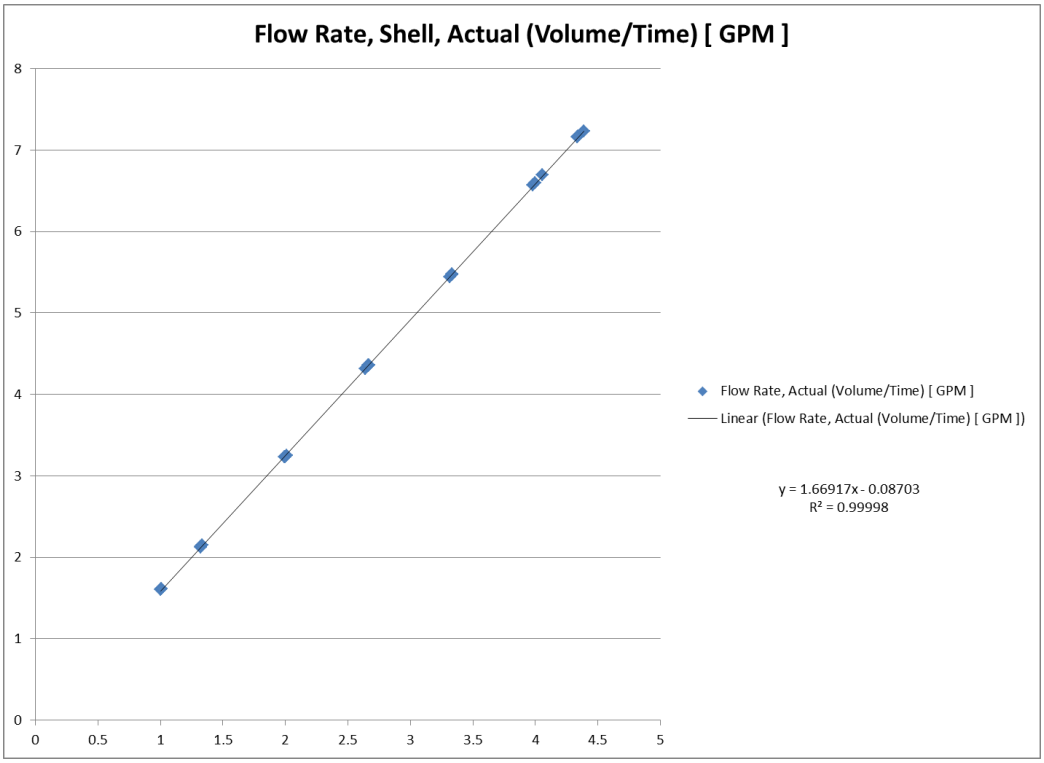

Figure 65: Calibration data points and curve fit, shell side flowmeter

APPENDIX C: EXPERIMENTAL PROCEDURES

The detailed procedures necessary to complete each test successfully are defined here. All phases of testing refer to Figure 6 and Table 9. This figure and table are repeated here for continuity with the step-by-step instructions that follow.

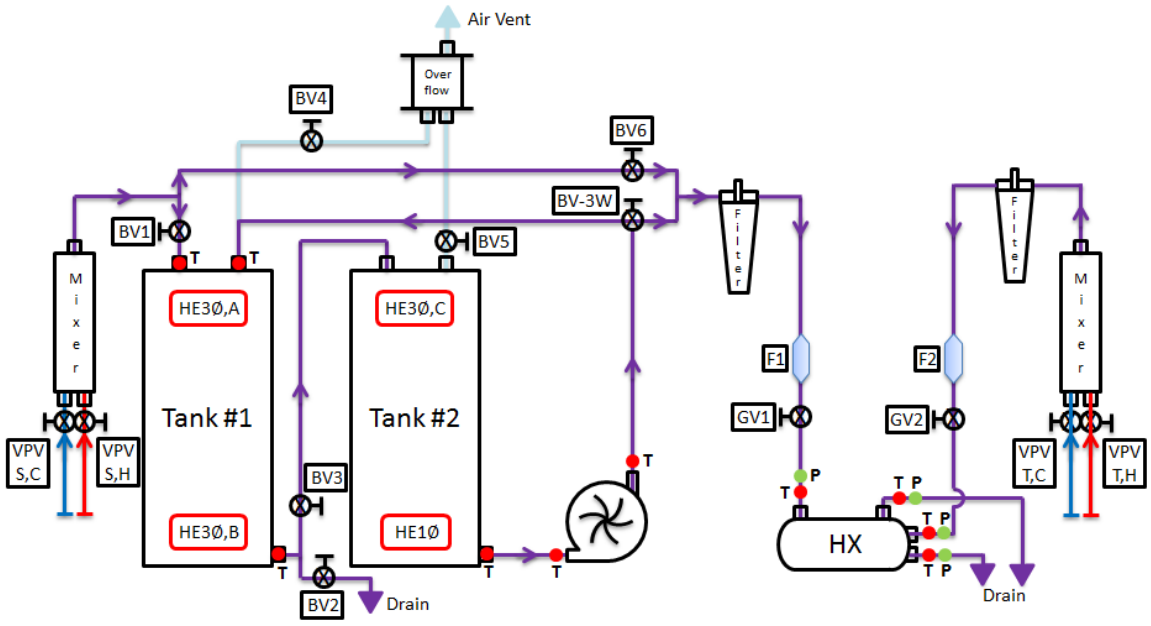

Figure 66: Experimental thermal emulator with labeled valves and instrumentation

Table 14: Control labels, names, and functions

Label	Name	Function
VPV-S,C	V-port valve, shell side, cold	Fine control of cold water flow rate into the system on the shell side of the emulator
VPV-S,H	V-port valve, shell side, hot	Fine control of hot water flow rate into the system on the shell side of the emulator; also used to control bypass flow rate
VPV-T,C	V-port valve, tube side, cold	Fine control of cold water flow rate into the system on the tube side of the emulator; also used to control bypass flow rate
VPV-T,H	V-port valve, tube side, hot	Fine control of hot water flow rate into the system on the tube side of the emulator
BV1	Ball valve, 1	Binary flow control (on/off); allows fluid into tanks, as well as to bypass recirculation tanks
BV2	Ball valve, 2	Binary flow control (on/off); To drain Tank #1
BV3	Ball valve, 3	Binary flow control (on/off); allows or prohibits

		flow between Tank #1 and Tank #2
BV4	Ball valve, 4	Binary flow control (on/off); air purge to atmosphere for Tank #1 during filling, and air vent during draining to prevent hydro lock
BV5	Ball valve, 5	Binary flow control (on/off); air purge to atmosphere for Tank #2 during filling, and air vent during draining to prevent hydro lock
BV6	Ball valve, 6	Binary flow control (on/off); allows or prohibits bypass of tanks for shell side
BV-3W	Ball valve, 3-way	Directs flow in 1 of 2 directions: Position #1 recirculates fluid through tanks; Position #2 drains to shell side of hx
GV1	Gate valve, 1	Main control valve for flow rate through shell side of hx
GV2	Gate valve, 2	Main control valve for flow rate through tube side of hx
HE3θ,A	Heating element, 3-phase, element A	1st of 3 heating elements for 3-phase power, cannot be operated independently of other 3-phase elements
HE3θ,B	Heating element, 3-phase, element B	2nd of 3 heating elements that operate in unison, cannot be operated independently of other 3-phase elements
HE3θ,C	Heating element, 3-phase, element C	3rd of 3 heating elements that operate in unison, cannot be operated independently of other 3-phase elements
HE1θ	Heating element, single phase, element 1	Single heating element, can be operated individually and independently from 3-phase heating elements

In order to simplify the process of conducting an experimental test repeatedly, a table was constructed of the labels and the valve position defined for when no testing is being conducted. This is the state that all controls should be placed when testing is completed each day; therefore, it is also the state for the warm-up phase. The warm-up phase is only completed once, prior to conducting any tests for the day. It is the process by which the software and hardware are all readied for testing. Table 15, below, shows these initial control positions, followed with step-by-step instructions to complete the warm-up phase of the experiment.

Table 15: Warm-up phase, initial control positions

VPV-S,C	Closed	BV1	Closed	BV5	Closed	GV1	Closed
VPV-S,H	Closed	BV2	Closed	BV6	Closed	GV2	Closed
VPV-T,C	Closed	BV3	Closed	BV-3W	Position #1	HE3θ	Off
VPV-T,H	Closed	BV4	Closed	-	-	HE1θ	Off

1.) Switch on electrical supply for thermal emulator DAQ components via switch on the power strip.

2.) Plug pump into the wall outlet.

3.) Plug heating elements supply cords into respective wall outlets.

4.) Power up DAQ computer.

5.) Connect USB cord from DAQ module to front lower USB port on the front of the DAQ computer.

6.) Run LabView by opening the "Test 10.vi" virtual instrumentation (VI).

7.) Enter proper values into required boxes within LabView VI for data collection:

   a. Thermocouple sampling rate: 10 Hz

   b. Flowmeter sampling rate: 10 Hz

   c. Path for output file: "C:\Users\carperjl\Desktop\Data\Warmup_DATE.txt" where DATE is the current date for the block of testing.

8.) Run the VI.

9.) Open the following valves in the order listed for the shell side:

   a. VPV-S,C

   b. BV6

   c. GV1: Open slowly while watching flow rate for shell side within VI

      i. Set flow rate to at least 4 GPM

      ii. Note: Maintain flow rate ***less than*** 7.5 GPM

10.) Open the following valves in the order listed for the tube side:

a. VPV-T,C

b. GV2: Open slowly while watching flow rate for tube side within VI

i. Set flow rate to at least 4 GPM

ii. Note: Maintain flow rate ***less than*** 7.5 GPM

11.) Wait at least 15 minutes for DAQ modules to reach steady-state operating temperatures and for cold water supply temperature to stabilize at steady-state value (minimal temperature variations within a reasonable amount of time).

12.) Thermal emulator has now completed warm-up phase.

With the warm-up phase complete, it is now possible to move onto filling the tanks with water. The first step is to identify which test is to be completed and the prescribed fluid conditions. Once the fluid conditions are known, it is possible to adjust the controls accordingly. Table 16 below shows the initial position of the controls, after completing the warm-up phase, followed with step-by-step instructions to fill the tanks.

Table 16: Tank filling phase, initial control positions

VPV-S,C	OPEN	BV1	Closed	BV5	Closed	GV1	OPEN
VPV-S,H	Closed	BV2	Closed	BV6	OPEN	GV2	OPEN
VPV-T,C	OPEN	BV3	Closed	BV-3W	Position #1	HE3θ	Off
VPV-T,H	Closed	BV4	Closed	-	-	HE1θ	Off

1.) Close BV6.

2.) Close VPV-S,C.

3.) Adjust GV2 to set desired flow rate for tube side of experiment.

4.) To fill tanks:

a. Open BV4 & BV5 to vent tanks to atmosphere.

b. Open BV3 to allow fluid flow from Tank #1 to Tank #2.

c. Open BV1 to allow water to enter Tank #1.

d. Adjust VPV-S,C and VPV-S,H to maintain temperature at TC01 as close as possible to desired shell side temperature.

    i. If desired shell side temperature is greater than 50 °C, only fill tanks via VPV-S,H; while keeping VPV-S,C closed.

e. Monitor air vent tank; as soon as water is seen rising in the vent tank:

    i. ***Immediately*** close BV4 and BV5 (the recirculation tanks are now pressurized and purged of air).

        1. Note: Air vent tank may ***NEVER*** become fully filled and pressurized with water or major leaks will occur!

    ii. Close VPV-S,C and VPV-S,H.

    iii. Close BV1.

    iv. Open BV4 to de-pressurize system.

    v. Close BV4 to close system.

With the tank filling phase complete, it is now possible to move onto recirculation and heating, if necessary. Table 17 below shows the initial position of the controls, after completing the warm-up phase, followed with step-by-step instructions to fill the tanks.

Table 17: Recirculation and heating phase, initial control positions

VPV-S,C	Closed	BV1	Closed	BV5	Closed	GV1	OPEN
VPV-S,H	Closed	BV2	Closed	BV6	OPEN	GV2	OPEN
VPV-T,C	OPEN	BV3	OPEN	BV-3W	Position #1	HE3θ	Off
VPV-T,H	Closed	BV4	Closed	-	-	HE1θ	Off

1.) Switch pump on via control switch on thermal emulator frame.

2.) Take note of audible tone that the pump generates as it recirculates fluid through the unpressurized tanks.

a. Tone should be reasonably low-pitched and not sound labored.

3.) If the temperature of the water in the tanks needs to be raised to reach the desired flow temperature for the shell side:

a. Switch on HE3θ in LabView VI by pressing ‘F5’ on the keyboard.

b. Switch on HE1θ in LabView VI by pressing ‘F6’ on the keyboard.

c. Note: Heating elements may only be powered for the following two cases:

i. Unpressurized system *and* pump ON

ii. Pressurized system *and* pump OFF

d. TC02 – TC06 are continuously monitored for desired temperature.

e. If tone of pump becomes much higher-pitched than under normal operating conditions or sounds labored, pressure build-up will need to be relieved:

i. BV4 is opened *slightly* to relieve pressure build-up.

ii. As soon as pump tone returns to normal, BV4 is again closed.

4.) While tank fluid is being recirculated and heated, cold bypass water is sent through shell side of heat exchanger for preliminary adjustments to GV1:

a. VPV-S,C is opened.

b. BV6 is opened.

c. GV1 is now adjusted to desired shell flow rate by monitoring the flow rate within LabView VI.

i. Note: The shell flow rate will need adjusted further once fluid in tanks has reached desired operating temperature due to differences in pressure from supply water and centrifugal pump.

5.) When recirculation fluid reaches the desired temperature:

   a. HE3θ is switched off.

   b. HE1θ is switched off.

6.) Fluid is now recirculating at desired temperature.

With the fluid recirculating at the desired temperature, it is now possible to move onto adjustment of GV1 to achieve the desired flow rate through the shell side of the heat exchanger. Table 18 below shows the initial position of the controls when beginning to make final adjustments to GV1, followed with step-by-step instructions to make necessary adjust both the tank fluid flow rate and the cold water supply flow rate.

Table 18: Shell flow rate adjustment phase, initial control positions

VPV-S,C	OPEN	BV1	Closed	BV5	Closed	GV1	OPEN
VPV-S,H	Closed	BV2	Closed	BV6	OPEN	GV2	OPEN
VPV-T,C	OPEN	BV3	OPEN	BV-3W	Position #1	HE3θ	Off
VPV-T,H	Closed	BV4	Closed	-	-	HE1θ	Off

1.) BV4 is opened *slightly* to draw air when tank fluid is directed through shell side of heat exchanger.

2.) ***Simultaneously*** make the following valve position changes:

   a. Close BV6.

   b. Switch BV-3W from Position #1 to Position #2.

3.) ***Immediately*** following (2.), above, open BV4 fully.

4.) Adjust GV1 to maintain desired flow rate through shell side of heat exchanger by monitoring the flow rate within LabView VI.

5.) As soon as GV1 is adjusted to desired flow rate, ***simultaneously*** make the following valve position changes:

   a. Open BV6.

b. Switch BV-3W from Position #2 to Position #1.

6.) ***Immediately*** following (5.), above, close BV4 fully.

7.) Adjust VPV-S,C to maintain desired flow rate through shell side of heat exchanger.

a. Note: This step is necessary due to different supply pressures between wall and pump fluid.

With the shell side flow rate adjusted properly, it is now possible to conduct the test and gather experimental data. Table 19 below shows the initial position of the controls when beginning the test, followed with step-by-step instructions for conducting the test and recording experimental data.

Table 19: Test phase, initial control positions

VPV-S,C	OPEN	BV1	Closed	BV5	Closed	GV1	OPEN
VPV-S,H	Closed	BV2	Closed	BV6	OPEN	GV2	OPEN
VPV-T,C	OPEN	BV3	OPEN	BV-3W	Position #1	HE3θ	Off
VPV-T,H	Closed	BV4	Closed	-	-	HE1θ	Off

1.) The currently running VI within LabView is stopped by pressing 'Escape' on the keyboard.

2.) BV4 is opened *slightly* to draw air when tank fluid is directed through shell side of heat exchanger.

3.) A new path is entered (filename) for the output of the experimental data:

a. Path for output file: "C:\Users\carperjl\Desktop\Data\FILENAME.txt" where FILENAME an appropriate name that will not be confusing at a later date.

4.) The VI is run.

5.) Data is recorded for 500 seconds with the same temperature cold water running through both the shell and tube side of the heat exchanger.

6.) At 500 seconds, ***simultaneously*** make the following valve position changes to introduce a step change in temperature on the shell side:

    a. Close BV6.

    b. Switch BV-3W from Position #1 to Position #2.

7.) ***Immediately*** following (6.), above, open BV4 fully.

8.) If the shell side flow rate is maintained at the desired value, continue to record data for 500 seconds after completing (6.), above.

9.) If the shell side flow rate is ***NOT*** maintained at the desired value:

    a. Stop the LabView VI and write data to file by pressing 'Escape' on the keyboard.

    b. ***Simultaneously*** make the following valve position changes:

        i. Open BV6.

        ii. Switch BV-3W from Position #2 to Position #1.

    c. ***Immediately*** following (9b.), above, close BV4 fully.

    d. Delete the file containing the bad data that was written when the VI was halted.

    e. It is now necessary to ***repeat*** the following phases:

        i. Filling fluid reservoirs,

        ii. Recirculation and heating,

        iii. Adjustment of gate valve, and

        iv. Conducting the test.

10.) After 1000 seconds have elapsed from the start of the recording, ***simultaneously*** make the following valve position changes to introduce a step change in temperature on the shell side (opposite direction):

a. Open BV6.

b. Switch BV-3W from Position #2 to Position #1.

11.) Continue to record data for 500 seconds after completing (10.), above.

12.) Stop the LabView VI and write data to file by pressing 'Escape' on the keyboard.

APPENDIX D: RESULTS

There were a total of 63 cases of data that was experimentally collected to cover a broad operating envelope of the heat exchanger. Of those 63 cases, the shell outlet temperature was examined in detail in the RESULTS & DISCUSSION section of this document for three of those cases: Cases 15, 37, and 42. All plots that were required to calculate the uncertainties and final outputs for the shell streams are included here for these three cases, as well as those covering the tube fluid streams. The plots are presented on a case by case basis and will repeat several of the plots that were presented previously, but they are included for continuity and completeness.

Case 15

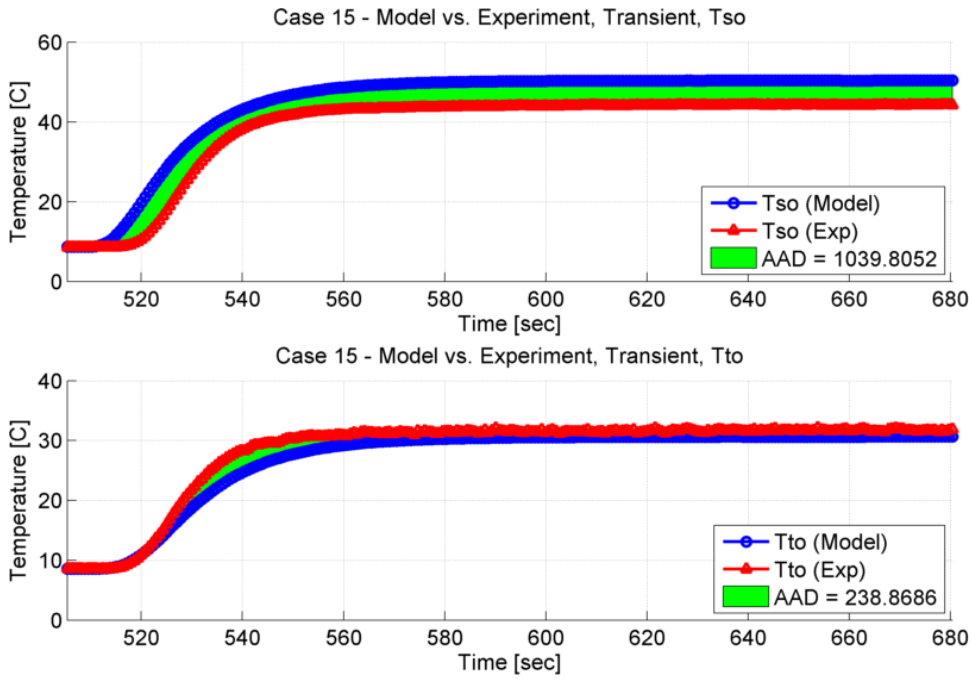

Figure 67: Case 15, Outlet Temperatures, Model & Experiment, AAD

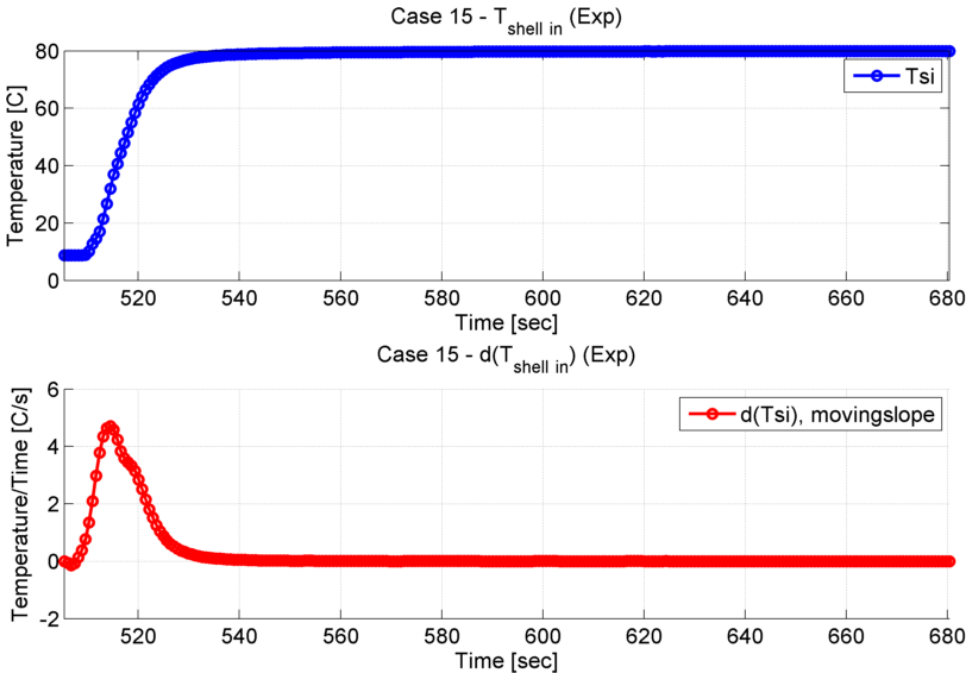

Figure 68: Case 15, Shell Inlet Temperature and Derivative of Shell Inlet Temperature (Experiment)

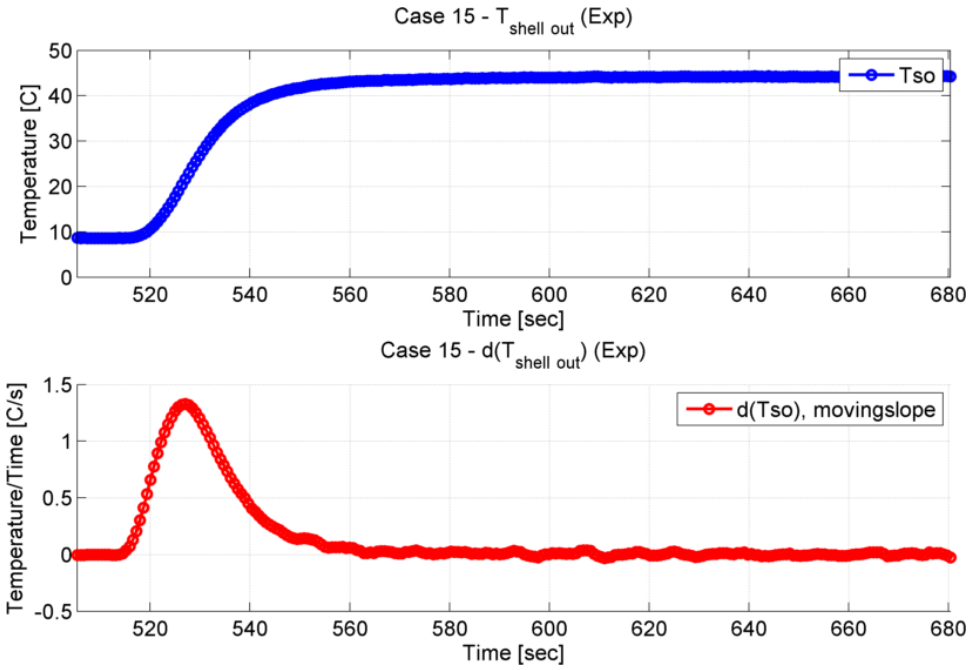

Figure 69: Case 15, Shell Outlet Temperature and Derivative of Shell Outlet Temperature (Experiment)

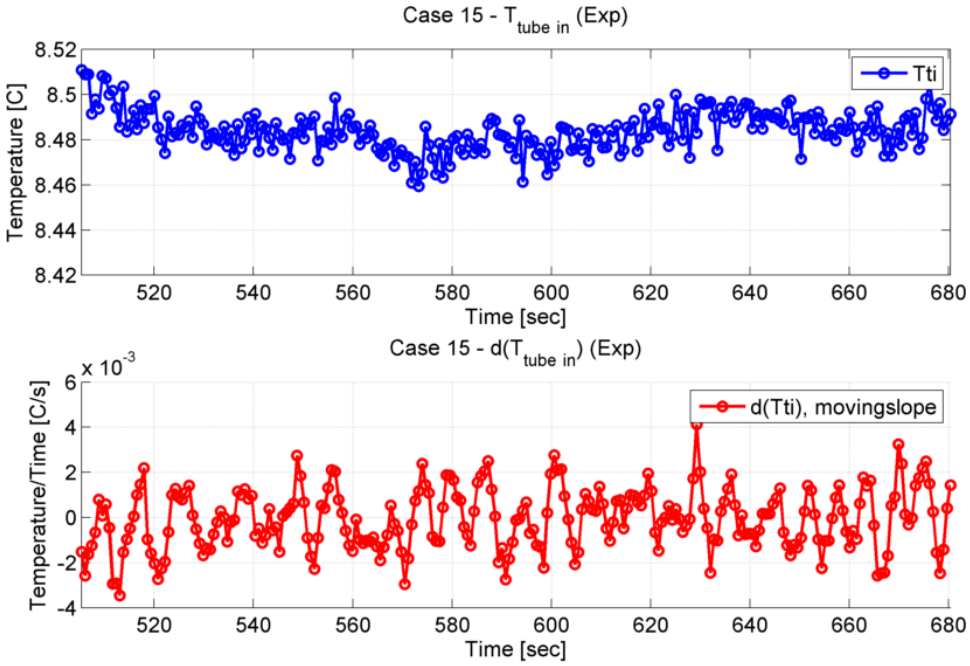

Figure 70: Case 15, Tube Inlet Temperature and Derivative of Tube Inlet Temperature (Experiment)

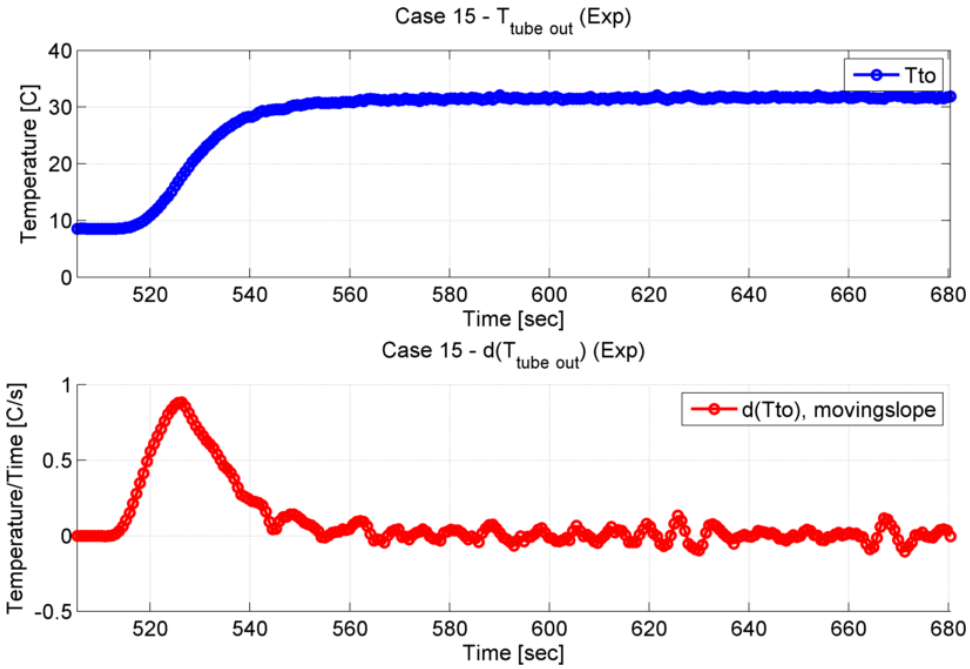

Figure 71: Case 15, Tube Outlet Temperature and Derivative of Tube Outlet Temperature (Experiment)

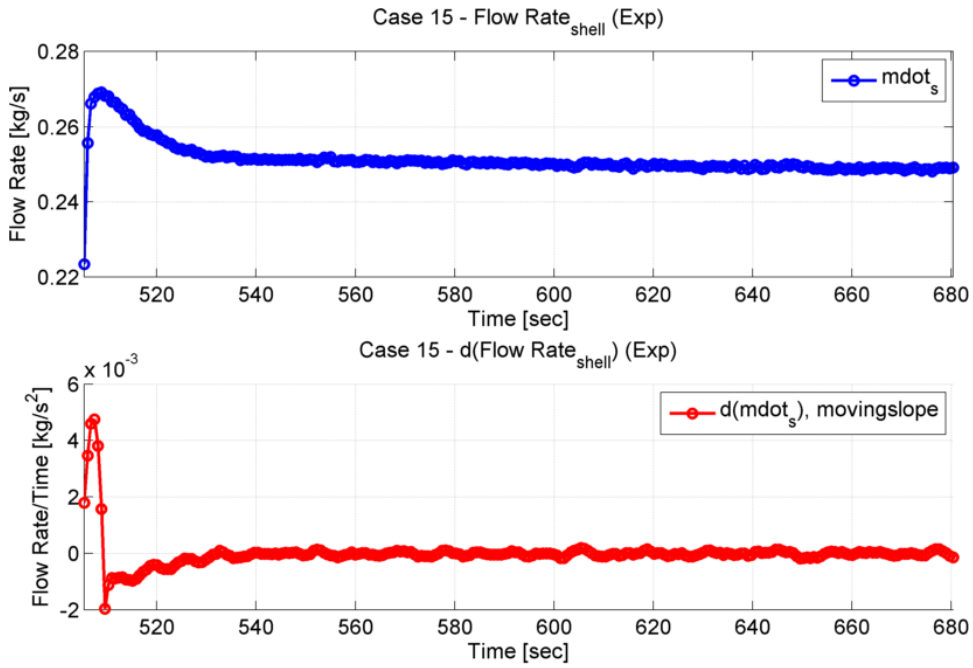

Figure 72: Case 15, Shell Mass Flow Rate and Derivative of Shell Mass Flow Rate (Experiment)

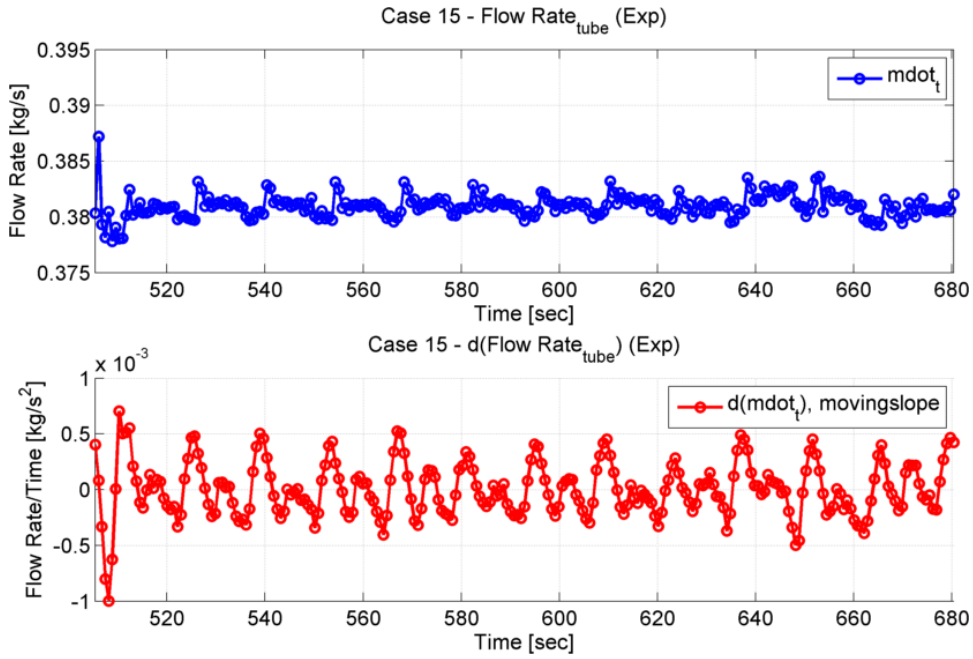

Figure 73: Case 15, Tube Mass Flow Rate and Derivative of Tube Mass Flow Rate (Experiment)

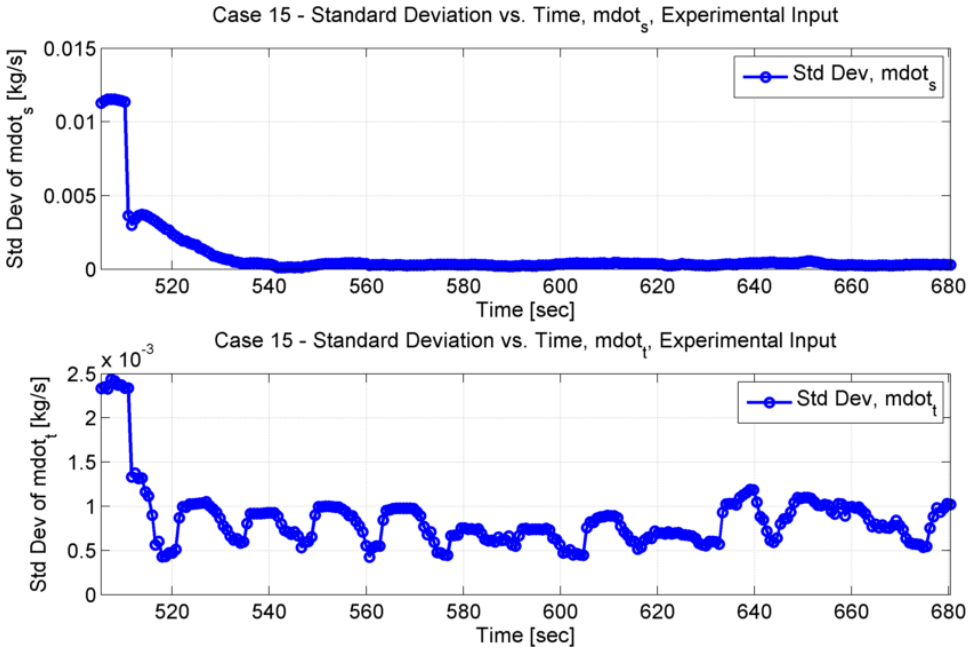

Figure 74: Case 15, Standard Deviation vs. Time, Mass Flow Rates

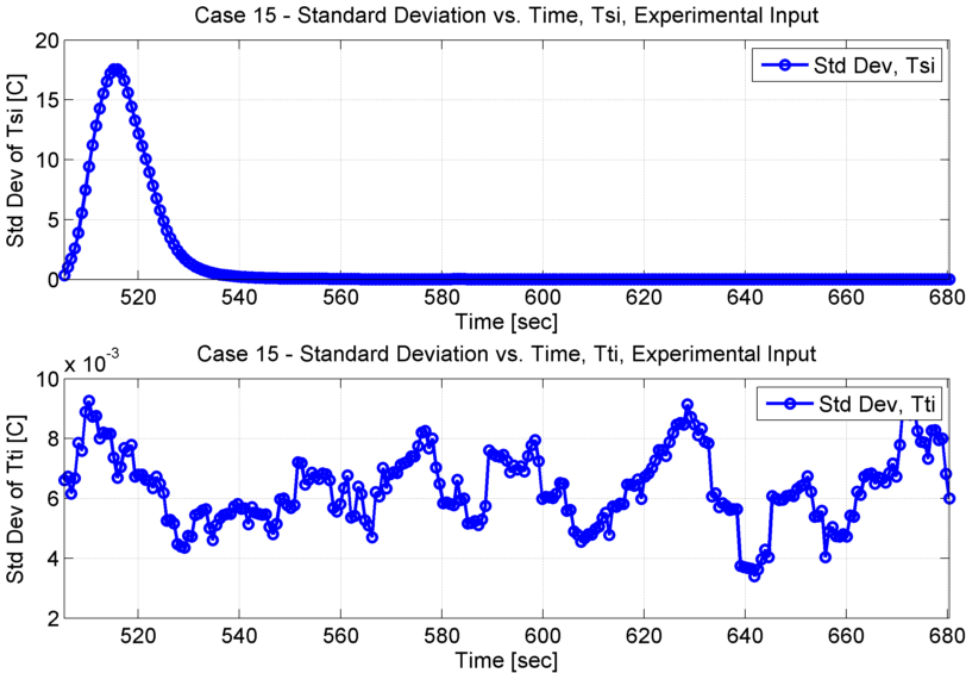

Figure 75: Case 15, Standard Deviation vs. Time, Inlet Temperatures

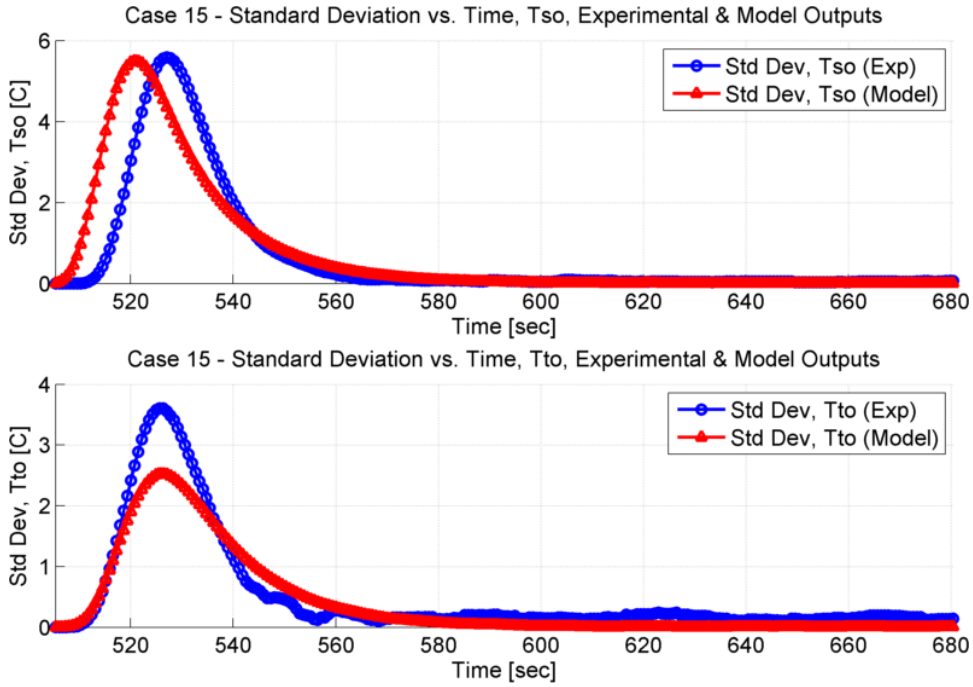

Figure 76: Case 15, Standard Deviation vs. Time, Outlet Temperatures

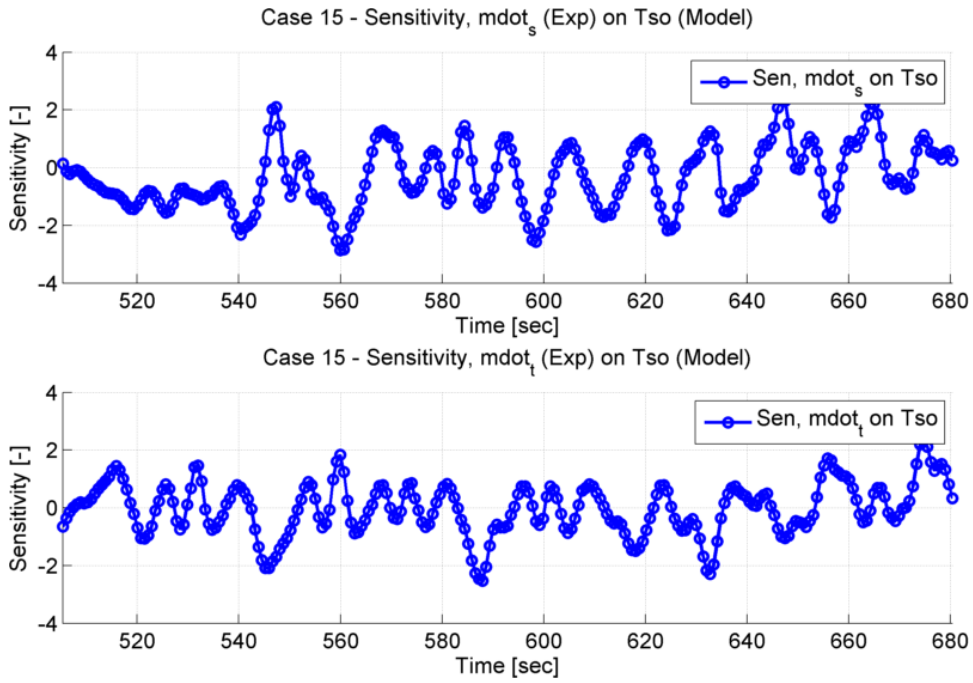

Figure 77: Case 15, Sensitivities vs. Time, Mass Flow Rates on Shell Outlet Temperature

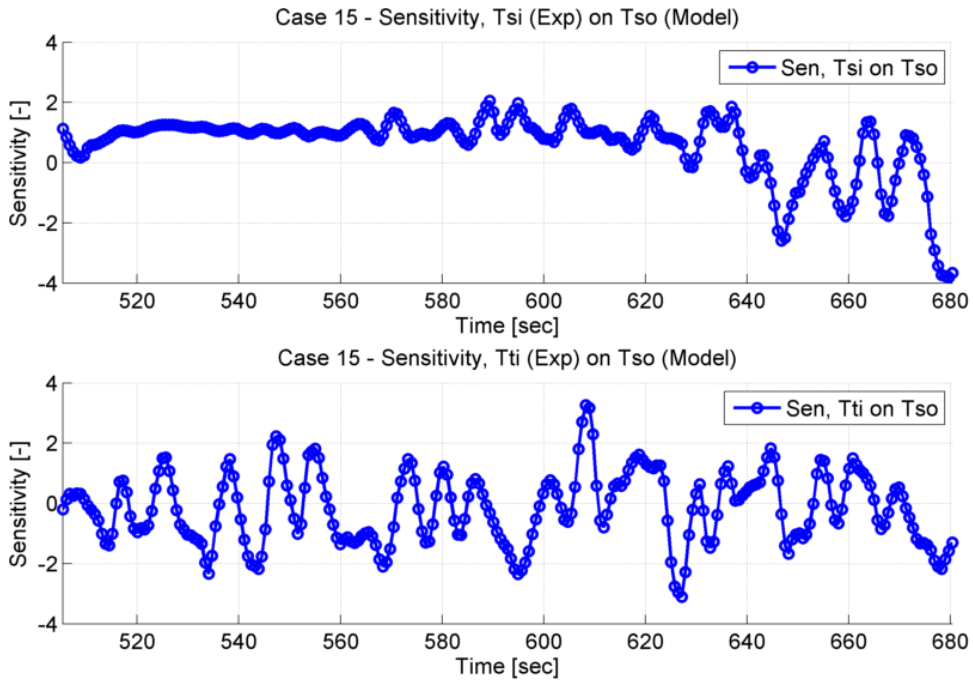

Figure 78: Case 15, Sensitivities vs. Time, Inlet Temperatures on Shell Outlet Temperature

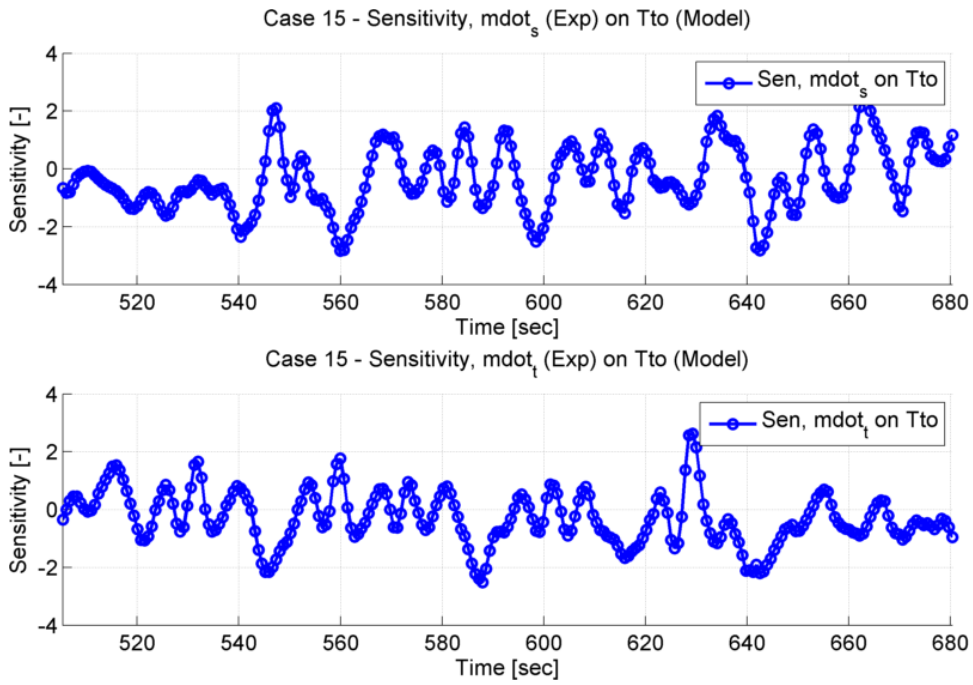

Figure 79: Case 15, Sensitivities vs. Time, Mass Flow Rates on Tube Outlet Temperature

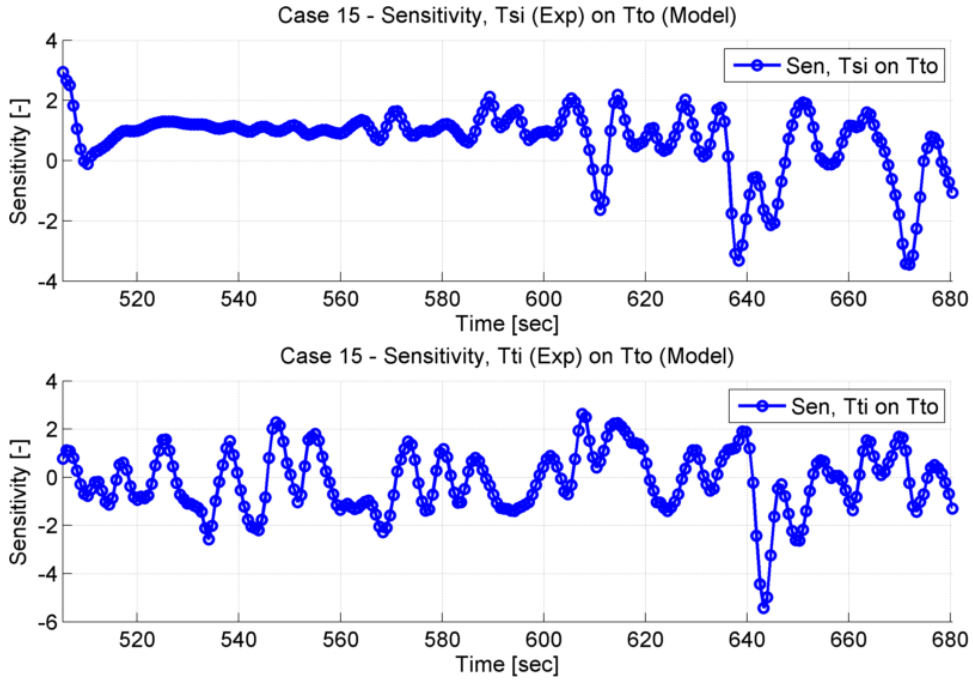

Figure 80: Case 15, Sensitivities vs. Time, Inlet Temperatures on Tube Outlet Temperature

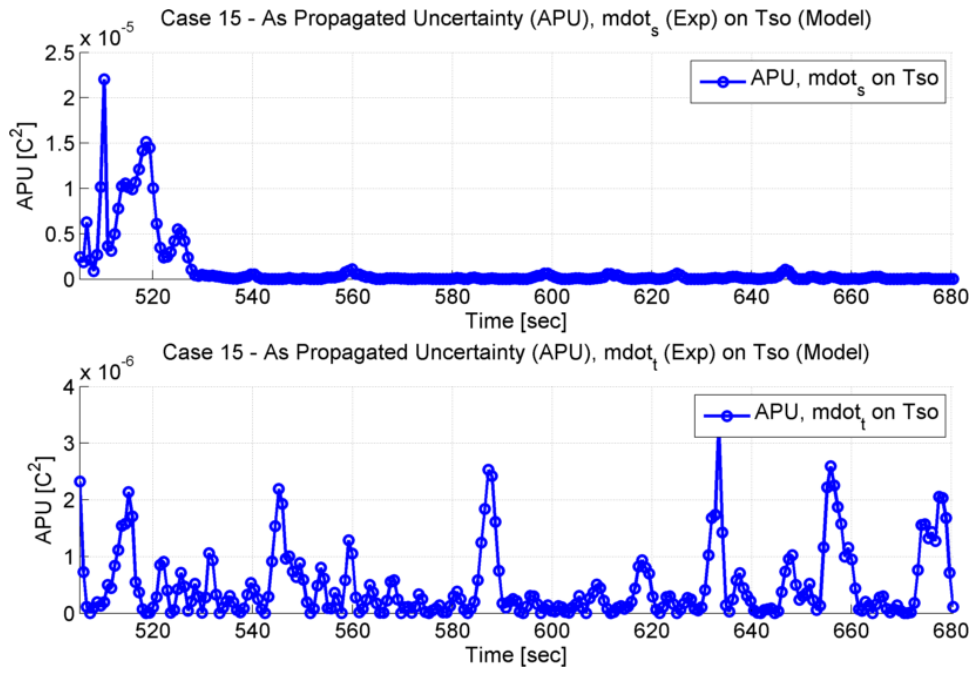

Figure 81: Case 15, As Propagated Uncertainties vs. Time, Mass Flow Rates on Shell Outlet Temperature

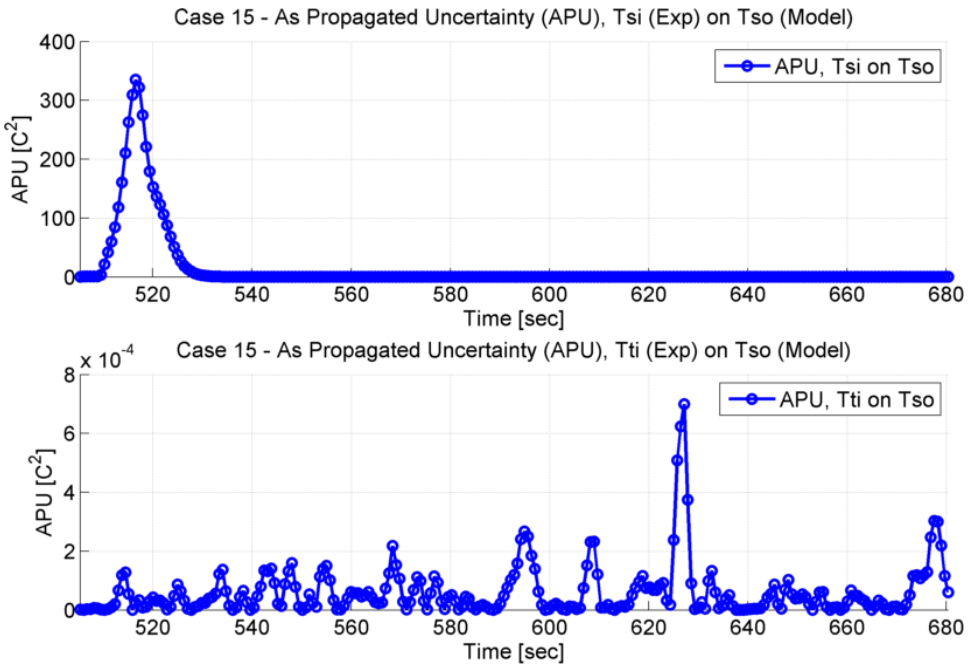

Figure 82: Case 15, As Propagated Uncertainties vs. Time, Inlet Temperatures on Shell Outlet Temperature

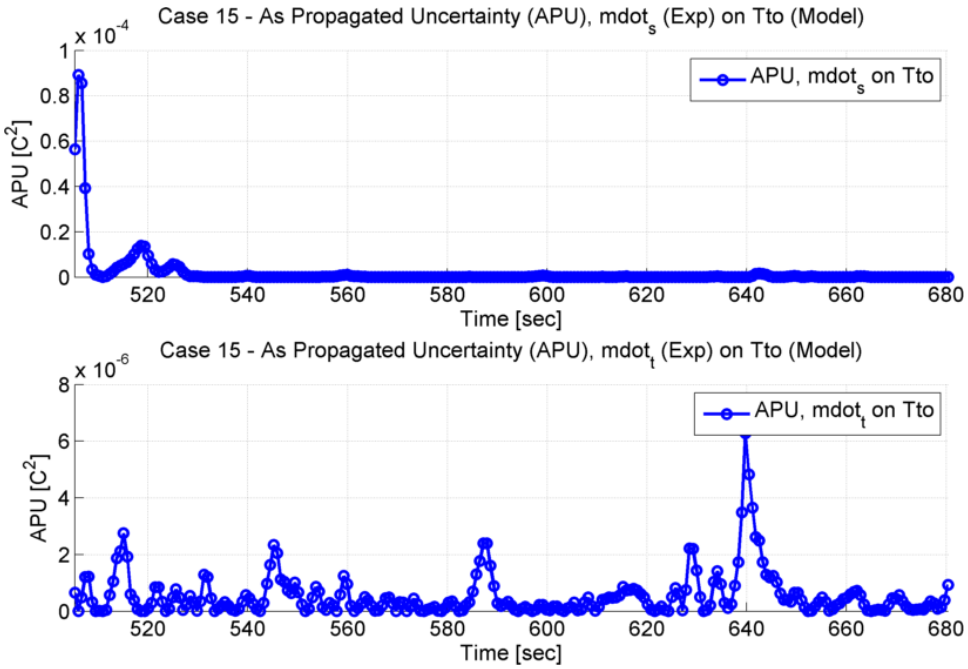

Figure 83: Case 15, As Propagated Uncertainties vs. Time, Mass Flow Rates on Tube Outlet Temperature

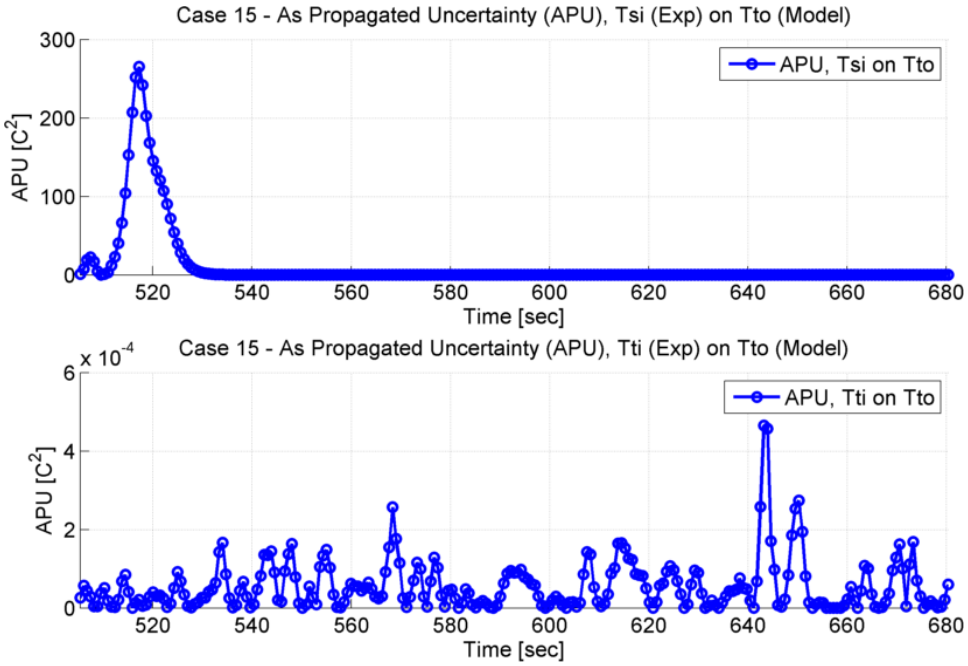

Figure 84: Case 15, As Propagated Uncertainties vs. Time, Inlet Temperatures on Tube Outlet Temperature

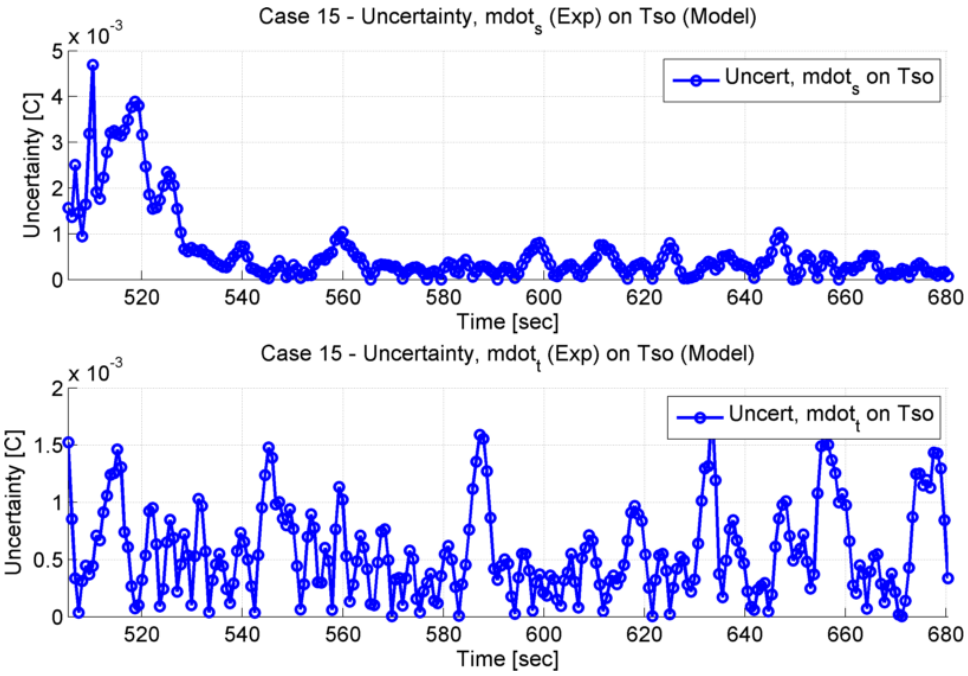

Figure 85: Case 15, Uncertainties vs. Time, Mass Flow Rates on Shell Outlet Temperature

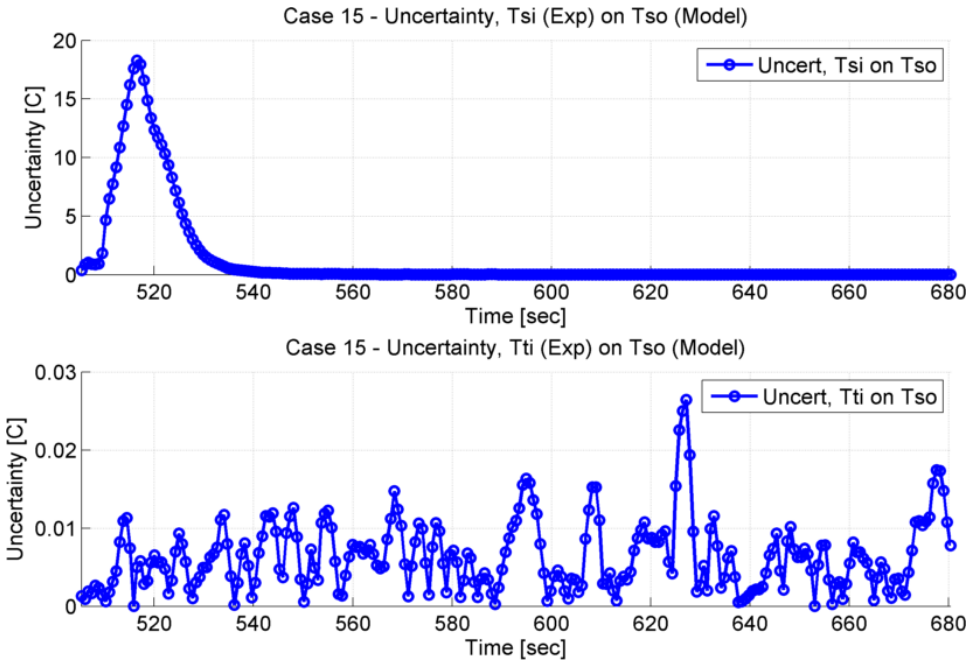

Figure 86: Case 15, Uncertainties vs. Time, Inlet Temperatures on Shell Outlet Temperature

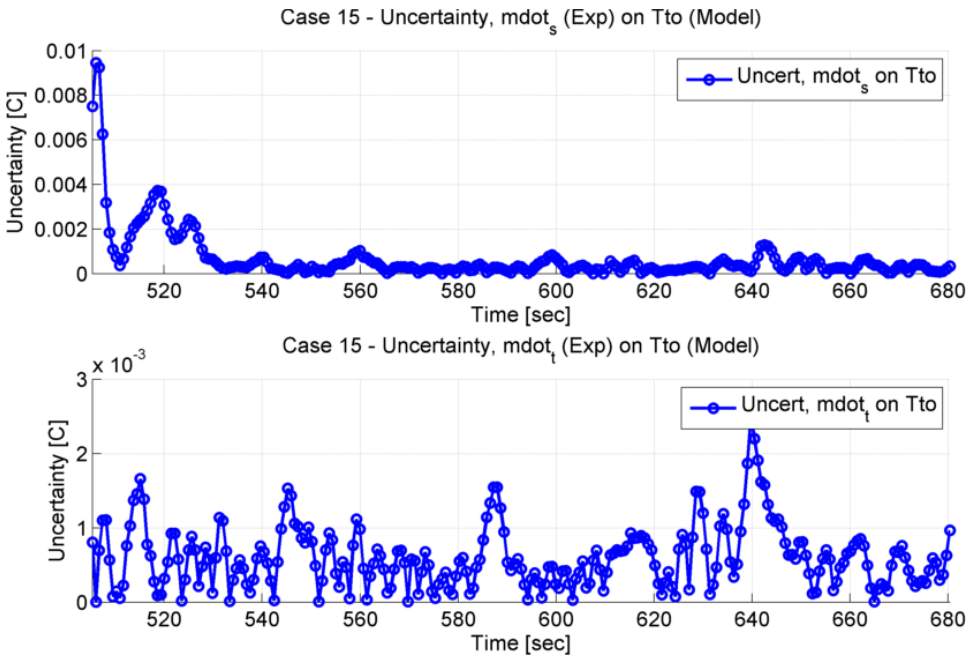

Figure 87: Case 15, Uncertainties vs. Time, Mass Flow Rates on Tube Outlet Temperature

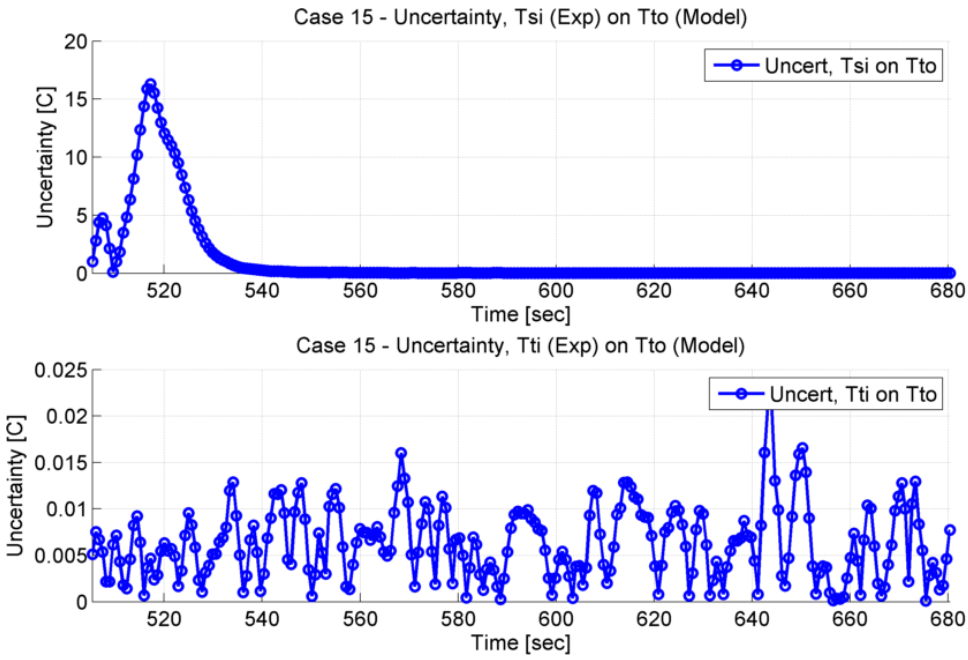

Figure 88: Case 15, Uncertainties vs. Time, Inlet Temperatures on Tube Outlet Temperature

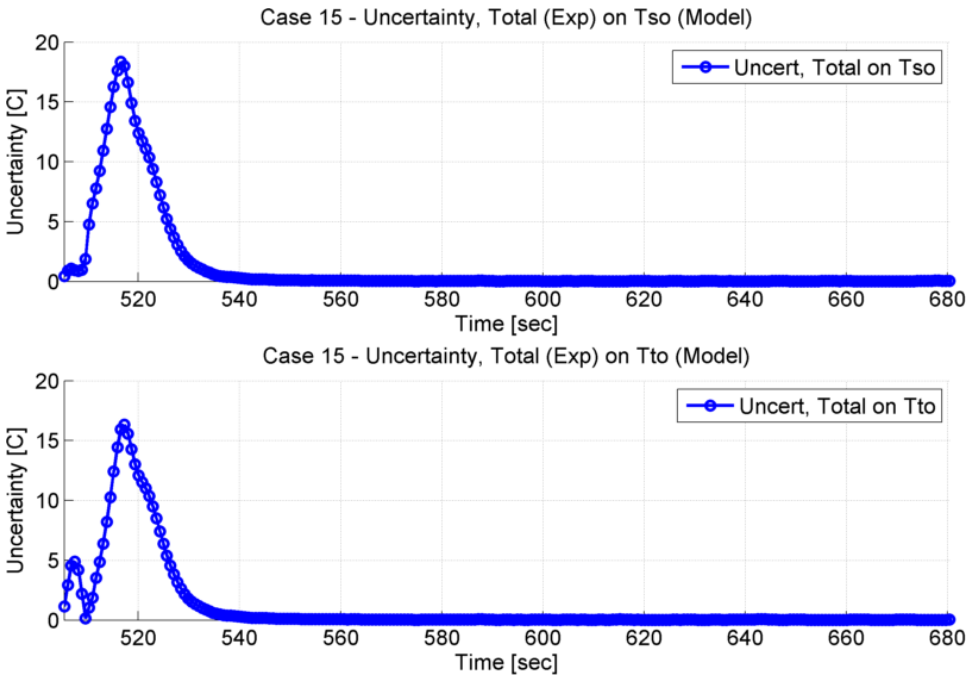

Figure 89: Case 15, Total Uncertainty on Outlet Temperatures

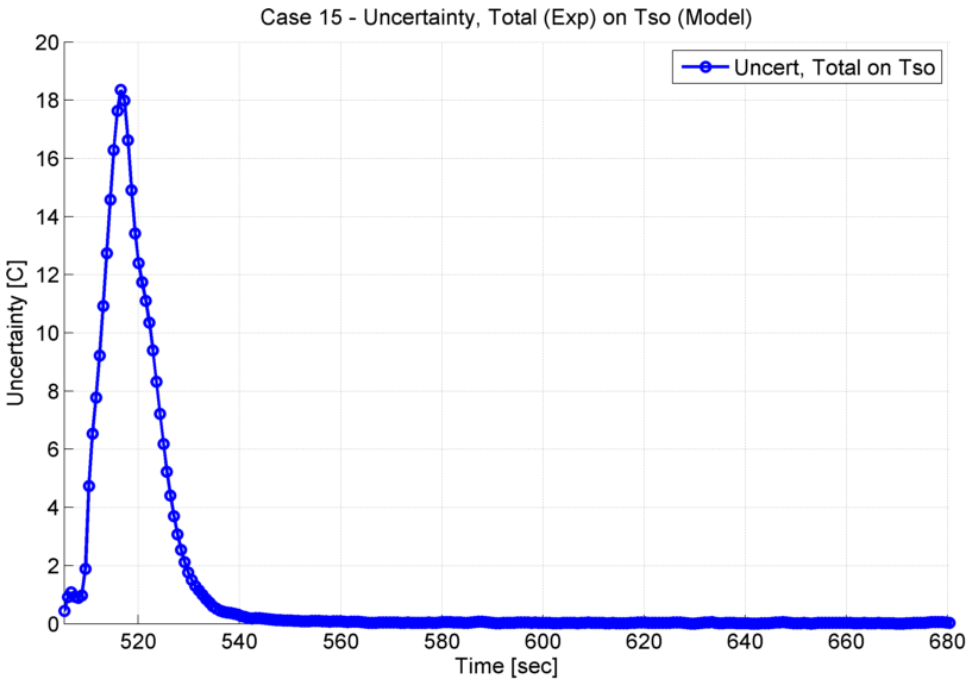

Figure 90: Case 15, Total Uncertainty on Shell Outlet Temperature

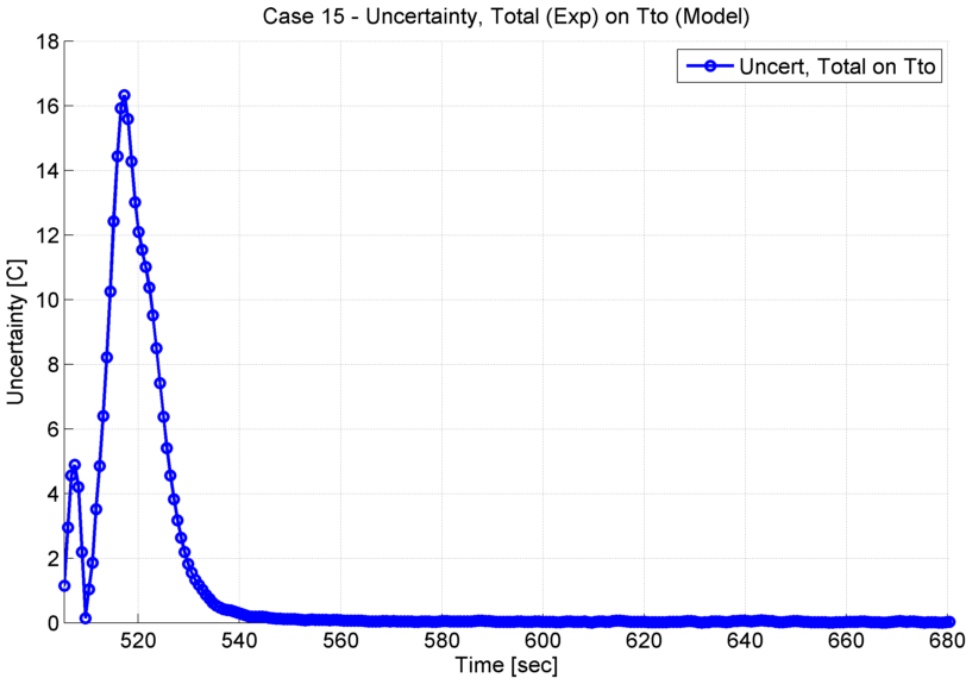

Figure 91: Case 15, Total Uncertainty on Tube Outlet Temperature

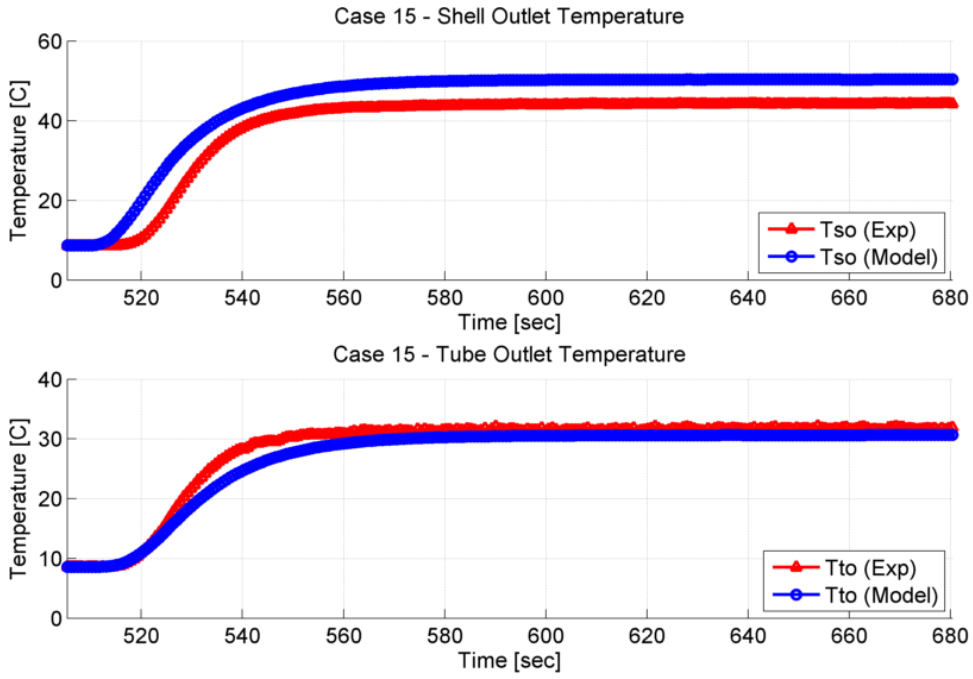

Figure 92: Case 15, Outlet Temperatures, Model & Experiment

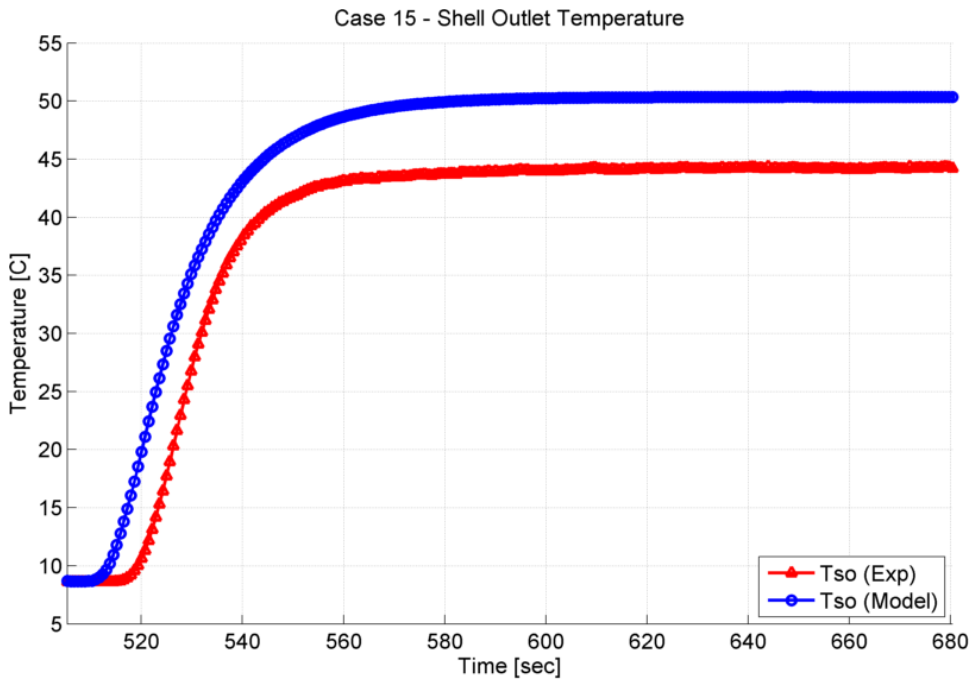

Figure 93: Case 15, Shell Outlet Temperature, Model & Experiment

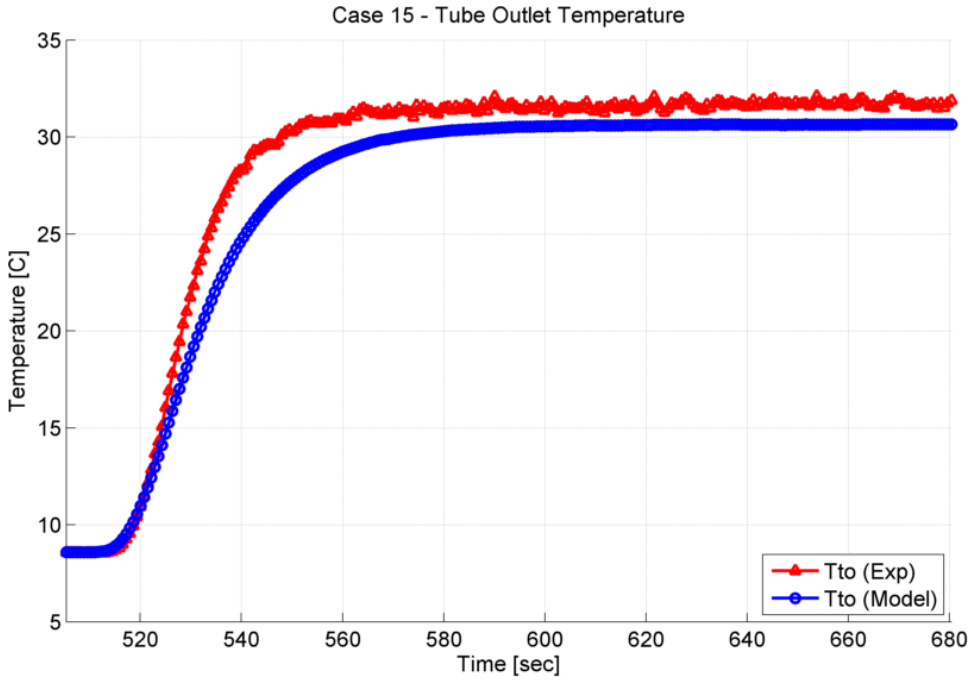

Figure 94: Case 15, Tube Outlet Temperature, Model & Experiment

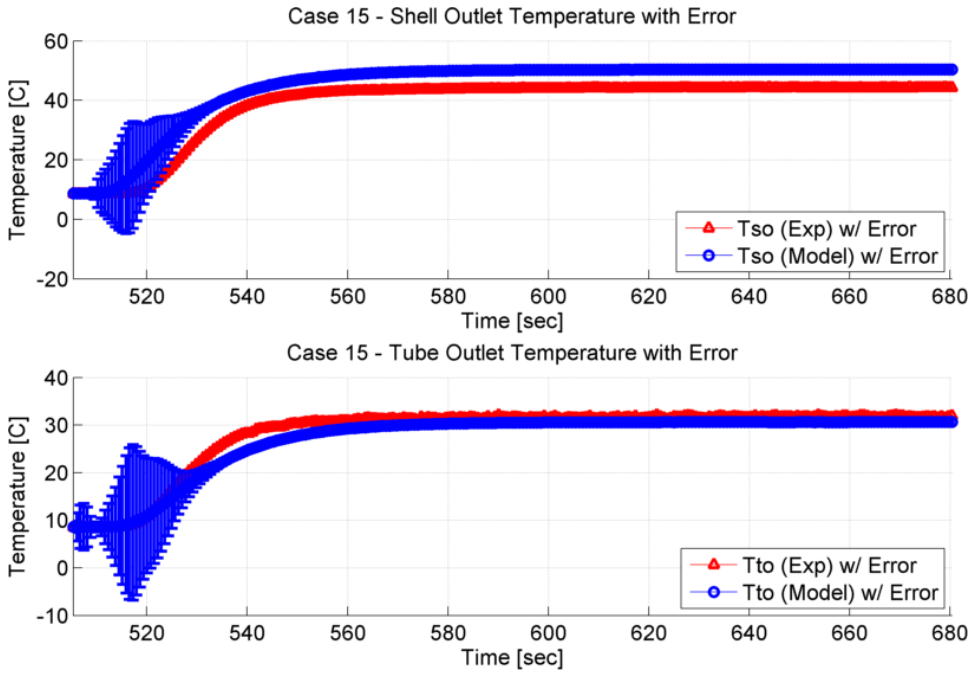

Figure 95: Case 15, Outlet Temperatures with Error, Model & Experiment

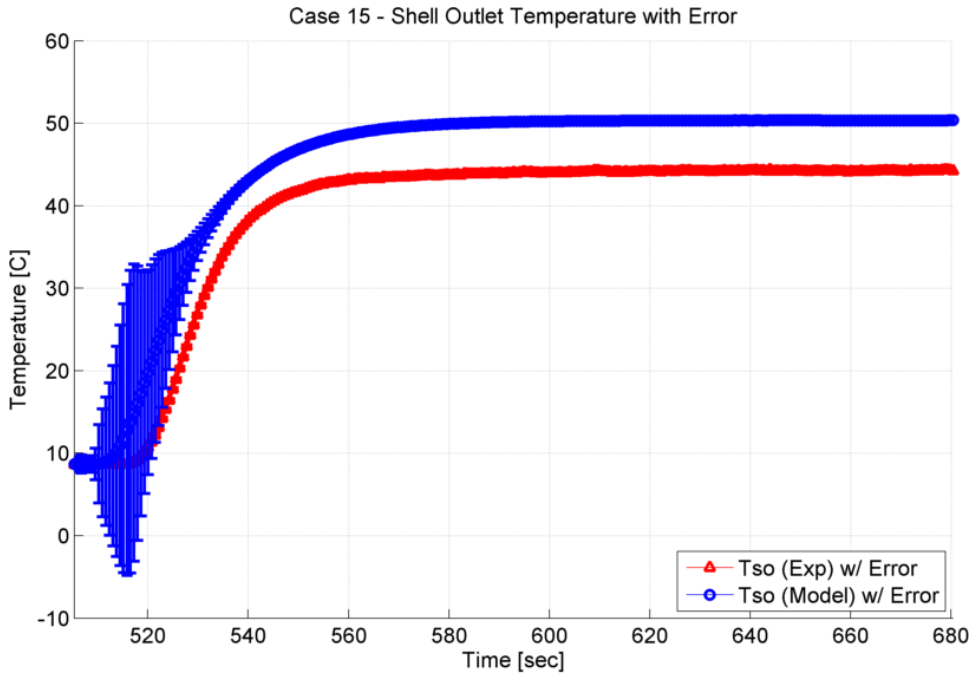

Figure 96: Case 15, Shell Outlet Temperature with Error, Model & Experiment

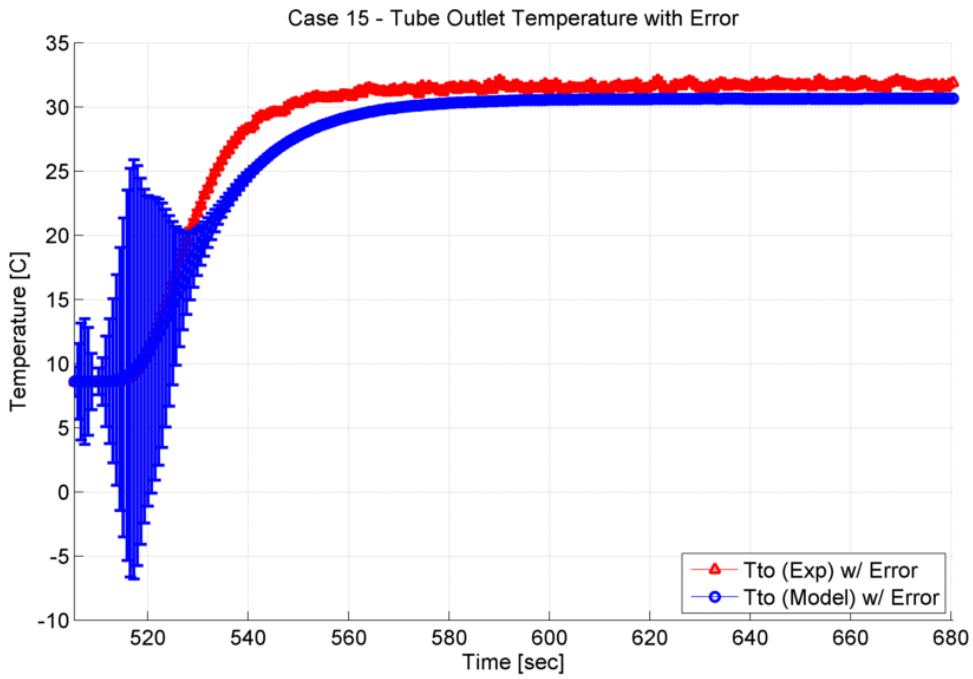

Figure 97: Case 15, Tube Outlet Temperature with Error, Model & Experiment

Case 37

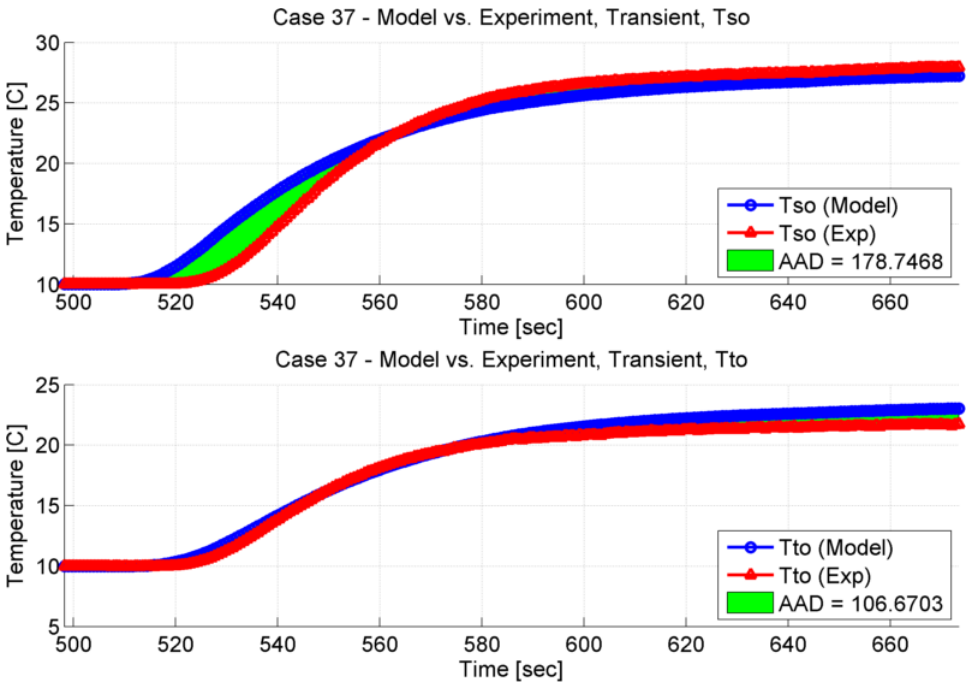

Figure 98: Case 37, Outlet Temperatures, Model & Experiment, AAD

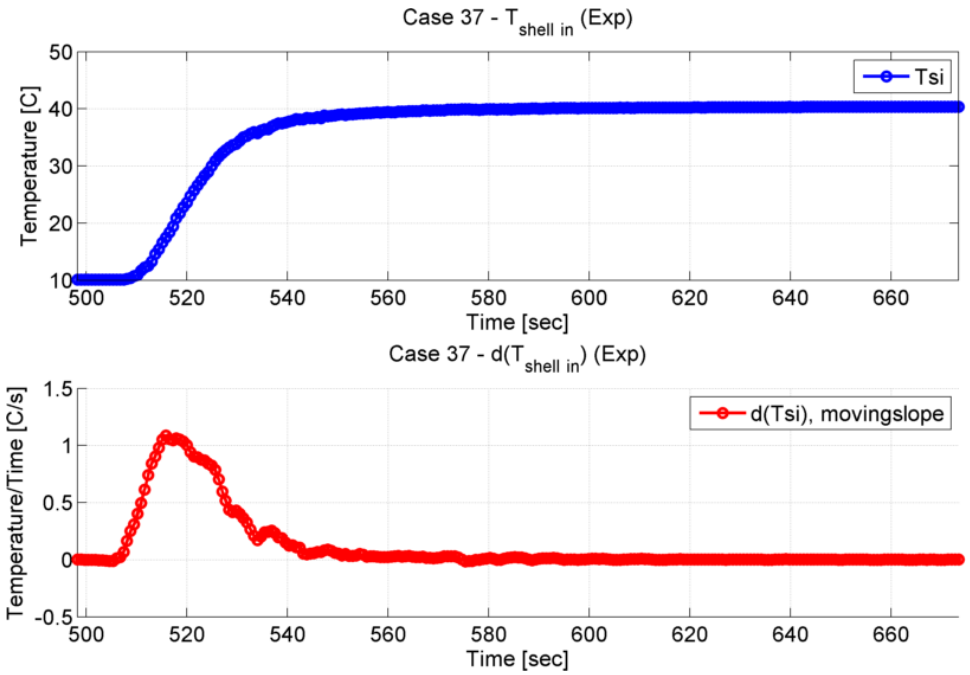

Figure 99: Case 37, Shell Inlet Temperature and Derivative of Shell Inlet Temperature (Experiment)

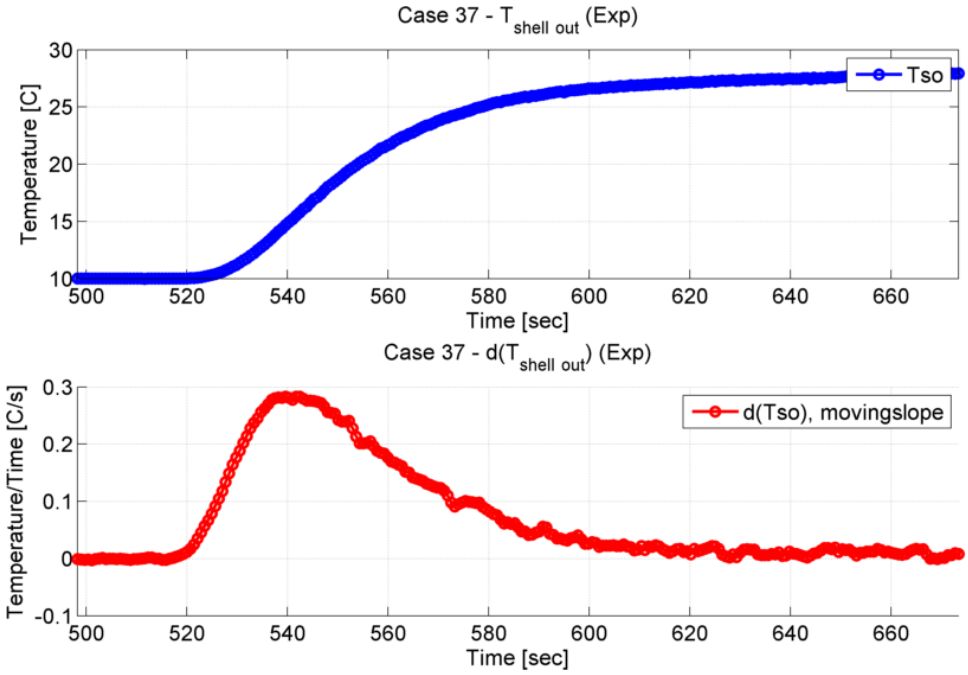

Figure 100: Case 37, Shell Outlet Temperature and Derivative of Shell Outlet Temperature (Experiment)

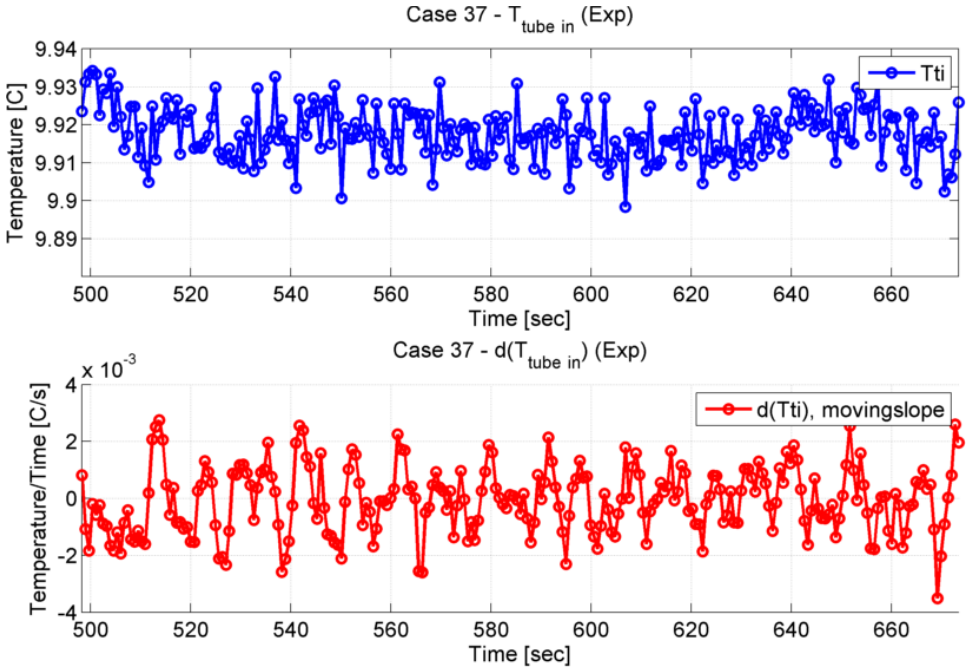

Figure 101: Case 37, Tube Inlet Temperature and Derivative of Tube Inlet Temperature (Experiment)

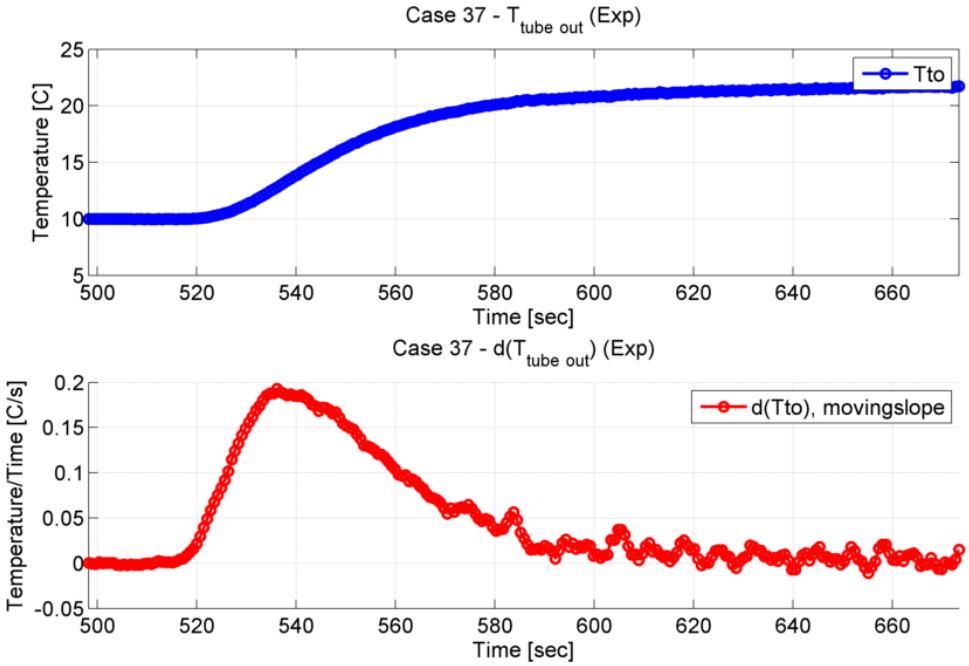

Figure 102: Case 37, Tube Outlet Temperature and Derivative of Tube Outlet Temperature (Experiment)

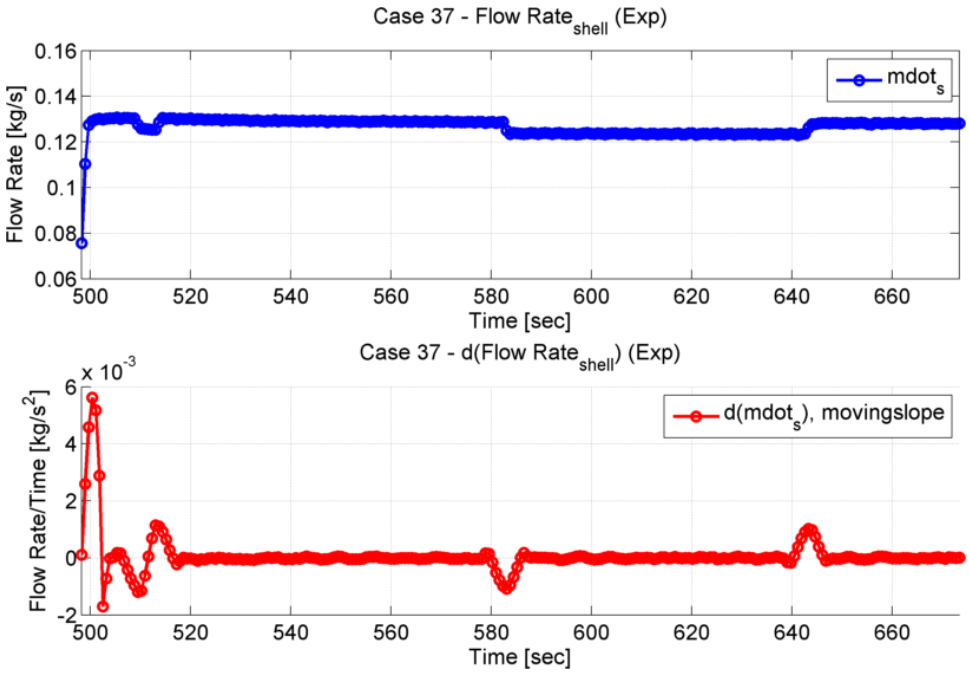

Figure 103: Case 37, Shell Mass Flow Rate and Derivative of Shell Mass Flow Rate (Experiment)

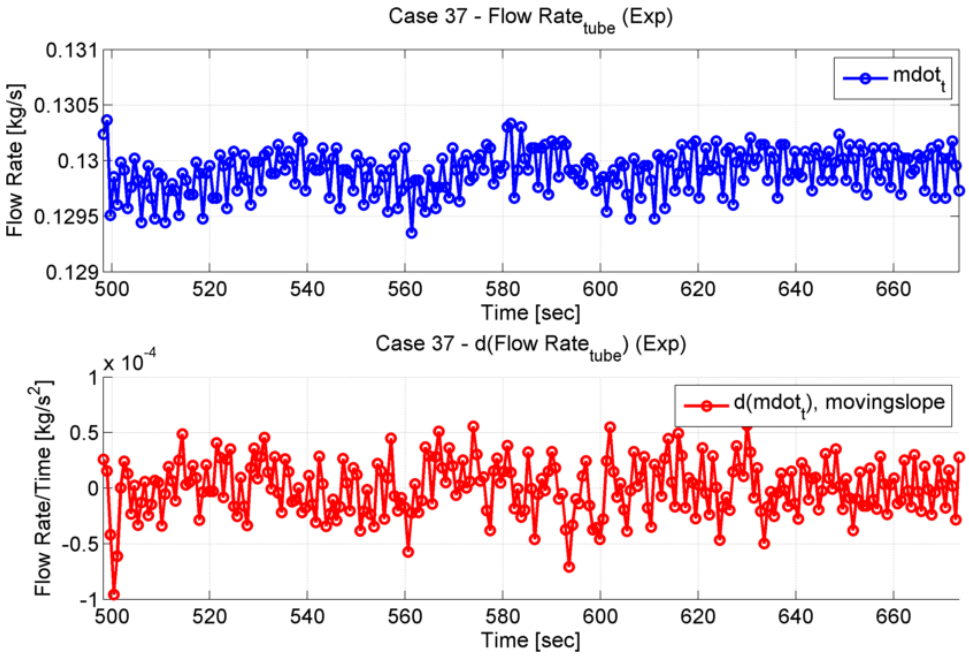

Figure 104: Case 37, Tube Mass Flow Rate and Derivative of Tube Mass Flow Rate (Experiment)

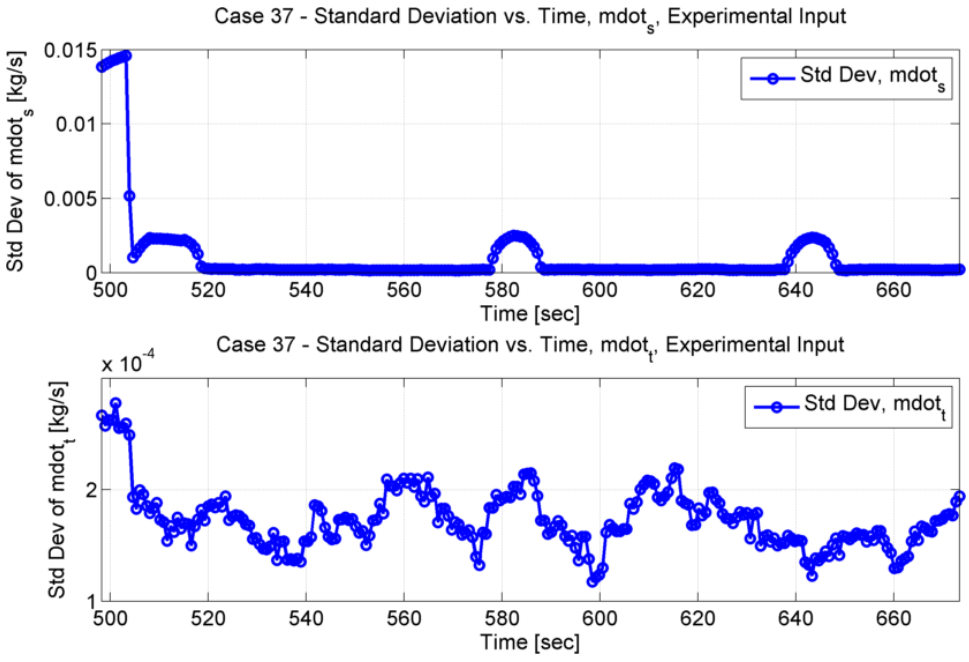

Figure 105: Case 37, Standard Deviation vs. Time, Mass Flow Rates

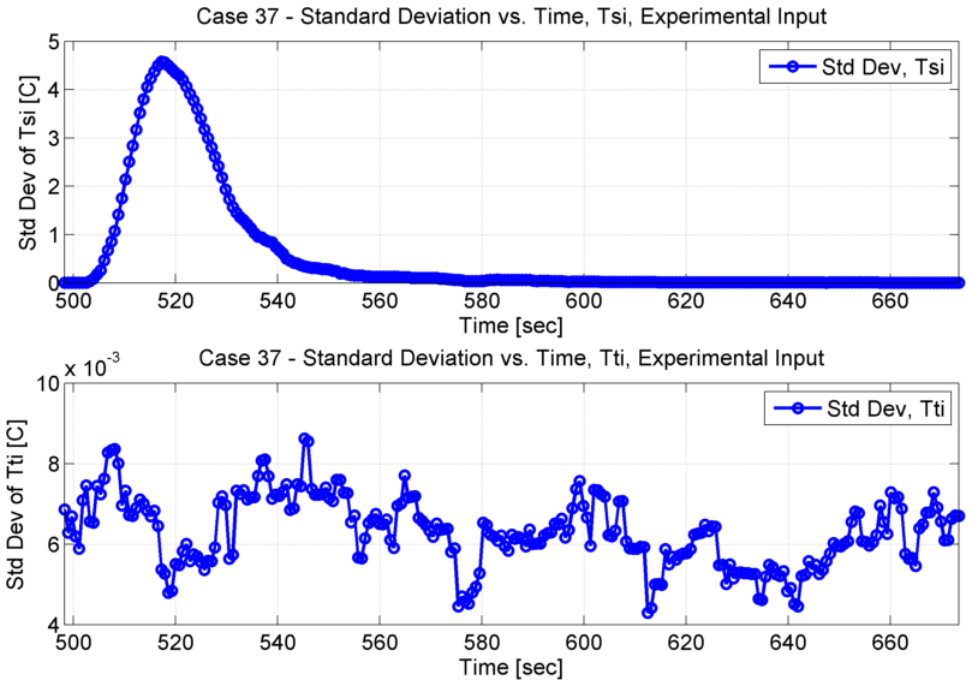

Figure 106: Case 37, Standard Deviation vs. Time, Inlet Temperatures

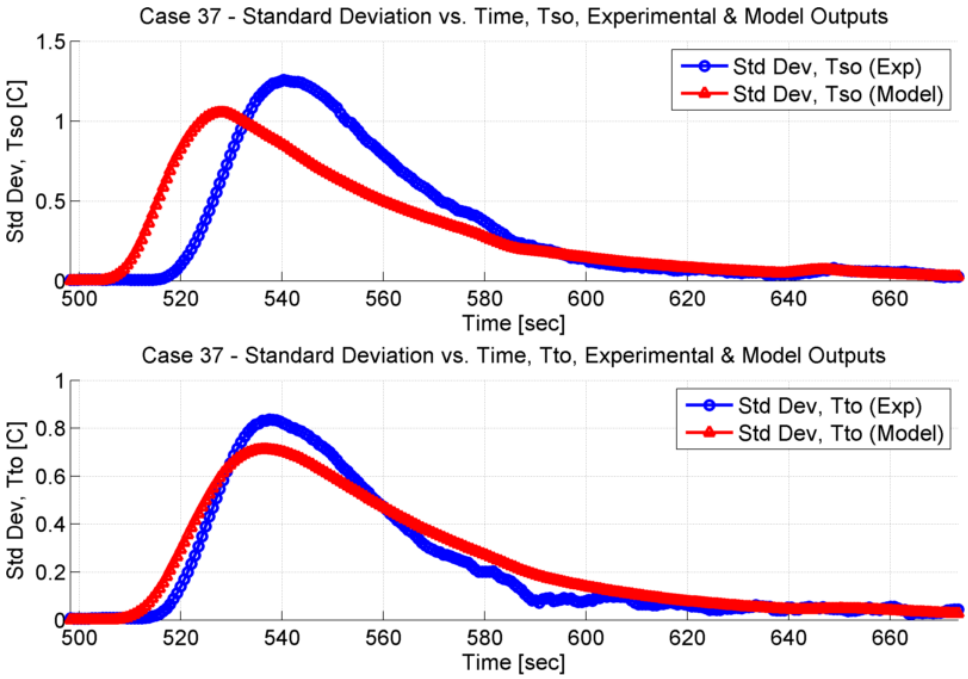

Figure 107: Case 37, Standard Deviation vs. Time, Outlet Temperatures

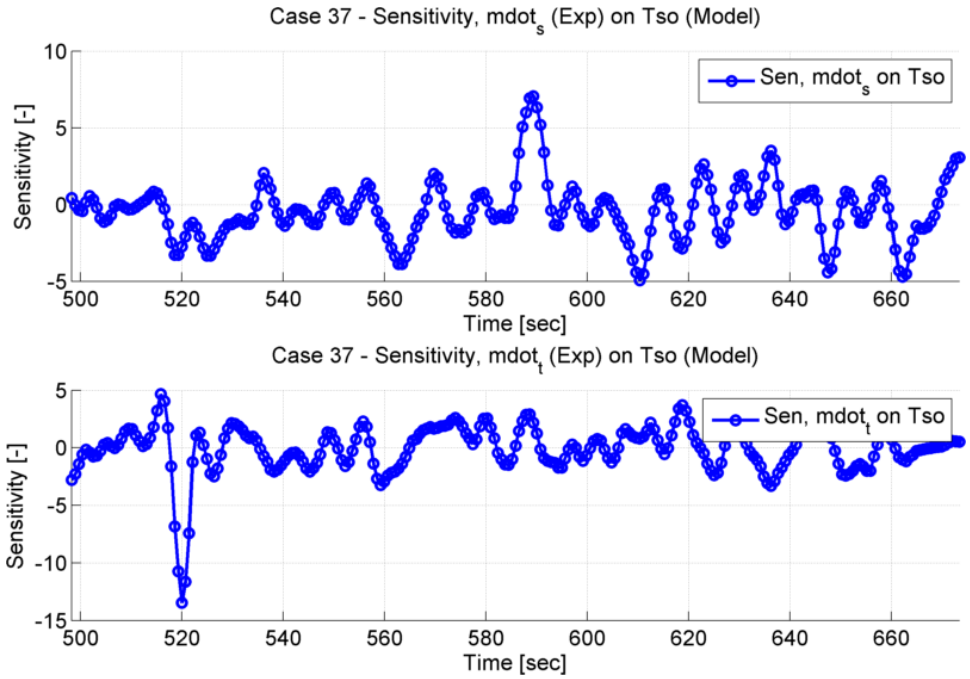

Figure 108: Case 37, Sensitivities vs. Time, Mass Flow Rates on Shell Outlet Temperature

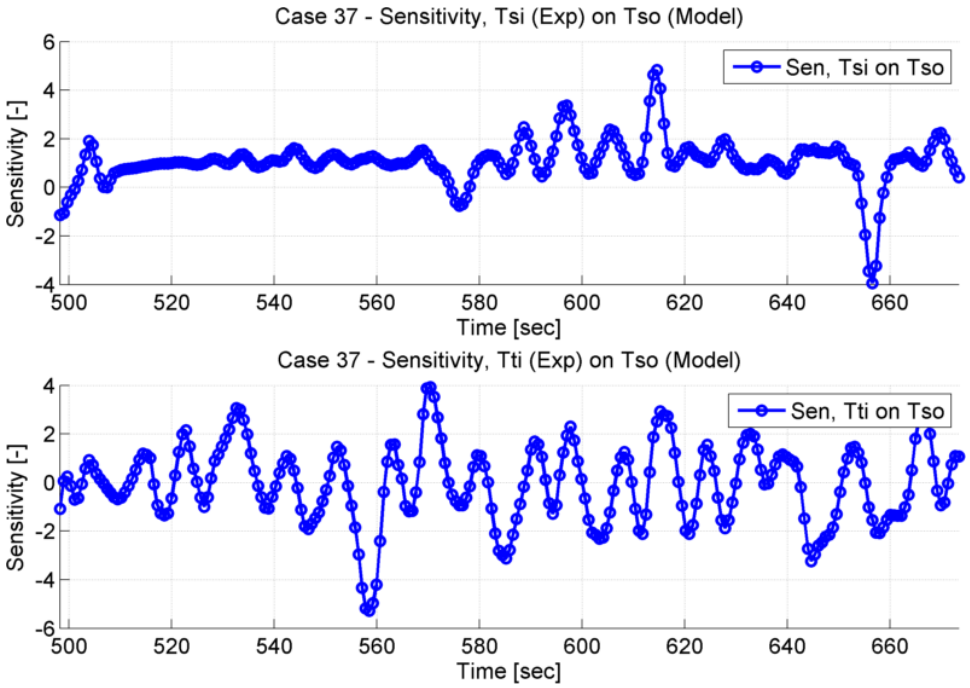

Figure 109: Case 37, Sensitivities vs. Time, Inlet Temperatures on Shell Outlet Temperature

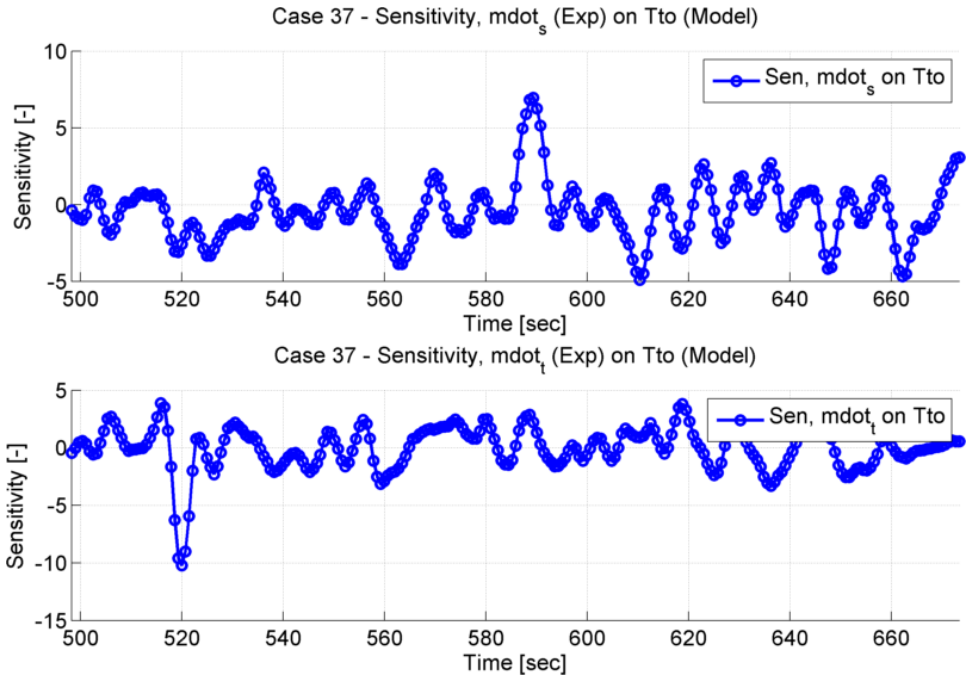

Figure 110: Case 37, Sensitivities vs. Time, Mass Flow Rates on Tube Outlet Temperature

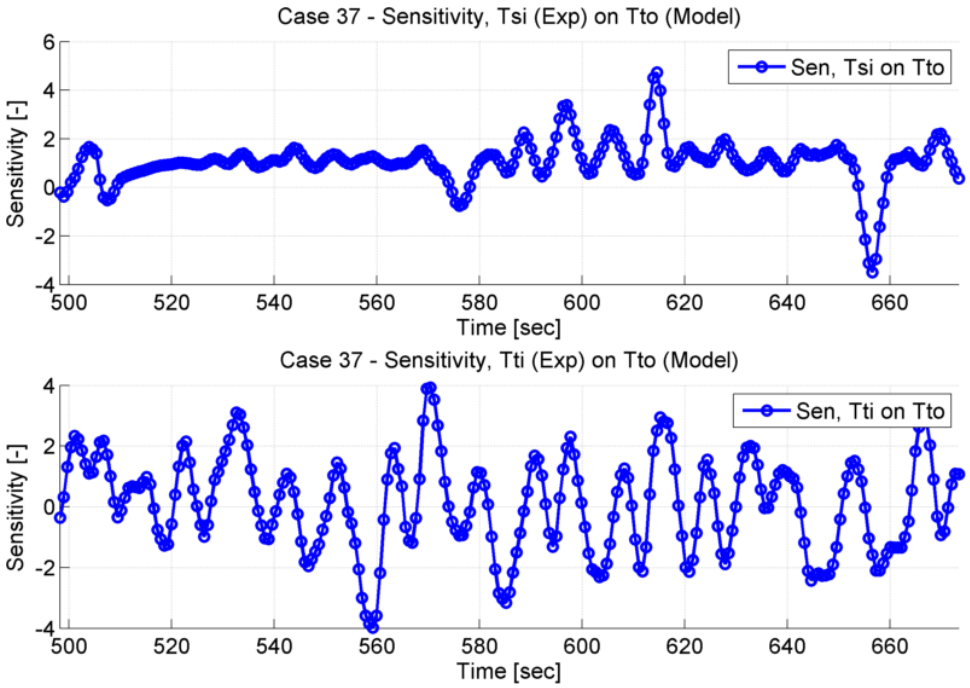

Figure 111: Case 37, Sensitivities vs. Time, Inlet Temperatures on Tube Outlet Temperature

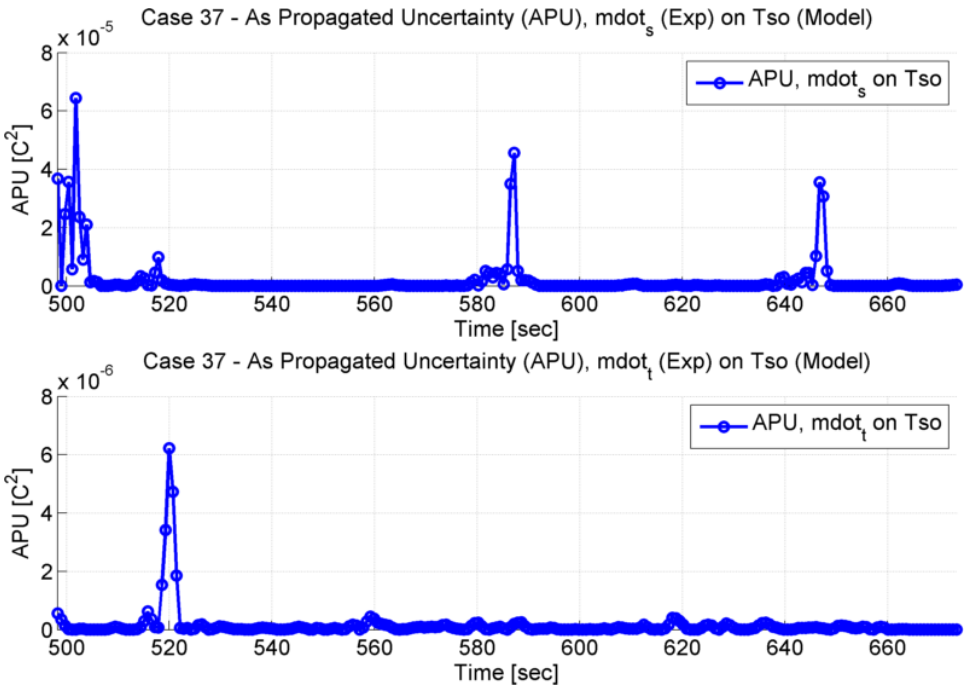

Figure 112: Case 37, As Propagated Uncertainties vs. Time, Mass Flow Rates on Shell Outlet Temperature

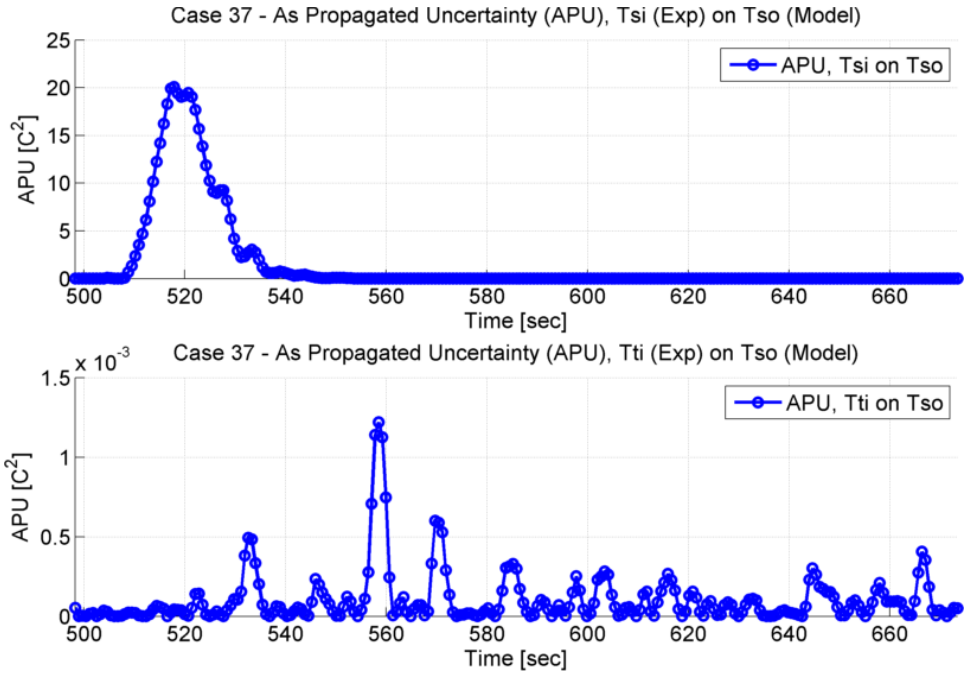

Figure 113: Case 37, As Propagated Uncertainties vs. Time, Inlet Temperatures on Shell Outlet Temperature

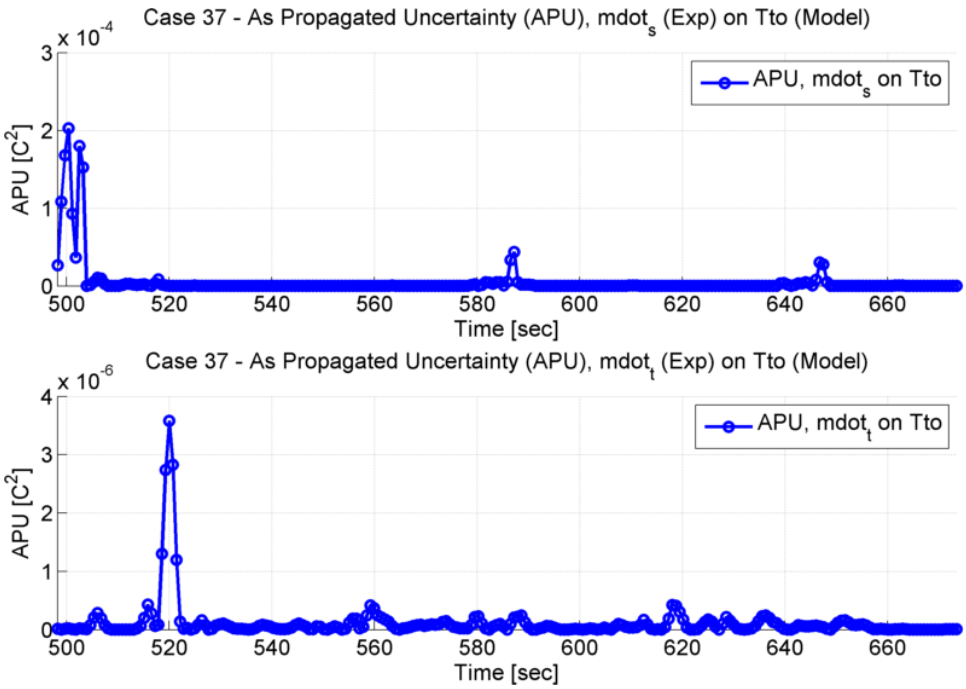

Figure 114: Case 37, As Propagated Uncertainties vs. Time, Mass Flow Rates on Tube Outlet Temperature

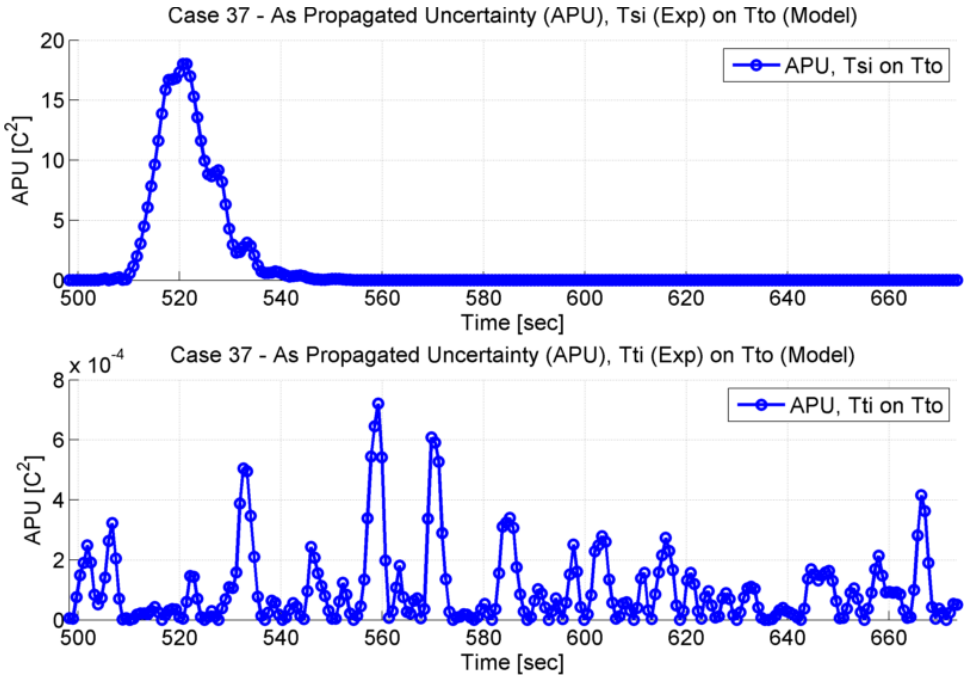

Figure 115: Case 37, As Propagated Uncertainties vs. Time, Inlet Temperatures on Tube Outlet Temperature

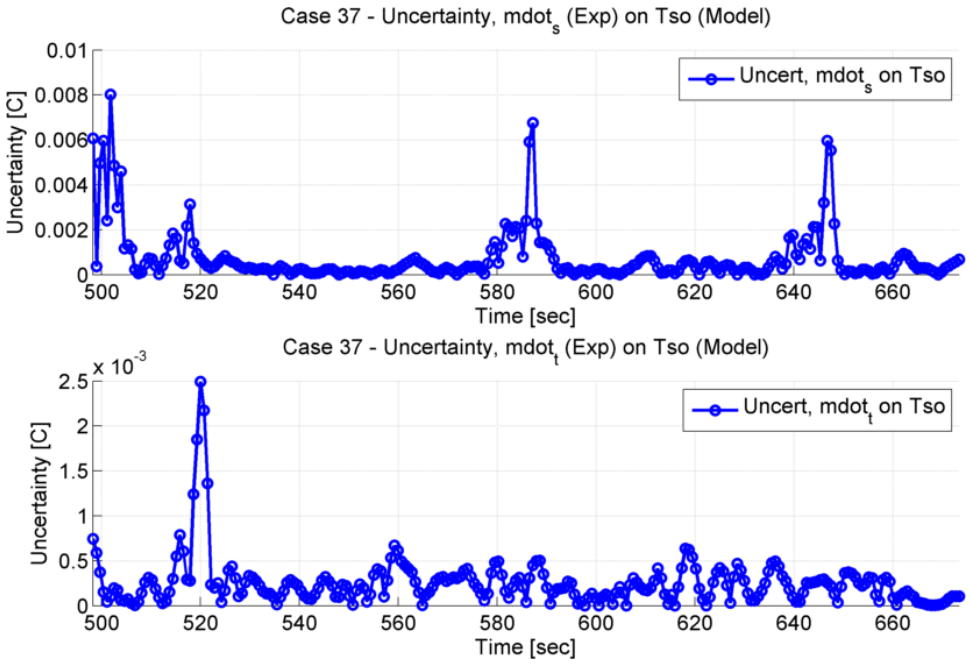

Figure 116: Case 37, Uncertainties vs. Time, Mass Flow Rates on Shell Outlet Temperature

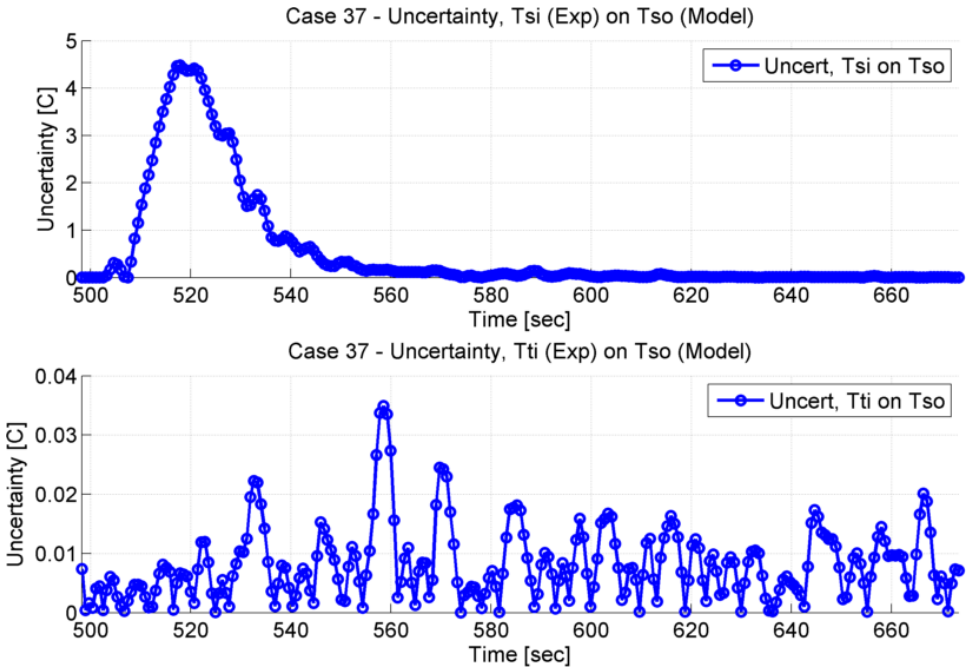

Figure 117: Case 37, Uncertainties vs. Time, Inlet Temperatures on Shell Outlet Temperature

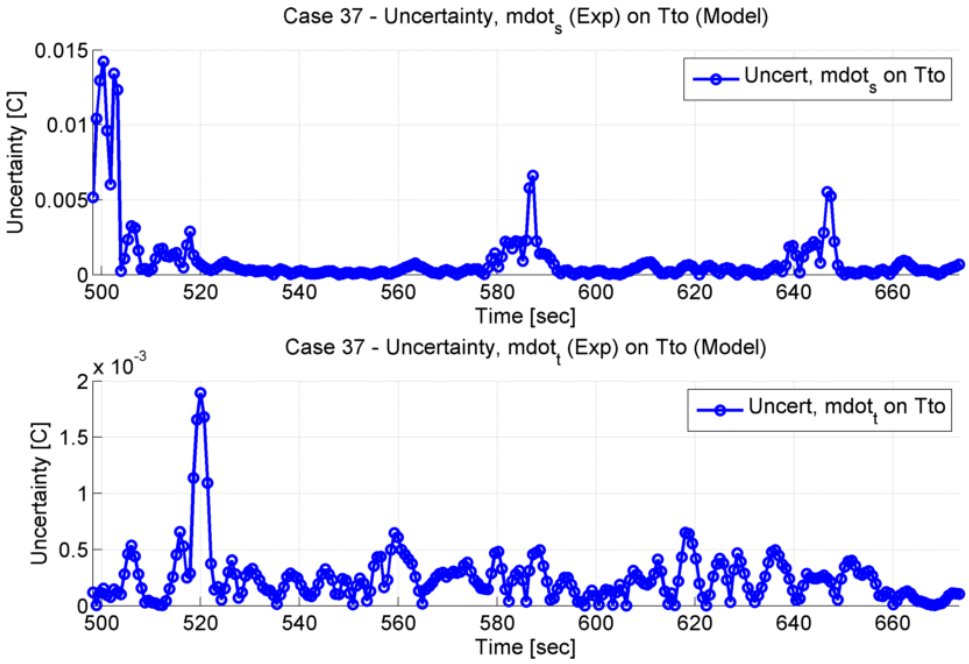

Figure 118: Case 37, Uncertainties vs. Time, Mass Flow Rates on Tube Outlet Temperature

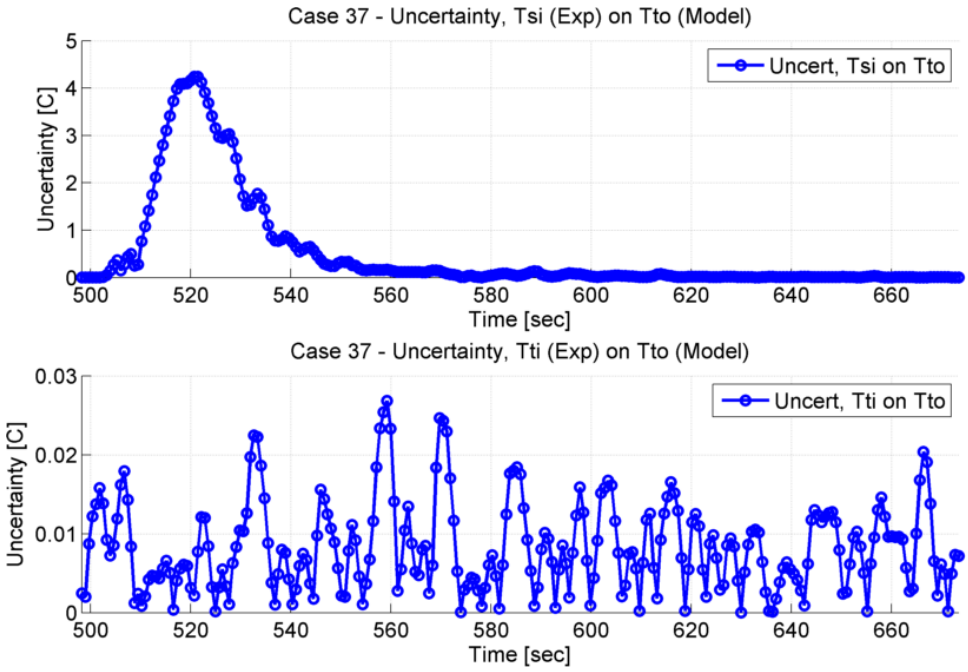

Figure 119: Case 37, Uncertainties vs. Time, Inlet Temperatures on Tube Outlet Temperature

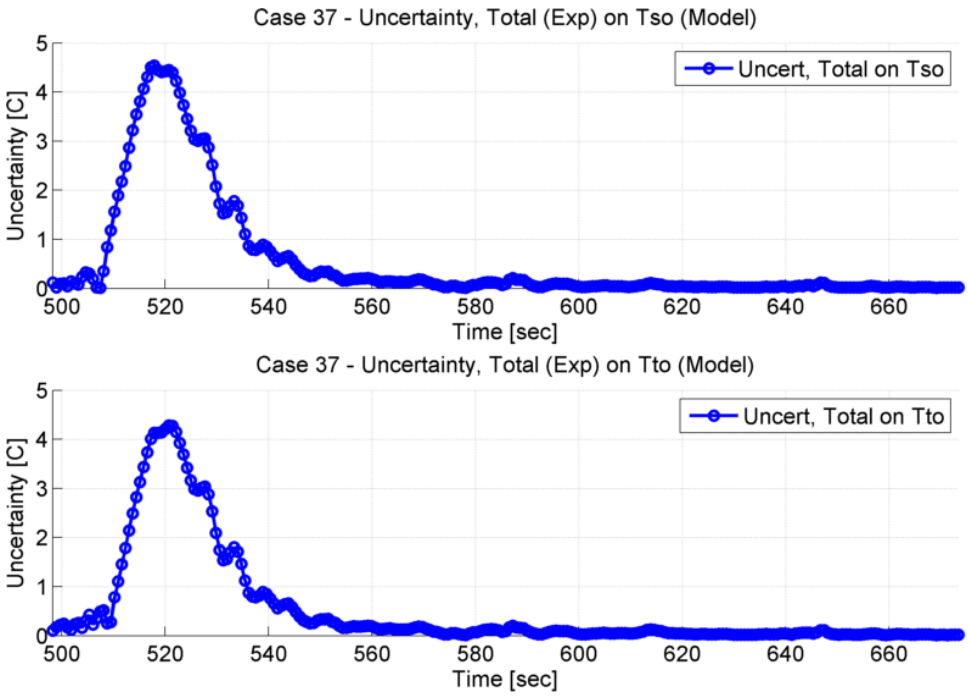

Figure 120: Case 37, Total Uncertainty on Outlet Temperatures

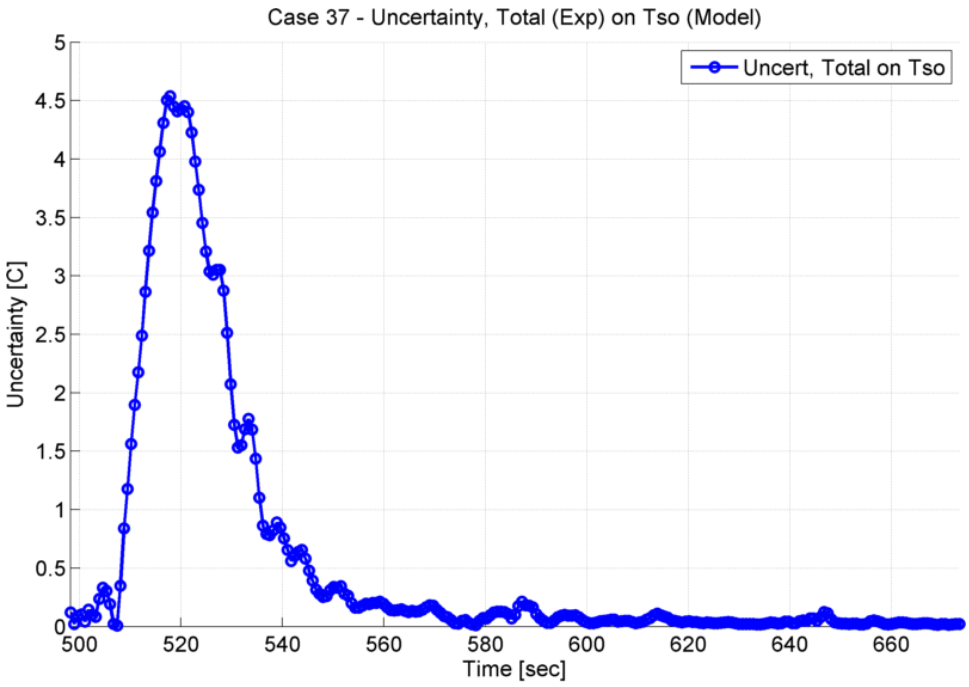

Figure 121: Case 37, Total Uncertainty on Shell Outlet Temperature

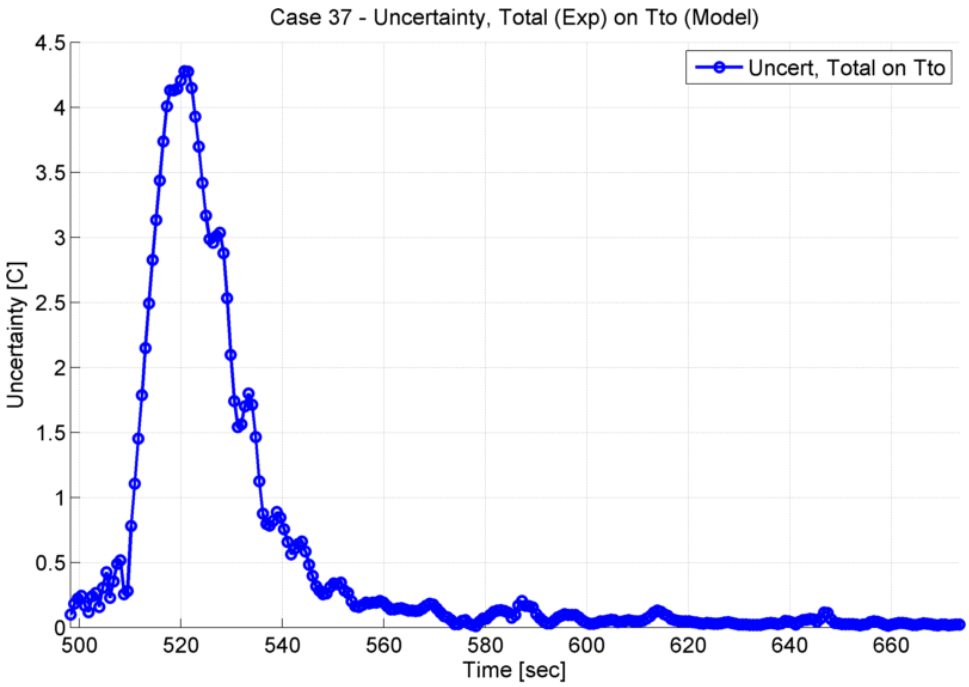

Figure 122: Case 37, Total Uncertainty on Tube Outlet Temperature

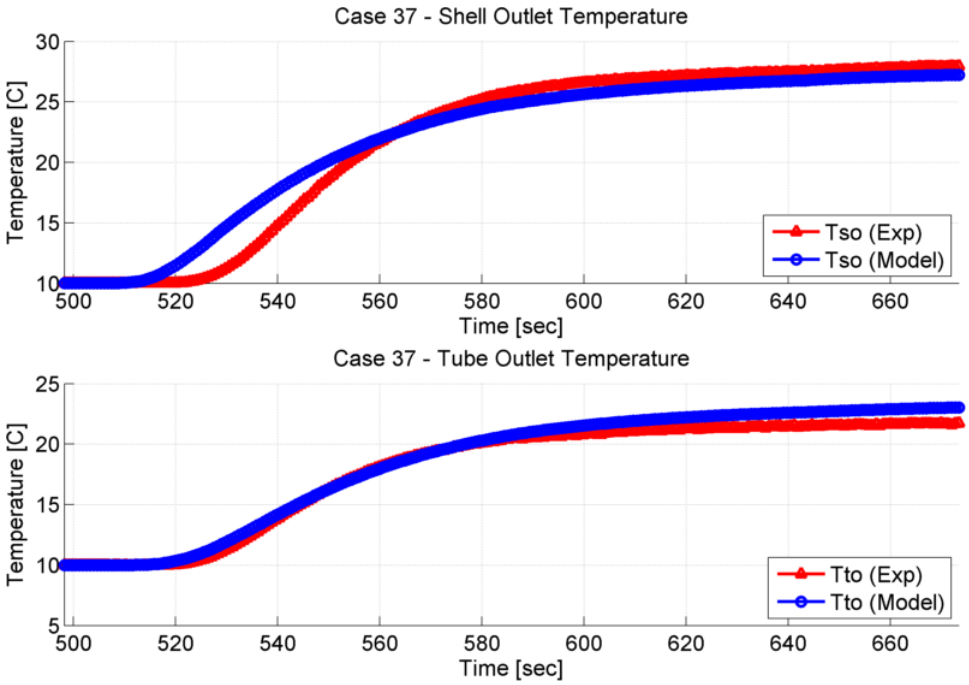

Figure 123: Case 37, Outlet Temperatures, Model & Experiment

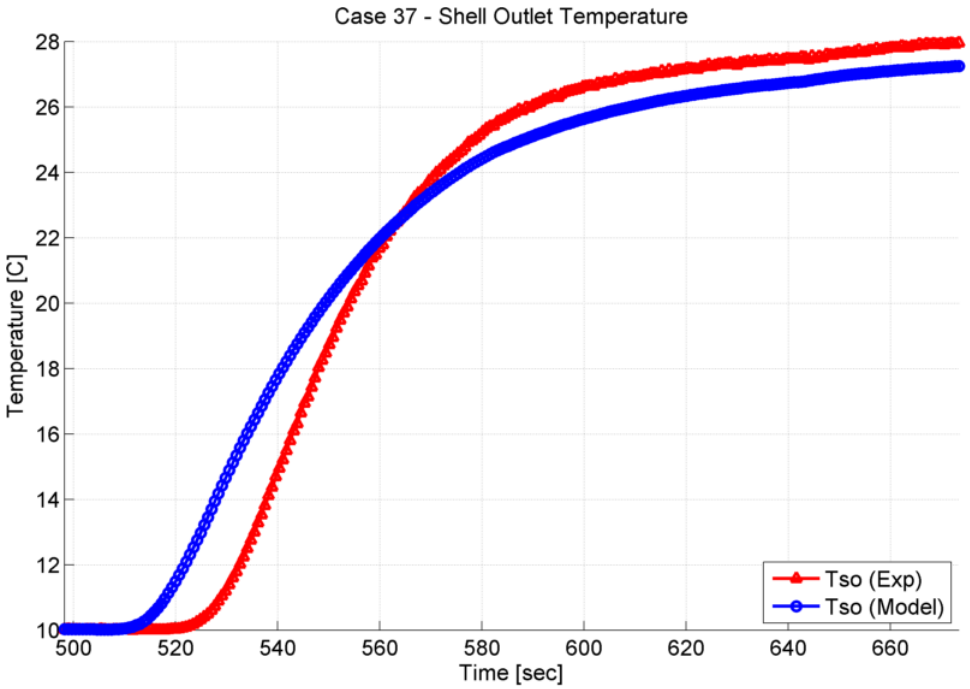

Figure 124: Case 37, Shell Outlet Temperature, Model & Experiment

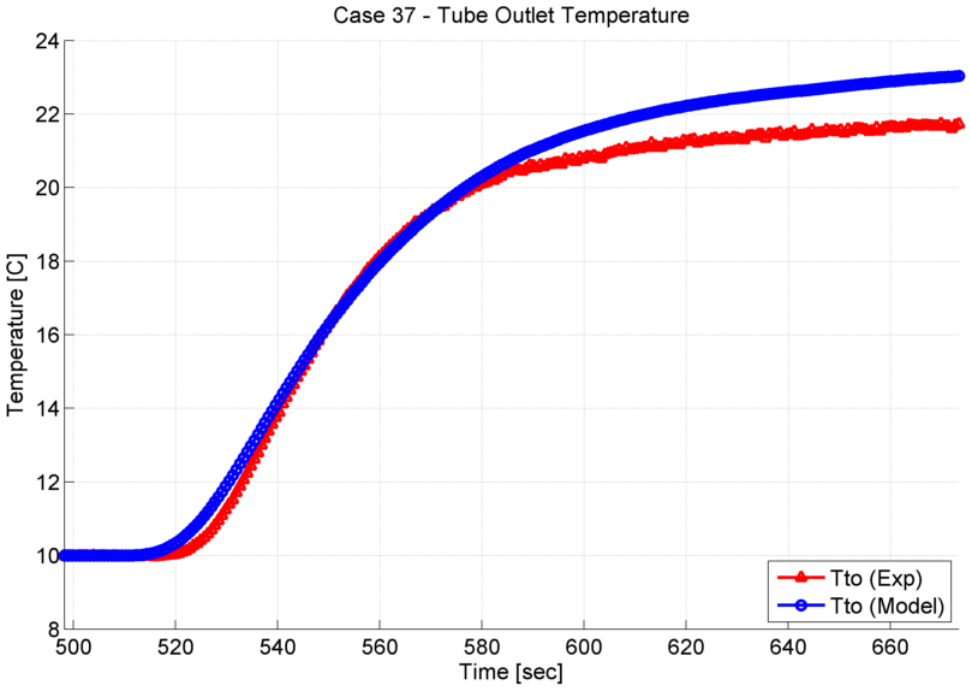

Figure 125: Case 37, Tube Outlet Temperature, Model & Experiment

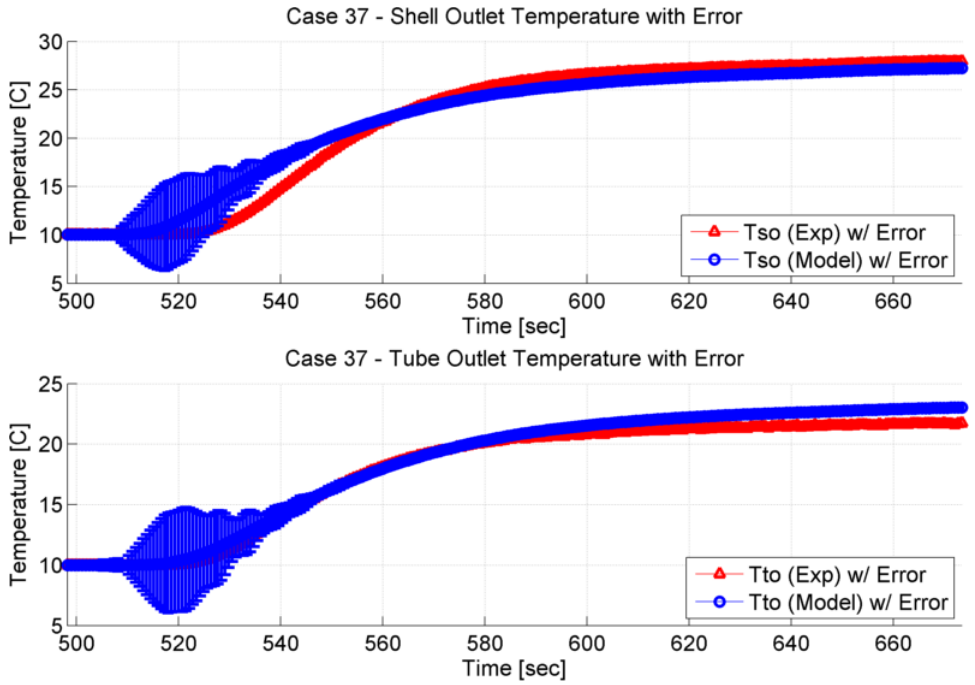

Figure 126: Case 37, Outlet Temperatures with Error, Model & Experiment

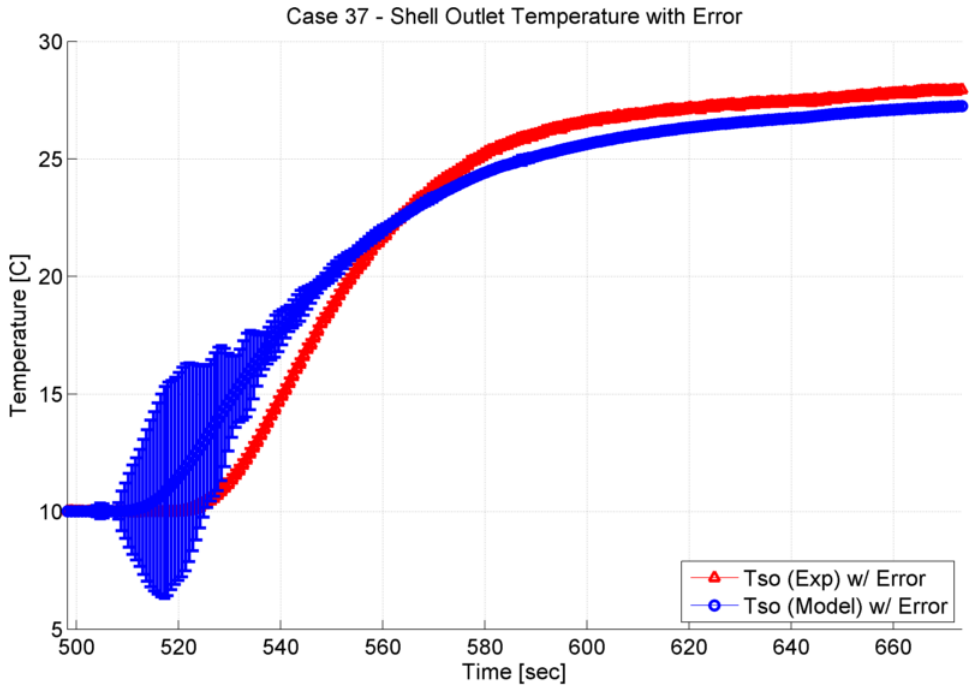

Figure 127: Case 37, Shell Outlet Temperature with Error, Model & Experiment

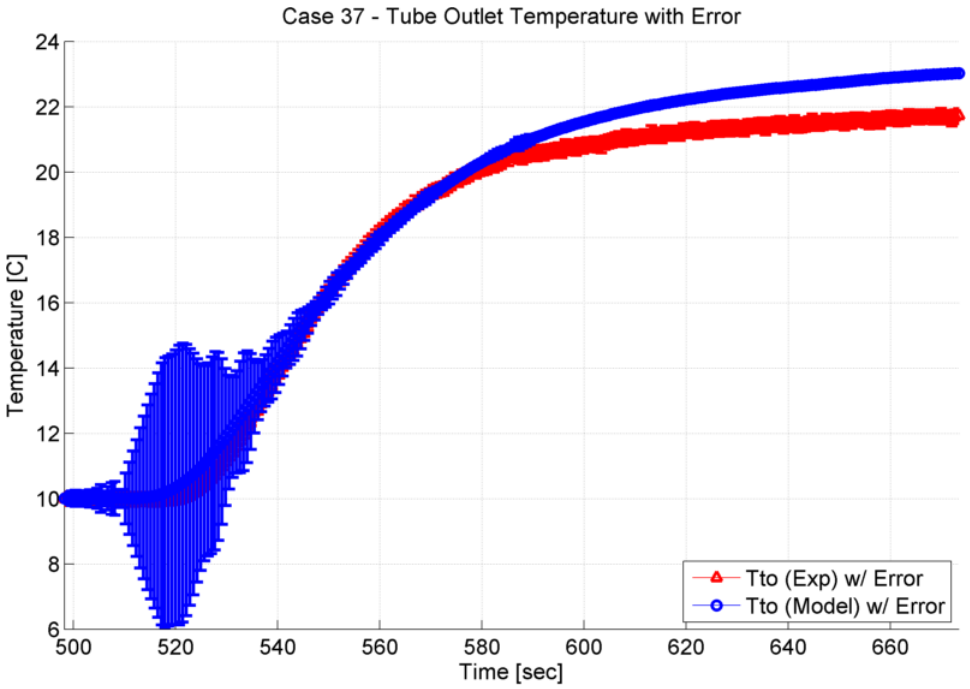

Figure 128: Case 37, Tube Outlet Temperature with Error, Model & Experiment

Case 42

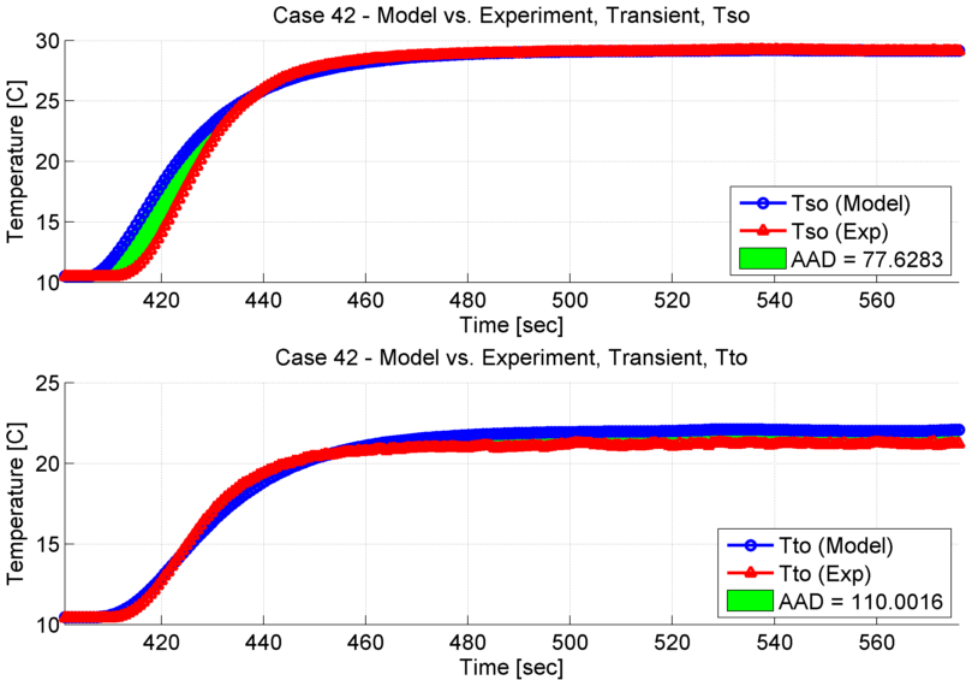

Figure 129: Case 42, Outlet Temperatures, Model & Experiment, AAD

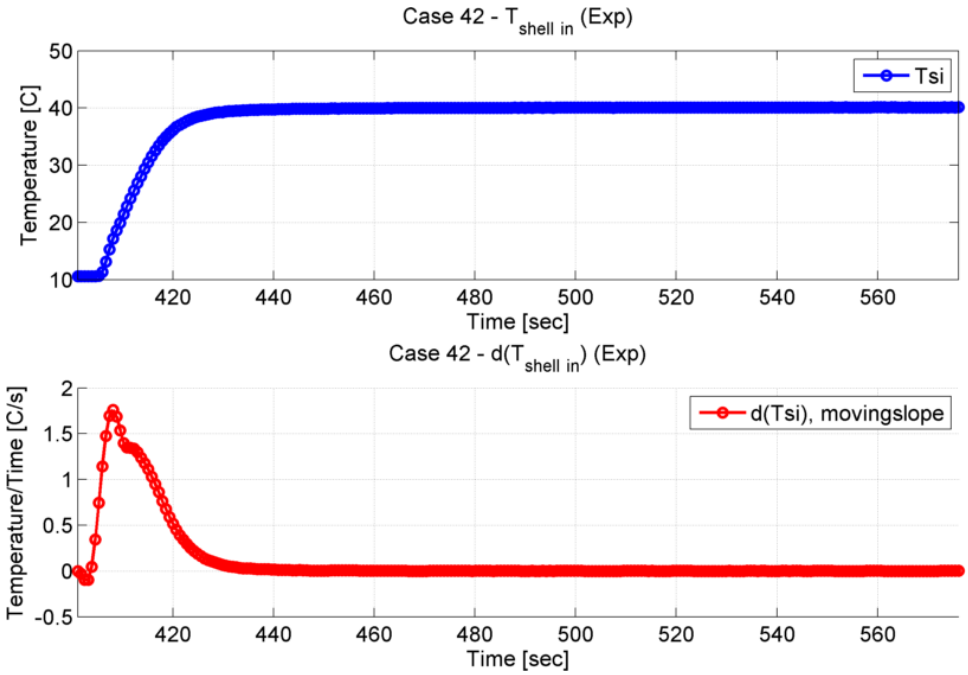

Figure 130: Case 42, Shell Inlet Temperature and Derivative of Shell Inlet Temperature (Experiment)

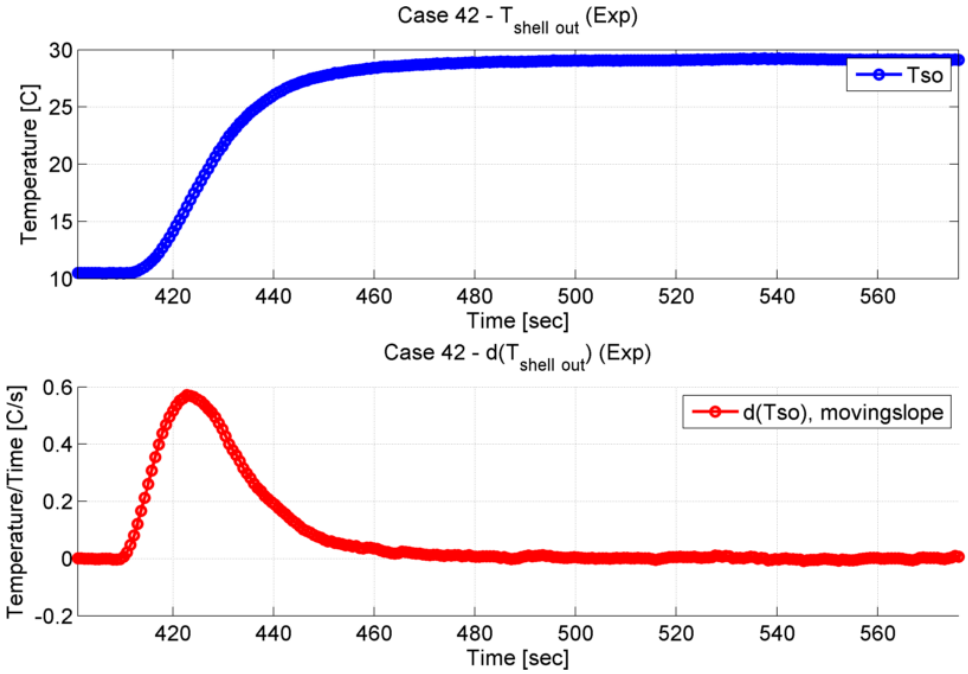

Figure 131: Case 42, Shell Outlet Temperature and Derivative of Shell Outlet Temperature (Experiment)

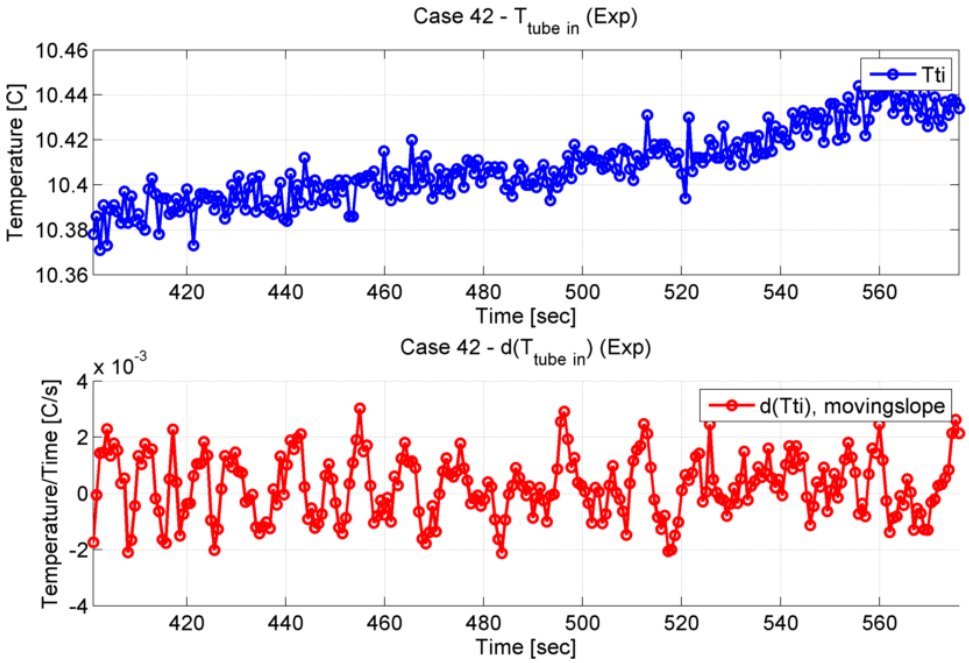

Figure 132: Case 42, Tube Inlet Temperature and Derivative of Tube Inlet Temperature (Experiment)

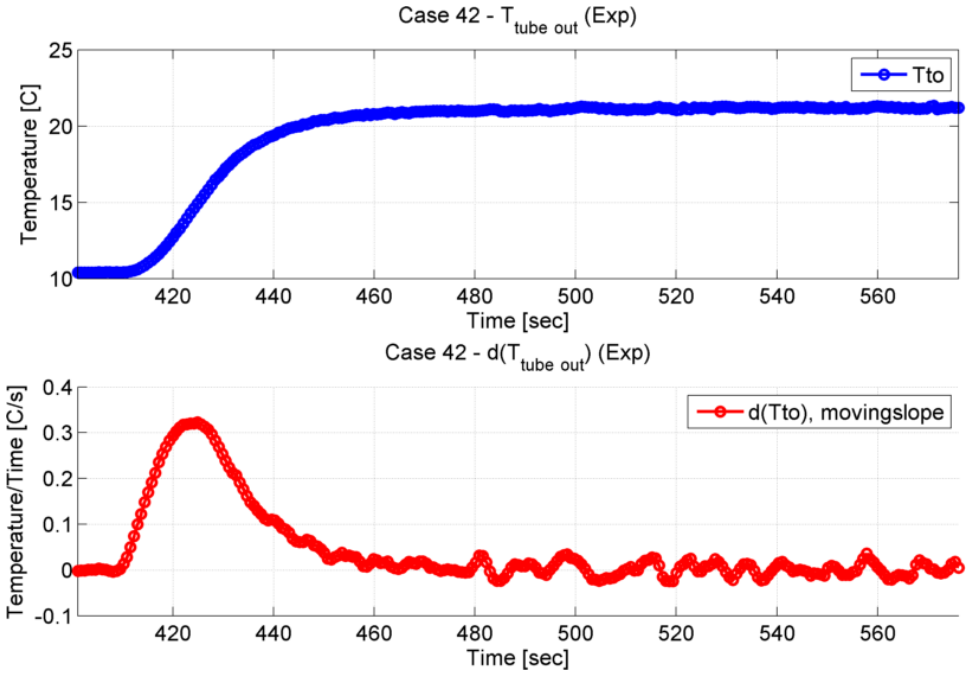

Figure 133: Case 42, Tube Outlet Temperature and Derivative of Tube Outlet Temperature (Experiment)

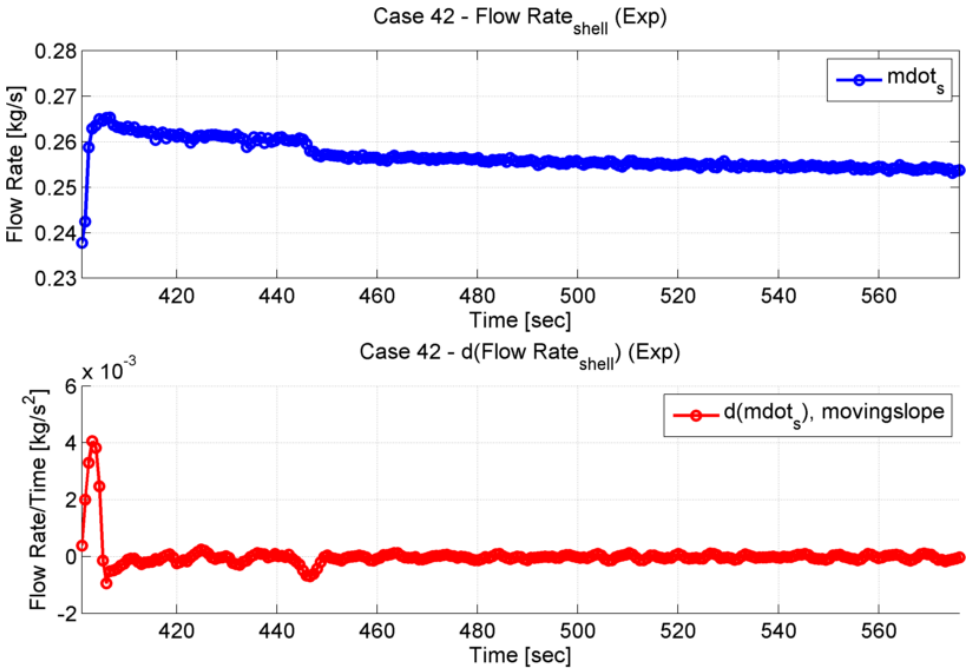

Figure 134: Case 42, Shell Mass Flow Rate and Derivative of Shell Mass Flow Rate (Experiment)

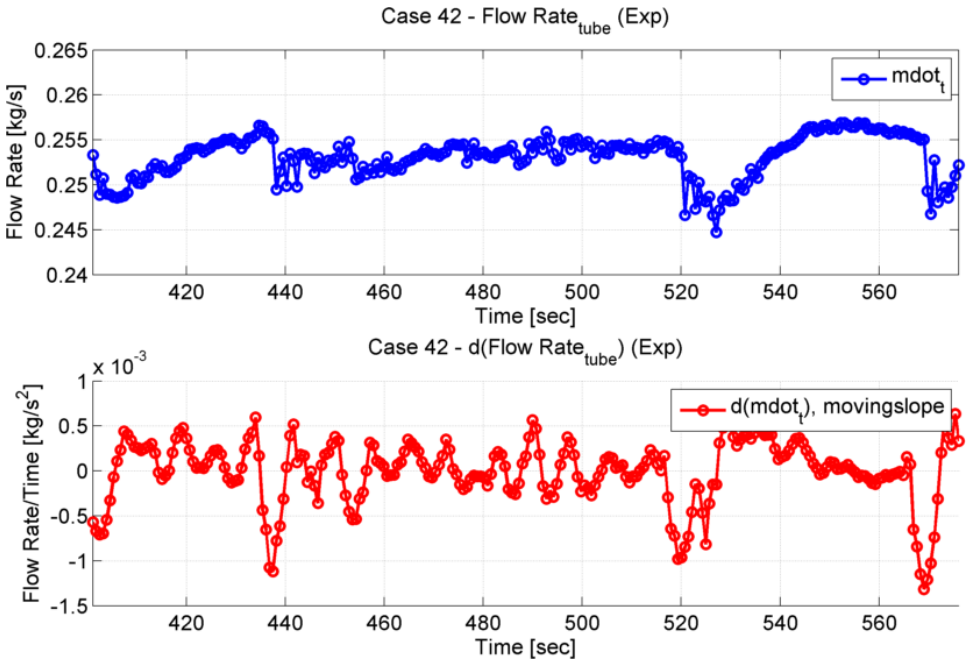

Figure 135: Case 42, Tube Mass Flow Rate and Derivative of Tube Mass Flow Rate (Experiment)

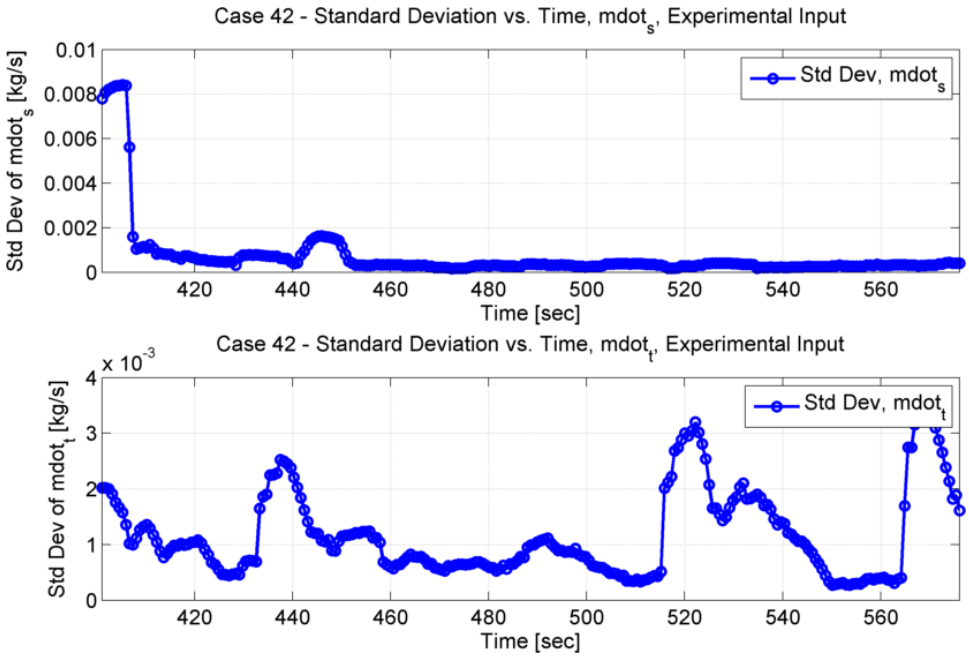

Figure 136: Case 42, Standard Deviation vs. Time, Mass Flow Rates

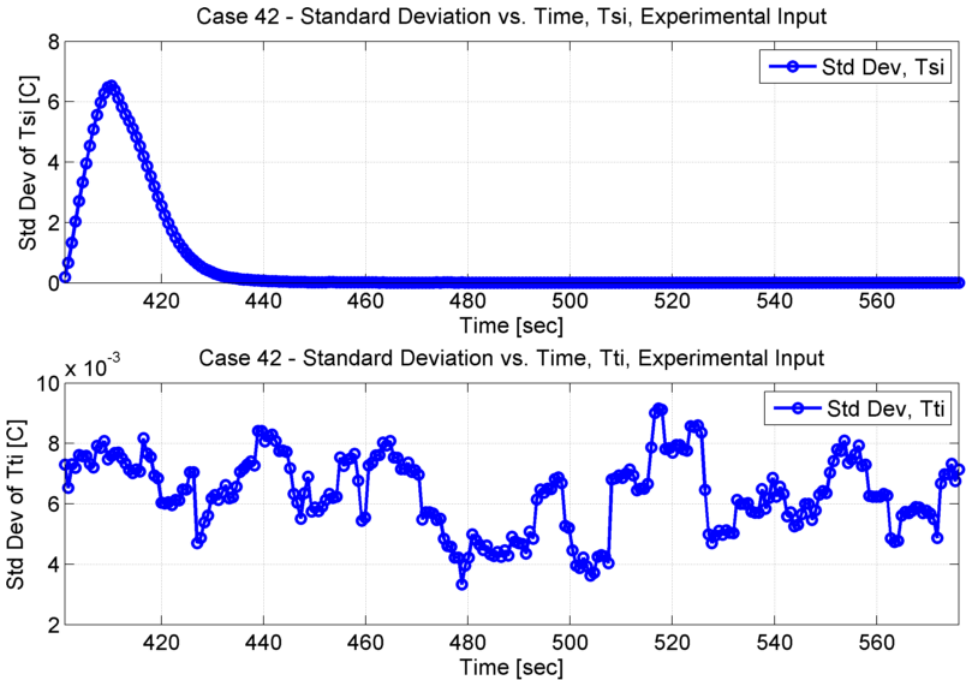

Figure 137: Case 42, Standard Deviation vs. Time, Inlet Temperatures

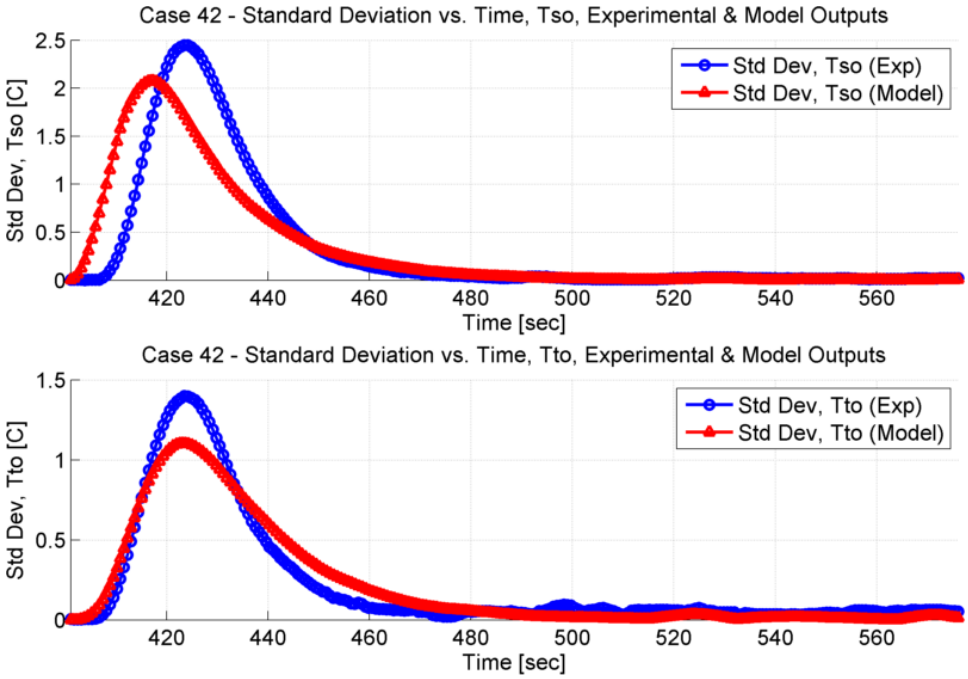

Figure 138: Case 42, Standard Deviation vs. Time, Outlet Temperatures

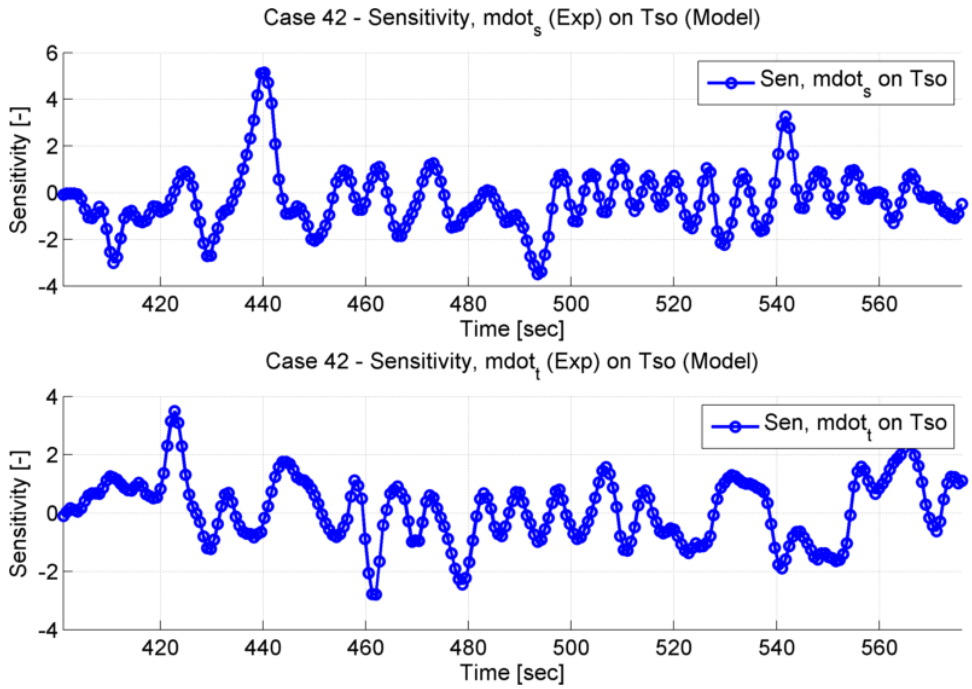

Figure 139: Case 42, Sensitivities vs. Time, Mass Flow Rates on Shell Outlet Temperature

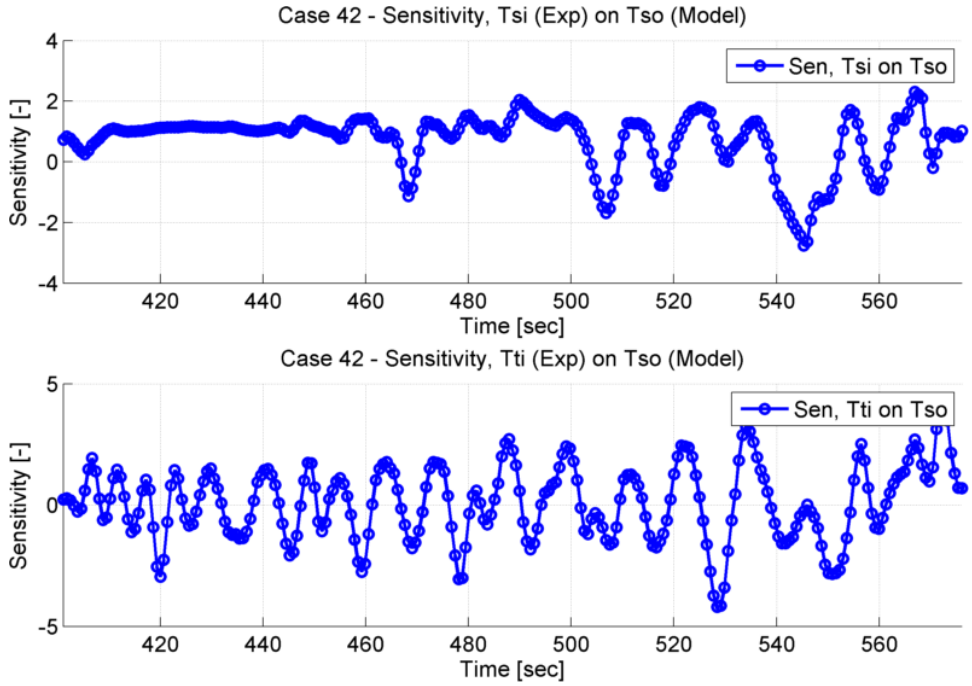

Figure 140: Case 42, Sensitivities vs. Time, Inlet Temperatures on Shell Outlet Temperature

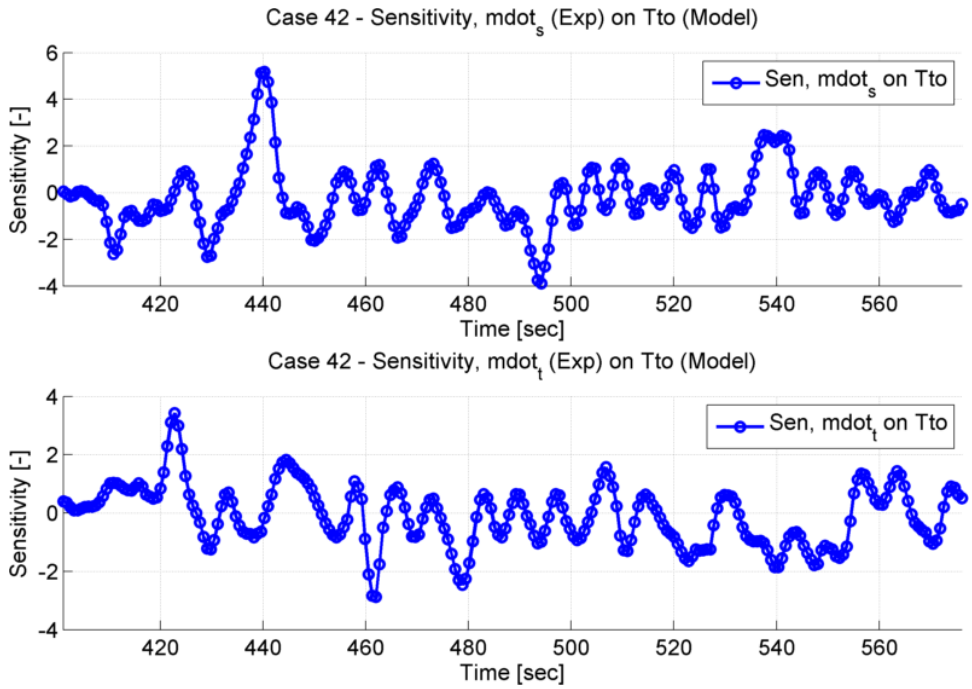

Figure 141: Case 42, Sensitivities vs. Time, Mass Flow Rates on Tube Outlet Temperature

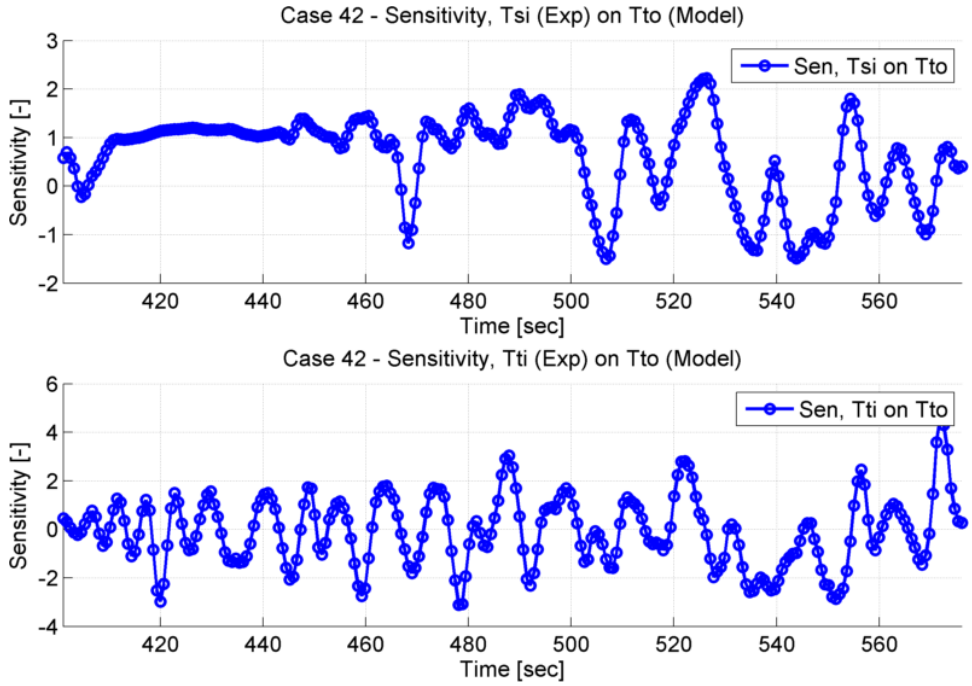

Figure 142: Case 42, Sensitivities vs. Time, Inlet Temperatures on Tube Outlet Temperature

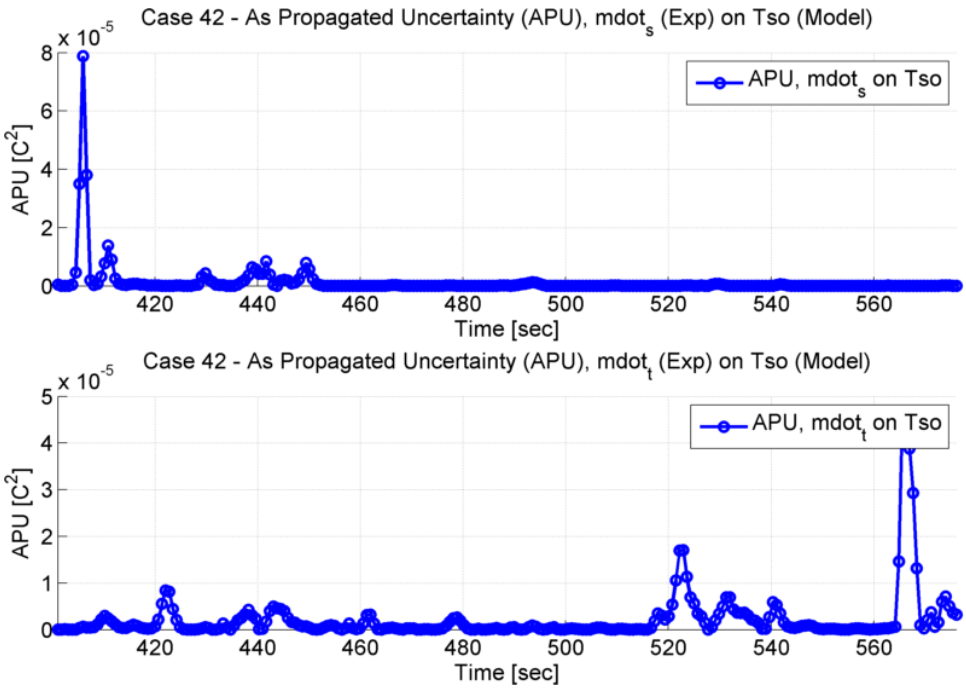

Figure 143: Case 42, As Propagated Uncertainties vs. Time, Mass Flow Rates on Shell Outlet Temperature

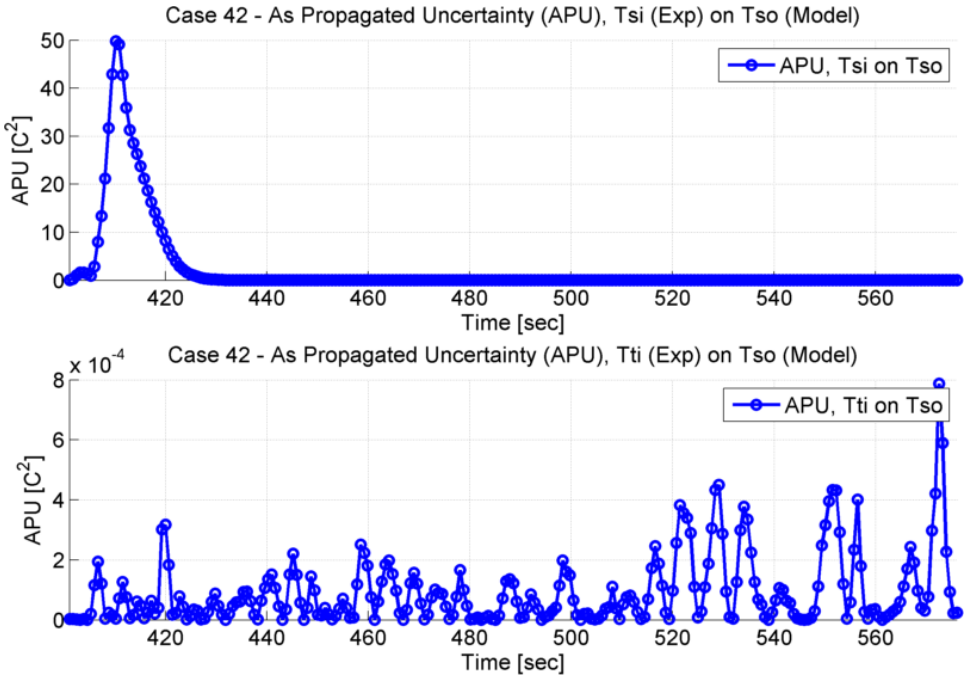

Figure 144: Case 42, As Propagated Uncertainties vs. Time, Inlet Temperatures on Shell Outlet Temperature

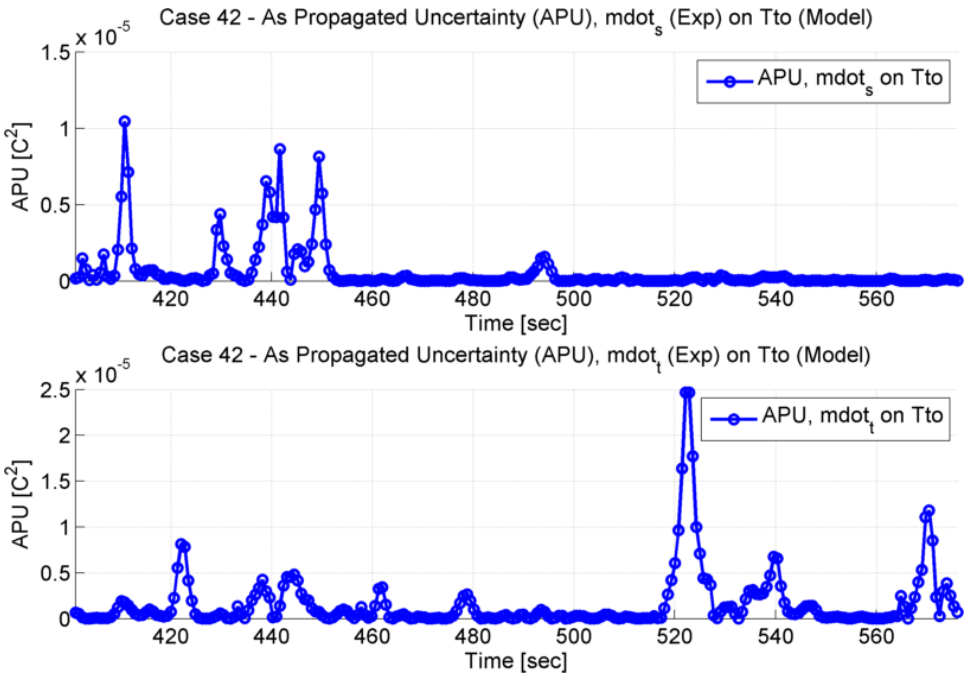

Figure 145: Case 42, As Propagated Uncertainties vs. Time, Mass Flow Rates on Tube Outlet Temperature

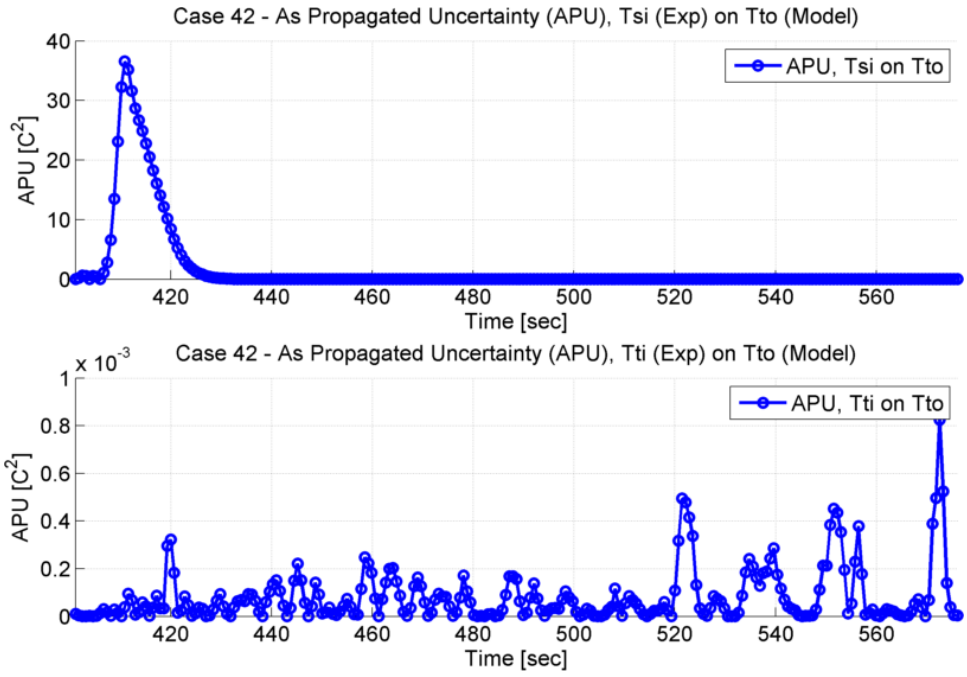

Figure 146: Case 42, As Propagated Uncertainties vs. Time, Inlet Temperatures on Tube Outlet Temperature

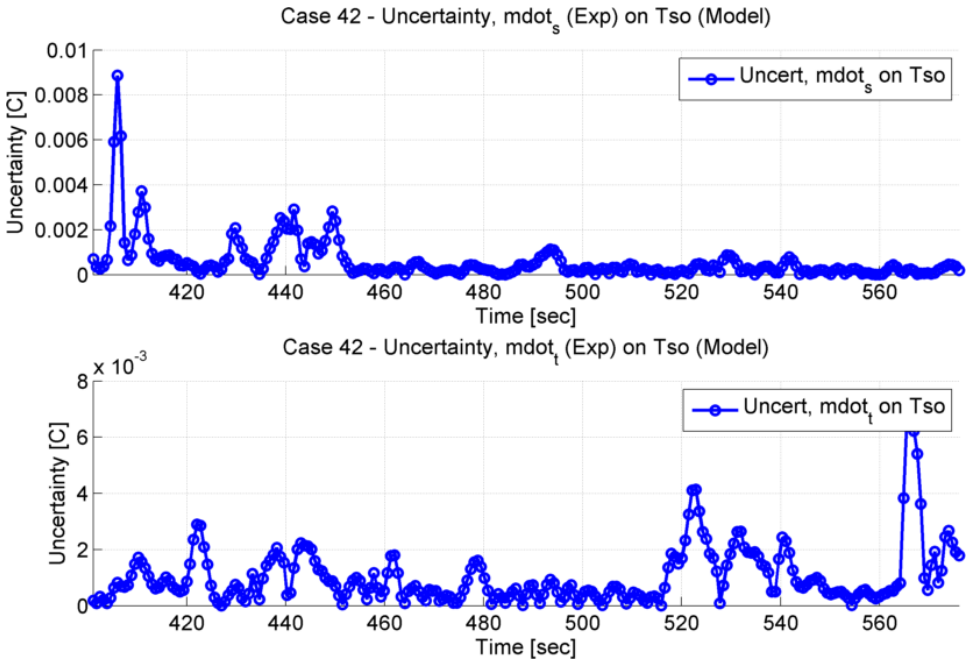

Figure 147: Case 42, Uncertainties vs. Time, Mass Flow Rates on Shell Outlet Temperature

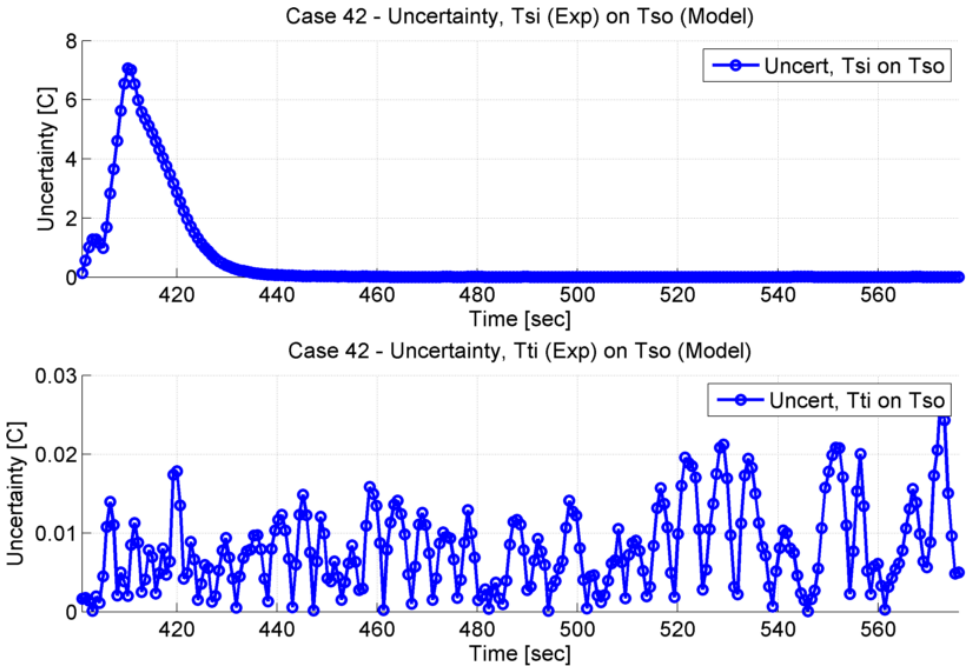

Figure 148: Case 42, Uncertainties vs. Time, Inlet Temperatures on Shell Outlet Temperature

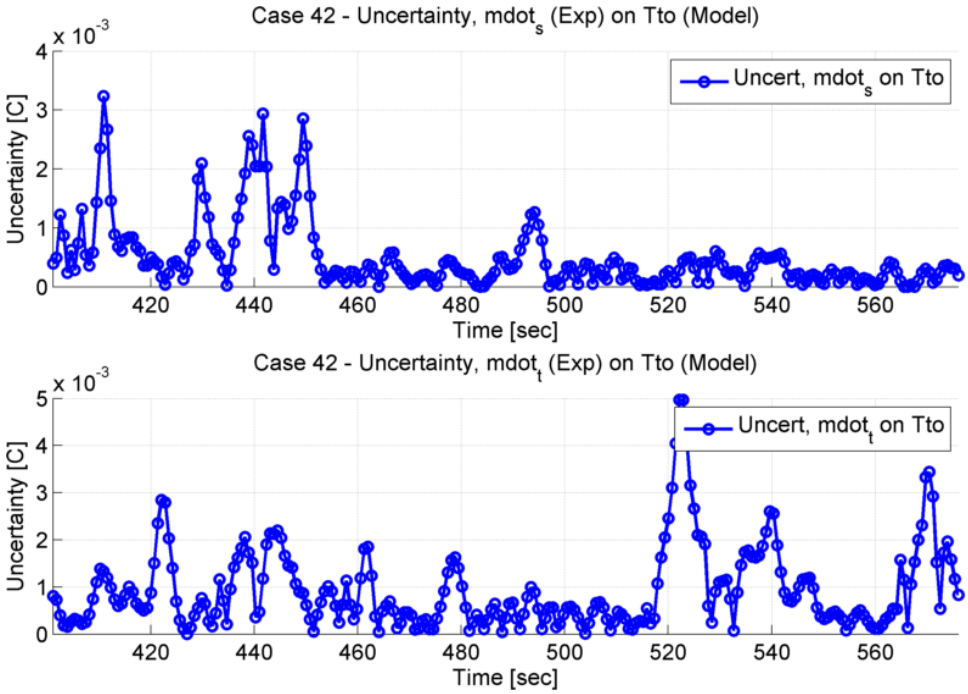

Figure 149: Case 42, Uncertainties vs. Time, Mass Flow Rates on Tube Outlet Temperature

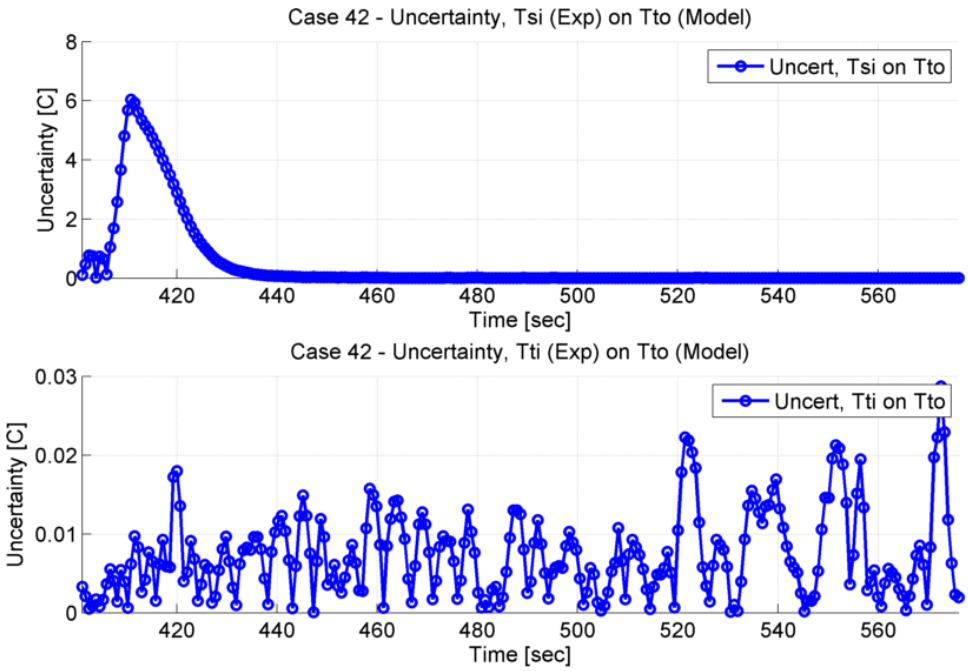

Figure 150: Case 42, Uncertainties vs. Time, Inlet Temperatures on Tube Outlet Temperature

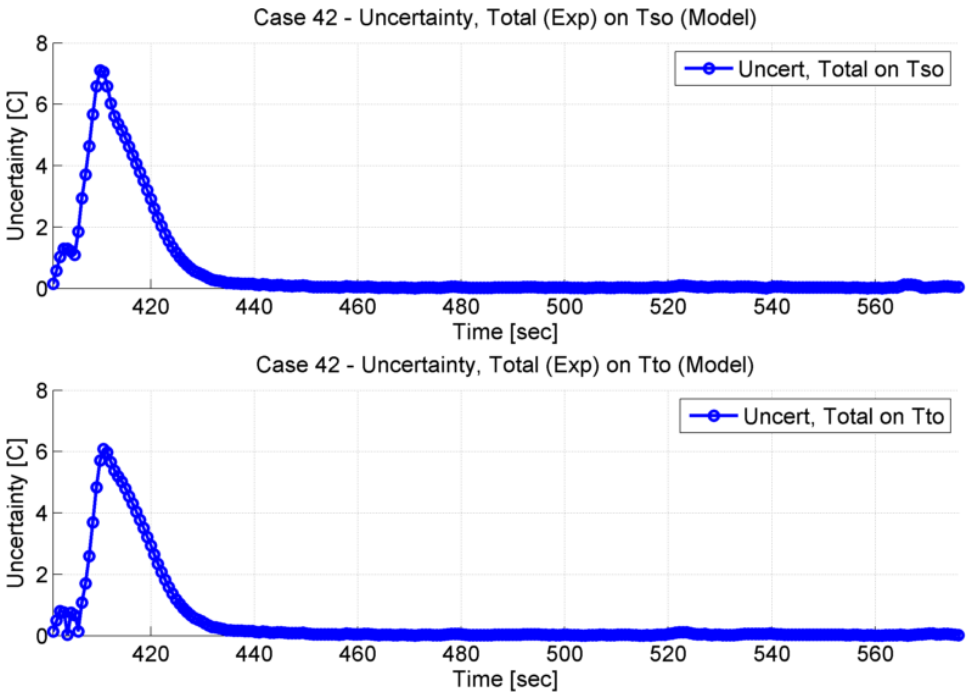

Figure 151: Case 42, Total Uncertainty on Outlet Temperatures

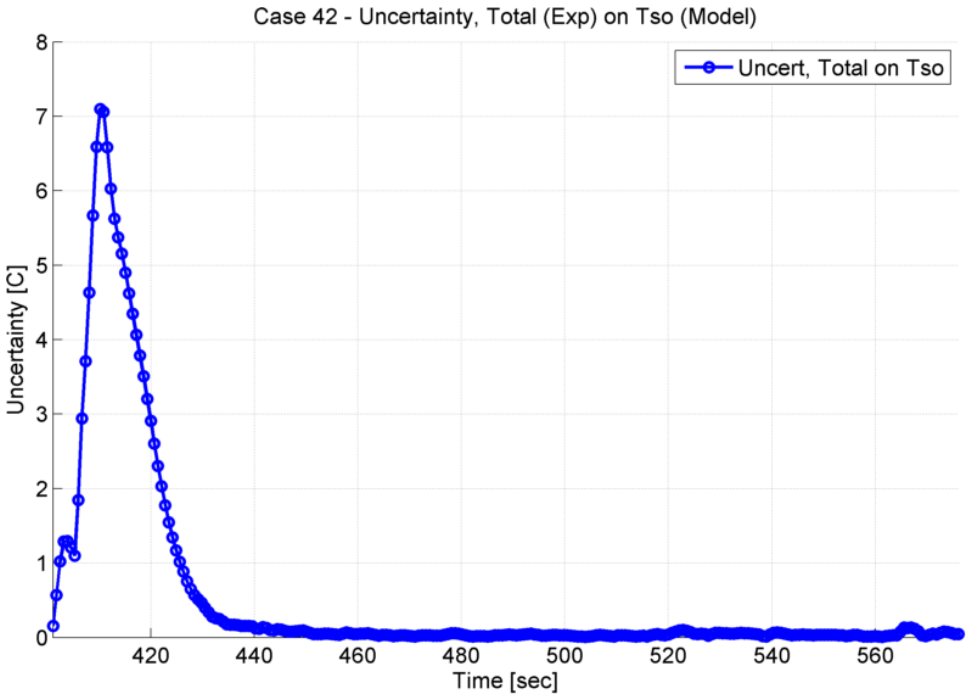

Figure 152: Case 42, Total Uncertainty on Shell Outlet Temperature

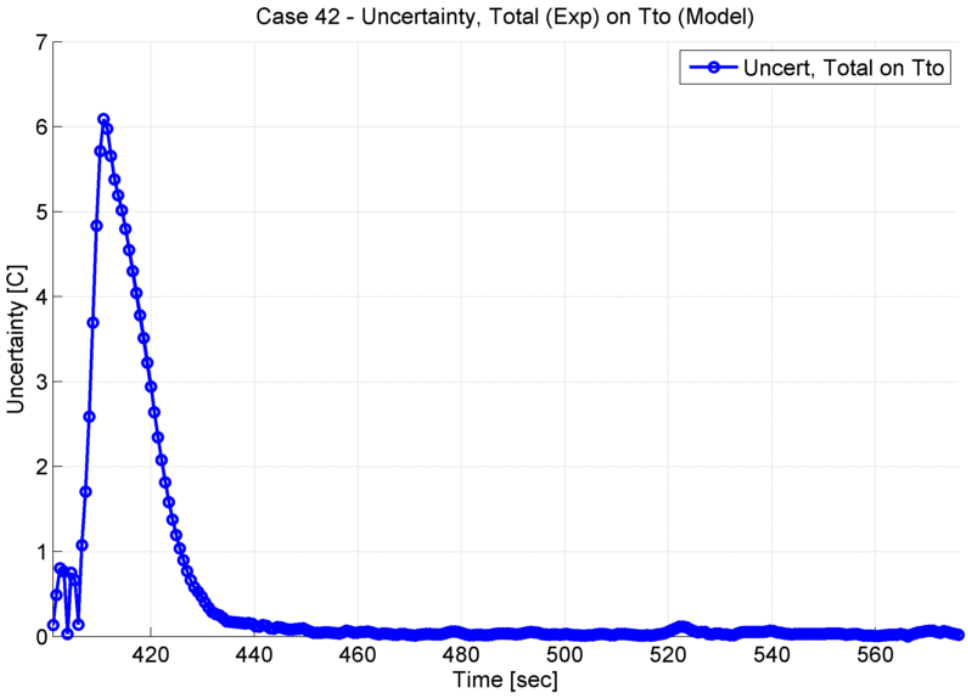

Figure 153: Case 42, Total Uncertainty on Tube Outlet Temperature

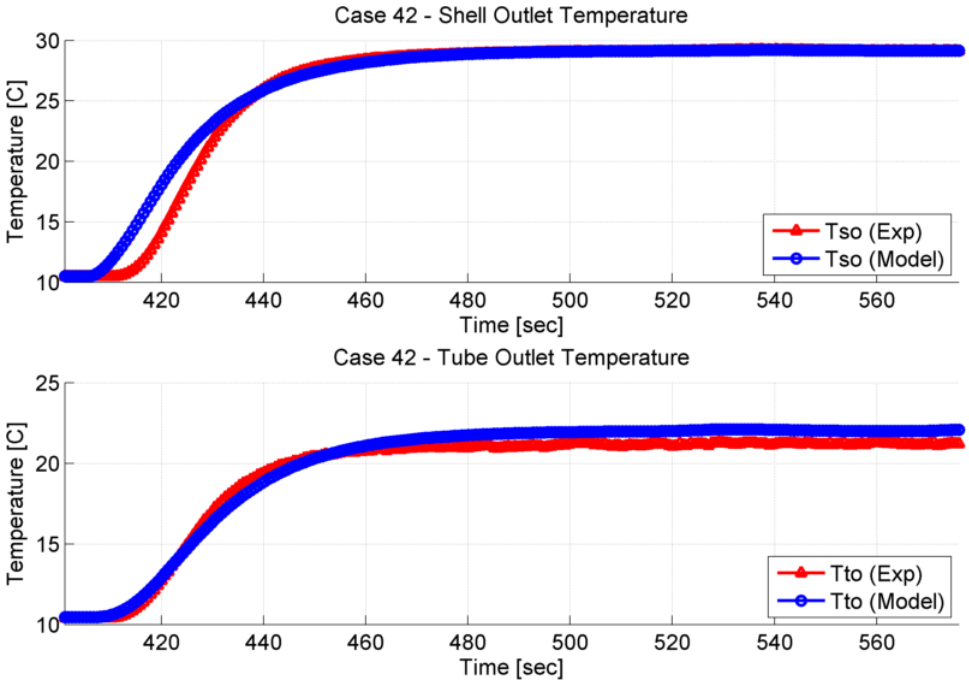

Figure 154: Case 42, Outlet Temperatures, Model & Experiment

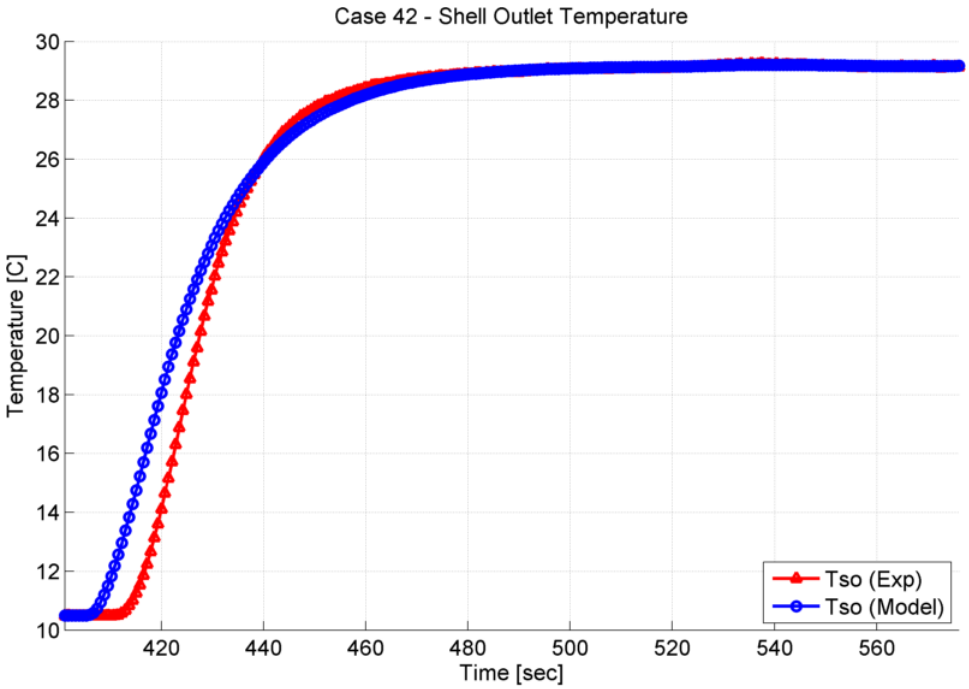

Figure 155: Case 42, Shell Outlet Temperature, Model & Experiment

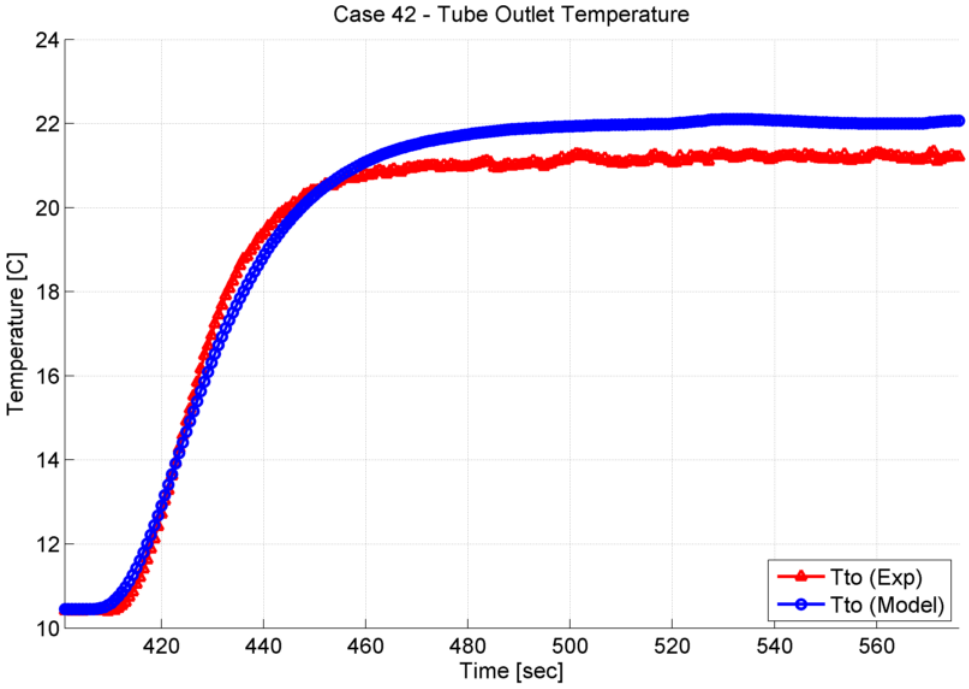

Figure 156: Case 42, Tube Outlet Temperature, Model & Experiment

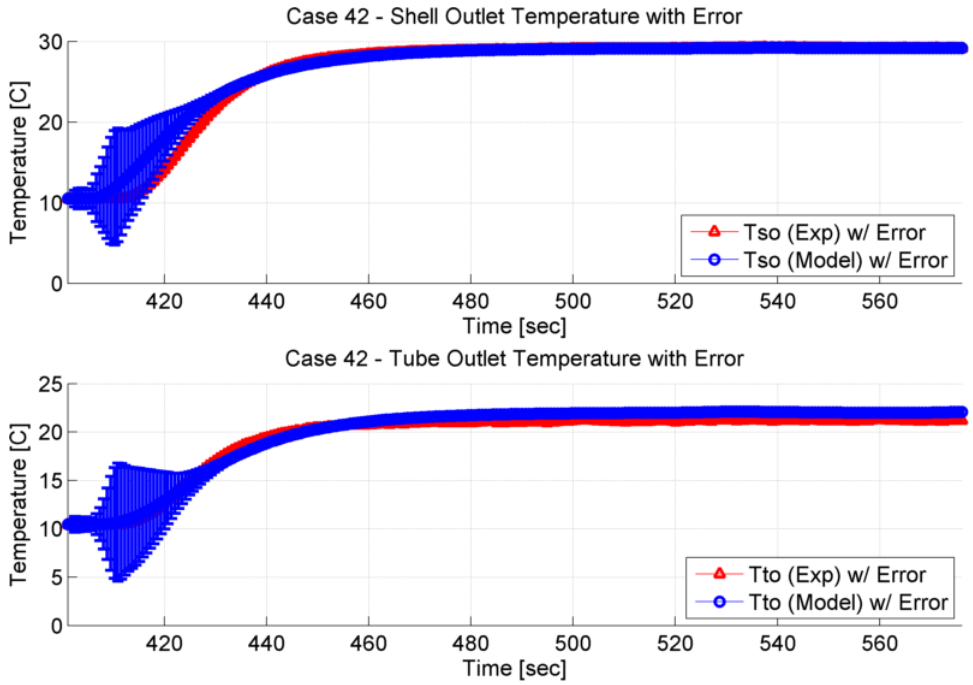

Figure 157: Case 42, Outlet Temperatures with Error, Model & Experiment

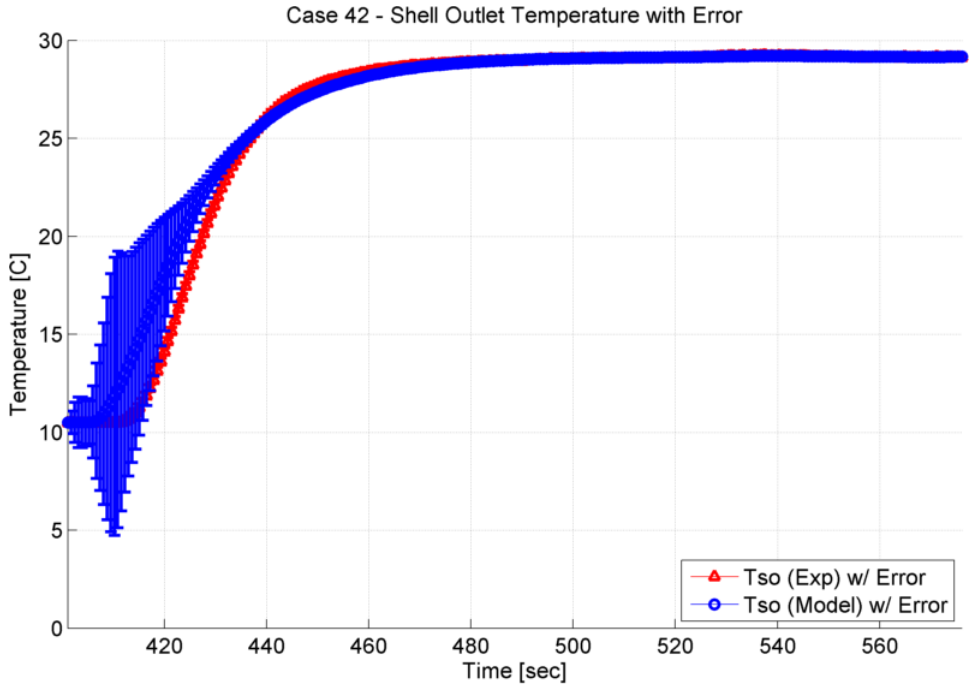

Figure 158: Case 42, Shell Outlet Temperature with Error, Model & Experiment

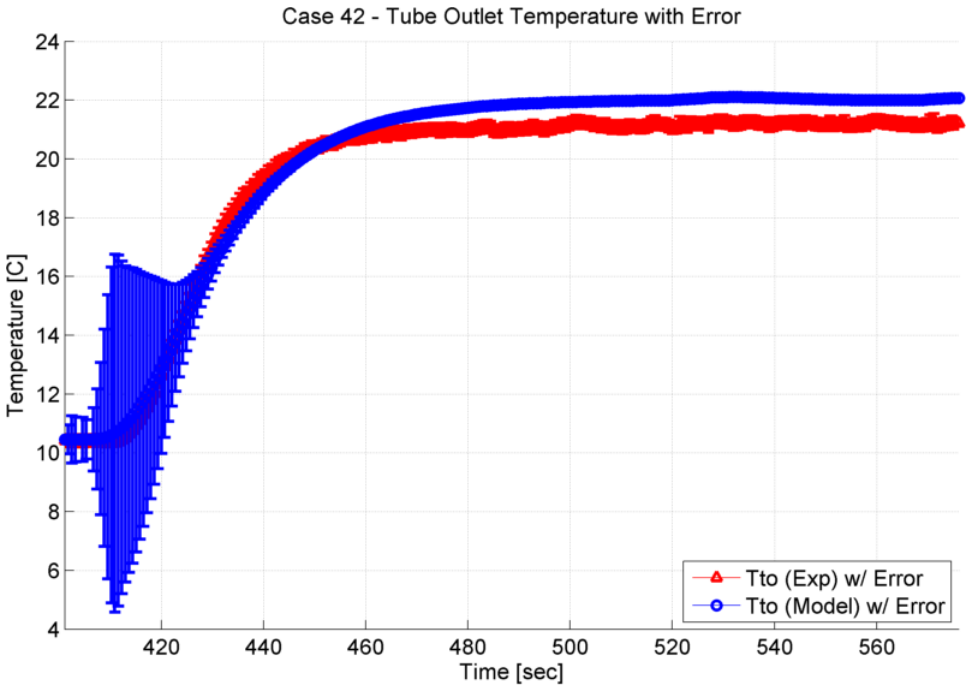

Figure 159: Case 42, Tube Outlet Temperature with Error, Model & Experiment

APPENDIX E: RECOMMENDATIONS FOR FUTURE WORK

One key finding from these efforts was that conducting several tests at each data point would prove useful. This type of testing is a standard practice such that average values may be calculated and answers can be relayed with some sort of statistical significance. Due to the nature of the experimental test rig, it was extremely difficult to obtain perfect replicate data points for one particular case; as such, emphasis was placed on collecting data for the test case that was of acceptable quality in all regions of the test. This meant ensuring minimal variation from the specified parameter for both temperature and flow rates. If a test was conducted that experienced high levels of variations, the test was re-run to attempt to reduce the standard deviation (since the uncertainties are a function of the standard deviation values).

Additionally, various factors played a role in the ability to successfully reproduce a test point. The manual operation of the valves that directed the flow throughout the loop was a source of inconsistency, the very nature of operating the valves by hand allowed the differences to exist between the cases. If the valves were operated by a solenoid, they could be controlled by the computer and timed much more consistently. This would make calculations for the time constant of the heat exchanger much more reliable. Manual temperature control of the fluid in the reservoirs / heating tanks was another factor. The heating elements were cycled on and off by hand, and as such, it was difficult to obtain the exact same temperature input, even for different cases (different flow rate, same temperature). Again, if a simple control scheme was introduced into the LabView program, more consistent temperatures could be maintained throughout the experiment.

Another important factor was due to the centrifugal pump that was utilized to circulate the fluid within the loop: it had no difficulties when the fluid was being recirculated, but provided very inconsistent flow rates when both the temperature was high and the fluid was switched to start pumping through the heat exchanger. It is believed that the pump was experiencing cavitation and as a result, pressure differential across the pump was lost. When this occurred, the pump either provided a lower flow rate than had been dialed in for the case, or would provide next to no flow. Occasionally the pump would experience a step up or down in the flow rate part way through, presumably as the air bubbles due to cavitation were pushed through the system. The nature of the reservoir tanks also created variation in the flow rates: as the level of fluid would decrease in one tank, the flow rate would also decrease slowly. As the fluid level drops in the tanks, the effects of gravity on the fluid pressure decreases, ultimately leading to a reduction of pressure at the backside of the pump. This small but steady change in pressure differential across the pump resulted in corresponding changes to the flow rate. When the fluid was drained from the first tank, the level of the fluid now "jumped" up to the top of the second tank, which again, resulted in a corresponding jump in flow rate part way through the test. These variations all contributed to higher standard deviations in the inputs, which in turn resulted in higher standard deviations and uncertainties in the outputs. A simple solution to this problem would be to utilize a positive displacement pump. One major advantage to these types of pumps is that they will consistently pump the same volume or mass flow rate, regardless of changes in viscosity or pressure differential across the pump. This type of change can provide flow

rates that are more stable and the use of fluids other than water, but at the tradeoff of a higher expense.

The cooling fluid was water that was pulled directly from the wall in the Wright State University laboratory. It was found through preliminary testing that regardless of flow rate, changes could be detected in the flow rates when water was being used elsewhere in the building. This resulted in the tests being completed at night when the number of people, and therefore water usage, was a minimum in the building. The experimental fluid loop could very easily detect when a toilet was flushed anywhere within the building as a relatively small drop was detected in the flow rate. When the temperature step change was induced, this also created a change in flow rate on both sides of the heat exchanger as well. This was most prevalent when using flow rates on the higher side of the test scheme, but was visible in virtually all tests. The flow rates could be dialed in with minimal variation from the set point prior to the step change, but as soon as the step change was induced, the flow rates would change. For example, the flow rate often jumped up slightly when the temperature step change was introduced to the system because now the total draw from the building's water system had just dropped abruptly by now drawing fluid from the reservoir tanks. A way to alleviate these issues would have been to utilize reservoir tanks for the cold side fluid as well as the hot side, and also implement a positive displacement pump as noted above. Another possible way to minimize changes in the flow rates would be to implement a pressure snubber on the supply lines to both sides of the heat exchanger. The snubber would serve to reduce the supply pressure to the experiment from the pressures seen in the entire water system. If the reduced pressure was set to a value below the typical drops that are seen due to

normal water usage, the flow rates provided to the experiment would always be consistent and steady.

A total of 63 tests were selected in a 3 factor design (for flow rates) along with 7 factors for the input temperature. Each test was very time consuming to run, and as such, any way that the number of tests can be reduced while still providing the necessary data for the analysis is beneficial. The total number of tests may have been able to be reduced with a better understanding of the design of experiments selection criteria. For example, it may have been more beneficial to only conduct a two factor analysis for each major input in the system to reduce the number of tests.

There was a delay between when the valve was switched to introduce the thermal step and when the thermal step was actually seen in the system. This is partially due to the fact that as opposed to using a specially designed flow straightening tube before and after the flow meters, a sufficient amount of straight pipe was used to allow the flow to fully develop. Due to this long length of pipe prior to entering the flowmeter and the heat exchanger, additional time was required for the fluid with a higher temperature to register at the entrance of the heat exchanger as it had to be pumped through the pipes first. If there was a way to introduce the step change physically very close to the entrance of the heat exchanger, these time delays could for all intents and purposes be ignored. A way to implement this could require placing the flowmeters downstream of the heat exchanger along with the flow control valves.

The flowmeters that were utilized in this experimental test rig were of the turbine variety. This was possible due to the selection of water as the working fluid on both sides of the heat exchanger. If the working fluid had been one that has a large change in

viscosity with changes in temperature, such as oil, a positive displacement flowmeter would have been required to accurately measure the flow rates.

REFERENCES

[1] Roberts, R., Eastbourn, S., and Maser, A., "Generic Aircraft Thermal Tip-to-Tail Modeling and Simulation," *AIAA/ASME/SAE/ASEE Joint Propulsion Conference & Exhibit*, San Diego, CA: 2011.

[2] Doty, A. P., "Nonlinear Uncertainty Quantification, Sensitivity Analysis, and Uncertainty Propagation of a Dynamic Electrical Circuit," University of Dayton, 2012.

[3] Doty, J. H., "Statistical Analysis and Assessment of Missile Performance Characteristics," *NATO/RTA/RTO, Air Vehicle Technology (AVT) Panel, Paper 12*, San Diego, CA: 2012, p. 69.

[4] ASME, "Standard for Verification and Validation in Computational Fluid Dynamics and Heat Transfer," 2009, p. 88.

[5] Young Touchstone, "F/HF/SSF Fixed Tube Bundle Heat Exchangers, Catalog 12," 2005, p. 8.

[6] Cengel, Y., *Heat and Mass Transfer: A Practical Approach*, New York, NY: McGraw-Hill, 2007.

[7] Theodore, L., *Heat Transfer Applications for the Practicing Engineer (Essential Engineering Calculations Series)*, Wiley, 2011.

[8] Cengel, Y. A., and Boles, M. A., *Thermodynamics: An Engineering Approach*, New York, NY: McGraw-Hill Higher Education, 2008.

[9] Fox, R. W., Pritchard, P. J., and McDonald, A. T., *Introduction to Fluid Mechanics*, Hoboken, NJ: John Wiley & Sons, Inc., 2009.

[10] Beckwith, T. G., Marangoni, R. D., and Lienhard V, J. H., *Mechanical Measurements*, Upper Saddle River, NJ: Pearson Prentice Hall, 2007.

[11] Omega Engineering, "Turbine Flowmeters with Economical Ball Bearing Design" Available: http://www.omega.com/pptst/FTB100.html.

[12] Omega Engineering, "Integral Signal Conditioners for Frequency, Voltage, or Current Output" Available: http://www.omega.com/pptst/FLSC18_28_34_35_51.html.

[13] Baker, R. C., *Flow Measurement Handbook: Industrial Designs, Operating Principles, Performance, and Applications*, Cambridge, UK: Cambridge University Press, 2000.

[14] Ohaus Corporation, "EB Series Compact Bench Scales," p. 2.

[15] Omega Engineering, "Super OMEGACLAD® XL Thermocouple Probes - Quick Disconnect Probes with Standard Size Connectors, Low Drift" Available: http://www.omega.com/pptst/KQXL_NQXL.html.

[16] Lauda, "Lauda Compact Thermostat Operating Instructions," 1989, p. 38.

[17] Isotech North America, "F250 Mk II Precision Thermometer," 1997, p. 57.

[18] Omega Engineering, "High Performance Pressure Transducer, Rugged All Stainless Steel Construction, State-of-the-Art Silicon Technology, 0 to 5 Vdc Output" Available: http://www.omega.com/pptst/PX309-5V.html.

[19] National Instruments, "NI CompactDAQ 4-Slot USB Chassis" Available: http://sine.ni.com/nips/cds/view/p/lang/en/nid/207535.

[20] National Instruments, "NI 9205 32-Ch ±200 mV to ±10 V, 16-Bit, 250 kS/s Analog Input Module" Available: http://sine.ni.com/nips/cds/view/p/lang/en/nid/208800.

[21] National Instruments, "NI 9213 ±78 mV, Thermocouple Input, 75 S/s, 16 Ch Module" Available: http://sine.ni.com/nips/cds/view/p/lang/en/nid/208788.

[22] National Instruments, "NI 9481 4-Channel Relay [30 VDC (2 A), 60 VDC (1 A), 250 VAC (2 A)]" Available: http://sine.ni.com/nips/cds/view/p/lang/en/nid/208827.

[23] Montgomery, D. C., *Design and Analysis of Experiments*, Hoboken, NJ: John Wiley & Sons, Inc., 2009.

[24] Roy, C. J., and Oberkampf, W. L., "A comprehensive framework for verification, validation, and uncertainty quantification in scientific computing," *Computer Methods in Applied Mechanics and Engineering*, vol. 200, Jun. 2011, pp. 2131–2144.

[25] Goodman, L., "On the Exact Variance of Products," *Journal of the American Statistical Association*, vol. 55, 1960, pp. 708–713.

[26] Saltelli, A., *The critique of modelling and sensitivity analysis in the scientific discourse. An overview of good practices*, presented at the Transatlantic Uncertainty Colloquium (TAUC), Washington, October 10-11: 2006.

[27] Intergovermental Panel on Climate Change (IPCC), *Background Papers - IPCC Expert Meetings on Good Practice Guidance and Uncertainty Management in National Greenhouse Gas Inventories*, 2002.

[28] MathWorks, "Floating-Point Numbers," *MATLAB Documentation Center* Available: http://www.mathworks.com/help/matlab/matlab_prog/floating-point-numbers.html.

[29] Oberkampf, W. L., and Roy, C. J., *Verification and Validation in Scientific Computing*, New York, NY: Cambridge University Press, 2010.

[30] MathWorks, "adtest - Anderson-Darling test," *MATLAB Documentation Center* Available: http://www.mathworks.com/help/stats/adtest.html.

[31] Trujillo-Ortiz, A., "AnDarksamtest," *MATLAB Central File Exchange* Available: http://www.mathworks.com/matlabcentral/fileexchange/17451-andarksamtest.

[32] MathWorks, "kstest2 - Two-sample Kolmogorov-Smirnov test," *MATLAB Documentation Center* Available: http://www.mathworks.com/help/stats/kstest2.html.